Investigating the functions of Phospholipase C-1, Ca^{2+}/H^{+} exchanger, and Secretory Phospholipase A_2 in growth, stress responses, and cellulose degradation in *Neurospora crassa*

A thesis submitted in partial fulfilment of the requirements
for the award of the degree of

DOCTOR OF PHILOSOPHY

by

Darshana Baruah

Department of Biosciences and Bioengineering
Indian Institute of Technology Guwahati
Guwahati - 781 039, Assam, India
February 2023

Investigating the functions of Phospholipase C-1, Ca^{2+}/H^{+} exchanger, and Secretory Phospholipase A_2 in growth, stress responses, and cellulose degradation in *Neurospora crassa*

A thesis submitted in partial fulfilment of the requirements
for the award of the degree of

DOCTOR OF PHILOSOPHY

by

Darshana Baruah

(Roll No. 166106007)

Under the supervision of

Prof. Ranjan Tamuli

Department of Biosciences and Bioengineering
Indian Institute of Technology Guwahati
Guwahati - 781 039, Assam, India

February 2023

Dedicated

to

Deuta-Maa & Family

INDIAN INSTITUTE OF TECHNOLOGY GUWAHATI

DEPARTMENT OF BIOSCIENCES AND BIOENGINEERING

Guwahati – 781 039

STATEMENT

I do hereby declare that the content embodied in this thesis entitled **"Investigating the functions of Phospholipase C-1, Ca^{2+}/H^{+} exchanger, and Secretory Phospholipase A_2 in growth, stress responses, and cellulose degradation in *Neurospora crassa*"** is the result of investigation carried out by me at the Department of Biosciences and Bioengineering, Indian Institute of Technology Guwahati, Guwahati, India under the guidance of Prof. Ranjan Tamuli.

In keeping with the general practice of reporting scientific observations, due acknowledgements have been made wherever the work described is based on the findings of other investigators.

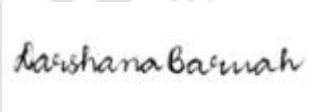

February 2023 **Darshana Baruah**

Roll No. 166106007
Department of Biosciences and Bioengineering
Indian Institute of Technology Guwahati
Guwahati, Assam, India

INDIAN INSTITUTE OF TECHNOLOGY GUWAHATI

DEPARTMENT OF BIOSCIENCES AND BIOENGINEERING

Guwahati – 781 039

CERTIFICATE

This is to certify that the work described in this thesis entitled **"Investigating the functions of Phospholipase C-1, Ca^{2+}/H^{+} exchanger, and Secretory Phospholipase A_2 in growth, stress responses, and cellulose degradation in *Neurospora crassa*"** by **Darshana Baruah (Roll No. 166106007)** for the award of **Doctor of Philosophy** is an authentic record of the results obtained from the research work carried out under our supervision in the Department of Biosciences and Bioengineering, Indian Institute of Technology Guwahati, Guwahati, India and this work has not been submitted elsewhere for a degree.

Dr. Ranjan Tamuli
Professor
Department of Biosciences and Bioengineering
Indian Institute of Technology Guwahati
Guwahati, Assam, India

Contents

Contents

Contents

Contents

Contents

List of Figures

List of Figures

List of Tables

List of Tables

Abbreviations

ANOVA	Analysis of Variance	N	Normal
bp	Base pair	NCBI	National Centre for Biotechnology Information
BLAST	Basic Local Alignment Tool		
BOD	Biological Oxygen Demand	NCU	*Neurospora crassa* unit
°C	Degree Celsius	NEB	New England Biolab
CDD	Conserved Domain Database	ng	Nanogram
cDNA	complementary Deoxyribonucleic Acid	nM	Nanomolar
cm	Centimetre	Ω	ohm
DNA	Deoxyribonucleic Acid	OD	Optical Density
ExPASy	Expert Protein Analysis System	ORF	Open Reading Frame
FGS	Fructose, Glucose, Sorbose	*p*	Probability
FGSC	Fungal Genetics Stock Centre	PAGE	Polyacrylamide Gel Electrophoresis
g	Gram	PCR	Polymerase Chain Reaction
g	Relative Centrifugal Force	pm	Picometre
GFP	Green Fluorescent Protein	psi	Pound-force per square inch
h	Hour	qRT-PCR	Quantitative Real-Time Polymerase Chain Reaction
hph	Hygromycin B Resistance Gene		
Jm^{-2}	Joule per square metre	RIP	Repeat Induced Point Mutation
KV	Kilovolt		
kb	Kilo base pair	RNA	Ribonucleic Acid
kDa	Kilo Dalton	rpm	Revolution per minute
LG	Linkage Group	RT-PCR	Reverse Transcription Polymerase Chain Reaction
m	Metre		
M	Molar	s	Second
mA	Milliampere	SCM	Synthetic Crossing Media
MEGA	Molecular Evolutionary Genetic Analysis	UCR	University of California Riverside
µg	Microgram	UK	United Kingdom
µl	Microlitre	USA	United States of America
µm	Micrometre	UV	Ultraviolet
µM	Micromolar	VM	Vogel's Minimal Medium
ml	Millilitre	V	Volt
mm	Millimetre	w/v	weight per volume
mM	Millimolar	w/w	weight per weight

Acknowledgements

The tenure at IIT Guwahati as a Ph.D. scholar has been an amazing experience for me, which I will cherish in my journey through life. It is full of my patience, and the constant support and encouragement of numerous individuals, including my mentors, teachers, colleagues, friends, and well-wishers. I take my utmost pleasure in expressing my deepest gratitude to each and everyone who supported me in several ways to complete my Ph.D. dissertation.

First and foremost, I would like to offer my sincere gratitude to my Ph.D. supervisor, Prof. Ranjan Tamuli, for his guidance, valuable suggestions, motivation, and constant support throughout my research work. I sincerely thank him for his humility in investing his valuable time and effort in instilling in me a scientific temperament and commendable work ethics.

I would also like to thank all the members of my doctoral committee, Prof. Pranab Goswami, Prof. Manish Kumar, and Prof. Sunanda Chatterjee, for their support and insightful suggestions during my progress review seminars, which helped in successful completion of my thesis.

I would like to convey my heartfelt gratitude to the current and former Directors of the Indian Institute of Technology Guwahati, for allowing me to pursue my doctoral studies on such a dynamic and natural campus. I would also like to thank the current and former Heads of the Department of Biosciences and Bioengineering for their assistance and support in carrying out my research. I wish to acknowledge all the staff members of the Department of Biosciences and Bioengineering for their possible support and for providing me the facilities to carry out my research work.

I would also like to express my sincere gratitude towards the Centre for Instrument Facility (CIF) and the Supercomputing Facility, Param-Ishan, IIT Guwahati, for allowing me to carry out the experiments, and Lakhminath Bezborua Central Library, IIT Guwahati, for providing me the books and the reading space.

I want to express my appreciation to the Ministry of Human Resources Development (MHRD), Government of India, for their support in the form of Ph.D. scholarships through IIT Guwahati, the Department of Science and Technology (DST) and the Department of Biotechnology (DBT), Govt. of India, for the research grants to my supervisor, which were vital in helping me complete my doctoral dissertation at IIT Guwahati. I also extend my gratitude to all the Indian taxpayers, because of whom all the government research funding and fellowships have become possible.

I'm grateful to the Fungal Genetics Stock Centre (FGSC) at the University of Missouri, Kansas, USA, for the *Neurospora* strains. I also want to thank Prof. Maria Celia Bertolini, for providing me with the *Neurospora* Δ*cre-1* and *Pn-cre-1* strains that I needed for my research work.

I am lucky to have the support, warmth, and fun-loving environment provided by the members of the Neurospora Research Group. I would like to thank all of the current lab members, Christy, Serena, Rahul, Surabhi, Sangeeta, Krishna, Megha, Rebecca, Ambika, Abhilash, Shomina, and Priyanuj and as well as the alumni members of this group – Dr. Rekha Deka, Dr. Ravi Kumar, Dr. Vijaya Laxmi, Dr. Ananya Barman, Dr. Dibakar Gohain, Dr. Ajeet Kumar, Dr. Avishek Roy, Pallavi, Shalini, Nayan, Divya, Mohit, and Aravind for their valuable suggestions and constant support. I would especially, like to mention Surabhi, who is more of a younger sister than a colleague, for her help and support in various aspects of my life at IIT Guwahati.

I'm fortunate to have a remarkable group of friends who have made my time at IIT Guwahati truly unforgettable. Alka, Anshuman, Debeni, Kuwari, Menan, Neelam, Prabhakar, Pratap, Satakshi, Surabhi, Sweta, and Vivek, your presence has enriched my life in countless ways. I would like to express my heartfelt gratitude to Ambika for introducing me to the wonderful world of squash. I am deeply indebted to Ekramul and Jaideep for their invaluable support throughout this journey. Your assistance has been instrumental in overcoming challenges and achieving my goals. During my Ph.D. tenure, I had the privilege of having Rima and Gaurav by my side, providing much-needed respite from the routine research discussions. Our lighter moments and shared laughter will forever hold a special place in my heart. I would like to express a special mention to Binita, Champs, Kasturi, Navaneeta, Rakesh, and Tanvi for their unwavering presence and support. You have been my pillars of strength, offering guidance and solace through both professional and personal highs and lows.

My Ph.D. endeavour would not have been completed without the never-ending love and endless support from my family. I am highly indebted to my parents for all the sacrifices they have made for my better future, for having faith in me and for giving me the freedom to make my own decisions. I would like to pay my heartfelt regards towards my grandparents and close relatives who have laid their sincere believe on me and supported me throughout my research work. My deepest thanks to my younger brother, Rishi, and my cousins for their unconditional love and support that motivated me throughout my entire life. Thank you.

Although it is not possible to pen down the names of each individual, I would like to thank each one of them for helping me and having trust in me.

Last but not least, I'm thankful to the Almighty, God, for showing me the right path to follow in all stages of my life, and giving me the courage and motivation to complete my research work successfully

Sincerely,

Darshana Baruah

Abstract

In this thesis work, I investigated the cell functions of three Ca^{2+} signaling genes encoding for a phospholipase C-1 (PLC-1), a Ca^{2+}/H^{+} exchanger (CPE-1), and a secretory phospholipase A_2 ($sPLA_2$) homologs in *N. crassa* using their knockout mutants. The Δ*plc-1*, Δ*cpe-1*, and Δ*splA*$_2$ mutants exhibited reduced survival during induced thermotolerance and increased sensitivity to alkaline pH, but had no effect during cell wall stress in *N. crassa*. Furthermore, deletion of PLC-1 resulted in increased period length and showed loss of temperature compensation at physiological temperature. In addition, the Δ*splA*$_2$ mutant exhibited hypersensitivity in the presence of dithiothreitol (DTT), which induces endoplasmic reticulum (ER) stress, rapid utilization of microcrystalline cellulose compared to the wild type, and increased extracellular protein secretion and glucose accumulation in the culture supernatants. However, when cultured on medium containing sucrose, glucose, xylose, glycerol, and sodium acetate as the carbon source, the Δ*plc-1*, Δ*cpe-1*, and Δ*splA*$_2$ mutants displayed growth like the wild type. The Δ*splA*$_2$ mutant was unable to grow on microcrystalline cellulose during ER stress. Moreover, studies using the double mutants revealed that *plc-1*, *cpe-1*, and *splA*$_2$ synthetically regulate the circadian clock, stress survival, and utilization of microcrystalline cellulose as a carbon source in *N. crassa*. Furthermore, the homokaryotic transformants expressing the *plc-1*, *cpe-1*, and *splA*$_2$ transgenes under the *ccg-1* promoter complemented the phenotypes of the Δ*plc-1*, Δ*cpe-1*, and Δ*splA*$_2$ mutants during stress conditions and growth on microcrystalline cellulose. qRT-PCR studies revealed differential expression of some important genes involved in regulating the circadian clock, stress responses, and cellulose degradation pathways in the Δ*plc-1*, Δ*cpe-1*, and Δ*splA*$_2$ single and double mutants, implying PLC-1, CPE-1, and $sPLA_2$ crosstalk with these cellular pathways in *N. crassa*. Further, to understand the molecular mechanism of $sPLA_2$ mediated cellulose degradation, I studied the interaction of *splA*$_2$ with *cre-1*, a carbon catabolite repressor. I found that *splA*$_2$ genetically interacts with *cre-1* to regulate vegetative growth and cellulose degradation in *N. crassa*. Further, I predicted the three dimensional protein structures of $sPLA_2$ and CRE-1. Therefore, this study concludes that the *plc-1*, *cpe-1*, and *splA*$_2$ genes are involved in a complex genetic interaction to regulate multiple cellular pathways in *N. crassa*.

Synopsis

Thesis title: Investigating the functions of Phospholipase C-1, Ca^{2+}/H^{+} exchanger, and Secretory Phospholipase A_2 in growth, stress responses, and cellulose degradation in *Neurospora crassa*

Objectives:

1. To investigate the cellular roles of the Ca^{2+} signaling genes *phospholipase C-1* (*plc-1*), *Ca^{2+}/H^{+} exchanger-1* (*cpe-1*), and *secretory phospholipase A_2* (*splA_2*) in circadian clock, stress responses, and cellulose degradation in *N. crassa*,
2. To investigate the crosstalk of *plc-1*, *cpe-1*, and *splA_2* genes in the regulation of circadian clock, stress responses, and cellulose degradation in *N. crassa*, and
3. To investigate the molecular basis of $sPLA_2$ mediated cellulose degradation in *N. crassa.*

Organization of the thesis:

Chapter 1: An introduction to *Neurospora crassa* biology and calcium signaling

Chapter 2: Materials and Methods

Chapter 3: The cell functions of the Ca^{2+} signaling genes *phospholipase C-1*, *Ca^{2+}/H^{+} exchanger-1*, and *secretory phospholipase A_2* in *N. crassa*

Chapter 4: Expression analysis of genes involved in the circadian clock, stress responses, and cellulose degradation in the *N. crassa* Δ*plc-1*, Δ*cpe-1*, and Δ*splA_2* mutants

Chapter 5: The *splA_2* gene interacts with the transcription factor CRE-1 to regulate growth and cellulose degradation in *N. crassa*

Chapter 6: Conclusions and Future Perspectives

Appendix

Bibliography

Chapter 1: An introduction to *Neurospora crassa* biology and calcium signaling

Neurospora crassa, which means "nerve spores" because of the nerve-like stripes in its sexual spores, is a filamentous fungus belonging to the phylum Ascomycetes, that primarily thrives on dead and burned vegetation in tropical and subtropical areas (Luque et al. 2012). *N. crassa* is an excellent eukaryotic model organism for studying several biological processes, including calcium (Ca^{2+}) signaling. Chapter 1 briefly describes about the history, life cycle, and Ca^{2+} signaling machinery of *N. crassa*. The Ca^{2+} ion has evolved as a universal second messenger molecule, influencing signaling pathways from fertilization to death in all eukaryotes (Berridge et al. 1998; Clapham 2007). The resting concentration of cytosolic free $[Ca^{2+}]_c$ is maintained at ~ 10^{-7} M, which is ~ 10^4 times lower than the extracellular Ca^{2+} concentration (Chin and Means 2000). The $[Ca^{2+}]_c$ level may transiently increase either due to extracellular Ca^{2+} or its release from the intracellular stores (Chin and Means 2000; Bootman et al. 2001; Clapham 2007). In eukaryotes, a minute change in the $[Ca^{2+}]_c$ is sensed by Ca^{2+}-sensing proteins that undergo a change in conformation and charge upon Ca^{2+} binding and activate the Ca^{2+} signaling pathway (Chin and Means 2000; Bootman et al. 2001). The analysis of *N. crassa* genome revealed that its Ca^{2+} signaling machinery is complex and comprises 48 Ca^{2+} signaling proteins. The *N. crassa* Ca^{2+} signaling machinery includes three Ca^{2+} channel proteins, nine Ca^{2+}/cation-ATPases, six recognizable Ca^{2+}/H^+ exchangers, two novel putative Ca^{2+}/Na^+ exchangers, four novel phospholipase C-δ subtype (PLC-δ) proteins, 23 Ca^{2+} and/or calmodulin (CaM) binding proteins, and one CaM, which are involved in triggering various cellular processes (Galagan et al. 2003; Borkovich et al. 2004; Zelter et al. 2004; Tamuli et al. 2013). In *N. crassa*, three Ca^{2+} signaling proteins, phospholipase C-1 (PLC-1), secretory phospholipase A_2 ($sPLA_2$), and a Ca^{2+}/H^+ exchanger (CPE-1) are found to be involved in sensing the increase in $[Ca^{2+}]_c$ (Galagan et al. 2003; Borkovich et al. 2004; Barman and Tamuli 2015, 2017). In response to external stimuli, PLC-1 produces inositol-1, 4, 5-trisphosphate (IP_3), which causes the release of Ca^{2+} from intracellular Ca^{2+} storage, resulting in a rise in $[Ca^{2+}]_c$, and diacylglycerol (DAG), which activates PKC. PKC activation and/or increased $[Ca^{2+}]_c$ function as a signal for the Ca^{2+} and/CaM binding $sPLA_2$ protein and CPE-1 in *N. crassa* (Barman and Tamuli 2017).

PLC-1 and $sPLA_2$ are phospholipase superfamily of proteins. The membrane-bound phosphoinositide-specific PLC-1 catalyses the hydrolysis of phosphatidylinositol 4, 5-bisphosphate (PIP_2) into two important second messengers; inositol-1, 4, 5-trisphosphate (IP_3) that induces Ca^{2+} release from intracellular Ca^{2+} stores to activate CaM-dependent enzymes, and diacylglycerol (DAG) that activates protein kinase C (PKC; Berridge and Irvin 1984; Rhee and Bae 1997; Clapham 2007). PLC-1 is necessary in many species, including yeast and filamentous fungi, for various cellular processes and pathogenicity. In *S. cerevisiae* and *C. albicans*, PLC1 homologs function in nutrition and stress-related responses (Flick and Thorner 1993; Kunze et al. 2005). In the fission yeast *S. pombe*,

the PLC1 homolog *plc1-1*, involved in ammonium sensing, is required for growth in a phosphate-rich medium (Fankhauser et al. 1995). The PLC1 homologs in *A. alternata*, *B. cinerea*, *C. neoformans*, and *M. oryzae* play a role in maintaining intracellular Ca^{2+} homeostasis, vegetative development, and pathogenicity (Schumacher et al. 2008; Rho et al. 2009; Lev et al. 2013; Tsai and Chung 2014). In *N. crassa*, the *plc-1*^{RIP} mutant showed reduced growth, aberrant hyphal morphology, hypersensitivity to low extracellular and elevated intracellular Ca^{2+} concentrations, and responded differently to the PLC inhibitor 3-nitrocoumarin (Gavric et al. 2007). However, investigating the *plc-1* knockout mutant, which had characteristics distinct from the *plc-1*^{RIP} mutant, showed that PLC-1 plays a role in hyphal tip development in *N. crassa* (Lew et al. 2015).

The $sPLA_2$ are low molecular weight, Ca^{2+}-dependent extracellular secretory proteins that hydrolyze the *sn*$_2$ ester linkage of glycerophospholipids and produce two signaling molecules, including free fatty acids (FFAs) and 1-acyl-lysophospholipid (1-acyl-LPL), which regulate a variety of biological processes, including atherosclerosis, eicosanoid biosynthesis, host defense, and inflammation in various organisms (Murakami and Kudo 2004; Boilard et al. 2010; Dennis et al. 2011). This class of proteins features a highly conserved region, including the His-Asp dyad sequence and a number of unique disulphide-bonded Cys residues for its stability (Murakami and Kudo 2004; Schaloske and Dennis 2006; Nakahama et al. 2010). The first characterised $sPLA_2$ in fungi was a dual localization protein that plays a role in nutritional limitation in the symbiotic fungus *T. borchii* (Soragni et al. 2001; Cavazzini et al. 2013). In *A. oryzae*, in response to carbon deprivation, oxidative stress, heat shock, and during or after conidiation, the sPlaA was significantly upregulated, whereas the sPlaB expression was barely detectable in any of these conditions (Nakahama et al. 2010). In *N. crassa*, the $sPLA_2$ protein encoded by NCU06650 is categorised as a member of the Ca^{2+} and/or CaM binding proteins, and contains a potential CaM binding site possessing the amino acid sequence TCHALANVYYAAVREFGRTKGELQ (Borkovich et al. 2004; Barman and Tamuli 2017).

Ca^{2+} exchangers act as Ca^{2+} pumps, transporting extracellular Ca^{2+} into the intracellular Ca^{2+} stores, while also exchanging positive ions across the membranes (Zelter et al. 2004; Tamuli et al. 2013). All the Ca^{2+} exchangers have conserved Ca^{2+} exchanger domains that allow them to transfer Ca^{2+} across the intracellular membranes (Galagan et al. 2003; Borkovich et al. 2004; Zelter et al. 2004; Tamuli et al. 2013). In *N. crassa*, CPE-1, a low-affinity Ca^{2+}/H^+ exchanger involved in maintaining intracellular Ca^{2+}, was found significantly different from the *S. cerevisiae* and *M. grisea* homologs in a phylogenetic analysis (Zelter et al. 2004).

Previous studies showed *N. crassa* homologs of the PLC-1, CPE-1, and $sPLA_2$ play a role in Ca^{2+} homeostasis, carotenoid accumulation, conidiation, and stress survival (Barman and Tamuli 2015,

2017). In *N. crassa*, *plc-1* genetically interacts with *cpe-1* and *splA*$_2$ during asexual and sexual development (Barman and Tamuli 2017). Further, *N. crassa* displays circadian rhythm in the vegetative developmental program that produces asexual spores (Nakashima 1981; Bell-Pederson et al. 1992; Aronson et al. 1994). Several other reports also suggested that Ca^{2+} signaling can influence circadian oscillators through multiple pathways. Inhibition of the inositol 1, 4, 5-trisphosphate receptor (IP_3R) or the endoplasmic reticulum Ca^{2+}-ATPase (SERCA) lengthens the period, suggesting that Ca^{2+} plays a role in modifying the molecular circadian clock in the liver of rats (Báez-Ruiz and Diaz-Munoz 2011). In *N. crassa*, increased $[Ca^{2+}]_c$ levels caused by the loss of NCA-2 resulted in shortened circadian period length (Wang et al. 2021). Furthermore, the alkaline pH and Ca^{2+} signaling pathways show crosstalk in *N. crassa* (Cupertino et al. 2012) and aberration of Ca^{2+} homeostasis in the ER causes protein unfolding, leading to ER stress (Ma and Hendershot 2004; Bravo et al. 2012; Hetz 2012). In the filamentous fungus *T. reesei*, PLC-1 mediated Ca^{2+} signaling pathway plays a crucial role in the regulation of cellulase overexpression under cellulase-inducing conditions (Chen et al. 2021). Recently, *N. crassa* is gaining prominence as a model organism to understand the physiology of lignocellulose degradation in fungi (Fan et al. 2015). However, there is no information on the role of PLC-1, CPE-1, and $sPLA_2$ in lignocellulose degradation, although phospholipases are associated with membrane remodelling. Therefore, in this study, I investigated the role of the *plc-1*, *cpe-1*, and *splA*$_2$ genes in regulating the circadian clock, stress responses, cellulose degradation, and other related cell functions in *N. crassa*. I also investigated the genetic interactions of the *plc-1*, *cpe-1*, and *splA*$_2$ genes in regulating these cell functions in *N. crassa*.

Chapter 2: Materials and Methods

This chapter describes the experimental procedures, chemicals, and reagents used in this study. Growth, maintenance, and crossing of *N. crassa* strains were carried out essentially as described previously (Westergaard and Mitchell 1947; Davis and de Serres 1970). The *N. crassa* wild type (WT) and the knockout mutant strains used in this work were obtained from the Fungal Genetics Stock Centre (FGSC, Manhattan, KS), and the remaining *N. crassa* strains were generated in our laboratory. Chemicals and reagents were purchased from reputed manufacturers and used after autoclaving or filter sterilising as needed. Cloning, polymerase chain reaction (PCR), reverse transcriptase PCR, quantitative real time PCR (qRT-PCR), and other molecular biology experiments were carried out according to the standard protocols (Sambrook and Russel 2001) or manufacturer's instructions. Microsoft Excel, SigmaPlot®, and Origin software tools were used to perform all statistical analysis on the experimental data and to generate the graphs.

Chapter 3: The cell functions of the Ca^{2+} signaling genes *phospholipase C-1*, Ca^{2+}/H^{+} *exchanger-1*, and *secretory phospholipase* A_2 in *N. crassa*

This chapter describes the cell functions of *plc-1*, *cpe-1*, and *splA*$_2$ in the circadian clock, stress responses, and cellulose degradation in *N. crassa*. In this chapter, I also studied the phenotypes of the double mutants of *plc-1*, *cpe-1*, and *splA*$_2$ to understand their genetic interactions in regulating these cell functions in *N. crassa*. I performed a circadian regulated conidiation assay at three different temperatures (20 °C, 25 °C, and 30 °C) to understand the role of *plc-1*, *cpe-1*, and *splA*$_2$ in maintaining circadian period length and temperature compensation in *N. crassa*. Deletion of PLC-1 resulted in an increased period length at 20 °C and 25 °C; however, the Δ*cpe-1* and Δ*splA*$_2$ mutants did not show a significant change in the period length at either of the temperatures. The Δ*plc-1*; Δ*cpe-1* and Δ*plc-1*; Δ*splA*$_2$ double mutants also showed period lengthening at 20 °C and 25 °C relative to the *ras-1*^{bd} strain; however, the clock phenotype is independent of the *cpe-1* and *splA*$_2$ interactions in *N. crassa*. I observed loss of temperature compensation, determined for 25 °C and 30 °C in the Δ*plc-1* mutant; whereas the Δ*plc-1*; Δ*cpe-1*, Δ*plc-1*; Δ*splA*$_2$, and Δ*cpe-1*; Δ*splA*$_2$ double knockouts showed no effect on temperature compensation. Under induced thermotolerance, the Δ*plc-1*, Δ*cpe-1*, Δ*splA*$_2$ single mutants, and the Δ*plc-1*; Δ*cpe-1* and Δ*plc-1*; Δ*splA*$_2$ double mutants showed reduced survival percentages compared to the WT. In uninduced thermotolerance, survival of the Δ*cpe-1* and Δ*splA*$_2$ was marginally higher than the WT, and no viable colony was observed in the Δ*plc-1*, Δ*plc-1*; Δ*cpe-1*, and Δ*plc-1*; Δ*splA*$_2$ mutants. In addition, the Δ*plc-1*, Δ*cpe-1*, Δ*splA*$_2$ single and their double mutants showed defects in the development of aerial hyphae at alkaline pH; however, normal growth was observed in acidic conditions. However, the Δ*plc-1*, Δ*cpe-1*, and Δ*splA*$_2$ single and double mutants were completely resistant to cell wall stress. I also observed a more than 50% reduction in the aerial hyphae height in the Δ*splA*$_2$, Δ*plc-1*; Δ*cpe-1*, and Δ*plc-1*; Δ*splA*$_2$ mutants in the presence of endoplasmic reticulum (ER) stress inducing agent, DTT. In addition, Δ*splA*$_2$ and Δ*cpe-1*; Δ*splA*$_2$ mutants showed an increase in cellulolytic activity, protein secretion, and glucose accumulation in the culture supernatants. On the other hand, the Δ*plc-1*, Δ*cpe-1*, Δ*plc-1*; Δ*cpe-1*, and Δ*plc-1*; Δ*splA*$_2$ mutants were unable to grow efficiently on microcrystalline cellulose (Avicel) containing media. Because, the lignocellulose degradation and ER stress pathways are interconnected in *N. crassa* (Fan et al. 2015), I investigated the ability of the Δ*splA*$_2$ mutant to utilize microcrystalline cellulose in the ER stress inducing condition. The Δ*splA*$_2$ mutant was unable to grow on microcrystalline cellulose during ER stress in *N. crassa*. However, WT and the Δ*plc-1*, Δ*cpe-1*, and Δ*splA*$_2$ single and double mutants showed no significant differences in growth rate and morphology when cultured on medium containing sucrose, glucose, xylose, glycerol, and sodium acetate as the carbon source. Complementation studies using the homokaryotic transformants expressing the *plc-1*, *cpe-1*, and *splA*$_2$ transgenes rescued the phenotype of

the Δ*plc-1*, Δ*cpe-1*, and Δ*splA*$_2$ mutants during heat shock, pH stress, ER stress, and cellulose degradation in *N. crassa*. Therefore, this study revealed that *plc-1*, *cpe-1*, and *splA*$_2$ genes genetically interact to regulate multiple cellular pathways in *N. crassa*.

Chapter 4: Expression analysis of genes involved in the circadian clock, stress responses, and cellulose degradation in the *N. crassa* Δ*plc-1*, Δ*cpe-1*, and Δ*splA*$_2$ mutants

The Ca^{2+} signaling machinery works in tandem with other signaling pathways to regulate cellular processes, resulting in signaling pathways to crosstalk (Sanders et al. 2002; Berridge et al. 2003). Therefore, to understand how PLC-1, CPE-1, and $sPLA_2$ interact and crosstalk with these signaling pathways in *N. crassa*, I performed qRT-PCR to determine the fold change in expression of some of the important cellular genes involved in circadian clock regulation, stress responses, and utilization of cellulose in the Δ*plc-1*, Δ*cpe-1*, Δ*splA*$_2$ single and double mutants.

In *N. crassa*, the core circadian clock consists of two major genes, *frequency* (*frq*) and *white collars* (*wc-1* and *wc-2*; Aronson et al. 1994; Crosthwaite et al. 1997). The altered period lengths observed in the Δ*plc-1*, Δ*plc-1*; Δ*cpe-1*, and Δ*plc-1*; Δ*splA*$_2$ mutants were related to the transcript levels of *frq* and *wc-1*. The Δ*plc-1*, Δ*plc-1*; Δ*cpe-1*, and Δ*plc-1*; Δ*splA*$_2$ mutants expressed considerably higher *frq* and *wc-1* at 20 °C than the *ras-1*^{bd}. However, the transcript levels of *frq* and *wc-1* were only marginally higher in the Δ*plc-1*, Δ*plc-1*; Δ*cpe-1*, and Δ*plc-1*; Δ*splA*$_2$ mutants compared to the *ras-1*^{bd} at 25 °C. Furthermore, there was no change in the *frq* and *wc-1* transcript levels in the Δ*cpe-1*, Δ*splA*$_2$, and Δ*cpe-1*; Δ*splA*$_2$ mutants. When *N. crassa* cells are subjected to sub-lethal heat shock temperatures, the heat shock proteins are induced (Kapoor et al. 1995; Yang and Borkovich 1999). In *N. crassa*, the heat shock response (HSR) is demonstrated by the abundant production of HSP60, HSP80, and HSP90; and HSP80 is a member of the HSP90 family of HSPs (Borkovich et al. 2004). The increased sensitivity of the Δ*plc-1*, Δ*cpe-1*, Δ*splA*$_2$ single mutants, as well as the Δ*plc-1*; Δ*cpe-1* and Δ*plc-1*; Δ*splA*$_2$ double mutants to heat shock, was attributed to lower expression of *hsp60* and *hsp80* compared to the WT. However, the transcript levels of *hsp60* and *hsp80* in the Δ*cpe-1*; Δ*splA*$_2$ were similar to the WT. Moreover, the expression of *plc-1* was considerably increased, whereas only a modest upregulation of *cpe-1* and *splA*$_2$ was observed following heat shock in the WT. The transcription factor PacC/Rim101, is the major regulator of the pH signaling pathway in *A. nidulans* and *S. cerevisiae* (Tilburn et al. 1995; Peñalva and Arst 2004). In *N. crassa*, the *pacC* ortholog, *pac-3* is highly upregulated in the alkaline condition compared to the ambient pH 5.8 (Cupertino et al. 2012). In alkaline stress, Δ*plc-1*, Δ*cpe-1*, Δ*splA*$_2$ single mutants and their double mutants Δ*plc-1*; Δ*cpe-1*, Δ*plc-1*; Δ*splA*$_2$, and Δ*cpe-1*; Δ*splA*$_2$ showed reduced expression of *pac-3*, which corresponds to the increased sensitivity of the mutants to alkaline stress. I also observed significant upregulation of *plc-1*, *cpe-1*, and *splA*$_2$ during the alkaline condition. However, at physiological and acidic pH, *pac-3* transcript levels remain basal in all

the mutants, indicating that Pac-3 has no effect in these pH conditions, which is consistent with the phenotypes of the *N. crassa* strains. In *N. crassa*, the expression of two UPR marker genes, *grp-78* and *pdi-1*, is used to assess the impact of ER stress (Bravo et al. 2012; Fan et al. 2015). I observed reduced expression of *grp-78* and *pdi-1* in the Δ*splA*$_2$, Δ*plc-1*; Δ*cpe-1*, and Δ*plc-1*; Δ*splA*$_2$ mutants in the presence of ER stress inducing agent, DTT. In addition, I observed no change in the transcript levels of *grp-78* and *pdi-1* in the Δ*plc-1*, Δ*cpe-1*, and Δ*cpe-1*; Δ*splA*$_2$ mutant strains. Moreover, ER stress induces the expression of *splA*$_2$ in *N. crassa*. Furthermore, the Δ*splA*$_2$ and Δ*cpe-1*; Δ*splA*$_2$ mutants showed increased expression of the major cellulolytic genes, *cbh-1*, *cbh-2*, and *endo-2*, which is correlated with the enhanced cellulose degradation ability of these mutants. On the other hand, I observed significant downregulation of the *cbh-1*, *cbh-2*, and *endo-2* genes in the Δ*plc-1*, Δ*cpe-1*, Δ*plc-1*; Δ*cpe-1*, and Δ*plc-1*; Δ*splA*$_2$ mutants. Moreover, the presence of putative binding sites for carbon source responsive elements, circadian control factors, ER stress-response elements, the fungal basic leucine zipper family, pH responsive regulators, and yeast stress response elements in the promoter regions of the *plc-1*, *cpe-1*, and *splA*$_2$ genes further supported that PLC-1, CPE-1, and sPLA$_2$ are critical for circadian clock regulation, stress survival, and cellulose utilization in *N. crassa*. Thus, PLC-1, CPE-1, and sPLA$_2$ interact with different molecules to regulate the circadian clock, stress responses, and cellulose degradation in *N. crassa*.

Chapter 5: The *splA*$_2$ gene interacts with the transcription factor CRE-1 to regulate growth and cellulose degradation in *N. crassa*

In this chapter, I investigated the interaction of *splA*$_2$ with the carbon catabolite repressor, CRE-1 to understand the cellulose degradation pathway in *N. crassa*. It was established that the zinc finger transcription factor CreA/CRE-1, a homolog of *S. cerevisiae* Mig1, regulates the utilization of alternate carbon sources in filamentous ascomycete fungi (Sun and Glass 2011). In *N. crassa*, the deletion of *cre-1* results in increased cellulolytic activity and increased expression of cellulolytic genes during growth on microcrystalline cellulose (Sun and Glass 2011). When grown on 2% microcrystalline cellulose as the sole carbon source, the Δ*cre-1* strain consumed microcrystalline cellulose faster than the WT, secreted 30% more extracellular protein, and showed 50% higher endoglucanase activity (Sun and Glass 2011). Further, the Δ*cre-1* mutant showed hypersensitivity to ER stress (Fan et al. 2015). In this study, I found that Δ*splA*$_2$ knockout mutants have similar phenotype like the Δ*cre-1* mutant during growth on microcrystalline cellulose and ER stress. Therefore, I generated the Δ*cre-1*; Δ*splA*$_2$ double mutant by crossing the single mutant strains of opposite mating type and phenotypes of the double mutant were studied to determine the genetic interaction of the *splA*$_2$ and *cre-1* genes in *N. crassa*.

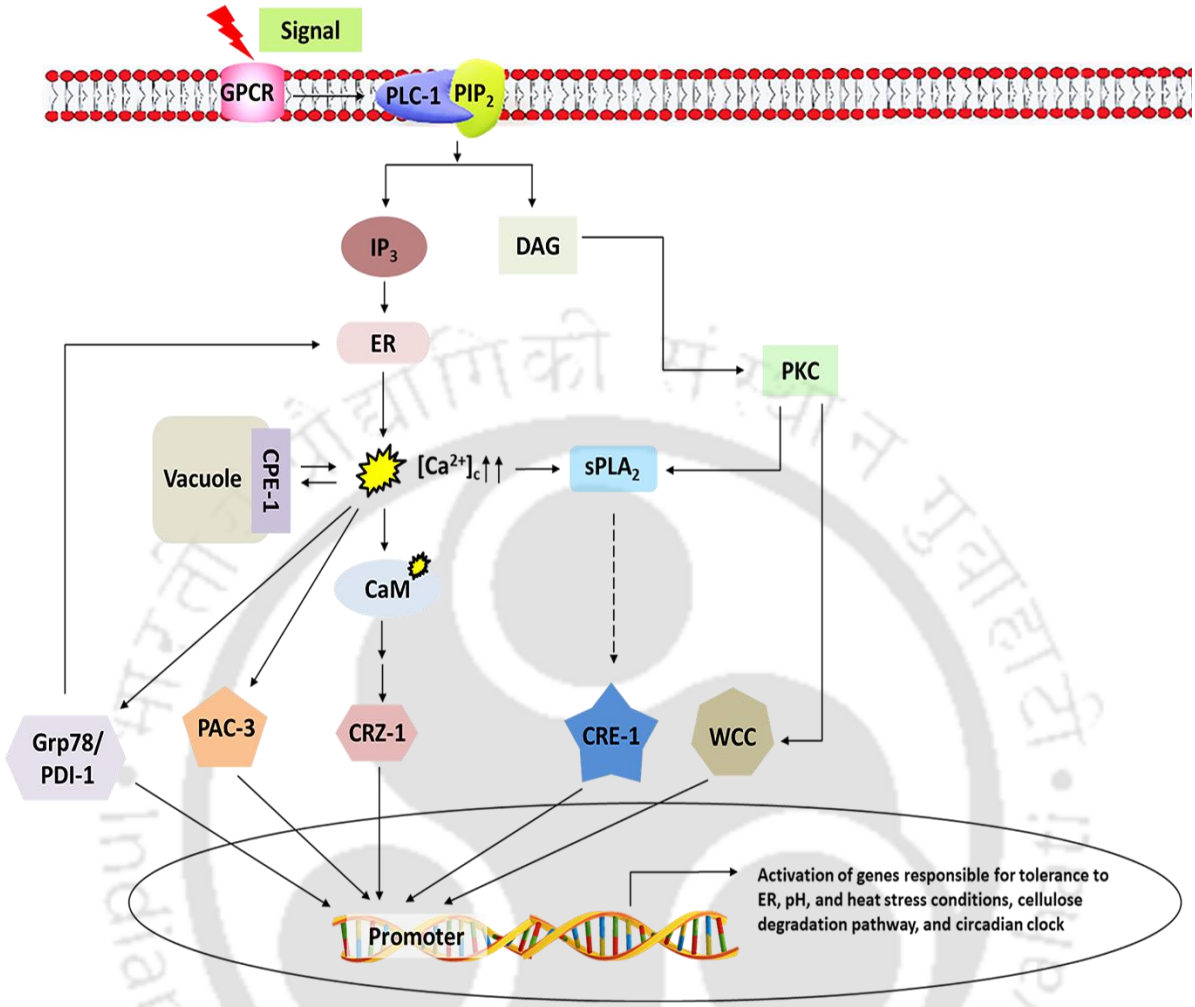

Figure 1: Possible mechanism of the PLC-1, CPE-1, and sPLA$_2$ mediated pathways in circadian clock, stress survival, and cellulose degradation in *N. crassa*. The *plc-1*, *cpe-1*, and *splA$_2$* genes act in coordination to maintain the intracellular Ca^{2+} homeostasis. Aberration of Ca^{2+} homeostasis triggers a number of morphological and physiological changes in *N. crassa*. GPCR: G-Protein coupled receptor; PLC-1: phospholipase C-1; PIP_2: phosphatidylinositol 4, 5-bisphosphate; IP_3: inositol-1, 4, 5-trisphosphate; DAG: diacylglycerol; PKC: protein kinase C; CPE-1: Ca^{2+}/H^+ exchanger; sPLA$_2$: secretory phospholipase A_2; CaM: calmodulin; PDI-1: protein disulphide-isomerase; PAC-3: pH response transcription factor; CRZ-1: calcineurin responsive zinc finger-1; CRE-1: carbon catabolite repressor; WCC: white collar complex.

The Δ*cre-1*; Δ*splA$_2$* double mutant synthetically showed numerous phenotypes such as colonial growth with reduced hyphal branching, a slower growth rate, reduced aerial hyphae with decreased

conidiation, and uneven septation, suggesting that *splA*$_2$ and *cre-1* interact to regulate growth in *N. crassa*. Furthermore, the Δ*cre-1*; Δ*splA*$_2$ double mutant was unable to grow during cell wall and ER stress, indicating their interaction is also required for cell wall integrity and the ER response pathway. Our main aim to generate the Δ*cre-1*; Δ*splA*$_2$ double mutant was to assess its ability to degrade microcrystalline cellulose. Compared to the WT and the parental single mutants, the Δ*cre-1*; Δ*splA*$_2$ double mutant exhibited enhanced cellulose degradation, as well as increased protein secretion and endoglucanase activity. But, unlike the Δ*splA*$_2$ and Δ*cre-1* single mutants, the Δ*cre-1*; Δ*splA*$_2$ double mutant did not form mycelial aggregates and remained as isolated colonies. Expression studies revealed significantly higher expression of *cbh-1* and *cbh-2* in the Δ*cre-1*; Δ*splA*$_2$ double mutant compared to the Δ*splA*$_2$ and Δ*cre-1* single mutants. Further, I checked the transcript levels of *splA*$_2$ in the Δ*cre-1* mutants. The expression of *splA*$_2$ was increased in the Δ*cre-1* mutant, implying sPLA$_2$ and CRE-1 might show protein-protein interaction. Therefore, this study suggested that *splA*$_2$ genetically interacts with *cre-1* to regulate vegetative growth and cellulose degradation in *N. crassa*.

I also predicted the three-dimensional protein structures of sPLA$_2$ and CRE-1 by protein structure modelling. The three-dimensional structures of sPLA$_2$ and CRE-1 were modelled based on threading and ab-initio methods by using I-TASSER. The modelled structures were then subjected to Molecular Dynamics Simulation, which significantly improved the stereochemical quality of the structures. Also, based on the RMSD plot obtained as a result of MD simulation studies, the modelled structures were found to be stable in the simulated environment, which makes the structures reliable for further structural studies. The I-TASSER modelled MD refined structures of sPLA$_2$ and CRE-1 obtained in this study were found to be significantly better than the existing AlphaFold predicted structures.

Chapter 6: Conclusions and Future Perspectives

This chapter summarizes the conclusions and future prospects of the current research work. In summary, this study showed that PLC-1, CPE-1, and sPLA$_2$ synthetically regulate the circadian clock, the acquisition of thermotolerance induced by heat shock, responses to alkaline pH and ER stress conditions, and utilization of cellulose and other alternate carbon sources in *N. crassa*. Further, differential expression of some key genes involved in circadian clock regulation, stress responses, and the cellulose degradation pathway in the Δ*plc-1*, Δ*cpe-1*, and Δ*splA*$_2$ mutants, suggested that PLC-1, CPE-1, and sPLA$_2$ crosstalk with these signaling pathways in *N. crassa*. In addition, *splA*$_2$ genetically interacted with *cre-1* to regulate vegetative growth and cellulose degradation in *N. crassa*.

Future direction of this research will be to establish additional molecular information about the pathways involving PLC-1, CPE-1, and sPLA$_2$ to understand the mechanism of stress tolerance and cellulose degradation in *N. crassa*. In addition, an insight into the structure-function relationship of *N.*

crassa PLC-1, CPE-1, and $sPLA_2$, specifically the low molecular weight $sPLA_2$, will reveal the mechanistic details. Therefore, it is anticipated that more in-depth knowledge about the mechanism of PLC-1, CPE-1, and $sPLA_2$ will be available in the near future, and might be useful for the application in degradation of cellulose.

Chapter 1: An Introduction to *Neurospora crassa* Biology and Calcium Signaling

1.1 The biology of *Neurospora crassa*, a model filamentous fungus

Neurospora, which means "nerve spores" because of the nerve-like stripes in its sexual spores, is a filamentous fungus that has been used as a model organism for decades to study eukaryotic cell biology, genetics, biochemistry, and molecular biology (Perkins 1992; Davis 2000; Davis and Perkins 2002; Galagan et al. 2003). *N. crassa*, a member of the phylum Ascomycota, was first identified as the causative organism of orange bread mould infestations in French bakeries, and was described as *Oidium aurantiacum* (Payen 1843) and *Penicillium sitophilum* (Montagne 1843). In the mid-1920s, Shear and Dodge described *N. crassa* as a heterothallic fungus with two mating types, *A* and *a* with eight asci, and in the mid-1930s, Bernard Lodge and Carl Lindegren established Mendelian inheritance in the individual asci (Shear and Dodge 1927; Dodge 1939; Perkins 1992). Furthermore, the genetic map of *N. crassa*'s sex chromosome was the first fungal chromosomal map (Lindegren 1936). Using *N. crassa*, Beadle and Tatum discovered that a gene's primary function is to control the synthesis of a specific enzyme, leading to the famous "one gene, one enzyme" hypothesis, for which they were awarded the Nobel Prize in Physiology or Medicine in 1958 (Beadle and Tatum 1941). And the whole genome sequencing project for *N. crassa* was completed in 2003 (Galagan et al. 2003). Thus, *N. crassa* established itself as a valuable eukaryotic model organism that has immensely contributed to our understanding of cellular differentiation and development, DNA methylation and repair, genome defense mechanisms, mitochondrial transport, and post-transcriptional gene silencing, among other biological processes (Davis 2000; Davis and Perkins 2002; Galagan et al. 2003). *N. crassa* is a multicellular, heterothallic, haploid organism with a 43 Mb completely sequenced genome, including 10,082 protein-coding genes divided into seven linkage groups (LG I-VII) with sizes ranging from 4 to 10.3 Mb each (Davis and de Serres 1970; Davis and Perkins 2002; Galagan et al. 2003). *N. crassa* is a heterotroph, and it utilizes a wide range of carbon and nitrogen sources, simple salts, a few trace elements, and a single vitamin, biotin (Davis and de Serres 1970; Perkins and Davis 2000). *N. crassa* possesses a diverse set of genome defense mechanisms, including a reversible post transcriptional gene silencing (PTGS) mechanism known as 'quelling' (Romano and Macino 1992) that occurs during the vegetative phase, a fungal specific transcriptional gene silencing (TGS) mechanism known as 'repeat-induced point mutation' (RIP; Cambareri et al. 1989) that occurs after fertilisation and before karyogamy, and another PTGS mechanism known as 'meiotic silencing' that occurs during the sexual phase (Shiu et al. 2001).

1.2 The life cycle of *N. crassa*

In comparison to unicellular yeasts, the multicellular fungus *N. crassa* has a more complex life cycle that includes both asexual (vegetative) and sexual phases (Raju 1992; Springer 1993). *N. crassa* enters the asexual phase in a nutrient-rich environment, producing branching multinucleated filaments or

vegetative hyphae that run parallel to the solid medium's surface (Springer 1993). The vegetative hyphae are divided into sections by incomplete internal cross walls or septa, which allow cellular organelles such as mitochondria and other inclusion bodies to travel between the cells (Springer 1993). The multicellular mycelium is formed by continued hyphal development and branching (Springer 1993). Specified aerial hyphae emerge from the mycelium in the absence of nutrients or in the presence of an air-water contact, giving rise to conidiophores, which then generate uninucleated asexual spores known as microconidia or multinucleated macroconidia (Springer 1993). Macroconidia are employed as a vegetative culture inoculum as well as a fertilising male parent in sexual crosses. Submerged cultures of *N. crassa* generally retain vegetative hyphae without conidiation; however, environmental triggers such as nitrogen or carbon limitation, as well as exposure to high temperatures, can cause conidiophores or conidia to develop (Cortat and Turian 1974; That and Turian 1978; Plesofsky-Vig et al. 1983; Guignard et al. 1984).

N. crassa is a heterothallic filamentous fungus with two non-switching mating types, *mat A* and *mat a*, defined by alternate DNA sequences known as idiomorphs at a single mating type locus. Nitrogen limitation, light, and cold temperatures trigger the sexual cycle, resulting in the formation of female reproductive structures known as protoperithecia (Raju 1992). A protoperithecium derived specialised hyphae (trichogyne) grows chemotropically towards a male cell of the opposite mating type, which is often a hyphal fragment, macroconidium, or microconidium. Following the fusion of the trichogyne with the conidium, the male nucleus is transported to the protoperithecium, where it begins the formation of the multicellular sexual apparatus known as the perithecium (matured protoperithecium). The male and female nuclei do not fuse right away, but rather reside as a dikaryon in ascogenous hyphae, which are specialised structures. At the apex of a specialised hook-shaped structure called the crozier, the paired male and female nuclei undergo a series of synchronised mitotic divisions. During karyogamy, the nuclei of the opposing mating type combine to produce a diploid zygote, which then undergoes two meiotic divisions and a post meiotic mitosis, generating an octad of eight ascospores, which are packed in a linear order in the ascus. The ascospores, once mature, are ejected in the direction of blue light through a beak (ostiole) at the perithecium's tip, and the discharged ascospores eventually germinate and form their own vegetative hyphae in the presence of adequate nutrients (Fig. 1.1; Raju 1980, 1992; Springer 1993; Kim et al. 2012).

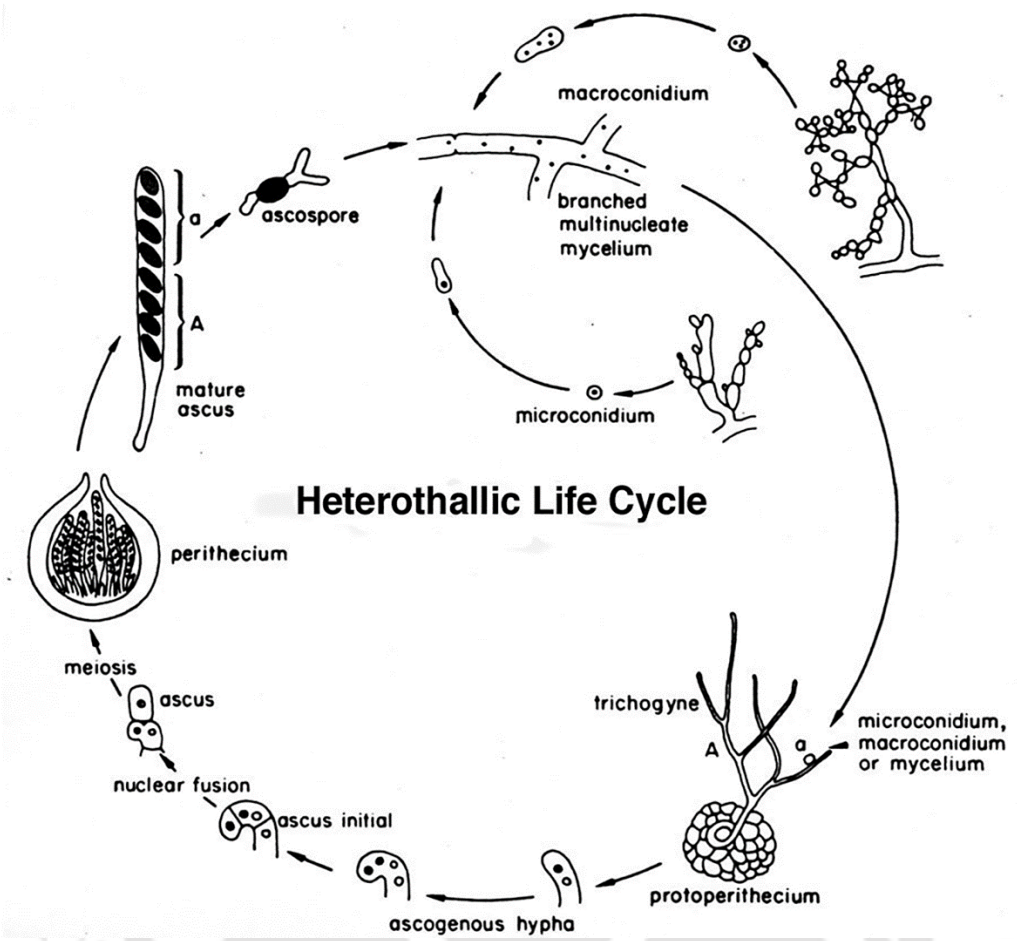

Figure 1.1: The life cycle of *N. crassa*. During the asexual cycle, the multinucleated and branching vegetative mycelium grows into aerial hyphae and generates asexual spores, either multinucleated macroconidium or uninucleated microconidium, which germinate to form new mycelium. The sexual cycle begins with the formation of the protoperithecium, a female reproductive structure. It is fertilised by a male parent's conidium or mycelium of the opposite mating type and matures into perithecium, which goes through a process of mitosis and meiosis to generate eight linearly organised ascospores within an ascus. The mature pigmented multinucleate ascospores grow into new hyphae and form the multicellular mycelium to complete the asexual cycle, or operate as a male or female parents to initiate another sexual cycle after being released. Fig. is adapted from the FGSC http://www.fgsc.net/Neurospora/sectionB2.htm).

1.3 The versatility and universality of calcium

Cells must signal for adaptation to changing environments. Signaling requires the use of messengers whose concentration changes across time and space (Clapham 2007). The calcium ion (Ca^{2+}) has evolved as a second messenger that dominates cell signaling (Clapham 2007). Ca^{2+} is a ubiquitous second messenger that regulates a wide range of cellular activities and adaptive responses (Berridge et

al. 1998, 2000). Ca^{2+} is a versatile signaling molecule because it allows a cell to accurately alter the cellular amounts of free and sequestered Ca^{2+} both in time and space (Campbell 1983; Berridge et al. 1988, 2000; Jaiswal 2001). Only Ca^{2+} has attained such flexibility in the environment, a critical property that is lacking among various other inorganic ions such as H^+, Na^+, K^+, Mg^{2+}, Ba^{2+}, and Zn^{2+} (Jaiswal 2001). The primordial ocean, where some of the first living species evolved, was enriched with ions from the earth's crust, such as Na^+, K^+, Cl^-, Ca^{2+}, and Mg^{2+} (Verkhratsky and Parpura 2014). The Ca^{2+} concentrations in the primordial ocean were possibly very low, maybe in the 100 nM range (Kazmierczak et al. 2013); therefore, the very first cells were expected to contain very little Ca^{2+} in their cytoplasm. Indeed, certain primitive species, such as cyanobacteria, have a low Ca^{2+} need and are alkalophilic (Gerloff and Fishbeck 1969; Brock 1973; Kazmierczak et al. 2013). As the earth's temperature dropped gradually, numerous chemical and biological interactions resulted in the increase of free extracellular Ca^{2+} ions in the environment (Jaiswal 2001). The increase of Ca^{2+} ions in the environment exerted a selection pressure, because low Ca^{2+} levels in the cytosol of primitive cells are required for the normal functioning of ATP and the utilization of DNA/RNA, both of which cannot tolerate high Ca^{2+} levels (Jaiswal 2001; Case et al. 2007; Williams 2007). Ca^{2+} causes phosphate precipitation, protein and nucleic acid aggregation, and lipid membrane disruption at concentrations greater than 10 μM (Jaiswal 2001; Case et al. 2007; Williams 2007). Each of these occurrences has a significant negative impact on the cell's ability to survive. As a result, it became critical for cells to hold Ca^{2+} in such a way that it was no longer toxic, resulting in the development of a Ca^{2+} homeostatic mechanism that kept cytosolic Ca^{2+} at a low level (Jaiswal 2001; Case et al. 2007; Verkhratsky and Parpura 2014). This might have been the driving force behind the evolution of Ca^{2+} pumps and internal Ca^{2+} storage, which allowed cells to maintain acceptable amounts of cytosolic free Ca^{2+} (Jaiswal 2001; Verkhratsky and Parpura 2014). Thus, the existence of numerous Ca^{2+} pumps and intracellular Ca^{2+} storage such as vacuoles, endoplasmic reticulum (ER), and mitochondria might have aided in the use of Ca^{2+} as a messenger molecule (Campbell 1988; Jaiswal 2001).

The flexibility of Ca^{2+} as a messenger molecule lies in its chemistry, which includes its molecular structure, binding strength, balance state, ionisation potential, and kinetic characteristics in biological processes (Jaiswal 2001). The Ca^{2+} ion has a high co-ordination number (6-8) that allows it to hold 4-12 oxygen atoms in its main co-ordination sphere (Swain and Amma 1989; Carugo et al. 1993; Jaiswal 2001). The Ca^{2+}-mediated protein-induced co-ordination shape is typically irregular due to its favourable ionic radius (100-120 pm) and electronic structure (Swain and Amma 1989; Carugo et al. 1993; Jaiswal 2001). In general, 6-7 oxygen atoms coordinate the Ca^{2+} ion in a pentagonal bipyramidal, monocapped trigonal, or split-vertex octahedral fashion (Fig. 1.2; Swain and Amma 1989). Unlike other divalent cations such as Zn^{2+} and Mg^{2+}, which have a higher affinity for nitrogen ligands, Ca^{2+} has the highest affinity for carboxylate oxygen, and interestingly, most proteins include carboxylate

oxygen containing acidic amino acids such as aspartic acid and glutamic acid (Ochiai 1991; Jaiswal 2001). Ca^{2+} that enters the cytoplasm through Ca^{2+} channels does not remain free and binds to a variety of Ca^{2+} binding proteins via a helix-loop-helix structural motif known as the EF-hand domain (Nakayama and Kretsinger 1994; Clapham 2007; Gifford et al. 2007). The Ca^{2+} binding loop between the two helices in the EF-hand domain contains 12 amino acids rich in acidic residues that provide negatively charged oxygen atoms for Ca^{2+} co-ordination (Fig. 1.3A) in a pentagonal bipyramidal geometry (Fig. 1.3B), which is the most preferable chemistry for Ca^{2+} co-ordination (Gifford et al. 2007). Due to its rapid rate of water exchange in metal aquo-complexes, Ca^{2+} may bind and dissociate from a protein 100 times quicker than Mg^{2+} at 25 °C (1×10^8 s^{-1} for Ca^{2+} and 7×10^5 s^{-1} for Mg^{2+}; Ochiai 1991; Jaiswal 2001; Williams 2007). Thus, the development of Ca^{2+} as a ubiquitous second messenger has been ascribed to all of these reasons.

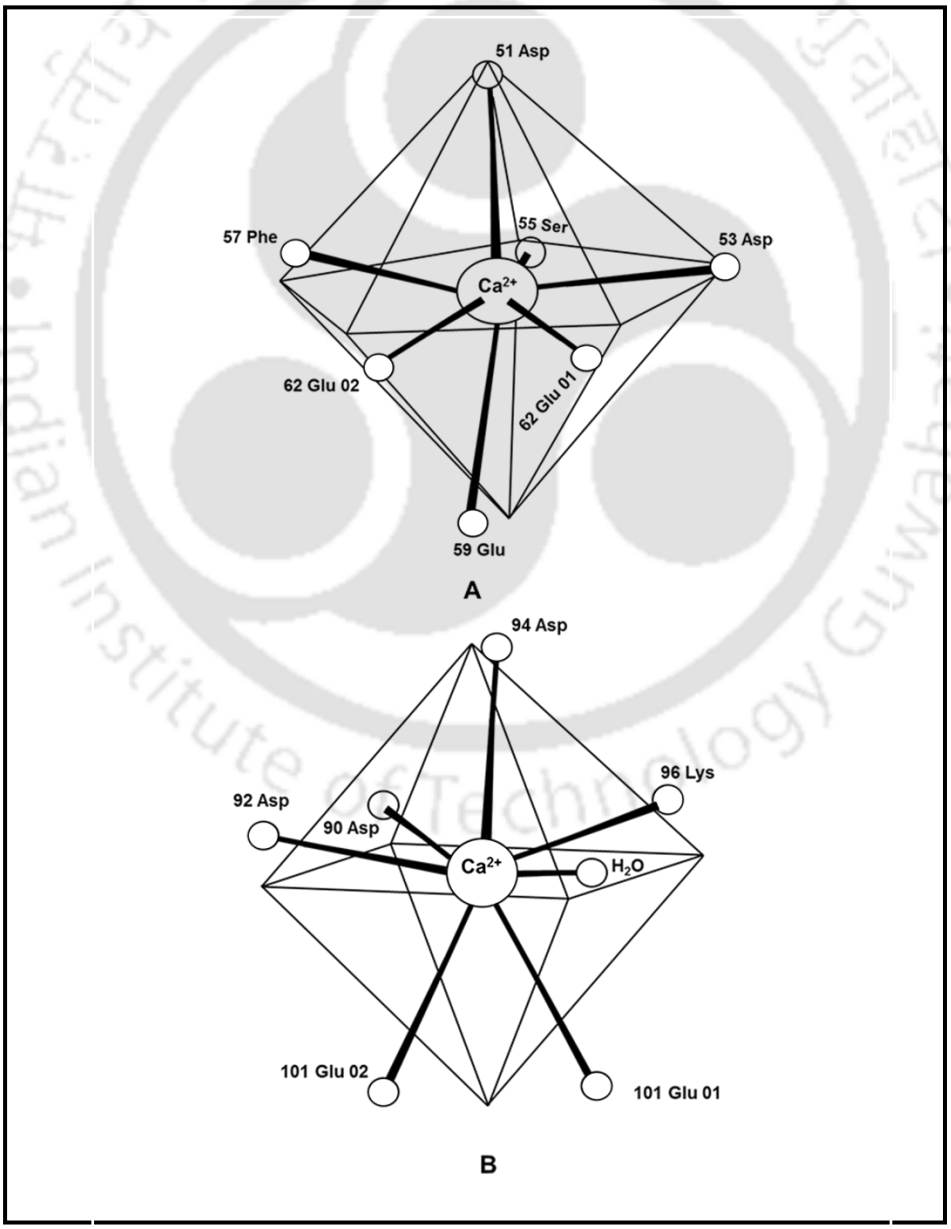

Figure 1.2: Co-ordination geometry of the Ca^{2+} ion in parvalbumin. Parvalbumin has six α helices, starting from A to F, and the loops between the helices C and D (CD site), E and F (EF site), bind to a Ca^{2+} ion (Kretsinger and Wasserman 1980). **A.** Pentagonal bipyramidal co-ordination geometry of Ca^{2+} in the CD site of parvalbumin. **B.** Monocapped trigonal prism or split-vertex octahedral co-ordination geometry of Ca^{2+} in the EF site of parvalbumin. Fig. is adapted from Swain and Amma (1989).

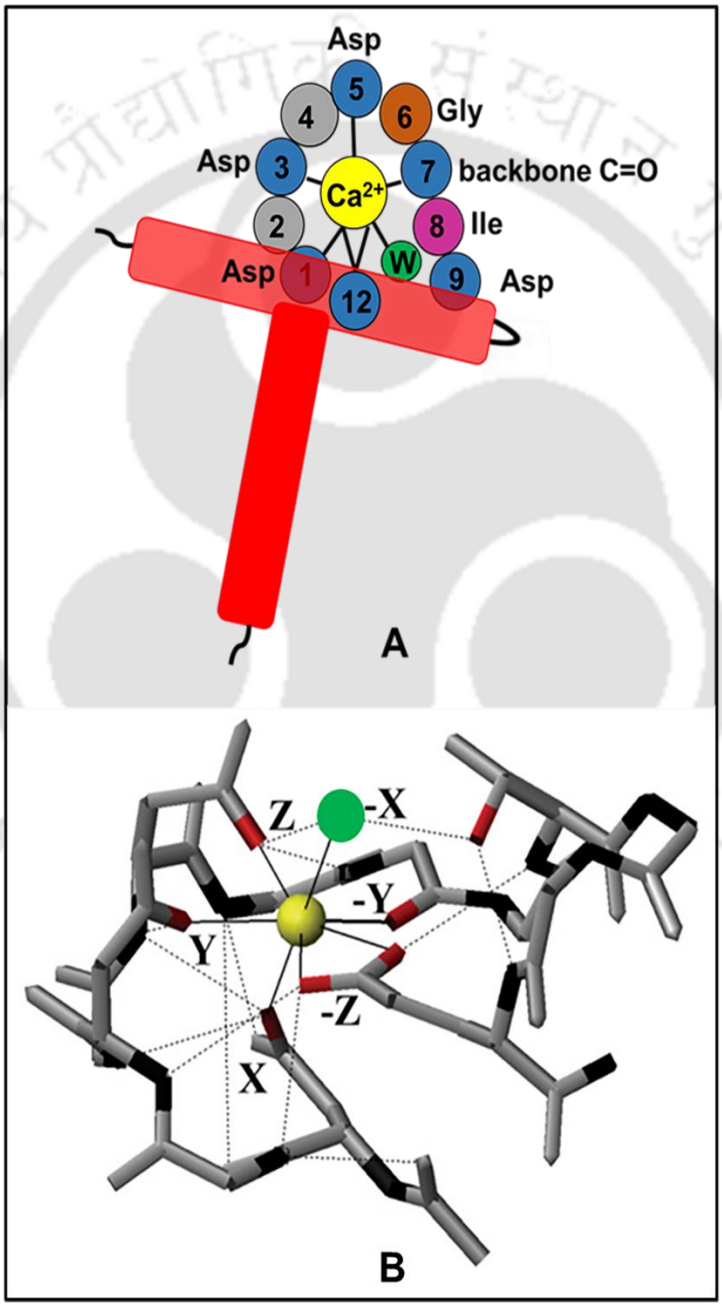

Figure 1.3: The co-ordination sphere of the Ca^{2+} binding loop in a typical EF-hand. A. A schematic diagram of the co-ordination sphere with the α-helices in red, the co-ordinating amino acid ligands in blue, and the water molecule (W) in green. Conserved glycine (Gly) residues that cause the bend in the loop are shown in brown. Purple represents the conserved hydrophobic amino acid residue that forms a short β-sheet in the paired EF-hand. **B.** Ca^{2+} co-ordination in the canonical EF-hand domain 1 (EF-1) of calmodulin (CaM) showing both pentagonal bipyramidal Ca^{2+} co-ordination (continuous lines) and hydrogen bonding (dotted lines). Fig. is adapted from Gifford et al. (2007).

1.4 The calcium signaling machinery in *N. crassa*

N. crassa has a wide range of environmental sensing pathways, making it an excellent model organism for signaling research. Signaling pathways mediated by G-protein-coupled receptors (GPCRs), histidine kinases (HKs), mitogen-activated protein kinases (MAPKs), and intracellular Ca^{2+} are various intracellular signaling pathways that operate in *N. crassa* (Fig. 1.4; Galagan et al. 2003). Ca^{2+} signaling is involved in a variety of biological activities in organisms (Berridge et al. 1998, 2000; Zelter et al. 2004; Clapham 2007). Binding of Ca^{2+} triggers changes in protein shape and charge, and thereby regulate the protein functions (Clapham 2007). *N. crassa*, like other organisms, is exposed to a variety of environmental stimuli, and its Ca^{2+} signaling machinery is critical for detecting these extracellular environmental changes and thriving in a variety of habitats (Li and Borkovich 2006; Tamuli et al. 2013; Kumar and Tamuli 2014). Ca^{2+} is primarily stored in intracellular stores such as vacuoles (> 90 percent of Ca^{2+} is sequestered in vacuoles), Golgi, endoplasmic reticulum (ER), plasma membrane vesicles, microsomes, and mitochondria in *N. crassa*; only a small amount (100 nM) of Ca^{2+} is present as free cytosolic Ca^{2+} ($[Ca^{2+}]_c$; Bowman et al. 2011). The Ca^{2+} pumps and transporters, as well as the cytoplasm's Ca^{2+} buffering capacity keep the resting level of $[Ca^{2+}]_c$ normally 100-350 nM in fungi (Halachmi and Eilam 1989; Iida et al. 1990; Miller et al. 1990), and 100-200 nM in plant and animal cells (Carafoli 1987; Gilroy et al. 1987; Johannes et al. 1991). Ca^{2+} signaling is initiated when $[Ca^{2+}]_c$ rises transiently to 500-1000 nM, either due to extracellular Ca^{2+} input or Ca^{2+} release from intracellular Ca^{2+} storage, in order to maintain the resting level of $[Ca^{2+}]_c$ (Bootman et al. 2001; Zelter et al. 2004).

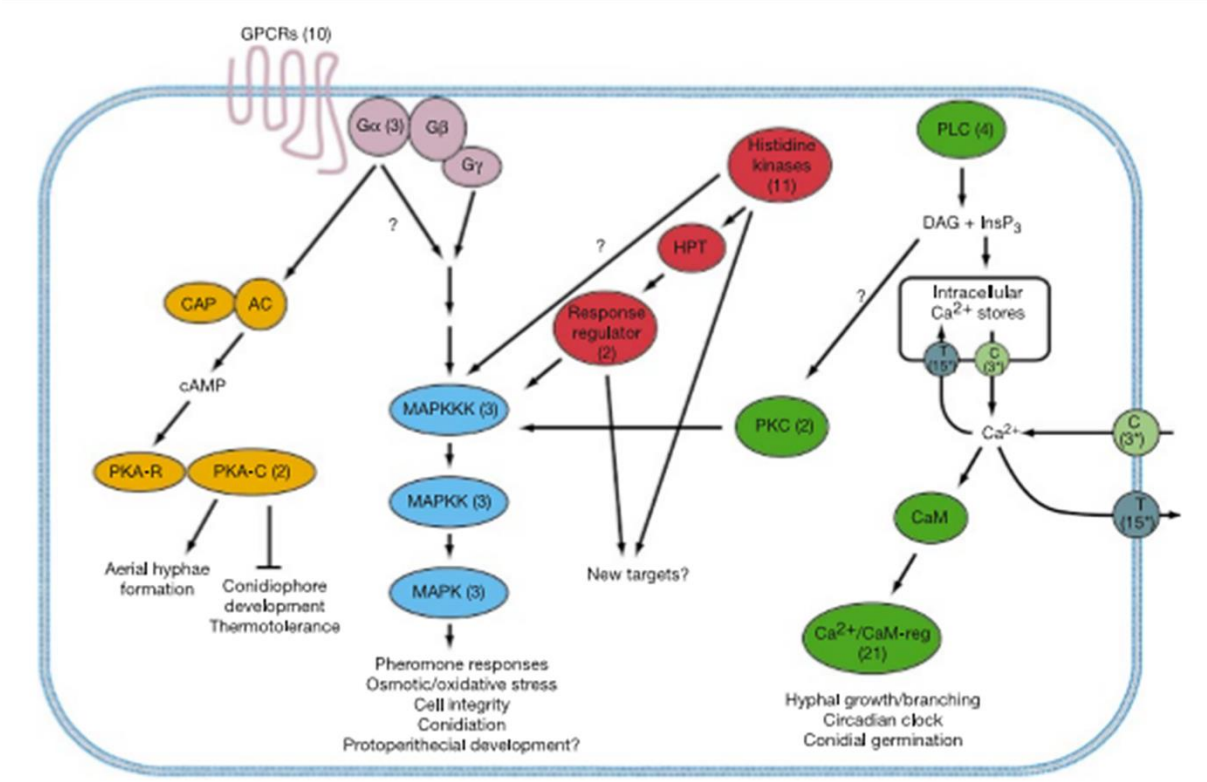

Figure 1.4: Overview of the major intracellular signaling pathways in *N. crassa*. AC: adenylyl cyclase; CaM: calmodulin; Ca^{2+}/CaM reg: calcium and calmodulin regulated protein; CAP: cyclase-associated protein; CT: Ca^{2+}-transport protein (P-type Ca^{2+}-ATPase, Ca^{2+}/H^{+} exchanger, Ca^{2+}/Na^{+} exchanger); CPC: Ca^{2+}-permeable channel protein; GPCR: G-protein-coupled receptor; Gα: G-protein α subunit; Gβ: G-protein β subunit; Gγ: G-protein γ subunit; HPT: histidine-containing phosphotransfer domain protein; MAPK: mitogen activated protein kinase; MAPKK: MAPK kinase; MAPKKK: MAPKK kinase; PKA-R: protein kinase A regulatory subunit; PKA-C: protein kinase A catalytic subunit; PLC: phospholipase C; PKC: protein kinase C. The intracellular second messenger molecules cAMP: 3′, 5′-cyclic adenosine monophosphate; DAG: diacylglycerol; IP_3: inositol-1, 4, 5-trisphosphate are also shown. Fig. is adapted from Galagan et al. (2003).

The *N. crassa* Ca^{2+} signaling machinery is complex (Fig. 1.5), possessing 48 Ca^{2+} signaling proteins involved in the pathway (Table 1.1; Borkovich et al. 2004; Tamuli et al. 2013). The *N. crassa* Ca^{2+} signaling machinery differs greatly from that of plant and animal cells, mainly in the second messenger systems linked with Ca^{2+} release from internal storage (Galagan et al. 2003; Borkovich et al. 2004; Zelter et al. 2004). The major components of the processes for Ca^{2+} release from internal stores in both plant and animal cells include inositol 1, 4, 5-trisphosphate (IP_3) receptors, ADP ribosyl cyclase, and ryanodine receptors, which are absent in *N. crassa* (Galagan et al. 2003; Borkovich et al. 2004). Furthermore, *N. crassa* lacks the extracellular Ca^{2+} sensing receptor proteins that have been identified

in animal cells for sensing changes in extracellular Ca^{2+} concentration (Brown et al. 1993; Galagan et al. 2003; Borkovich et al. 2004). *N. crassa* is unique in that it has both Ca^{2+}/Na^{+} and Ca^{2+}/H^{+} exchangers, whereas animals only have Ca^{2+}/Na^{+} exchangers and plants possess only Ca^{2+}/H^{+} exchangers (Borkovich et al. 2004). These striking variations imply that proteins or signaling components responsible for intracellular Ca^{2+} release are yet to be discovered in *N. crassa*. Our lab is focusing on understanding the Ca^{2+} signaling mechanism in *N. crassa*, which might be a promising target for antifungal drugs. The Ca^{2+} signaling proteins in *N. crassa* are described below.

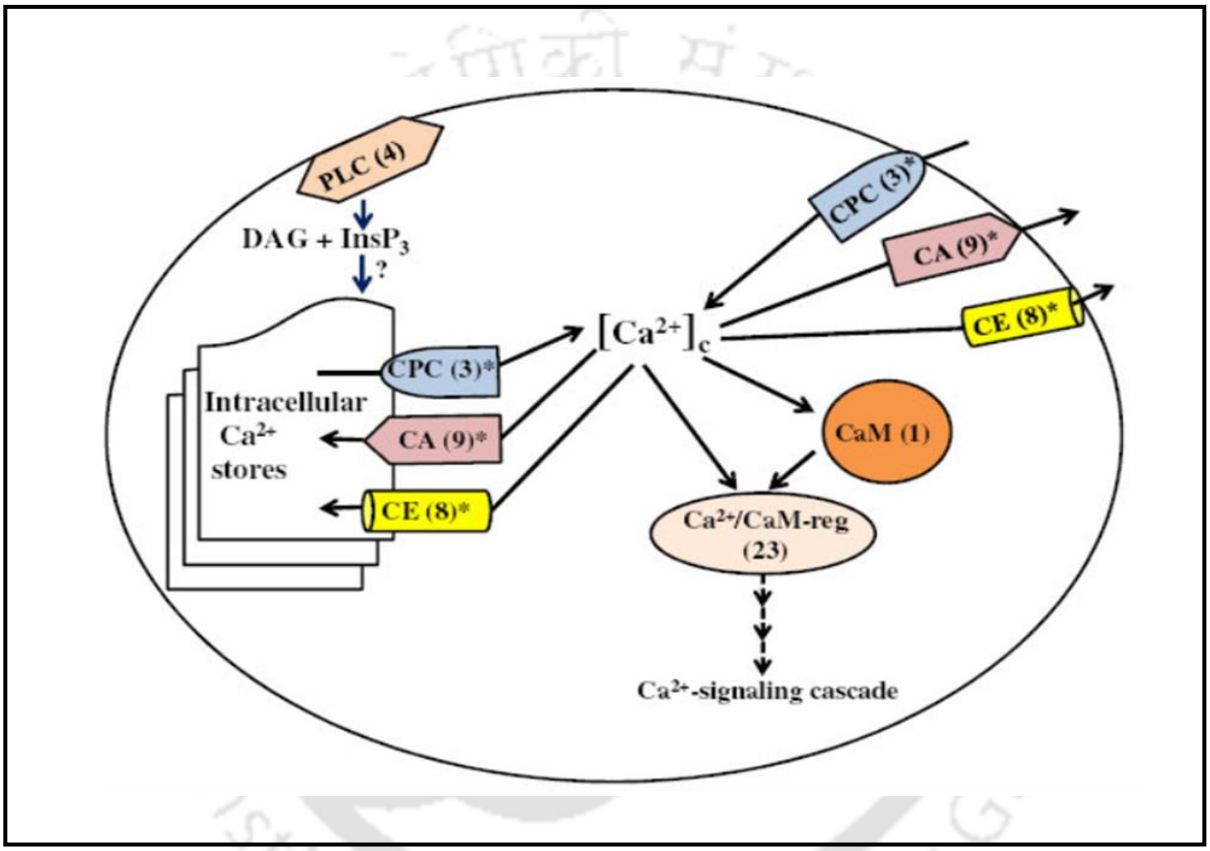

Figure 1.5: Overview of the calcium signaling system in *N. crassa*. The Ca^{2+} signaling proteins are CPC: Ca^{2+} permeable channel; CA: Ca^{2+}-and cation-ATPases; CT: Ca^{2+}/H^{+} and Ca^{2+}/Na^{+} exchanger; PLC: phospholipase C; CaM: Calmodulin; and Ca^{2+}/CaM-reg: Ca^{2+} and/or calmodulin binding proteins. The intracellular second messengers are IP_3: inositol 1,4,5-trisphosphate and DAG: 1,2-diacylglycerol. Numbers in parentheses indicate the number of identified genes in each class, and the asterisk indicates the location of the membrane localized proteins. Fig. is adapted from Tamuli et al. (2013).

1.4.1 Ca^{2+}-permeable channels: Ca^{2+}-permeable channels are the membrane-localized channel proteins that regulate passive Ca^{2+} passage across membranes into the cytoplasm (Bootman et al. 2001; Zelter et al. 2004). The NCU02762, NCU06703, and NCU11680 genes in *N. crassa* encode three different Ca^{2+}-permeable channel proteins, classified as group I, II, and III, respectively (Zelter et

al. 2004). The NCU06703 gene encodes the mating-induced death-1 (MID-1) protein, a stretch-triggered mechanosensitive Ca^{2+}-permeable channel that plays a crucial role in regulating ion transport via Ca^{2+} homeostasis (Lew et al. 2008).

1.4.2 Ca^{2+} and cation-ATPases: Ca^{2+} and cation-ATPases are membrane-localized ATP-driven proteins that regulate Ca^{2+} efflux across biological membranes (Hao et al. 1994; Moller et al. 1996). *N. crassa* possesses nine ATPases, seven of which are Ca^{2+}-ATPases and two are cation-ATPases. NCU03305, NCU04736, NCU05154, NCU03292, and NCU08147 genes encode the Ca^{2+}-ATPases NCA-1, NCA-2, NCA-3, PMR-1, and PH-7 ATPases, respectively (Benito et al. 2000). NCA-2 deficiency causes slow growth, Ca^{2+} sensitivity, increased intracellular Ca^{2+} level, and female sterility, but NCA-1 and NCA-3 deficiency had no effect on growth or Ca^{2+} distribution (Bowman et al. 2011; Laxmi and Tamuli 2015). Another Ca^{2+}-ATPase, TRM-9 encoded by NCU04898 is involved in growth, Ca^{2+} sensitivity, and heat shock caused cell death in *N. crassa* (Laxmi and Tamuli 2015).

1.4.3 Ca^{2+}/H^{+} exchangers: Ca^{2+}/H^{+} exchangers are crucial for pumping Ca^{2+} ions out of the cell as well as delivering Ca^{2+} into organelles for intracellular Ca^{2+} storage to maintain Ca^{2+} equilibrium (Zelter et al. 2004). Two H^{+} ions are exchanged per Ca^{2+} ion translocation across membranes in *N. crassa* (Miller et al. 1990). *N. crassa* has six Ca^{2+}/H^{+} exchangers encoded by the NCU07075, NCU00916, NCU00795, NCU06366, NCU07711, and NCU05360 genes (Galagan et al. 2003; Borkovich et al. 2004).

1.4.4 Ca^{2+}/Na^{+} exchangers: Ca^{2+}/Na^{+} exchangers cause the exit of Ca^{2+} out of the cytoplasm and also allow Ca^{2+} into the cell (Lytton 2007). The NCU02826 and NCU08490 genes encode two Ca^{2+}/Na^{+} exchangers found in *N. crassa*.

1.4.5 Phospholipase C-δ subtype proteins: Four novel phospholipase C-δ subtype proteins (PLC-δ) encoded by the NCU01266, NCU02175, NCU06245, and NCU11415 genes have been discovered in *N. crassa* (Galagan et al. 2003; Borkovich et al. 2004). PLC-δ is a phosphoinositide specific phospholipase that hydrolyzes the plasma membrane phospholipid phosphatidylinositol 4, 5-bisphosphate (PIP_2) to produce IP_3 and DAG (Berridge and Irvin 1984; Berridge 1987, 1993). Ca^{2+} is released from intracellular Ca^{2+} storage vacuoles when IP_3 is present (Cornelius et al. 1989). In *N. crassa*, no recognised IP_3 receptors have been discovered (Galagan et al. 2003; Borkovich et al. 2004). Protein kinase C (PKC) is activated by DAG, but none of the *N. crassa* PKC has a C2 domain with Ca^{2+} binding sites (Schmitz and Heinisch 2003; Borkovich et al. 2004). The *plc-1*^{RIP} mutant and PLC-1 expressed by the NCU06245 gene had a spreading colonial morphology with defects in growth, hyphal size, and branching pattern (Garnjobst and Tatum 1967; Gavric et al. 2007).

1.4.6 Calmodulin: Only one calmodulin (CaM) was found in *N. crassa*, and it was represented by the NCU04120 gene (Galagan et al. 2003; Borkovich et al. 2004). CaM is required for cell viability and modulates DNA repair, circadian clock, DNA synthesis, and cell proliferation in both Chinese hamster ovary (CHO) and human cell lines (Chafouleas et al. 1984; Chard 1987; Pavelic 1987; Capelli et al. 1993; Mirzayans et al. 1995; Sadakane and Nakashima 1996; Suresh and Subramanyam 1997; Galagan et al. 2003; Borkovich et al. 2004). In *N. crassa*, calmodulin (*cmd*) is an essential gene and is linked to proper vegetative growth, ultraviolet (UV) survival, and sexual development (Laxmi and Tamuli 2015, 2017).

1.4.7 Ca^{2+} and/or CaM binding proteins: There are 23 Ca^{2+} and/or CaM binding proteins in the *N. crassa* genome (Galagan et al. 2003; Borkovich et al. 2004). Ca^{2+} and/or CaM binding proteins are involved in the control of $[Ca^{2+}]_c$ and contain multiple conserved domains, including an N-terminal catalytic domain, a Ca^{2+} binding EF-hand domain, an autoinhibitory domain, and an overlapping CaM binding domain (Tamuli et al. 2013). CaMK-1, CaMK-2, CaMK-3, and CaMK-4 are four Ca^{2+}/CaM dependent kinases encoded by the NCU09123, NCU02283, NCU06177, and NCU09212 genes, respectively, in *N. crassa* (Galagan et al. 2003). CaMK-1 mutants have a phase delay, a light-induced phase shift in the circadian conidiation rhythm, a short period lengthening, and a delayed growth phenotype (Yang et al. 2001). The Ca^{2+}/CaM dependent kinases in *N. crassa* are involved in growth, oxidative stress survival, and other processes (Kumar and Tamuli 2014). Calcineurin is a heterodimer containing a CaM binding catalytic subunit, calcineurin A (CNA-1), and a Ca^{2+} binding regulatory subunit, calcineurin B (CNB-1), and these two subunits interact physically in *N. crassa* (Klee et al. 1979; Winkler et al. 1984; Tamuli et al. 2016). Calcineurin is involved in the maintenance of an apical Ca^{2+} gradient as well as growth and development in *N. crassa* (Prokisch et al. 1997; Kothe and Free 1998; Tamuli et al. 2016). The NCU04379 gene encodes the Ca^{2+} and/or CaM binding neuronal calcium sensor-1 (NCS-1), which is involved in growth, Ca^{2+} stress tolerance, UV survival, and germling fusion (Deka et al. 2011; Palma-Guerrero et al. 2013). The NCU08980 gene encodes another Ca^{2+} and/or CaM binding protein, NDE-1, which is an external NADPH dehydrogenase in *N. crassa* mitochondria (Melo et al. 1999, 2001; Borkovich et al. 2004; Carneiro et al. 2007). The NADPH oxidation activity of the NDE-1 protein is Ca^{2+}-dependent and features a Ca^{2+} binding motif (Melo et al. 1999, 2001).

Table 1.1: Ca^{2+} signaling proteins in *N. crassa*

Sl. No.	NCU No.	Gene name	Protein name	Protein type	Best overall[b] (e-value; organism; protein name; accession number)
1	02762	*cch-1*	Cch-1	Ca^{2+} permeable channel	0; *Verticillium dahlia* (Cch1); EGY18507.1
2	06703	*mid-1*	MID-1	Ca^{2+} permeable channel	2*e*-97; *Paracoccidioides brasiliensis* (MID-1); EEH23338.1
3	11680			Ca^{2+} permeable channel	0; *Ajellomyces dermatitidis* (Yvc1); EGE78766.1
4	03305	*nca-1*	NCA-1	Ca^{2+}-ATPase	0; *Trichophyton tonsurans* (SCA-1); EGD96734.1
5	04736	*nca-2*	NCA-2	Ca^{2+}-ATPase	0; *Magnaporthe oryzae* (Plasma membrane calcium transporting ATPase 3); EHA56671.1
6	05154	*nca-3*	NCA-3	Ca^{2+}-ATPase	0; *Glomerella graminicola* (Calcium translocating P-type ATPase); EFQ29373.1
7	03292	*pmr-1*	PMR-1	Ca^{2+}-ATPase	0; *Uncinocarpus reesii* (PMR-1); XP_002541437.1
8	08147	*ph-7*	PH-7	Ca^{2+}-ATPase	0; *G. graminicola* (Potassium/sodium efflux P-type ATPase); EFQ36596.1
9	04898	*trm-9*	TRM-9	Ca^{2+}-ATPase	0; *Cordyceps militaris* (Cation transporting ATPase 4); EGX91104.1
10	03818	*trm-10*	TRM-10	Ca^{2+}-ATPase	0; *V. dahlia* (Neo1p); EGY18069.1

11	07966	*trm-1*	TRM-1	Cation-ATPase	0; *T. tonsurans* (Cta3p); EGD97988.1
12	10143	*atp-11*	ATP-11	Cation-ATPase	0; *C. militaris* (ATPase type 13A2); EGX92563.1
13	07075	*cax*	CAX	Ca^{2+}/H^{+} exchanger	0; *G. graminicola* (Calcium/proton exchanger); EFQ30300.1
14	00916	*trm-15*	TRM-15	Ca^{2+}/H^{+} exchanger	2*e*-176; *Aspergillus fumigatus* (Membrane bound cation transporter); XP_001481534.1
15	00795	*trm-14*	TRM-14	Ca^{2+}/H^{+} exchanger	1*e*-149; *A. niger* (Membrane bound cation transporter); XP_001400827.2
16	06366	*trm-18*	TRM-18	Ca^{2+}/H^{+} exchanger	0; *Sclerotinia sclerotiorum* (Ca^{2+}/H^{+} antiporter); XP_001589752.1
17	07711	*trm-19*	TRM-19	Ca^{2+}/H^{+} exchanger	4*e*-160; *T. tonsurans* (Vacuolar calcium ion transporter/H^{+} exchanger); EGD98067.1
18	05360	*trm-17*	TRM-17	Ca^{2+}/H^{+} exchanger	0; *Metarhizium anisopliae* (Calcium permease); EFY95914.1
19	02826	*trm-16*	TRM-16	Ca^{2+}/Na^{+} exchanger	0; *V. albo-atrum* (Sodium/calcium exchanger protein); XP_003004985.1
20	08490	*trm-20*	TRM-20	Ca^{2+}/Na^{+} exchanger	1*e*-83; *A. niger* (Sodium/calcium transporter); XP_001397155.1
21	01266	*plc-2*	PLC-2	Phospholipase C	0; *Sordaria macrospora* (Phosphoinositide-specific phospholipase C); XP_003348116.1

22	06245	*plc-1*	PLC-1	Phospholipase C	0; *G. graminicola* (Phosphatidylinositol-specific phospholipase C); EFQ28596.1
23	11415	*inl-7*	INL-7	Phospholipase C	0; *G. graminicola* (Phosphatidylinositol-specific phospholipase C); EFQ31595.1
24	02175	*inl-15*	INL-15	Phospholipase C	3*e*-125; *Botryotinia fuckeliana* (BcPLC2); CCD34776.1
25	04120	*cmd*	CaM	Calmodulin	1*e*-103; *Gibberella zeae* (CaM); XP_382067.1
26	03804	*cna-1*	CNA-1	Ca^{2+} and/or CaM binding protein	0; *S. macrospora* (Serine/threonine-protein phosphatase 2B catalytic subunit protein); XP_003352213.1
27	03833	*cnb-1*	CNB-1	Ca^{2+} and/or CaM binding protein	2*e*-119; *Trichoderma reesei* (Calcineurin beta subunit); EGR44907.1
28	09265	*cnx-1*	CNX-1	Ca^{2+} and/or CaM binding protein	0; *S. macrospora* (cnx1); XP_003347545.1
29	05225[c]	*nde-1*	NDE-1	Ca^{2+} and/or CaM binding protein	0; *M. oryzae* (Mitochondrial NADH dehydrogenase); EHA47323.1
30	02115			Ca^{2+} and/or CaM binding protein	0; *M. oryzae* (EF-hand domain containing protein); EHA48778.1
31	01564	*mic-4*	MIC-4	Ca^{2+} and/or CaM binding protein	0; *M. oryzae* (Calcium dependent mitochondrial carrier protein); EHA48778.1
32	06948			Ca^{2+} and/or CaM binding protein	2*e*-54; *Mycosphaerella graminicola* (Calcium ion

					binding, calmodulin); EGP88834.1)
33	04379	*ncs-1*	NCS-1	Ca^{2+} and/or CaM binding protein	4*e*-126; *Grosmannia clavigera* (Neuronal calcium sensor 1); EFX03580.1
34	02738	*pef-1*	PEF-1	Ca^{2+} and/or CaM binding protein	2*e*-130; *V. dahlia* (Peflin); EGY21808.1
35	09871	*nup-34*	NUP-34	Ca^{2+} and/or CaM binding protein	4*e*-33; *V. dahlia* (Centrin-3); EGY16271.1
36	01241	*mic-2*	MIC-2	Ca^{2+} and/or CaM binding protein	0; *T. reesei* (Mitochondrial carrier protein); EGR44893.1
37	06347	*ask-2*	ASK-2	Ca^{2+} and/or CaM binding protein	0; *S. macrospora* (Actin cytoskeleton–regulatory complex protein); XP_003350109.1
38	06617	*cdc4-2*	CDC4-2	Ca^{2+} and/or CaM binding protein	7*e*-93; *V. albo-atrum* (Myosin regulatory light chain cdc4); XP_003009631.1
39	03750	*cmd-2*	CMD-2	Ca^{2+} and/or CaM binding protein	8*e*-74; *B. fuckeliana* (Calmodulin); XP_001560827.1
40	08980	*nde-2*	NDE-2	Ca^{2+} and/or CaM binding protein	0; *G. clavigera* (Alternative NADH-dehydrogenase); EFX03867.1
41	02283	*camk-2*	CaMK-2	Ca^{2+} and/or CaM binding protein	0; *S. macrospora* (Calcium/calmodulin-dependent protein kinase type I); XP_003344498.1
42	09123	*camk-1*	CaMK-1	Ca^{2+} and/or CaM binding protein	0; *Sporothrix schenckii* (Calcium/calmodulin-dependent kinase); AAV80434.1

43	09212	*camk-4*	CaMK-4	Ca^{2+} and/or CaM binding protein	0; *V. dahliae* (Serine/threonine-protein kinase srk1); EGY15110.1
44	02814	*prd-4*	PRD-4	Ca^{2+} and/or CaM binding protein	0; *G. clavigera* (Serine/threonine-protein kinase chk2); EFX01629.1
45	06650	*spp-3*	SPP-3	Ca^{2+} and/or CaM binding protein	3*e*-61; *Nectria haematococca* (Phospholipase A2); XP_003042542.1
46	02411			Ca^{2+} and/or CaM binding protein	0; *G. graminicola* (Microtubule-associated protein); EFQ31793.1
47	06177	*camk-3*	CaMK-3	Ca^{2+} and/or CaM binding protein	0; *M. grisea* (CMKK2); ACM41720.1
48	04265	*inv*	INV	Ca^{2+} and/or CaM binding protein	7*e*-85; *Bacillus megaterium* (Betafructosidase FruA); AEN90524.1

[a]Adapted from Tamuli et al. 2013. [b]BLASTp search was performed at NCBI (http://blast.ncbi.nlm.nih.gov/Blast.cgi; Altschul et al. 1990, 1997, 2005) with default parameters for each of the 48 Ca^{2+} signaling proteins against the non-redundant protein sequence databases, and the respective best overall match in other organisms with an *e*-value has been indicated. [c]NCU05225 was indicated as NCU08980.1 in Borkovich et al. 2004.

1.5 The Ca^{2+} signaling proteins are important for Ca^{2+} homeostasis

Although cytosolic Ca^{2+} is important as an intracellular signal in fungi, increased Ca^{2+} levels are toxic to the cell; therefore, the $[Ca^{2+}]_c$ is tightly controlled (Berridge et al. 1988; Sanders et al. 2002; Tamuli et al. 2013). The Ca^{2+} signaling proteins such as PLC-δ subtype proteins (PLC-δ), Ca^{2+} and/or CaM binding secretory phospholipase A_2 protein ($sPLA_2$), and Ca^{2+} exchangers govern key cellular processes in fungi and other species, including *N. crassa* (Barman and Tamuli 2015). Here, I briefly describe the functions of PLC, $sPLA_2$, and Ca^{2+} exchangers in different fungi.

1.5.1 Phospholipase C

Phospholipases are ubiquitous enzymes that catalyse the hydrolysis of phospholipids to produce free fatty acids (FFAs) and a variety of lipophilic signaling molecules such as DAG, phosphatidic acid (PA),

and lysophospholipids (Köhler et al. 2006; Hong et al. 2016). Phospholipases are categorised as Phospholipase A (PLA_1 and PLA_2), Phospholipase B (PLB), Phospholipase C (PLC), and Phospholipase D (PLD) based on the site of cleavage of an ester bond inside a phospholipid molecule (Fig. 1.6A; Köhler et al. 2006). PIP_2 is hydrolyzed by the membrane-bound phosphoinositide-specific PLC, producing two essential second messengers, IP_3 and DAG (Fig. 1.6B; Berridge and Irvin 1984; Berridge 1987, 1993). IP_3 causes Ca^{2+} to be released from the intracellular Ca^{2+} reserves, whereas DAG binds to the Ca^{2+}-dependent C2 domain, activating the PKC enzyme (Berridge and Irvin 1984; Nishizuka 1984; Berridge 1987; Cornelius et al. 1989; Berridge 1993; Clapham 2007). The majority of eukaryotic PLCs have five conserved domains that include two catalytic domains X and Y, an N-terminal pleckstrin homology (PH) domain for membrane phospholipid interaction, a C-terminal Ca^{2+} -dependent C2 domain for phospholipid binding, and an EF-hand motif for Ca^{2+} binding and PH-phospholipid interaction (Fig. 1.6C; Bristol et al. 1988; Watson and Arkinstall 1994; Sutton et al. 1995; Yamamoto et al. 1999). The orthologs of PLC have been identified across different species, including yeast, mould, and filamentous fungi, and PLC regulates a variety of cellular and biological activities (Table 1.2).

In *Saccharomyces cerevisiae*, the *Plc1p* deletion-insertion mutants were viable, but phenotypic defects such as slower growth at restricted temperatures (23 °C), lethality with multiple morphological aberrations at nonpermissive temperatures (above 35 °C) or on synthetic media or media containing a high concentration of fermentable carbon sources were observed (Flick and Thorner 1993; Payne and Fitzgerald-Hayes 1993; Yoko-o et al. 1993). The *Plc1p* deletion-insertion mutants also showed osmosensitivity and sensitivity to nitrogen limitation at permissive temperatures (23 to 30 °C), as well as defects in utilizing non-fermentable carbon sources other than glucose (Flick and Thorner 1993). Expression of rat PLC-1 in the *Plc1p* mutant improved growth deficiencies of the mutant, suggesting that PLC-1 is involved in growth, nutrition, and stress responses in *S. cerevisiae* (Yoko-o et al. 1993). In the fission yeast *Schizosaccharomyces pombe*, *plc1-1* deficient strains grew slowly on normal minimal medium (MM), formed morphologically abnormal cells, showed temperature sensitivity in rich medium, and displayed UV sensitivity (MM; Andoh et al. 1995; Fankhauser et al. 1995; Andoh et al. 1998). The growth deficiency was largely inhibited in low inositol and low phosphate MM harbouring high nitrogen concentrations, suggesting a function for *plc1-1* in the ammonium sensing system (Fankhauser et al. 1995).

In the opportunistic fungal pathogen *Alternaria alternata*, deletion of PLC-1 resulted in significant morphological defects, including vegetative growth deficiency, swollen hyphae, decreased sporulation with delayed germination, and disturbance of Ca^{2+} homeostasis (Tsai and Chung 2014). The *plc1* mutants also generated little or no necrosis on excised citrus leaves, suggesting that PLC-1

may play a role in pathogenicity in *A. alternata* (Tsai and Chung 2014). The *plc1* is required for *A. alternata* proliferation, infection structure differentiation, and secondary metabolism in response to physiochemical cues on the pear fruit surface (Huang et al. 2020). In the grey mould fungus *Botrytis cinerea*, *bcplc1* is an essential gene (Schumacher et al. 2008). The *bcplc1* knock down mutant generated by RNA-mediated gene silencing forms tiny compact colonies with fewer aerial hyphae and altered hyphal morphology, as well as showed dramatically lowered conidiation and germination (Schumacher et al. 2008). BcPLC1 is also required for virulence and regulates the expression of BCG-1 (encoding the GTP binding subunit) and CN (encoding calcineurin) dependent genes in *B. cinerea* (Schumacher et al. 2008). The genome of *Candida albicans* possesses three putative PI-PLCs, *CaPLC1*, *CaPLC2*, and *CaPLC3* (Bennett et al. 1998; Andaluz et al. 2001). *CaPLC1* resembles the mammalian PI-PLC-δ isoform, whereas *CaPLC2* and *CaPLC3* are similar to bacterial PI-PLCs (Bennett et al. 1998; Andaluz et al. 2001). In *C. albicans* also, *CaPLC1* is an essential gene since knocking out *CaPLC1* did not result in any null mutants, and the PI-PLC specific inhibitor 1-O-octadecyl-2-O-methyl-rac-glycero-3-phosphorylcholine (ET-18) totally restricted *C. albicans* cells from growing (Kunze et al. 2005). The *CaPLC1* conditional mutants showed phenotypes similar to *S. cerevisiae Plc1p* deletion-insertion mutants, including osmosensitivity (high concentrations of sorbitol or NaCl), sensitivity to lower (18 °C) or higher (43 °C) temperatures, reduced growth in non-glucose carbon sources (such as galactose), sensitivity to nocodazole which inhibits chromosome segregation, and reduced growth in filamentous growth inducing media (Kunze et al. 2005). However, the *CaPLC2* and *CaPLC3* are non-essential for survival, since deletion of *Caplc2* or *Caplc3* caused no phenotypic abnormalities under various growth and stress producing circumstances (Knechtle et al. 2005; Kunze et al. 2005).

In *Coprinopsis cinerea*, a tiny ink-cap mushroom, *CcPLC1*, *CcPLC2*, and *CcPLC3* are three potential PLC genes that showed considerable similarity to the *S. cerevisiae PLC-1* (Oh et al. 2012). All three *CcPLC*s are expressed differentially throughout distinct stages of the *C. cinerea* life cycle (Oh et al. 2012). In response to the PLC inhibitor U73122, the wild type *C. cinerea* strain exhibited several phenotypic defects, including inhibition of oidia and basidiospore germination, reduced hyphal growth with irregular hyphal tips, open clamp connections with aberrant clamp cells (branch like structures), and protoplast inhibition (Oh et al. 2012). In *Cryptococcus neoformans*, selective disruption of *Cnplc1* abolishes three major traits of cryptococcal pathogenicity, including melanin production due to decreased cell wall associated melanin producing laccase 1 (*lac*1) expression, growth at the host physiological temperature (37 °C), and secretion of cell associated CnPlb1 (Chayalkulkeeree et al. 2008). The growth of the *C. neoformans* wild type strain is inhibited in the presence of PLC inhibitor U73122, while the MICs (Minimum Inhibitory Concentrations) of the azole drugs, amphotericin B, and flucytosine were significantly reduced in the *Cnplc1* deleted strain, suggesting that *plc1* could be a

potential antifungal drug target (Chayalkulkeeree et al. 2008). *C. neoformans PLC1* regulates virulence and homeostasis by providing IP_3 as a substrate for Arg1 Kinase (Lev et al. 2013). However, deletion of *Cnplc2* caused no phenotypic alterations in *C. neoformans* and demonstrated virulence equivalent to the wild type (Chayalkulkeeree et al. 2008). In *Cryphonectria parasitica*, the *cplc*1 null mutant exhibited few morphological abnormalities, such as bright orange coloured colonies with slower mycelial development and no aerial mycelium, thinner and abrupt vegetative hyphae, and decreased conidiation, but no temperature or osmosensitivity (Chung et al. 2006). Furthermore, *lac*1 transcript was not accumulated when *cplc*1 was disrupted, indicating that *cplc*1 is important for *lac*1 gene expression (Chung et al. 2006). Furthermore, both the *cplc*1 null mutant and the hypo virulent strain displayed similar necrosis on excised chestnut tree bark, suggesting that *cplc1* has no involvement in pathogenicity (Chung et al. 2006). The genome of *Fusarium graminearum* possesses six putative PLC encoding genes, *FgPLC1*, *FgPLC2*, *FgPLC3*, *FgPLC4*, *FgPLC5*, and *FgPLC6*; and all these six FgPLCs are expressed variably throughout the mycelia (Zhu et al. 2015). In response to U73122, wild type *F. graminearum* showed dose-dependent decreases in mycelial growth, colony formation, conidiation and conidial germination, perithecium suppression, and downregulation of trichothecene biosynthetic Tri5 and Tri6 genes in the mycelia (Zhu et al. 2015). In *F. graminearum*, only *FgPLC1* is required for hyphal development, plant infection, and sexual or asexual development, and it is thought to be functionally connected to MAP kinases (Zhu et al. 2016).

In the rice blast filamentous ascomycete *Magnaporthe oryzae*, the PLC inhibitor neomycin inhibits Ca^{2+} inflow at the germ tube apex and appressoria, suggesting that PLC may play a role in intracellular Ca^{2+} homeostasis (Rho et al. 2009). Reduced growth rate, osmosensitivity (glycerol or NaCl), decreased conidiation with altered conidial shape, suppression of perithecium formation, aberrant appressoria development, and non-invasive hyphae were seen after targeted disruption of *MoPLC1* (Rho et al. 2009). The *MoPLC2* and *MoPLC3* deleted strains showed normal vegetative growth, conidia, and appressorium morphology; however, conidia production was significantly reduced, and multiple appressoria on separate germ tubes were formed from a single conidium, most likely due to a cell wall integrity defect (Choi et al. 2011). Complementation with a wild type allele of *MoPLC1* and a mouse *PLC-δ1* independently restored most of the phenotypic defects, indicating that PLC-mediated regulation of Ca^{2+} flow is functionally conserved between two kingdoms (Rho et al. 2009). Complementation with a wild type allele of the *MoPLC2* and *MoPLC3* genes also supplemented the phenotypic defects of *MoPLC2* and *MoPLC3* deletion mutants, indicating PLC acts as a regulator of Ca^{2+} flow and pathogenesis (Choi et al. 2011). In the filamentous fungus *Trichoderma reesei*, PLC serves as an essential link between cAMP and Ca^{2+} signaling in cellulase production (Chen et al. 2021).

Table 1.2: Summary of the functions of PLC in different organisms

Organisms	Proteins	Functions	Reference
Alternaria alternata	AaPLC	Vegetative growth, sporulation, Ca^{2+} homeostasis, and virulence	Tsai and Chung 2014; Huang et al. 2020
Botrytis cinerea	BcPLC1	Vegetative growth, conidiation, virulence, and regulates transcription of BCG-1 and CN encoding genes	Schumacher et al. 2008
Candida albicans	CaPLC1	Viability, thermotolerance, osmoregulation, and growth on non glucose carbon sources	Bennett et al. 1998; Andaluz et al. 2001; Kunze et al. 2005
Coprinopsis cinerea	CcPLCs	Oidia and basidiophore germination, and hyphal morphology	Oh et al. 2012
Cryphonectria parasitica	CPLC	Vegetative growth, conidiation, and *lac*1 gene expression	Chung et al. 2006
Cryptococcus neoformans	CnPLC1	Ca^{2+} homeostasis, *lac*1 gene expression, growth at host physiological temperature, and virulence	Chayalkulkeeree et al. 2008; Lev et al. 2013
Fusarium graminearum	FgPLCs	Vegetative and sexual development, conidiation, appressorium formation, and trichothecene biosynthesis	Zhu et al. 2015, 2016

Magnaporthe oryzae	MoPLC1	Vegetative and sexual development, Ca^{2+} homeostasis, conidiation, appressorium formation, osmoregulation, and pathogenicity	Rho et al. 2009; Choi et al. 2011
Saccharomyces cerevisiae	Plc1p	Growth at nonpermissive temperatures (above 35 °C), survival under hyperosmotic stress, utilization of galactose, raffinose, or glycerol as a carbon source at permissive temperature	Flick and Thorner 1993; Yoko-o et al. 1993
Schizosaccharomyces pombe	Plc1-1	Vegetative growth, and ammonium sensing	Andoh et al. 1995, 1998; Fankhauser et al. 1995
Trichoderma reesei	PLC	Cellulase production	Chen et al. 2021

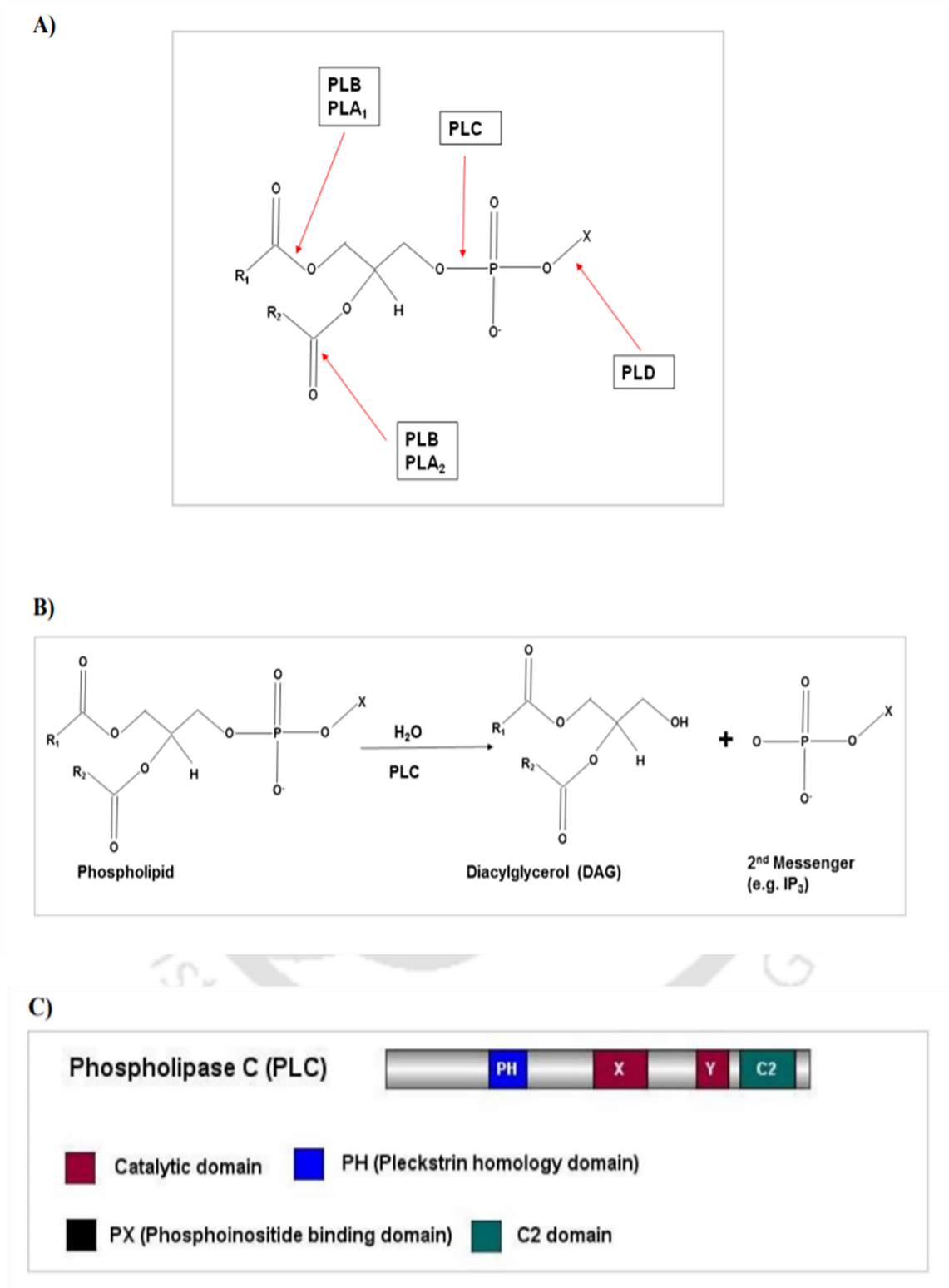

Figure 1.6: Mechanism of action and domain organization of PLC. **(A)** Phospholipases A_1 (PLA_1), A_2 (PLA_2), B (PLB), C (PLC), and D (PLD) hydrolyze various carbon atoms on a phospholipid backbone. The red arrow indicates the location of action of the phospholipases PLA_1, PLA_2, PLB, PLC,

and PLD on a phospholipid (Köhler et al. 2006). The letter X denotes polar head groups (e.g. choline, serine etc.). **(B)** Phosphatidylinositol-4, 5-bisphosphate (PIP_2) is hydrolyzed by PLC to IP_3 and DAG. **(C)** The domain organization of the PLC. Fig. is adapted from Barman and Tamuli (2018).

1.5.2 Secretory Phospholipase A_2

The phospholipase A (PLA) superfamily, which catalyses the hydrolysis of membrane phospholipids into FFAs and other lipid soluble molecules, is divided into two types based on the site of ester linkage cleavage; PLA_1 cleaves at the sn_1 ester linkage, whereas PLA_2 cleaves at the sn_2 ester bond of glycerophospholipids (Fig. 1.6A; Ghannoum 2000; Arioka et al. 2005; Köhler et al. 2006). The low molecular weight (Mw: 13-19 kDa) Ca^{2+}-dependent extracellular secretory proteins are a member of the PLA_2 superfamily ($sPLA_2$). $sPLA_2$ are secretory enzymes that regulate a variety of biological processes such as atherosclerosis, eicosanoid production, host defense, and inflammation in a wide range of species, from bacteria to fungi, plants, and mammals (Murakami and Kudo 2004; Boilard et al. 2010; Dennis et al. 2011). They were first discovered in mammalian pancreatic juice and cobra venom, and subsequently found in reptiles, insects, plants, bacteria, viruses, and fungi (Nakashima et al. 2003; Nevaleinen et al. 2012, 2013). The primary amino acid sequence of $sPLA_2$ includes a highly conserved His-Asp dyad, a number of unique disulphide bonded Cys residues that contribute to the stability of these enzymes, and a N terminal signal peptide residue for secretion, which is cleaved upon internalisation in the ER or the periplasm (Murakami and Kudo 2004; Schaloske and Dennis 2006; Nakahama et al. 2010; Dennis et al. 2011; Cavazzini et al. 2013). In addition, the secretory actions of $sPLA_2$ are regulated by the N terminal signal peptide and cellular Ca^{2+} concentrations (Murakami and Kudo 2004; Dennis et al. 2011; Cavazzini et al. 2013). The catalytic core of most $sPLA_2$ enzymes lacks a catalytic Ser but includes a firmly bound water molecule that functions as a potential nucleophile (Verheij et al. 1980; Scott et al. 1990; Pickard et al. 1996). Based on its structural and functional features, $sPLA_2$ has been classified into I, II, III, V, IX to XIV groups (Matoba et al. 2002).

The ectomycorrhizal ascomycete *Tuber borchii* was the first fungal species to identify and describe $sPLA_2$ activity (TbSP1; Soragni et al. 2001). In *T. borchii*, TbSP1 is expressed in nutrient-depleted environments (carbon and nitrogen limitation) and has a signaling role in enhancing the *T. borchii* mycorrhizal establishment with a particular host plant (Miozzi et al. 2005; Nakahama et al. 2010). TbSP1 (Mw: 19 kDa) has a predicted N-terminal signal peptide with a pre-protein cleavage site, a conserved Arg-Gly-Asp motif, a conserved catalytic His, Ca^{2+} binding residues, and disulphide linked Cys residues, forming a new XIV subfamily within the PLA_2 superfamily (Soragni et al. 2001; Kohler et al. 2006). *Helicosporium sp.* HN1 encodes a 15 kDa secreted protein, p15, that also belongs to group XIV (Wakatsuki et al. 1999, 2001). The core amino acid sequence of p15 has a conserved region of four Cys residues, that are needed for its stability (Wakatsuki et al. 1999, 2001). This secretory protein

stimulates neurite outgrowth and differentiation in neurons from the rat pheochromocytoma PC12 cell line by activating L-type Ca^{2+} channels, which in turn activates a downstream signaling cascade (Wakatsuki et al. 1999, 2001). Scp15 (Mw: 14 kDa), isolated from *Streptomyces coelicolor*, is comparable to *Helicosporium sp.* p15, includes four Cys residues, and has neurite stimulating action in PC12 cells (Nakashima et al. 2003). The saprotrophic ascomycete *Aspergillus oryzae* has two unique putative $sPLA_2$ proteins designated as sPlaA and sPlaB in its genome (Machida et al. 2005; Kobayashi et al. 2007; Nakahama et al. 2010). Both sPlaA and sPlaB have different physiological features; sPlaA has the maximum enzyme activity for Ca^{2+} under acidic pH conditions with external secretion, whereas sPlaB has the highest enzyme activity for Ca^{2+} at a neutral to alkaline pH with intracellular localization (Nakahama et al. 2010). Only sPlaA expression was shown to be significantly elevated in response to carbon deprivation, oxidative stress, heat shock, and during or after conidiation, but sPlaB expression was hardly detectable in any of the conditions (Nakahama et al. 2010).

Table 1.3: Summary of the functions of $sPlA_2$ in different organisms

Organisms	Proteins	Functions	Reference
Tuber borchii	TbSP1P1	Nutrient acquisition	Soragni et al. 2001
Aspergillus oryzae	sPlaA	Oxidative stress, heat shock, and conidiation	Nakahama et al. 2010
Helicosporium sp.	p15	Neurite outgrowth and differentiation of neurons in rat	Wakatsuki et al. 1999, 2001
Streptomyces coelicolor	Scp15	Neurite stimulating activity in rat	Nakashima et al. 2003
Mus musculus		Innate immune response	Balestrieri et al. 2009
Homo sapiens		Anti-inflammatory role in immune complex mediated arthritis	Boilard et al. 2010

1.5.3 Ca^{2+} exchangers

Ca^{2+} exchangers are Ca^{2+} transporting proteins that operate to lower high $[Ca^{2+}]_c$ by removing the excess cytosolic Ca^{2+} from the cell and transferring into intracellular Ca^{2+} stores by the simultaneous exchange of positive ions across membranes powered by ATP hydrolysis (Zelter et al. 2004). Ca^{2+} exchangers contain conserved domains; however, little is known about the precise cellular function of any of the Ca^{2+} exchangers in fungi (Zelter et al. 2004). Vcx1p/Hum1p, the *S. cerevisiae* vacuolar Ca^{2+}/H^+ exchanger, is negatively regulated by calcineurin and is implicated in the fast sequestration of cytosolic Ca^{2+} into vacuoles as well as the transport of cadmium (Cd^{2+}; Cunningham and Fink 1996; Miseta et al. 1999; Pittman et al. 2004). *C. neoformans*, a human pathogenic fungus, encodes VCX1, a vacuolar Ca^{2+} exchanger implicated in calcineurin-dependent Ca^{2+} tolerance and a putative cryptococcosis virulence determinant (Kmetzsch et al. 2010, 2013). Six unique Ca^{2+}/H^+ exchangers and two Ca^{2+}/Na^+ exchangers are found in *N. crassa* (Galagan et al. 2003; Borkovich et al. 2004; Zelter et al. 2004). In *N. crassa*, the Ca^{2+}/H^+ exchanger CAX, a homolog of *S. cerevisiae* Vcx1p/Hum1p, is crucial in maintaining $[Ca^{2+}]_c$ levels, and mutants lacking *cax* accumulate relatively little Ca^{2+} in the dense vacuolar fraction (Bowman et al. 2011). In *M. oryzae*, knocking out Vcx1 genes resulted in reduction in growth rate, sporulation and appressorium formation but had no effect on pathogenicity (Nguyen et al. 2008). In the insect-pathogenic fungus *Beauveria bassiana*, which has five Vcx1 homologs, deletion of individual Vcx1 genes leads to a moderate reduction in pathogenicity and has no effect on the development of this fungus on conventional media, but it does have a minor effect on high Ca^{2+} media (Hu et al. 2014). In summary, the Ca^{2+} exchanger appears to have the common function of sequestering high Ca^{2+} concentrations, whereas its impacts on growth and pathogenicity are very species-specific.

1.5.4 *Neurospora crassa* homologs of *plc-1*, *cpe-1*, and *splA*$_2$

The genome of *N. crassa* contains four PLC-δ subtype proteins, six novel Ca^{2+}/H^+ exchangers, and two distinct $sPLA_2$ proteins (Galagan et al. 2003; Borkovich et al. 2004; Zelter et al. 2004). In this study, I focused on the NCU06245, NCU06366, and NCU06650 genes that encode the phospholipase C-1 (PLC-1), the Ca^{2+}/H^+ exchanger-1 (CPE-1), and the secretory phospholipase A_2 ($sPLA_2$) proteins, respectively, in *N. crassa*. The NCU06245, which encodes PLC-1 of 711 amino acid residues, is genetically mapped from position 2027776-2031034 (-) at the right arm of linkage group three in the super contig three and its genomic sequence has two exons separated by one intron (LG IIIR). The NCU06245 encoded PLC-1 has sequence similarity to *A. capsulatus*, *C. higginsianum*, and *M. grisea* PLC-1 homologs (Barman and Tamuli 2015). Sequence analysis of the NCU06245 homolog revealed *N. crassa* PLC-1 lacks the PH domain, but consists of Ca^{2+} and H^+ binding residues essential for its catalytic activity (Barman and Tamuli 2015). However, the NCU06245 gene is highly variable across the *N. crassa* natural isolates (Gavric et al. 2007). Polymorphisms in the NCU06245 gene resulted in

N. crassa specific coding sequence variants for amino acid positions 200-250 (Gavric et al. 2007). The NCU06366 gene designated *cpe-1* encodes a putative Ca^{2+}/H^{+} exchanger of 505 amino acid residues involved in maintaining intracellular levels of Ca^{2+} and is found to be significantly different from homologs found in *S. cerevisiae* and *M. grisea* in a phylogenetic analysis (Zelter et al. 2004). The NCU06366 has nine transmembrane domains as predicted by TMHMM software and is genetically mapped in the super contig four from position 2765568-2768250 (-) at the right arm of the linkage group IV (LG IVR; Zelter et al. 2004; Barman and Tamuli 2015). In addition, *N. crassa* possesses two $sPLA_2$ proteins encoded by NCU06650 and NCU09423 (Barman and Tamuli 2015; Takayanagi et al. 2015). The NCU06650 gene encodes a conserved hypothetical secretory phospholipase A_2 protein of 186 amino acid residues (Barman and Tamuli 2015; Takayanagi et al. 2015); and is genetically mapped from position 4123065-4123980 (-) at the right arm of linkage group five (LG VR) in super contig five and has two exons in its genomic sequence (Barman and Tamuli 2015). The NCU06650 encoded $sPLA_2$ has a 19 amino acids long N-terminal signal peptide residues (1-30) likely for secretion, a highly conserved region (residues 122-153) that contains a catalytic histidine residue, and two disulphide-bonded Cys residues similar to the *T. borchii* $sPLA_2$ homolog, and belongs to the group XIV $sPLA_2$ group of enzyme (Soragni et al. 2001; Barman and Tamuli 2015; Takayanagi et al. 2015). It has a potential CaM binding site with the amino acid sequence TCHALANVYYAAVREFGRTKGELQ, which is missing from the NCU09423 encoded $sPLA_2$ (Borkovich et al. 2004; Barman and Tamuli 2015).

Studies on the *N. crassa plc-1*, *cpe-1*, and *splA*$_2$ genes revealed their roles in the regulation of $[Ca^{2+}]_c$ homeostasis, carotenoid accumulation, and survival under stress conditions (Barman and Tamuli 2015). In response to an increase in cytosolic $[Ca^{2+}]_c$ caused by the divalent ionophore A23187, *N. crassa* strains lacking *plc-1*, *cpe-1*, and *splA*$_2$ showed growth abnormalities, suggesting that these genes are involved in maintaining Ca^{2+} homeostasis (Barman and Tamuli 2015). The Δ*plc-1*, Δ*cpe-1*, and Δ*splA*$_2$ knockout mutants also showed considerably greater carotenoid content at 8 °C, 22 °C, and 30 °C, as well as enhanced UV survival under carotenoid accumulation conditions (Barman and Tamuli 2015). In addition, *plc-1*, *cpe-1*, and *splA*$_2$ deletion mutants demonstrated lower survival in hydrogen peroxide (H_2O_2) induced oxidative stress (Barman and Tamuli 2015). Complementation with the wild type alleles of *plc-1*, *cpe-1*, and *splA*$_2$ restored the phenotypic defects caused by the divalent ionophore A23187, during carotenoid accumulation and oxidative stress in *N. crassa* (Barman 2017).

Studies on their double mutants revealed that the genetic interactions of *plc-1* with *cpe-1* and *splA*$_2$ loci are important for vegetative and sexual development in *N. crassa* (Barman and Tamuli 2017). Colonial morphology, aberrant hyphal branching, a slower growth rate, shorter aerial hyphae, reduced biomass accumulation, early conidiation with delayed germination, inappropriate conidiation of submerged cultures, and lower carotenoid accumulation were also observed in the Δ*plc-1*; Δ*cpe-1* and

Δ*plc-1*; Δ*splA*$_2$ double mutants (Barman and Tamuli 2017). The Δ*plc-1*; Δ*cpe-1* and Δ*plc-1*; Δ*splA*$_2$ double mutants had abnormal hyphal morphology on ionophore A23187 containing medium, as well as increased sensitivity to Ca^{2+}, UV, oxidative stress, and were female sterile (Barman and Tamuli 2017). However, the Δ*cpe-1*; Δ*splA*$_2$ double mutant, had no synthetic effect on growth, sexual development, Ca^{2+}, or UV stress, demonstrating that *cpe-1* and *splA*$_2$ do not interact genetically in *N. crassa* (Barman and Tamuli 2017).

Although previous studies shed light on the functions of the homologs of PLC-1, CPE-1, and sPLA$_2$ in *N. crassa*, a detailed molecular pathway including their localization and structural information remained elusive. Moreover, previous studies showed that the extracellular signals mediated by Ca^{2+} and cAMP affect the mammalian circadian clock (O'Neill and Reddy 2012). Circadian rhythms are ubiquitous biological oscillations with an approximately 24 h period. The model filamentous fungus *N. crassa* displays circadian rhythm in the vegetative developmental program (Nakashima 1981; Bell-Pederson et al. 1992; Aronson et al. 1994). Previous studies also showed that the cytosolic Ca^{2+} regulates the expression of heat shock proteins under heat stress in fungi (Zhang et al. 2016). In addition, the Ca^{2+} signaling pathway crosstalks with the alkaline pH signaling pathway in *N. crassa* (Cupertino et al. 2012). Moreover, disruption of Ca^{2+} homeostasis in the endoplasmic reticulum (ER) causes protein unfolding, leading to ER stress (Ma and Hendershot 2004; Bravo et al. 2012; Hetz 2012). Although PLC-1, CPE-1, and sPLA$_2$ are involved in the process of sensing the cytosolic Ca^{2+} in *N. crassa*, their function in response to heat, pH, and ER stress are not clear. In the filamentous fungus *T. reesei*, PLC-1 mediated Ca^{2+} signaling pathway plays a crucial role in the regulation of cellulase overexpression under cellulase-inducing conditions (Chen et al. 2021). Furthermore, *N. crassa* has recently gained importance as a model organism to obtain a more detailed understanding of the physiology of lignocellulose degradation across fungi, as a near full genome deletion set is available. However, no evidence for the role of PLC-1, CPE-1, and sPLA$_2$ in biomass degradation was previously available, although phospholipases are associated with membrane remodelling. Therefore, in this study, I investigated the role of the *plc-1*, *cpe-1*, and *splA*$_2$ genes in regulating the circadian clock, stress responses, cellulose degradation, and other related cell functions in *N. crassa*. The three broad objectives of this study are as given below:

1. To investigate the cellular roles of the Ca^{2+} signaling genes *phospholipase C-1* (*plc-1*), *Ca^{2+}/H^+ exchanger-1* (*cpe-1*), and *secretory phospholipase A*$_2$ (*splA*$_2$) in circadian clock, stress responses, and cellulose degradation in *N. crassa*,
2. To investigate the crosstalk of *plc-1*, *cpe-1*, and *splA*$_2$ genes in the regulation of circadian clock, stress responses, and cellulose degradation in *N. crassa*, and
3. To investigate the molecular basis of sPLA$_2$ mediated cellulose degradation in *N. crassa*.

Chapter 2: Materials and Methods

2.1 Materials

2.1.1 Laboratory chemicals and reagents used in this study

Table 2.1 lists all the chemicals and reagents used in this study. Glasswares used were obtained from Borosil (Mumbai, India) and Jain Scientific Glasswares (Ambala, India). The Plasticwares were procured from either Tarsons (Kolkata, India) or Genaxy (New Delhi, India).

Table 2.1: List of laboratory chemicals and reagents used in this study

Chemicals/Reagents	Chemical Formula	Make	Catalogue No.
Ammonium iron (II) sulphate hexahydrate	$Fe(NH_4)_2(SO_4)_2.6H_2O$	MERCK	103792
Ammonium molybdate tetrahydrate	$(NH_4)_6Mo_7O_{24}.4H_2O$	SRL	014892
Ammonium nitrate	NH_4NO_3	Fisher Scientific	21445
Ammonium per sulphate (APS)	$(NH_4)_2S_2O_8$	SRL	0148134
L-Arginine	$C_6H_{14}N_4O_2$	HIMEDIA	PCT0302-25G
Avicel^R PH-101	N/A	SIGMA-ALDRICH	11365
D-Biotin	$C_{10}H_{16}N_2O_3S$	SRL	0248120
Boric acid	H_3BO_3	SRL	0244112
Bromophenol blue	$C_{19}H_{10}Br_4O_5S$	SRL	0240168
Calcium chloride dihydrate	$CaCl_2.2H_2O$	SRL	0349152
Calcium D-pantothenate	$C_{18}H_{32}CaN_2O_{10}$	HIMEDIA	CMS178-100G
Cetyltrimethyl ammonium bromide (CTAB)	$C_{19}H_{42}BrN$	aMResco	0833-500G
Chloroform	$CHCl_3$	SRL	0328101
Citric acid monohydrate	$C_6H_8O_7.H_2O$	SRL	0348216
Copper sulphate pentahydrate	$CuSO_4.5H_2O$	SRL	0347102
Diethyl pyrocarbonate (DEPC)	$C_6H_{10}O_5$	SRL	46791
Dimethyl sulphoxide (DMSO)	C_2H_6OS	MERCK	109678
Di-sodium hydrogen arsenate	$Na_2HAsO_4.7H2O$	SIGMA-ALDRICH	6756
Absolute ethanol	C_2H_5OH	MERCK	1.00983.0511
Ethidium bromide (EtBr)	$C_{21}H_{20}BrN_3$	SRL	054817
EDTA	$C_{10}H_{16}N_2O_8$	SRL	18240
EGTA	$C_{14}H_{24}N_2O_{10}$	HIMEDIA	MB130-10G
Ferrous sulphate heptahydrate	$FeSO_4.7H_2O$	RANKEM	F0044
Formaldehyde	CH_2O	SRL	AS017-500ML
D-Fructose	$C_6H_{12}O_6$	SRL	064855
Glacial acetic acid	CH_3COOH	MERCK	1.93402.0521
D-Glucose	$C_6H_{12}O_6$	SRL	42738
L-Glutamine	$C_5H_{10}N_2O_3$	HIMEDIA	PCT0308-100G
Glycerol (glycerin) anhydrous	$C_3H_8O_3$	SRL	072929
Glycine	$C_2H_5NO_2$	SRL	69422
Hydrochloric acid	HCl	HIMEDIA	AS003-500ML
Hydrogen peroxide	H_2O_2	MERCK	61765305001730
HEPES buffer	$C_8H_{18}N_2O_4S$	SRL	084023
Isopropanol	C_3H_7OH	SRL	092956
Lithium chloride	LiCl	SRL	124919
Magnesium chloride hexahydrate	$MgCl_2.6H_20$	HIMEDIA	GRM3922-500G
Magnesium sulphate heptahydrate	$MgSO_4.7H_2O$	Qualigens	18955

Manganous chloride tetrahydrate	$MnCl_2.4H_2O$	SRL	1348152
Manganous sulphate monohydrate	$MnSO_4.H_2O$	Qualigens	25255
Methanol	CH_3OH	HIMEDIA	AS058-500ML
N,N′-Methylenebisacrylamide	$C_7H_{10}N_2O_2$	SRL	38516
β-Mercaptoethanol	C_2H_6OS	SRL	1324196
MOPS buffer	$C_7H_{15}NO_4S$	HIMEDIA	RM660-100G
Phenol: Chloroform: Isoamyl alcohol (25:24:1)	N/A	SRL	69031
Potassium acetate	$C_2H_3O_2K$	HIMEDIA	GRM3930-500G
Potassium hydroxide	KOH	RANKEM	P0390
Potassium nitrate	KNO_3	TITAN	761
Potassium phosphate dibasic	K_2HPO_4	HIMEDIA	GRM1045-500G
Potassium phosphate monobasic	KH_2PO_4	HIMEDIA	GRM249-500G
Silica gel (6-12 mesh)	N/A	SIGMA-ALDRICH	214426-1KG
Sodium acetate anhydrous	$C_2H_3NaO_2$	HIMEDIA	TCO23-500G
Sodium arsenate dibasic heptahydrate	$Na_2HAsO_4.7H_2O$	HIMEDIA	10048-95-0
Sodium bicarbonate dihydrate	$Na_3C_6H_5O_7.2H_2O$	SRL	89399
Sodium carbonate anhydrous	Na_2CO_3	SRL	64079
Sodium citrate dihydrate	$Na_3C_6H_5O_7.2H_2O$	HIMEDIA	GRM255-500G
Sodium dodecyl sulphate (SDS)	$NaC_{12}H_{25}SO_4$	SRL	194821
Sodium hydroxide	NaOH	TITAN	439
Sodium molybdate dihydrate	$Na_2MoO_4.2H_2O$	SRL	1947166
Sodium nitrate	$NaNO_3$	HIMEDIA	GRM416-500G
Sodium potassium tartrate tetrahydrate	$C_4H_4O_6KNa{\cdot}4H_2O$	SRL	18241
Sodium sulphate anhydrous	Na_2SO_4	SRL	59977
D-Sorbitol	$C_6H_{14}O_6$	SRL	14281
Sorbose	$C_6H_{12}O_6$	LOBA Chemie	0607700025
Sucrose	$C_{12}H_{22}O_{11}$	MERCK	61839805001730
Sulphuric acid	H_2SO_4	HIMEDIA	AS015-500ML
Tetramethylethylenediamine (TEMED)	$(CH_3)_2NCH_2CH_2N(CH_3)_2$	HIMEDIA	MB026-100ML
Tris base	$C_4H_{11}NO_3$	RANKEM	T0350
Triton X-100	N/A	SRL	64518
D-Xylose	$C_5H_{10}O_5$	SRL	84974
Yeast extract	N/A	SRL	34266
Zinc sulphate heptahydrate	$ZnSO_4.7H_2O$	SRL	264745
Dithiothreitol (DTT)	$C_4H_{10}O_2S_2$	SRL	17315
Skimmed milk powder	N/A	HIMEDIA	M530-500G
Ampicillin sodium salt	$C_{16}H_{18}N_3NaO_4S$	HIMEDIA	MB104-5G
Hygromycin B	N/A	HIMEDIA	PCT1503-20ML
Bacto-agar	N/A	HIMEDIA	GRM026-500G
Prestained protein ladder	N/A	BIORAD	1610374
Bradford reagent	N/A	HIMEDIA	ML106-500ML
Agarose	N/A	Invitrogen	16500-500
TRIzol™ reagent	N/A	Invitrogen	15596026
SYBR Green Real-Time PCR Mix	N/A	Life Technologies	4472903
100 bp DNA Ladder	N/A	NEB	B7025S
1 Kb DNA Ladder	N/A	NEB	B7025S
Blue Gel Loading Dye (6X)	N/A	NEB	B7024S
Taq DNA Polymerase	N/A	NEB	M0273S
Phusion® High-Fidelity DNA Polymerase	N/A	NEB	M0530S
Plasmid DNA Isolation Kit	N/A	Qiagen	12123

PCR Purification Kit	N/A	Qiagen	28104
Pancreatic RNAse A	N/A	Promega	A7973
Verso cDNA Synthesis Kit	N/A	Thermo Scientific	AB-1453/A

Not Applicable (N/A): Chemical formula doesn't exist.

2.1.2 *N. crassa* strains used in this study

N. crassa strains used in this study were obtained from the Fungal Genetics Stock Centre (FGSC) and the laboratory of Maria Celia Bertolini and were also generated in our laboratory.

1. **Strains acquired from the Fungal Genetics Stock Centre (FGSC):** *N. crassa* wild type (WT) strains *74-OR23-IV* A (FGSC 2489) and *ORS-SL6* a (FGSC 4200), Ca^{2+} signaling mutants Δ*plc-1*, Δ*cpe-1*, and Δ*splA*$_2$, and the *ras-1*^{bd} strains were obtained from the Fungal Genetics Stock Centre (FGSC; University of Missouri, Kansas City, MO 64110; McCluskey et al. 2010; Table 2.2).

2. **Strains acquired from the laboratory of Maria Celia Bertolini, Brazil:** Δ*cre-1* and *Pn-cre-1* strains were obtained from the laboratory of Maria Celia Bertolini, Department of Biochemistry and Organic Chemistry, Sao Paulo State University, Brazil (Table 2.2).

3. **Strains generated in our laboratory:** Δ*plc-1*; Δ*cpe-1*, Δ*plc-1*; Δ*splA*$_2$, Δ*cpe-1*; Δ*splA*$_2$ (Barman and Tamuli 2017), and Δ*cre-1*; Δ*splA*$_2$ double mutants used in this study were generated in the laboratory by crossing the individual knockout mutant strains of opposite mating types. Δ*plc-1* (60), Δ*cpe-1* (74), and Δ*splA*$_2$ (4) strains were generated by crossing each of the single mutants with the *ras-1*^{bd} strain. For the generation of Δ*plc-1*; Δ*cpe-1* (3), Δ*plc-1*; Δ*splA*$_2$ (37), and Δ*cpe-1*; Δ*splA*$_2$ (72), each of the confirmed single mutants carrying the *ras-1*^{bd} allele of opposite mating types were crossed among themselves. Previously, my senior colleague Ananya Barman cloned the *plc-1*, *cpe-1*, and *splA*$_2$ genes into the *Sma* I site of the *his-3* targeting vector pMF272 and transformed the Δ*plc-1*, Δ*cpe-1*, and Δ*splA*$_2$ mutants and generated the P_{ccg-1}::*plc-1*::*gfp*, P_{ccg-1}::*cpe-1*::*gfp*, and P_{ccg-1}::*splA*$_2$::*gfp* homokaryotic strains (Table 2.2). The gene expression in the homokaryotic transformant strains is controlled by the *ccg-1* promoter, which is a constitutive promoter.

Table 2.2: List of *N. crassa* strains used in this study

FGSC No. (a/A) or Strain Name	NCU No. or Strain Type	Genotype	Source
4200/2489	Wild Type (WT)	WT *mat a/A*	FGSC
11411/NA	06245	Δ*plc-1*:: *hph*; *mat a/A*	FGSC
11407/11408	06366	Δ*cpe-1*:: *hph*; *mat a/A*	FGSC
11246/11247	06650	Δ*splA*$_2$:: *hph*; *mat a/A*	FGSC
18633	08807	Δ*cre-1*:: *hph*; *mat a*	FGSC
1858/1859	08823	*ras-1*^{bd}; *mat a/A*	FGSC
Δ*plc-1*; Δ*cpe-1*	Double mutant	Δ*plc-1*:: *hph*; Δ*cpe-1*:: *hph*; *mat a/A*	Our Laboratory (Barman and Tamuli 2017)
Δ*plc-1*; Δ*splA*$_2$	Double mutant	Δ*plc-1*:: *hph*; Δ*splA*$_2$:: *hph*; *mat a/A*	Our Laboratory (Barman and Tamuli 2017)
Δ*cpe-1*; Δ*splA*$_2$	Double mutant	Δ*cpe-1*:: *hph*; Δ*splA*$_2$:: *hph*; *mat a/A*	Our Laboratory (Barman and Tamuli 2017)
Δ*cre-1*; Δ*splA*$_2$	Double mutant	Δ*cre-1*:: *hph*; Δ*splA*$_2$:: *hph*; *mat a/A*	Our Laboratory (This study)
Δ*plc-1* (60)	Single mutant	Δ*plc-1*:: *hph*; *ras-1*^{bd}; *mat A*	Our Laboratory (This study)
Δ*cpe-1* (74)	Single mutant	Δ*cpe-1*:: *hph*; *ras-1*^{bd}; *mat a*	Our Laboratory (This study)
Δ*splA*$_2$ (4)	Single mutant	*ras-1*^{bd}; Δ*splA*$_2$:: *hph*; *mat a*	Our Laboratory (This study)
Δ*plc-1*; Δ*cpe-1* (3)	Double mutant	Δ*plc-1*:: *hph*; Δ*cpe-1*:: *hph*; *ras-1*^{bd}; *mat a*	Our Laboratory (This study)
Δ*plc-1*; Δ*splA*$_2$ (37)	Double mutant	Δ*plc-1*:: *hph*; *ras-1*^{bd}; Δ*splA*$_2$:: *hph*; *mat A*	Our Laboratory (This study)
Δ*cpe-1*; Δ*splA*$_2$ (72)	Double mutant	Δ*cpe-1*:: *hph*; *ras-1*^{bd}; Δ*splA*$_2$:: *hph*; *mat a*	Our Laboratory (This study)
P$_{ccg-1}$::*plc-1*::*gfp*	Homokaryotic	Δ*plc-1*::*hph*::*P*$_{ccg-1}$::*plc-1*::*gfp hop A*	Barman 2017 (Thesis)

P_{ccg-1}::cpe-1::gfp	Homokaryotic	*Δcpe-1::hph::P_{ccg-1}::cpe-1::gfp hop A*	Barman 2017 (Thesis)
P_{ccg-1}::$splA_2$::gfp	Homokaryotic	*Δ$splA_2$::hph::P_{ccg-1}::$splA_2$::gfp hop A*	Barman 2017 (Thesis)
Pn-cre-1	Homokaryotic	*his-3::Pn-cre-1-gfp*	Sun and Glass 2011

2.1.3 Media for bacterial growth, antibiotics, and other commonly used reagents

1. **Bacterial media:** Luria Bertani **(**LB) broth and agar were purchased from Himedia (Mumbai, India) and used according to the manufacturer's protocol. Before use, the media were autoclaved to sterilize them.

2. **Ampicillin:** A 100 mg/ml stock solution of ampicillin was prepared by dissolving 500 mg of ampicillin powder in 5 ml of sterile distilled water. The solution was filter sterilized, and it was stored at -20 °C.

3. **Hygromycin B:** A hygromycin B solution of 50 mg/ml concentration was obtained from Himedia (Mumbai, India) in a ready-to-use form.

4. **Glufosinate ammonium/Basta®:** Glufosinate ammonium, also known as Basta®, was obtained from Sigma-Aldrich (USA). A 100 mg/ml stock solution was prepared by dissolving 100 mg of glufosinate ammonium powder in 1 ml of sterile distilled water, and stored as aliquots of 200 µl at -20 °C.

5. **Pantothenate solution:** To prepare a stock solution of 1 mg/ml, 100 mg of calcium D-pantothenate were dissolved in 100 ml of distilled water, autoclaved, and then stored at 4 °C for further use.

6. **1 M sorbitol:** To prepare 100 ml of 1 M sorbitol, 18.21 g of sorbitol was properly dissolved in 70 ml of distilled water, adjusted to the final volume of 100 ml, and then sterilized by autoclaving.

7. **8 M LiCl:** To prepare 100 ml of 8 M LiCl, 33.9 g of LiCl was dissolved in a final volume of 100 ml of DEPC-treated distilled water, and then sterilized by autoclaving before use.

8. **3 M Na-acetate (pH 5.2):** For 100 ml, 24.61 g of Na-acetate was dissolved in 70 ml of distilled water, adjusted the pH to 5.2 with glacial acetic acid, and then made up the volume by adding distilled water. The solution was sterilized by autoclaving before use.

9. **5 M $CaCl_2$:** 73.5 g of $CaCl_2.2H_2O$ was dissolved in distilled water to make a final volume of 100 ml and then sterilized by autoclaving.

10. **10 N NaOH:** With constant stirring, 40 g NaOH pellet was slowly dissolved in 80 ml of ice cold distilled water, the final volume was adjusted to 100 ml. After autoclaving, the solution was kept at room temperature.

11. **2 M KCl:** 14.9 g of KCl was dissolved in a final volume of 100 ml, autoclaved, and stored at room temperature.

12. **1 M glycine:** For 100 ml, 7.5 g of glycine was dissolved in 80 ml of distilled water, volume adjusted, autoclaved, and then stored at room temperature.

13. **EtBr:** To prepare a 10 mg/ml stock solution, 10 mg of EtBr was dissolved in 1 ml of sterile distilled water, and then stored at room temperature.

14. **10% SDS:** 10 g of SDS was added to 80 ml of distilled water in a magnetic stirrer and heated at 65 °C with constant stirring. The final volume was adjusted to 100 ml, and then stored at room temperature.

15. **1 M Tris-HCl (pH 7.5/8.0):** 12.11 g of Tris base was dissolved in 70 ml of distilled water, adjusted the pH to 7.5/8.0 by adding concentrated HCl, and made up the volume to 100 ml with distilled water. The solution was sterilized by autoclaving.

16. **1.5 M Tris-HCl (pH 8.8):** 18.17 g of Tris base was dissolved in 70 ml of distilled water, adjusted the pH to 8.8 by adding concentrated HCl, and made up the volume to 100 ml with distilled water. The solution was sterilized by autoclaving.

17. **0.5 M Tris-HCl (pH 6.8**): 6.06 g of Tris base was dissolved in 70 ml of distilled water, adjusted the pH to 6.8 by adding concentrated HCl, and the volume was made up to 100 ml with distilled water. The solution was sterilized by autoclaving.

18. **0.5 M EDTA (pH 8.0):** 18.61 g of EDTA was added to 70 ml of distilled water with constant stirring, and the pH was adjusted to 8.0 by adding concentrated NaOH. The final volume was adjusted to 100 ml, and the solution was sterilized by autoclaving.

19. **0.5 M EGTA (pH 8.0):** 19.02 g of EGTA was added to 60 ml of distilled water with constant stirring, and the pH was adjusted to 8.0 by adding concentrated NaOH. The final volume was adjusted to 100 ml, and the solution was sterilized by autoclaving.

20. **1 M $MgCl_2$:** 20.33 g of $MgCl_2.6H_2O$ was dissolved in a final volume of 100 ml distilled water and autoclaved to sterilize.

21. **1X TE:** 1X TE is a solution of 10 mM Tris-HCl (pH 8.0) and 1 mM EDTA (pH 8.0) stored at 4 °C.

22. **50X TAE:** 1 L of the 50X TAE stock solution was made by mixing 242 g of Tris base, 57.1 ml of glacial acetic acid, and 100 ml of 0.5 M EDTA (pH 8.0), and adjusting the final volume to 1 L with distilled water. The solution was autoclaved and stored at 4 °C.

23. **10X MOPS buffer:** After properly dissolving 4.18 g of MOPS in DEPC-treated water, 2 ml of 1 M Na-acetate solution (20 mM) and 2 ml of 0.5 M EDTA (10 mM) were added to the solution. The pH was adjusted to 7.0 by adding concentrated NaOH. The solution was filter sterilized using a 0.45 µm syringe filter, and then stored at room temperature in the dark.

24. **1 M HEPES buffer (pH 7.5):** For 10 ml, 2.38 g of HEPES was dissolved in 6 ml of distilled water, adjusted the pH to 7.5 with NaOH solution, and then made up the volume. The solution was then stored at -20 °C after being filter sterilized through a 0.45 µm syringe.

25. **0.5 M $NaHCO_3$:** 0.21 g of $NaHCO_3$ was dissolved in a final volume of 10 ml of distilled water, and then stored at room temperature.

26. **10% Na-deoxycholate:** 1 g of Na-deoxycholate was dissolved in a final volume of 10 ml distilled water, and then stored at room temperature.

27. **100 mM DTT:** 0.15 g of DTT was dissolved in 1 ml of 100 mM HEPES buffer (pH 7.5) and stored at -20 °C in the dark.

28. **Alkaline Lysis Solution I:** Alkaline lysis solution I comprises 50 mM glucose, 25 mM Tris-HCl (pH 8.0), and 10 mM EDTA (pH 8.0). The solution was sterilized by autoclaving and stored at 4 °C.

29. **Alkaline Lysis Solution II:** Alkaline lysis solution II is always prepared fresh prior to use and contains 0.2 N NaOH and 1% SDS.

30. **Alkaline Lysis Solution III:** To prepare a 100 ml alkaline lysis solution III, 60 ml of 5 M potassium acetate, 11.5 ml of glacial acetic acid, and 23.5 ml of distilled water were mixed together. The solution was sterilized by autoclaving and stored at 4 ºC.

31. **Lysis buffer for *N. crassa* genomic DNA isolation:** The DNA lysis buffer is comprised of 10 mM Tris-HCl (pH 7.5), 0.5 M NaCl, 10 mM EDTA, 1% SDS, and 1% CTAB.

32. **Lysis buffer for *N. crassa* RNA isolation:** The RNA lysis buffer contains 100 mM Tris-HCl (pH 8.0), 0.6 M NaCl, 10 mM EDTA (pH 8.0), 4.5% SDS, and 2% β-mercaptoethanol.

33. **Arsenomolybdate Reagent:** 2.5 g of ammonium molybdate was dissolved in 45 ml of distilled water, and 2.5 ml of H_2SO_4 was added to the solution. After that, 0.3 g of disodium hydrogen arsenate dissolved in 25 ml of distilled water was also added, mixed thoroughly, incubated at 37 °C for 24 to 48 h, and then stored at room temperature in the dark.

34. **Alkaline Copper Tartrate:** For a volume of 100 ml, 96 ml of Solution A is mixed with 4 ml of Solution B before use.
    Solution A: Solution A contains 2.54 g of anhydrous sodium carbonate, 2 g of sodium bicarbonate, 2.5 g of potassium tartrate, and 20 g of anhydrous sodium sulphate in 100 ml of distilled water.
    Solution B: 15 g of copper sulphate is mixed in a small volume of distilled water. One drop of H_2SO_4 was added and made up the volume to 100 ml.

35. **Skimmed Milk:** Sterile milk was prepared by dissolving 3.5 g of skimmed milk powder in 50 ml of deionized water, autoclaved, and stored at 4 °C.

2.1.4 Solutions for growth, maintenance, and crossing of *N. crassa* strains

(i) Biotin Solution: 5 mg of biotin was dissolved in 100 ml of 50% (v/v) ethanol and stored at 4 °C.

(ii) Trace Element Solution: To prepare a trace element solution, the following chemicals were added sequentially with constant stirring in 90 ml of distilled water. The final volume was brought to 100 ml, and 1 ml of chloroform was added as a preservative. The solution was then kept at 4 °C.

Trace Element Solution

$C_6H_8O_7.H_2O$	5.00 g
$ZnSO_4.7H_2O$	5.00 g
$Fe(NH_4)_2(SO_4)_2.6H_2O$	1.00 g
$CuSO_4.5H_2O$	0.25 g
$MnSO_4.H_2O$	0.05 g
H_3BO_3	0.05 g
$Na_2MoO_4.2H_20$	0.05 g

(iii) Vogel's Medium N (VGN): To prepare 50X Vogel's Medium N (Vogel 1956, 1964), the following chemicals were added sequentially in 75 ml of distilled water with constant stirring. The final volume of the solution was adjusted to 100 ml, and chloroform was added as a preservative.

50X Vogel's Medium N (VGN)

$Na_3C_6H_5O_7.2H_2O$	12.5 g
KH_2PO_4	25 g
NH_4NO_3	10 g
$MgSO_4.7H_2O$	1 g
$CaCl_2.7H_2O$ (Predissolved in 5 ml H_2O)	0.5 g
Biotin Solution	500 µl
Trace Element Solution	500 µl
Chloroform	300 µl

Vogel's Minimal Medium (VM)

Vogel's Medium N	1X
Sucrose	1.5% (w/v)

VM Agar

Vogel's Medium N	1X
Sucrose	1.5% (w/v)
Agar	1.5% (w/v)

(iv) 4X Synthetic Crossing Medium (SCM): 4X Synthetic Crossing Medium (Westergaard and Mitchell 1947) was prepared by dissolving the following chemicals sequentially in 80 ml of distilled water with constant stirring. The volume of the solution was adjusted to 100 ml and sterilized by autoclaving.

4X Synthetic Crossing Medium (SCM)

KNO_3	0.4 g
K_2HPO_4	0.28 g
KH_2PO_4	0.2 g
$MgSO_4.7H_2O$	0.2 g
$CaCl_2.2H_2O$	40 mg
NaCl	40 mg
Biotin Solution	20 µl
Trace Element Solution	20 µl

SCM Agar	
SCM	1X
Glucose	1.5% (w/v)
Agar	1.5% (w/v)

(v) 10X FGS (Fructose, Glucose, and Sorbose) Stock: 10X FGS stock was prepared by dissolving the following chemicals in 80 ml of distilled water. The volume of the solution was adjusted to 100 ml and sterilized by autoclaving.

10X FGS Stock	
Fructose	5% (w/v)
Glucose	5% (w/v)
Sorbose	20% (w/v)

FGS Agar	
FGS	1X
Vogel's Medium N	1X
Agar	1.5% (w/v)

Top Agar	
FGS	1X
Vogel's Medium N	1X
Agar	2.8% (w/v)

(vi) Medium for Circadian Clock Study

Circadian Clock Medium (Park and Lee 2004)

Vogel's Medium N	1X
Glucose	0.1% (w/v)
L-Arginine	0.17% (w/v)
Biotin	50 ng/ml
Agar	1.5% (w/v)

2.1.5 Primers used in this study

Custom oligonucleotide primers were procured from Bioserve India (Hyderabad, India) as well as from Integrated DNA Technologies (USA).

Table 2.3: List of primers used for confirmation of the knockout mutants and the homokaryotic strains

S. No.	Primers	Sequence (5′→3′)	Source
1	HI-NCU06245-F	AGTTGGTCGCCTCCTAGAAC	Barman and Tamuli 2015
2	HI-NCU06366-F	CTGCAAGGAGGCTAATTCGG	Barman and Tamuli 2015
3	HI-NCU06650-F	GCCGGACGGCAACTGAATAT	Barman and Tamuli 2015
4	HI-NCU08807-F	CCTCGTATGGATAAAGTGGCA	This study
5	5HPHR	ATCCACTTAACGTTACTGAAATC	Deka et al. 2011
6	PLC-1-GFP-5F	ATGCCAGCAGCTGTCCATGG	Barman 2017 (Thesis)
7	PLC-1-GFP-5R	CAACCTCAACTTCTTGCTTATC	Barman 2017 (Thesis)
8	CPE-1-GFP-5F	ATGACATCGCCCTACCATGC	Barman 2017 (Thesis)
9	CPE-1-GFP-5R	ATGATGACCACCCTCCGACC	Barman 2017 (Thesis)
10	$sPLA_2$-GFP-5F	ATGAAGTTCTTCTCTGCCCTC	Barman 2017 (Thesis)
11	$sPLA_2$-GFP-5R	ATAATACAACGGATCCTCGCC	Barman 2017 (Thesis)
12	CRE-1-ORF-5F	ATGCAACGCGTACAGTCAGC	This study
13	CRE-1-ORF-5R	TTACAACCGGTCCATCATCTC	This study
14	Pccg-1-Fw	CCATCATCAGCCAACAAAGC	Barman 2017 (Thesis)
15	GFP-Rv	AACTTGTGGCCGTTTACGTC	Barman 2017 (Thesis)

2.2 Methods

2.2.1 Growth conditions

Neurospora strains were grown and maintained as previously described in Davis and de Serres 1970. For vegetative growth, strains were routinely grown on VM agar (Vogel 1956, 1964). Crossing and sexual development (Westergaard and Mitchell 1947) and ascospore germination (Davis and de Serres 1970) were performed in SCM and FGS agar, respectively. For growing the respective auxotroph, inositol and pantothenic acid stocks were prepared and added to the growth media at a concentration of 0.05 and 0.01 mg/ml, respectively (http://www.fgsc.net/methods/stanford.html; Murray and Perkins 1963). FGS agar media mixed with Basta® or Ignite® (Pall 1993) at a concentration of 400 µg/ml was used to select the *N. crassa* transformants. Hygromycin was used at a concentration of 220 µg/ml for screening the *N. crassa* knockout mutants having the *hph* cassette (Colot et al. 2006).

2.2.2 Setting up crosses and harvesting ascospores

As previously described, crosses were carried out between *N. crassa* strains of opposite mating types (Westergaard and Mitchell 1947; Davis and de Serres 1970). Agar plugs of both strains were placed on SCM agar approximately 2 cm apart in a 55-mm Petri plate and allowed to cross for three to four weeks at 22 °C in a BOD incubator. After 21-25 days, ascospores were harvested by rinsing the lids with 1 ml of sterile distilled water. Ascospores were then heat activated for 45 min in a shaking water bath at 65 °C, plated on FGS agar, and incubated overnight at 30 °C. The germinated ascospores were picked under a dissection microscope by cutting out a small agar block and transferring them to VM agar slants, followed by incubation at 30 °C.

2.2.3 Maintenance of stock

For long-term storage, the *N. crassa* strains were kept as silica stocks. Strains were first cultured in VM agar for 3 days in the dark at 30 °C and then for 4 days in the light at room temperature. Before usage, silica gels (6-12 mesh, Grade 40) were autoclaved, dried at 60 °C, and then chilled to room temperature. Dried silica was placed in 4.5 ml cryo-tubes. 1 ml of autoclaved skimmed milk (5%) was added to each of the culture tubes and vortexed vigorously. The spore suspension is then pipetted out and dispensed into the pre-chilled cryo-tubes containing silica gels and vortexed vigorously for a few min to break up any clumps. The tubes were then kept at room temperature and vortexed regularly for another 8-10 days before being stored at -20 °C for further use.

2.2.4 Conidial cell count

For conidial counting, *N. crassa* strains were inoculated on VM agar and incubated at 30 °C in the dark for 2 days, followed by incubation under light for 4 days. Conidia were harvested from the mycelial surface in sterile distilled water, vortexed gently to make a conidial suspension, and counted using a haemocytometer under a trinocular inverted microscope (Axio Vert.A1 FL, Carl Zeiss, Germany).

2.2.5 Scoring for antibiotic resistance in *N. crassa*

To screen for antibiotic resistance, conidia were streaked onto 1.5% FGS plates supplemented with the antibiotic of interest. The commonly used antibiotics for screening in *N. crassa* were Hygromycin B (440 µg/ml from a 50 mg/ml stock in water; Colot et al. 2006) and Basta® or Ignite® (400 µg/ml from a 100 mg/ml stock in water; Pall 1993).

2.2.6 Growth rate assay

For radial growth, mycelial plug was inoculated in the centre of a 90-mm Petri dish with VM agar and incubated at 30 °C. The colony growth was marked until the 18^{th} h at an interval of 3 h, starting at the 12^{th} h to obtain the radial growth rate. Apical growth was evaluated using a conventional race tube experiment (Ryan et al. 1943). The race tube, partially filled with VM agar, was inoculated with a mycelial plug at one end, incubated at 30 °C, and the growth front was marked every 24 h for 3 days.

Apical growth rate was determined by measuring the distance between the inoculation point and the hyphal growth front and plotting against time. Both radial and apical growth rates were measured in cm/h.

2.2.7 Aerial hyphae analysis

For the development of aerial hyphae, 1 x 10^6 conidia were inoculated into sterile test tubes containing VM liquid and incubated in the dark at 30 °C for three days and then at room temperature for four days. The height of the aerial hyphae was measured and then photographed.

2.2.8 Circadian regulated conidiation assay

A medium containing 1X Vogel's salts, 0.1% D-glucose, 0.17% L-arginine, 50 ng/ml biotin, and 1.5% agar was used to culture the *N. crassa* strains in race tubes to study circadian regulated conidiation (Park and Lee 2004; Deka and Tamuli 2013). To determine the period length, *N. crassa* strains were inoculated at one end of the race tubes, incubated at 20 °C, 25 °C, and 30 °C for 24 h under constant light, and then shifted to constant darkness. The growth front was marked once per day for 7 days under the red safe light. The tubes were then moved to a light and the positions of the conidial bands were marked. Period lengths were calculated by multiplying the distance between conidial bands by the inverse of the slope of the growth front versus time (http://www.fgsc.net/teaching/circad.htm). The Q_{10} value was calculated using the formula: $Q10 = \left(\frac{R2}{R1}\right) 10/(T2 - T1)$, where R_1 and R_2 are frequency of period lengths at T_1 and T_2 temperatures, respectively (Lakin-Thomas 1998; Sorek and Levy 2012).

2.2.9 Thermotolerance assay

For the thermotolerance assay, 1 x 10^6 conidia/ml were inoculated and allowed to germinate in VM liquid at 30 °C and 200 rpm for 2 h. Two-hour old germlings were then exposed to three different conditions for 30 min: 30 °C (control), 30 °C (uninduced), and 44 °C (induced). Germlings exposed at 30 °C (uninduced) and 44 °C (induced) were then subjected to lethal heat shock at 52 °C for 20 min. Finally, the germlings were plated on FGS agar and incubated at 30 °C for 24 h (Yang and Borkovich 1999). The percentage of colonies that survived was calculated by dividing the number of viable colonies on the heat treated conditions (induced or uninduced) by the number of colonies on the control (30 °C) and multiplying by 100.

2.2.10 pH tolerance assay

For the pH stress assay, 1 x 10^6 conidia were inoculated in sterile test tubes containing VM liquid of pH 3.8, 4.8, 5.8, 6.8, and 7.8, and then incubated in the dark at 30 °C for three days followed by four days at room temperature in the light. Height of the aerial hyphae was measured and then photographed. The average percentage (%) of aerial hyphae height was calculated relative to the height of the strain in VM liquid (pH 5.8), which is considered as 100%.

2.2.11 Cell wall stress assay

The cell wall stress assay was performed with cell wall stress drugs, Congo Red (1 mg/ml; Cat. No. GRM508-10G, Himedia), and SDS (0.01%). Conidia were inoculated on petri plates with 1.5% bacto-agar mixed with the drugs in VM medium at 30 °C for 24 h, and radial growth was measured. The average percentage (%) of colony growth rate was calculated relative to the colony growth of the strain in VM without drugs, which is considered as 100%.

2.2.12 Endoplasmic reticulum (ER) stress assay

For endoplasmic reticulum stress, 1 x 10^6 conidia were inoculated in sterile test tubes containing VM liquid supplemented with 0 mM, 0.5 mM, 1 mM, and 2 mM concentrations of Dithiothreitol (DTT; Cat. No. 17315, SRL) and incubated in the dark at 30 °C for three days, followed by four days at room temperature. Height of the aerial hyphae was measured and then photographed. The average percentage (%) of aerial hyphae height was calculated relative to the height of the strain in VM liquid without DTT (0 mM), which is considered as 100%.

2.2.13 Cellulose degradation assay

For the cellulose degradation assay, an equal amount of conidia were inoculated in 100 ml flasks containing 25 ml of 1X Vogel's Medium with 2% microcrystalline cellulose (Avicel^R PH-101; Cat. No. 11365, Sigma-aldrich) as the sole carbon source and incubated at 30 °C with shaking at 200 rpm for 5 days in the light. The cellulose degradation ability was inferred based on the ability of the strains to grow on microcrystalline cellulose, appearance of transparent media, the total protein secreted, and the amount of glucose accumulated in the culture supernatants. The total protein was estimated by Bradford Assay, and the reducing glucose accumulated in the culture supernatant was estimated by the Nelson-Somogyi Method.

2.2.14 Isolation of *N. crassa* genomic DNA

The strains were grown in VM liquid at 30 °C and 200 rpm for three days. The mycelial mass was harvested by filtration, lyophilized, and ground to a fine powder using a mortar and pestle. In 2 ml micro centrifuge tubes, 150 mg of mycelial powder from each sample was weighed, and suspended in 1 ml of DNA lysis buffer. The tubes were heated at 65 °C for 30 min before being centrifuged at 12,000 x g for 10 min. The supernatants were transferred to fresh 2 ml micro centrifuge tubes, and 500 µl of phenol: chloroform: isoamyl alcohol (25:24:1) was added to the supernatants. The tube contents were mixed for 15 min in a rotary mixer before being centrifuged for 10 min at 12,000 x g. The aqueous phase was collected in 1.5 ml micro centrifuge tubes, and 600 µl of chloroform was added to eliminate any residual phenol. The tubes were centrifuged at 12,000 x g for 10 min. In 1.5 ml micro centrifuge tubes, the aqueous phase was collected, and genomic DNA was precipitated by adding 1 ml of 100% ethanol to each sample. After gently inverting the tubes a few times, the genomic DNA was pelleted

by centrifuging at 12,000 x g for 10 min. The pellets were washed with 70% ethanol by centrifuging for another 10 min at 12,000 x g and allowed to air dry for 15 min at room temperature. The pellets were then dissolved in 30 µl of 1X TE buffer (pH 8.0) and kept at 4 °C. All the centrifugation steps were carried out at ambient temperature.

2.2.15 Isolation of RNA from *N. crassa*

For RNA isolation, 1 x 10^6 conidia of the desired *N. crassa* strains were inoculated in 25 ml of liquid VM and cultured for 16 h at 30 °C and 200 rpm (or otherwise mentioned). Mycelia obtained by filtration was ground into a fine powder in a mortar and pestle using liquid nitrogen. The mycelial powder (25 mg) of each sample was transferred immediately into 2 ml micro centrifuge tubes containing 300 µl of TRIzol™ reagent (Cat. No. 15596026, Invitrogen, USA), followed by the addition of 750 µl of RNA lysis buffer and 750 µl of phenol: chloroform: isoamyl alcohol (25:24:1) solution. The tubes were allowed to mix for 20 min in a rotary mixer before being centrifuged at 10,000 x g for 10 min. The top aqueous phase was transferred to fresh 1.5 ml micro centrifuge tubes, and 750 µl of 8 M LiCl was added. The tubes were then kept overnight at 4 °C. The mixtures were vortexed briefly and centrifuged at 10,000 x g for 10 min. The isolated pellets were suspended in 300 µl of DEPC-treated double-distilled water along with 30 µl of 3 M Na-acetate (pH 5.2), and then 750 µl of 100% ethanol was added. The mixtures were kept at -20 °C for 2 h before being centrifuged for 10 min at 10,000 x g. The RNA pellets were washed with 70% ethanol and kept for air drying at room temperature for 10 to 15 min before being dissolved in 30 µl of RNAse-free water. The RNA was then stored at -80 °C or used to prepare cDNA. All the centrifugation steps were carried out at ambient temperature.

2.2.16 Quantification of nucleic acids

The concentration of nucleic acids was determined based on the optical density (OD) at 260 nm using a Nanodrop spectrophotometer (Eppendorf, Germany). The concentrations were then calculated using the empirical relationships: an OD_{260} of 1 corresponds to ~ 50 µg/ml of double-stranded DNA, ~ 40 µg/ml of single-stranded DNA and RNA, and ~ 20 µg/ml of single-stranded oligonucleotides, respectively. By evaluating the OD_{260}/OD_{280} ratio, the purity of nucleic acids was assessed. Pure RNA and DNA preparations have OD_{260}/OD_{280} ratios of 2.0 and 1.8, respectively.

2.2.17 Polymerase Chain Reaction (PCR)

The routine Polymerase Chain Reaction (PCR) was conducted according to the manufacturer's instructions using Taq DNA Polymerase (Cat. No. M0273S, New England Biolabs, USA). Phusion® High-Fidelity DNA Polymerase (Cat. No. M0530S, New England Biolabs, USA) was used for cloning purposes, because standard Taq DNA Polymerase isolated from *Thermus aquaticus* lacks the proofreading activity (3′-5′ exonuclease activity). Depending on the size of the amplicon and the

annealing temperature of the primers, the PCR conditions varied. Every PCR was done using a thermal cycler (Arktik Thermal Cycler, Thermo Fisher Scientific, USA).

2.2.18 Reverse Transcription PCR for cDNA synthesis

For gene expression studies, reverse transcription PCR (RT-PCR) was performed to synthesise the cDNA. The Verso cDNA Synthesis Kit (Cat. No. AB-1453/A, Thermo Scientific, USA) was used for the cDNA synthesis. Each 20 µl reaction contained ~ 1 µg of total RNA. Cycling conditions for one cycle of cDNA synthesis were 50 °C for 45 min followed by 95 °C for 2 min.

2.2.19 Real-time Quantitative PCR (qRT-PCR)

Total RNA extracted from *N. crassa* was used for gene expression experiments using real-time quantitative PCR (qRT-PCR). The qRT-PCR was carried out on a real-time PCR machine (ABI 7500 Fast, Applied Biosystems, USA and AriaMx Real-Time PCR System, Agilent, India) with a final reaction volume of 10 µl of SYBR® Select Master Mix (Cat. No. 4472903, Life Technologies, USA). In all, 4.5 µl of cDNA (100 ng), 0.25 µl of forward primer, 0.25 µl of reverse primer, and 5 µl of SYBR® Select Master Mix were used in a 10 µl reaction mixture. The following PCR reaction conditions were used: 95 °C for 10 min, followed by 40 cycles of 95 °C for 15 sec, and 60 °C for 1 min. The relative expression levels of the target genes were determined using the $2^{-\Delta\Delta C}{}_{T}$ method (Livak and Schmittgen 2001), and *β-tubulin* expression was employed as the endogenous control.

2.2.20 Agarose gel electrophoresis

For loading, 1 µl of DNA sample was mixed with 1 µl of 6X Blue Gel Loading Dye (0.25% bromophenol blue, 0.25% xylene cyanol, 30% glycerol) and 4 µl of 1X TAE. The samples were loaded on 0.8% to 1.5% agarose gels prepared with 1X TAE containing 0.5 µg/ml EtBr, depending on the size of the DNA fragments to be resolved. At 5 Vcm-1, electrophoresis was done in a 1X TAE running buffer. Standard DNA size markers were run alongside the samples to estimate the size of the DNA fragments. The EtBr stained DNA samples were viewed in a gel documentation system (Bio print ST4, Vilber Lormat, France). A 1.2% agarose gel containing 1X MOPS buffer, 2.2 M formaldehyde, and 0.5 µg/ml EtBr was used for resolving RNA samples.

2.2.21 Sequence analysis

BLAST (Basic Local Alignment Search Tool) analysis (Altschul et al. 1990, 1997, 2005) was carried out using NCBI software tools. The conserved domains in the protein were identified using the Conserved Domain Database (CDD; Marchler-Bauer and Bryant 2004; Marchler-Bauer et al. 2009). The protein sequences were aligned with Clustal X (Thompson et al. 1997) and then visualised with GeneDoc (Nicholas 1997). Molecular Evolutionary Genetic Analysis Version 6 (MEGA 6; Felsenstein 1985; Rzhetsky and Nei 1992; Tamura et al. 2013) was used to make phylogenetic trees from the sequence alignments.

2.2.22 3D Protein Structure Prediction, Validation, Refinement and Molecular Dynamics Simulation Analysis

2.2.22.1 Sequence retrieval

The amino acid sequences in the FASTA format of the proteins were obtained from UniProtKB and FungiDB databases.

2.2.22.2 Structure modelling

The protein structure modelling was performed using the I-TASSER (Iterative Threading ASSEmbly Refinement) tool by Zhang Lab (https://zhanggroup.org/I-TASSER), which uses threading and ab-initio methods.

2.2.22.3 Molecular Dynamics Simulation analysis

The dynamic nature of the I-TASSER modelled proteins in the simulated environment were studied using Molecular Dynamics (MD) Simulation, and was performed using the GROMACS 2020 software package (https://manual.gromacs.org/current/download.html). MD Simulation involves the following steps: 1) Initially protein topology file is generated by converting the PDB format of proteins to GROMACS and by choosing the relevant forcefield, in this CHARMM27 all atom force field was used. 2) The protein was then placed in a dodecahedron box with 1 nm distance space from the edge of the protein. 3) Solvation within the defined box was performed using a generic equilibrated 3-point solvent model. 4) The system was then neutralized by using the genion tool in GROMACS by adding appropriate amount of chlorine and sodium ions depending on the charge of the system. 5) The steric clashes and inappropriate geometry within the proteins were reduced with the energy minimization step involving the Lincs constraint algorithm and steepest decent algorithm, both the algorithms were applied simultaneously to constrain the various interactions present within the protein. 6) The biological system was simulated by equilibrating the experiment parameters such as temperature and pressure at 300 K and 1 atm respectively. 7) After the system was well equilibrated with the desired temperature and pressure, position restraints were released and MD simulation run for 100 ns timescale for data collection was performed by using the high facility supercomputer system (Param-Ishan) available at IITG. The time dependent change in the conformation of the proteins was given by the parameter RMSD, which is the root mean square deviation of the protein structure over the time scale with respective to the initial structure at t = 0 ns and the RMSD of the proteins over the 100 ns timescale were plotted by using qtgrace tool (https://sourceforge.net/projects/qtgrace/).

2.2.22.4 Model validation

The stereochemical quality of the modelled structures were analysed by Ramachandran plots, which is a plot between the torsion angles phi and psi of each residue. The plot is obtained using the PROCHECK program within the Saves v 6.0 webserver (https://saves.mbi.ucla.edu/). The MD refined

models of proteins were also validated by using ProSA (https://prosa.services.came.sbg.ac.at/prosa.php), which is a widely used tool in the validation of modelled protein structures that is based on statistical analysis of all available experimental protein structures in PDB.

2.2.22.5 Molecular visualization

The modelled three-dimensional structures of the proteins were visualized using PyMOL software (https://pymol.org/2). Then, the percentage of amino acids involved in forming the secondary structures such as helices, beta-sheets, and random coils of modelled proteins were obtained from DSSPweb (http://bioinformatica.isa.cnr.it/SUSAN/NAR2/dsspweb.html).

2.3 Databases and Software Programs used in this study

1. **Basic Local Alignment Search Tool (BLAST):** Nucleotide or protein sequences were compared to sequence databases using BLAST (Altschul et al. 1990, 1997, 2005). This is available online at http://blast.ncbi.nlm.nih.gov/Blast.cgi.

2. **Clustal X:** For multiple sequence alignment of DNA or protein sequences, Clustal X software was employed (Thompson et al. 1997). Clustal X can be accessed online at http://www.clustal.org/clustal2/#Webservers.

3. **ExPASy Translate tool:** The ExPASy Translate Tool was used to translate the nucleotide sequences into protein sequences. It can be found online at http://web.expasy.org/tools/DNA.

4. **Conserved Domain Database (CDD):** Conserved Domain Database (CDD) was used to identify the conserved domains present in the proteins (Marchler-Bauer and Bryant 2004; Marchler-Bauer et al. 2009). It can be found online at http://www.ncbi.nlm.nih.gov/Structure/cdd/wrpsb.cgi.

5. **GeneDoc:** GeneDoc software was used to identify conserved domains in aligned DNA or protein sequences (Nicholas 1997). It is available online at http://www.nrbsc.org/gfx/genedoc/.

6. **Molecular Evolutionary Genetic Analysis Version 6 (MEGA 6):** The MEGA 6 software was used to find the evolutionary relationship among the organisms or gene sequences (Tamura et al. 2013), which is available online at http://www.megasoftware.net/.

7. ***Neurospora crassa* genome databases:** A genome resource for *Neurospora* is available at http://fungidb.org. The web site for the Fungal Genetics Stock Centre is http://www.fgsc.net/.

8. **NCBI:** NCBI was used to retrieve the proteins or nucleic acid sequences at http://www.ncbi.nlm.nih.gov/.

9. **EMBL:** EMBL was used for retrieving the primary sequence of proteins or nucleic acids. This is available at http://embl.org/.

10. **UniProt:** UniProt was used to retrieve the primary sequence of proteins. This is available at https://www.uniprot.org/.

11. **Primer3:** Primer3 software was used for analysis of the secondary structure of oligonucleotide primers. It is available online at http://bioinfo.ut.ee/primer3-0.4.0/.

12. **Site for reverse-complement:** The Sequence Manipulation Suite (SMS) software package was used to convert a DNA sequence into a reverse-complement sequence. It is available at http://www.bioinformatics.org/sms/index.html.

13. **MatInspector:** It is a software tool that utilizes a large library of matrix descriptions for transcription factor binding sites in DNA sequences. It is available at https://www.genomatix.de/matinspector/.

Chapter 3: The cell functions of the Ca^{2+} signaling genes *phospholipase C-1*, *Ca^{2+}/H^{+} exchanger-1*, and *secretory phospholipase A_2* in *N. crassa*

3.1 Introduction

The calcium ion (Ca^{2+}) has evolved as a universal second messenger molecule, impacting signaling pathways for almost all biological processes ranging from fertilization to death in all eukaryotes. Therefore, Ca^{2+} is considered a "molecule of life and death" (Berridge et al. 1998; Clapham 2007). The resting concentration of cytosolic free Ca^{2+} ($[Ca^{2+}]_c$) is ~ 10^{-7} M, which is 10^4 times lower than the concentration of Ca^{2+} in the extracellular fluid (Chin and Means 2000). This provides the necessary potential for importing Ca^{2+} into the cells, where Ca^{2+} can act as a secondary messenger molecule (Chin and Means 2000). The $[Ca^{2+}]_c$ level may transiently increase either due to the entry of extracellular Ca^{2+} or its release from internal stores (Chin and Means 2000; Bootman et al. 2001; Clapham 2007). Ca^{2+} plays an essential role in cell signaling, essential for cell survival; however, high concentrations of Ca^{2+} are toxic to the cell (Cerella et al. 2010). Therefore, an effective system for regulating the $[Ca^{2+}]_c$ is very much essential. In eukaryotes, a minute change in the $[Ca^{2+}]_c$ is detected by specific Ca^{2+}-sensing proteins that undergo a change in conformation and charge upon Ca^{2+} binding and initiate the Ca^{2+} signaling processes (Chin and Means 2000; Bootman et al. 2001). The *N. crassa* is an excellent model organism to study the cell functions of the Ca^{2+} signaling proteins. The genome analysis has revealed that the Ca^{2+} signaling machinery in *N. crassa* is complex and comprises of 48 mostly uncharacterized Ca^{2+} signaling proteins, including three Ca^{2+} channel proteins, nine Ca^{2+}/cation-ATPases, six recognizable Ca^{2+}/H^+ exchangers, two novel putative Ca^{2+}/Na^+ exchangers, four novel phospholipase C-δ subtype (PLC-δ) proteins, 23 Ca^{2+} and/or calmodulin (CaM) binding proteins, and one CaM, and these proteins are involved in triggering various cellular processes (Galagan et al. 2003; Borkovich et al. 2004; Zelter et al. 2004). In *N. crassa*, the Ca^{2+} signaling proteins, phospholipase C (PLC), secretory phospholipase A_2 ($sPLA_2$), and Ca^{2+} exchangers are found to be involved in sensing the increase in $[Ca^{2+}]_c$ (Galagan et al. 2003; Borkovich et al. 2004; Barman and Tamuli 2015, 2017).

The PLC and $sPLA_2$ are phospholipase superfamily of proteins. The membrane-bound phosphoinositide-specific PLC catalyses the hydrolysis of phosphatidylinositol 4, 5-bisphosphate (PIP_2) into two important second messengers, inositol-1, 4, 5-trisphosphate (IP_3), which induces Ca^{2+} release from intracellular Ca^{2+} stores to activate CaM-dependent enzymes, and diacylglycerol (DAG), that binds at the Ca^{2+}-dependent C2 domain and activates protein kinase C (PKC; Berridge and Irvin 1984; Rhee and Bae 1997; Clapham 2007). In some organisms, including filamentous fungi, PLC is required for a variety of cellular activities as well as pathogenicity. In the budding yeast *S. cerevisiae*, Plc1p functions in nutritional and stress-related responses (Flick and Thorner 1993). PLC1 homolog, *plc1-1*, is involved in ammonium sensing and is required for growth in a phosphate-rich medium in the fission yeast *S. pombe* (Fankhauser et al. 1995). In the grey mould fungus *B. cinerea* and citrus fungal pathogen *A. alternata*, PLC1 homolog, is required for vegetative development, conidiation,

germination, and pathogenicity (Schumacher et al. 2008; Tsai and Chung 2014). In the human pathogenic fungus *C. albicans*, the PLC1 homolog, CaPLC1 is an essential gene, and its conditional mutant showed growth sensitivity to osmotic and heat stress, as well as impaired growth in galactose medium (Kunze et al. 2005). CnPlc1, a homolog of the mammalian PI-PLC-δ, is required for pathogenicity and cellular homeostasis in the encapsulated yeast and human pathogen *C. neoformans* (Lev et al. 2013). In the rice-blast fungus *M. oryzae*, PI-PLC-δ isoform MoPLC1 regulates intracellular Ca^{2+} fluxes and is essential for fungal development, appressorium formation, and pathogenicity (Rho et al. 2009). The *plc-1* mutant of *N. crassa*, generated through repeat-induced point mutation (RIP; Selker and Garrett 1988), was viable, but showed reduced growth, aberrant hyphal morphology, greater sensitivity to low extracellular and elevated intracellular Ca^{2+} concentrations, and responded differently to the PLC inhibitor 3-nitrocoumarin (Gavric et al. 2007). Another study found that the *plc-1* knockout mutant had characteristics distinct from the RIP mutant, and PLC-1 plays a function in hyphal tip development in *N. crassa* (Lew et al. 2015).

The sPLA$_2$ are low molecular weight (Mw: 13-19 kDa), Ca^{2+}-dependent extracellular secretory proteins that hydrolyze the *sn*$_2$ ester linkage of glycerophospholipids, resulting in two signaling molecules, free fatty acids (FFAs) and 1-acyl-lysophospholipid (1-acyl-LPL), which regulate numerous biological processes such as atherosclerosis, eicosanoid biosynthesis, host defense, and inflammation in various organisms (Murakami and Kudo 2004; Boilard et al. 2010; Dennis et al. 2011). This family of proteins has a highly conserved region that includes a His-Asp dyad sequence responsible for catalysis and several unique disulphide-bonded Cys residues for their stability (Murakami and Kudo 2004; Schaloske and Dennis 2006; Nakahama et al. 2010). In fungi, the first described sPLA$_2$ was a dual localization protein that plays a role in nutritional limitation in the symbiotic fungus *T. borchii* (Soragni et al. 2001; Cavazzini et al. 2013). In *A. oryzae*, two sPLA$_2$s (sPlaA and sPlaB) have different physiological features. sPlaA shows the highest enzymatic activity for Ca^{2+} under acidic pH with external secretion, whereas the sPlaB has the highest enzyme activity for Ca^{2+} with intracellular localization at a neutral to alkaline pH (Nakahama et al. 2010). In response to carbon deprivation, heat shock, oxidative stress, and during or after conidiation, the sPlaA was found to be significantly upregulated, whereas sPlaB was barely expressed in these conditions (Nakahama et al. 2010). In *N. crassa*, sPLA$_2$ encoded by the NCU06650 gene has an N-terminal signal peptide residue (1-30) presumably for secretion, a highly conserved region (residues 122-153) that includes a catalytic histidine residue, and two disulphide-bonded Cys residues similar to the sPLA$_2$ homolog of *T. borchii* and belongs to the group XIV (GXIV) sPLA$_2$ group of enzymes (Soragni et al. 2001; Barman and Tamuli 2015; Takayanagi et al. 2015). It contains a putative CaM binding site with the amino acid sequence TCHALANVYYAAVREFGRTKGELQ (Borkovich et al. 2004; Barman and Tamuli 2017).

The Ca^{2+} exchangers are another group of Ca^{2+} signaling genes that maintain Ca^{2+} homeostasis during steep increases in intracellular Ca^{2+} induced by environmental changes or signal transduction triggered by events like hormone response, hyperosmotic shock, and response to mating pheromones (Borkovich et al. 2004). Ca^{2+} exchangers function as Ca^{2+} pumps, transferring excess Ca^{2+} out of the cell and into the intracellular Ca^{2+} stores, while simultaneously exchanging positive ions across membranes (Zelter et al. 2004; Tamuli et al. 2013). To transport Ca^{2+} across intracellular membranes, all the Ca^{2+} exchangers possess conserved Ca^{2+} exchanger domains (Galagan et al. 2003; Borkovich et al. 2004; Zelter et al. 2004; Tamuli et al. 2013). The *cpe-1* gene (NCU06366) encodes a putative Ca^{2+}/H^{+} exchanger involved in maintaining intracellular levels of Ca^{2+} and is significantly different from homologs found in *S. cerevisiae* and *M. grisea* in a phylogenetic analysis (Zelter et al. 2004).

Previously, *N. crassa* homologs of the PLC-1, CPE-1, and sPLA$_2$ have been shown to play a role in Ca^{2+} homeostasis, carotenoid accumulation, conidiation, and stress survival (Barman and Tamuli 2015, 2017). Moreover, the *plc-1* genetically interacts with *cpe-1* and *splA*$_2$ during vegetative and sexual development in *N. crassa* (Barman and Tamuli 2017). In this study, I examined how these three Ca^{2+} signaling genes regulate various cell processes in *N. crassa*. Because the Ca^{2+} signaling proteins interact to maintain Ca^{2+} homeostasis and other signaling processes, I also studied the genetic interaction of the *plc-1*, *cpe-1*, and *splA*$_2$ genes in regulating various cell functions in *N. crassa*.

3.2 Results

3.2.1 Circadian Regulated Conidiation Assay

3.2.1.1 The *plc-1* gene, but not *cpe-1* and *splA*$_2$, regulates the period length in *N. crassa*

Circadian rhythms are ubiquitous biological oscillations with an approximately 24 h period. This rhythm is affected by various abiotic factors, including light and temperature. The extracellular signals, mediated by Ca^{2+} and cAMP affect the circadian clock in mammals (O'Neill and Reddy 2012). The model filamentous fungus *N. crassa*, which has a unique Ca^{2+} signaling machinery, displays circadian rhythm during the vegetative developmental program (Nakashima 1981; Bell-Pederson et al. 1992; Aronson et al. 1994). Therefore, I investigated the role of the *plc-1*, *cpe-1*, and *splA*$_2$ genes in regulating the period length in constant darkness at three different temperatures (20 °C, 25 °C, and 30 °C). In *N. crassa*, the asexual conidiation occurs every 22 h completing one circadian rhythm (Liu and Bell-Pedersen 2006). The period lengths of the *ras-1*^{bd} and the mutants were calculated as described in Materials and Methods (Table 3.1; Fig. 3.1). In the *N. crassa* wild-type (WT) strain, rhythmic conidiation is suppressed due to the accumulation of CO_2, a respiratory by-product. Therefore, all strains used for this study carry the *ras-1*^{bd} allele (Appendix II), allowing clear visualization of conidial bands despite CO_2 accumulation without affecting the clock mechanism (Sargent and Kaltenborn 1972;

Belden et al. 2007). The *ras-1*^{bd}, known as *band* (*bd*) mutant, has a T79I point mutation in *ras-1* and has a period length of ~ 22.4 h at 25 °C (Belden et al. 2007). The period length of the clock in the *ras-1*^{bd} control strain is longer at 20 °C and shorter at 30 °C than at 25 °C (Gardner and Feldman 1981; Table 3.1; Fig. 3.1). The Δ*plc-1* exhibited altered period length at 20 °C and 25 °C compared to the *ras-1*^{bd} strain. At both temperatures of 20 °C and 25 °C, the Δ*plc-1* mutant displayed period lengthening, whereas Δ*cpe-1* and Δ*splA*$_2$ mutants did not show significant period length changes in either temperature (Table 3.1; Fig. 3.1). The *plc-1* was previously found to genetically interact with *cpe-1* and *splA*$_2$ in *N. crassa* (Barman and Tamuli 2017); therefore, I tested if this interaction also regulates the period length. The Δ*plc-1*; Δ*cpe-1* and Δ*plc-1*; Δ*splA*$_2$ double mutants had extended periods at 20 °C and 25 °C relative to the *ras-1*^{bd} strain, while the Δ*cpe-1*; Δ*splA*$_2$ double mutant did not show much period length changes suggesting the clock phenotype is independent of the *cpe-1* and *splA*$_2$ interaction (Table 3.1; Fig. 3.1). These results suggested that the *plc-1* gene is epistatic to both *cpe-1* and *splA*$_2$ for period length at 20 °C and 25 °C. Taken together, *plc-1*, but not *cpe-1* or *splA*$_2$, plays a vital role in regulating the period length in *N. crassa*.

Table 3.1: Period length of the Δ*plc-1*, Δ*cpe-1*, Δ*splA*$_2$ single and double mutants at different temperatures

Strains	[+]Period length ± SD (h)		
	20 ºC	**25 ºC**	**30 ºC**
ras-1^{bd}	23.5 ± 0.1	22.0 ± 0.2	20.4 ± 0.1
Δ*plc-1* (60)	25.2 ± 0.1 (***)	23.4 ± 0.2 (***)	19.7 ± 0.2 (**)
Δ*cpe-1* (74)	23.5 ± 0.3	21.3 ± 0.2 (**)	19.6 ± 0.1 (***)
Δ*splA*$_2$ (4)	23.3 ± 0.6	21.4 ± 0.2 (**)	20.0 ± 0.3
Δ*plc-1*; Δ*cpe-1* (3)	24.5 ± 0.3 (**)	23.4 ± 0.3 (**)	20.9 ± 0.1 (**)
Δ*plc-1*; Δ*splA*$_2$ (37)	24.3 ± 0.2 (**)	23.5 ± 0.5 (**)	20.8 ± 0.9
Δ*cpe-1*; Δ*splA*$_2$ (73)	23.3 ± 0.4 (*)	22.0 ± 0.3	20.1 ± 0.4

[+]Results are shown as mean ± standard deviation for three independent experiments (n = 3) with *P-values* < 0.05 (*), < 0.01 (**), and < 0.001 (***) compared with the *ras-1*^{bd} strain as measured by a one-way ANOVA test. The number in parentheses represent the progeny which carries the knockout alleles in the *ras-1*^{bd} background for each of the single and double mutants as described in Appendix II.

(A)

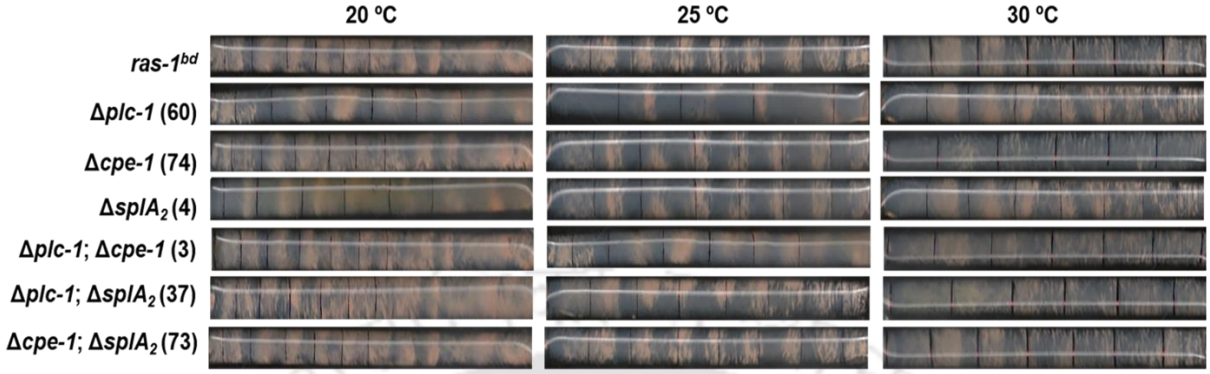

(B)

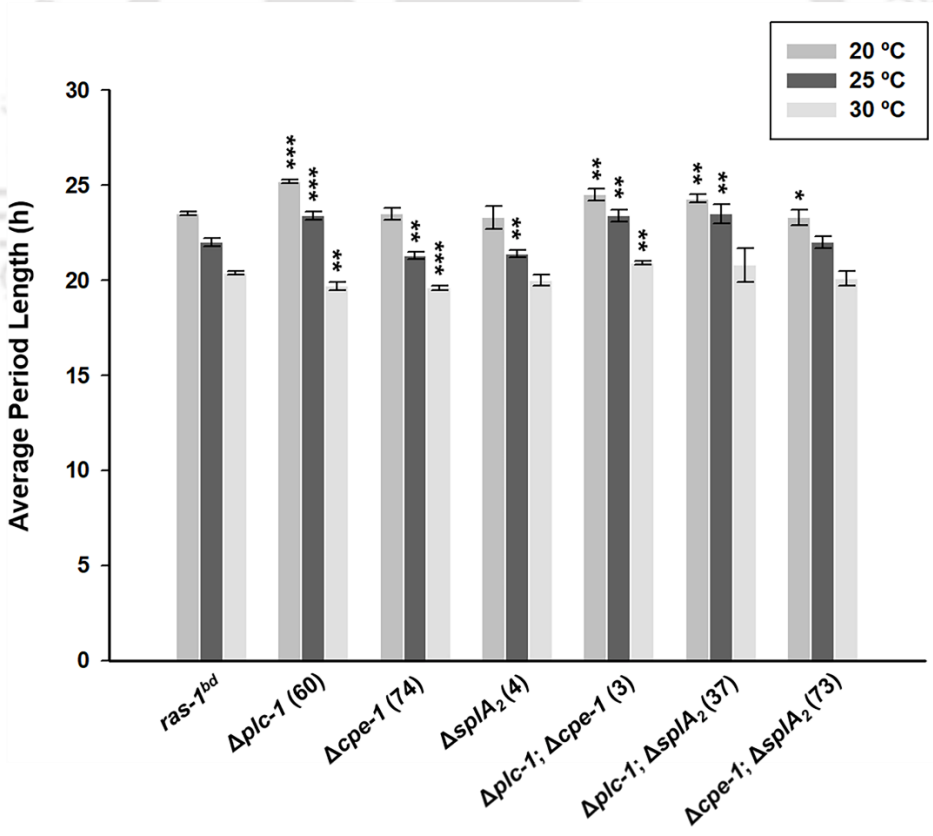

Figure 3.1: Circadian regulated conidiation assay of the *ras-1*^{bd} and the Δ*plc-1*, Δ*cpe-1*, Δ*splA*$_2$ single mutants and their double mutants. (A) The *ras-1*^{bd}, Δ*plc-1*, Δ*cpe-1*, Δ*splA*$_2$ single mutants and their double mutants were assayed for circadian regulated conidiation at 20 °C, 25 °C, and 30 °C using race tubes. The growth front was marked every 24 h, shown by the black lines, and the conidial bands

are seen as the orange bands. **(B)** A plot showing the period length of the *ras-1*^{bd} and the Δ*plc-1*, Δ*cpe-1*, Δ*splA*$_2$ single mutants and their double mutants under circadian regulated conidiation conditions at 20 °C, 25 °C, and 30 °C. Error bars indicate standard deviations calculated from the data for three independent experiments (n = 3). Asterisks indicate statistically significant values, **P<0.05*, ***P<0.01*, ****P<0.001*.

3.2.1.2 Loss of PLC-1 influences temperature compensation in *N. crassa*

Because period length shows temperature compensation over the physiological range of temperature, I also determined the Q_{10} values to investigate the role of the *plc-1*, *cpe-1*, and *splA*$_2$ genes in temperature compensation. The circadian clock has a free-running period that operates at approximately the same rate over a wide range of temperatures, a phenomenon known as temperature compensation and described as Q_{10} (Pittendrigh 1960; Sorek and Levy 2012; Avello et al. 2019). In general, circadian rhythms have Q_{10} ranging between 0.8 – 1.2 (Saunders 1977; Mattern et al. 1982). The Q_{10} value ranged between 0.8 – 1.2 for the strains lacking *cpe-1* and *splA*$_2$, indicating that the circadian clock in these mutants shows temperature compensation (Table 3.2). However, the Q_{10} value was 1.41 for the Δ*plc-1* mutant between 25 °C and 30 °C, suggesting a loss of temperature compensation of the circadian clock in this mutant in this temperature range (Table 3.2). The Q_{10} values of the Δ*plc-1*; Δ*cpe-1*, Δ*plc-1*; Δ*splA*$_2$, and Δ*cpe-1*; Δ*splA*$_2$ double mutants remained within the range, suggesting their genetic interaction has no role in temperature compensation (Table 3.2).

Table 3.2: Q_{10} values of the Δ*plc-1*, Δ*cpe-1*, Δ*splA*$_2$ single mutants and their double mutants at different temperature range

Strains	Q_{10} values		
	T_1 = 20 °C, T_2 = 25 °C	T_1 = 25 °C, T_2 = 30 °C	T_1 = 20 °C, T_2 = 30 °C
ras-1^{bd}	1.14	1.16	1.15
Δ*plc-1* (60)	1.16	**1.41**	1.28
Δ*cpe-1* (74)	1.22	1.18	1.20
Δ*splA*$_2$ (4)	1.18	1.14	1.20
Δ*plc-1*; Δ*cpe-1* (3)	1.10	1.25	1.17
Δ*plc-1*; Δ*splA*$_2$ (37)	1.07	1.28	1.17
Δ*cpe-1*; Δ*splA*$_2$ (73)	1.12	1.20	1.16

Calculation of Q_{10}: $Q_{10} = (R_2/R_1)^{10/(T2-T1)}$

R_1 and R_2 are frequency of period lengths at T_1 and T_2 temperatures, respectively (Sorek and Levy 2012). Q_{10} for normal circadian rhythms ranges from 0.8 – 1.2 (Saunders 1977; Mattern et al. 1982). Bold font indicates a loss of temperature compensation in a strain at the given temperatures.

3.2.2 Thermotolerance Assay

3.2.2.1 The Δ*plc-1*, Δ*cpe-1*, Δ*splA*$_2$ single and double mutants showed sensitivity to the heat shock condition

Previous studies on heat shock proteins have shown that the cytosolic Ca^{2+} participates in heat shock signal transduction and regulates downstream events in filamentous fungi (Kapoor et al. 1990); therefore, I investigated the role of *plc-1*, *cpe-1*, and *splA*$_2$ genes in the acquisition of thermotolerance. Induced thermotolerance is the increased survival of cells pre-incubated at a sub-lethal heat shock temperature followed by exposure to a lethal temperature. In contrast, uninduced thermotolerance is the survival of cells on exposure to a lethal temperature without pre-incubation at a sub-lethal heat shock temperature (Kapoor et al. 1990). Heat shock proteins are produced when *N. crassa* cells are exposed to sub-lethal heat shock temperatures, thereby protecting the cells from death (Kapoor et al. 1995; Yang and Borkovich 1999). I determined the survival of the WT, Δ*plc-1*, Δ*cpe-1*, and Δ*splA*$_2$ single mutants and their double mutants on exposure to a lethal temperature (52 °C) with and without pre-exposure to a sub-lethal heat shock temperature of 44 °C. The number of viable colonies was counted, and the percent survival was determined as discussed earlier in Materials and Methods (Chapter 2). The Δ*plc-1*, Δ*cpe-1*, and Δ*splA*$_2$ mutants showed reduced survival percentages than the

WT under induced thermotolerance condition (Table 3.3; Fig. 3.2). In contrast, survival of the Δ*cpe-1* and Δ*splA*$_2$ was marginally higher than the WT, and no viable colony was observed in the Δ*plc-1* mutant in uninduced thermotolerance condition (Table 3.3; Fig. 3.2). In addition, the Δ*plc-1*; Δ*cpe-1* and Δ*plc-1*; Δ*splA*$_2$ double mutants showed a significant reduction in survival percentage in both induced and uninduced thermotolerance conditions compared to the WT (Table 3.3; Fig. 3.2). However, the survival percentage of Δ*cpe-1*; Δ*splA*$_2$ double mutant during heat shock temperatures was comparable to the WT (Table 3.3; Fig. 3.2). Furthermore, the *plc-1*, *cpe-1*, and *splA*$_2$ homokaryotic strains displayed survival percentages similar to the WT under both induced and uninduced thermotolerance and complemented the mutant phenotype (Table 3.3; Fig. 3.2). These findings suggested that the *plc-1*, *cpe-1*, and *splA*$_2$ genes might play a role in survival at lethal temperatures. Moreover, *plc-1* genetically interacts with *cpe-1* and *splA*$_2$ in acquiring induced thermotolerance, possibly to induce the heat shock proteins for cell survival.

Table 3.3: Percent survival of the WT, Δ*plc-1*, Δ*cpe-1*, Δ*splA*$_2$ mutants, and the homokaryotic transformants after heat shock

Strains	[+]Percent survival upon exposure to heat shock (52 ºC)	
	Induced (44 ºC)	**Uninduced (30 ºC)**
WT	72.5 ± 2.9	0.31 ± 0.12
Δ*plc-1*	53.7 ± 2.5 (***)	0.12 ± 0.03
Δ*cpe-1*	55.8 ± 2.8 (**)	1.90 ± 0.31
Δ*splA*$_2$	47.7 ± 3.3 (***)	1.43 ± 0.31
Δ*plc-1*; Δ*cpe-1*	51.2 ± 1.0 (***)	0.77 ± 0.28
Δ*plc-1*; Δ*splA*$_2$	52.7 ± 2.3 (***)	0.16 ± 0.06
Δ*cpe-1*; Δ*splA*$_2$	73.02 ± 2.5	1.53 ± 0.33
P$_{ccg-1}$::*plc-1*::*gfp*	76.4 ± 0.89	1.77 ± 0.82
P$_{ccg-1}$::*cpe-1*::*gfp*	74.9 ± 1.7	1.16 ± 0.06
P$_{ccg-1}$::*splA*$_2$::*gfp*	75.1 ± 1.2	1.43 ± 0.33

[+]Results are shown as mean ± standard deviation for three independent experiments (n = 3) with *P-values* < 0.05 (*), < 0.01 (**), and < 0.001 (***) compared with the WT strain as measured by a one-way ANOVA test.

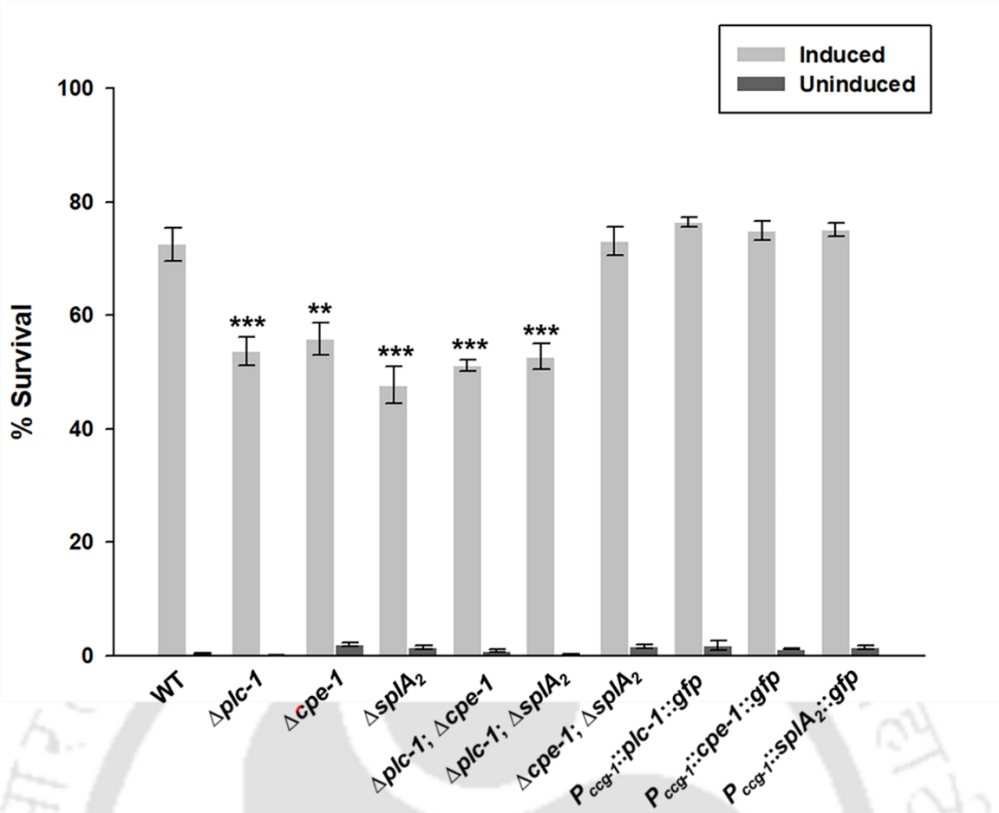

Figure 3.2: Thermotolerance assay of the WT, Δ*plc-1*, Δ*cpe-1*, Δ*splA*$_2$ mutants, and the homokaryotic transformant strains. Viability of the WT, Δ*plc-1*, Δ*cpe-1*, Δ*splA*$_2$ mutants, and the homokaryotic transformant strains after exposure to 52 °C lethal temperature with (induced) and without (uninduced) pre-exposure to a sub-lethal heat shock temperature of 44 °C. Error bars indicate the standard deviations calculated from the data for three independent experiments (n = 3). Asterisks indicate statistically significant values, *$P<0.05$, **$P<0.01$, ***$P<0.001$.

3.2.3 pH Tolerance Assay

3.2.3.1 The Δ*plc-1*, Δ*cpe-1*, and Δ*splA*$_2$ single and double mutants are sensitive to alkaline pH condition

The extracellular pH is an environmental condition to which any microorganism needs to adapt. The stress response induced by a change in the extracellular pH triggers a signal transduction pathway in several fungi, including *N. crassa* (Virgilio et al. 2016). In *N. crassa*, the alkaline pH signaling pathway crosstalks with the Ca^{2+} signaling pathway (Virgilio et al. 2017). Alkaline pH also regulates the expression of *calcineurin responsive zinc finger-1* (*crz-1*), a major downstream target of the Ca^{2+} signaling pathway in *N. crassa* (Virgilio et al. 2017). The *plc-1*, *cpe-1*, and *splA*$_2$ genes are essential for maintaining Ca^{2+} homeostasis and survival during stress conditions in *N. crassa* (Barman and Tamuli 2015, 2017). I performed a pH tolerance assay to investigate the effect of extracellular pH on the WT,

Δ*plc-1*, **Δ*cpe-1***, **Δ*splA*$_2$** single and double mutants. Aerial hyphae development of the strains was determined under acidic and alkaline conditions by inoculating ~ 10^6 conidia in VM liquid media with different pH conditions (pH 3.8, 4.8, 5.8, 6.8, and 7.8), and incubating the cultures at 30 °C under constant darkness for three days and then under light for four days. *N. crassa* grows optimally at an ambient pH of 5.8, and this was used as the control pH condition in this study. Under the acidic pH conditions, the Δ*plc-1*, Δ*cpe-1*, and Δ*splA*$_2$ single and their double mutants showed normal growth of aerial hyphae (Table 3.4; Fig. 3.3). At alkaline pH conditions, WT and the mutants showed decreased aerial hyphae growth compared to that in the ambient pH condition. However, at pH 7.8, the Δ*plc-1*, Δ*cpe-1*, Δ*splA*$_2$, Δ*plc-1*; Δ*cpe-1*, Δ*plc-1*; Δ*splA*$_2$, and Δ*cpe-1*; Δ*splA*$_2$ mutants showed severely reduced aerial hyphae compared to the WT (Table 3.4; Fig. 3.3). In addition, the $P_{ccg\text{-}1}$::*plc-1*::*gfp*, $P_{ccg\text{-}1}$::*cpe-1*::*gfp*, and $P_{ccg\text{-}1}$::*splA*$_2$::*gfp* homokaryotic transformant strains displayed aerial hyphae growth similar to the WT strain and rescued the growth defects of the Δ*plc-1*, Δ*cpe-1*, and Δ*splA*$_2$ mutants under alkaline pH conditions (Table 3.4; Fig. 3.3). These results suggested that *plc-1*, *cpe-1*, and *splA*$_2$ are necessary for alkaline pH stress tolerance. In addition, *plc-1*, *cpe-1*, and *splA*$_2$ might positively interact in the pH regulating pathway under alkaline conditions. In addition, normal growth phenotype of the *N. crassa* strains in the acidic conditions indicate that these genes are dispensable for survival under the acidic pH condition (Table 3.4; Fig. 3.3).

Table 3.4: Average aerial hyphae height (%) of the WT, Δ*plc-1*, Δ*cpe-1*, Δ*splA*$_2$ mutants, and the homokaryotic transformants under acidic and alkaline pH

Strains	[+]Average aerial hyphae height (%) in VM with different pH				
	3.8	**4.8**	**5.8**	**6.8**	**7.8**
WT	102.06 ± 5.58	98.15 ± 15.77	100 ± 0.00	80.86 ± 3.55 (***)	82.19 ± 6.44 (**)
Δ*plc-1*	100.22 ± 9.52	106.70 ± 10.72	100 ± 0.00	68.45 ± 8.12 (**)	59.54 ± 6.21 (***)
Δ*cpe-1*	102.60 ± 3.00	96.81 ± 14.83	100 ± 0.00	58.70 ± 8.71 (**)	46.86 ± 7.68 (***)
Δ*splA*$_2$	100.06 ± 11.29	96.93 ± 9.08	100 ± 0.00	53.75 ± 2.79 (***)	40.83 ± 3.00 (***)
Δ*plc-1*; Δ*cpe-1*	91.64 ± 8.57	85.46 ± 9.34 (*)	100 ± 0.00	37.25 ± 3.92 (***)	20.98 ± 3.05 (***)
Δ*plc-1*; Δ*splA*$_2$	90.11 ± 10.53	98.35 ± 5.33	100 ± 0.00	67.37 ± 3.53 (***)	38.24 ± 1.30 (***)
Δ*cpe-1*; Δ*splA*$_2$	97.94 ± 4.75	97.78 ± 7.78	100 ± 0.00	62.92 ± 4.53 (***)	50.53 ± 7.19 (***)

P$_{ccg-1}$::*plc-1*::*gfp*	95.93 ± 2.47 (*)	95.66 ± 2.08 (*)	100 ± 0.00	94.85 ± 2.09 (*)	87.56 ± 3.28 (**)
P$_{ccg-1}$::*cpe-1*::*gfp*	94.42 ± 1.41 (**)	97.08 ± 2.01	100 ± 0.00	93.12 ± 2.22 (**)	83.04 ± 3.88 (**)
P$_{ccg-1}$::*splA*$_2$::*gfp*	106.69 ± 7.98	106.73 ± 8.9	100 ± 0.00	88.33 ± 4.77 (*)	87.22 ± 5.45 (*)

[+]Results are shown as mean ± standard deviation for three independent experiments (n = 3) with *P-values* < 0.05 (*), < 0.01 (**), and < 0.001 (***) compared with the control condition (pH 5.8) as measured by a one-way ANOVA test.

(A)

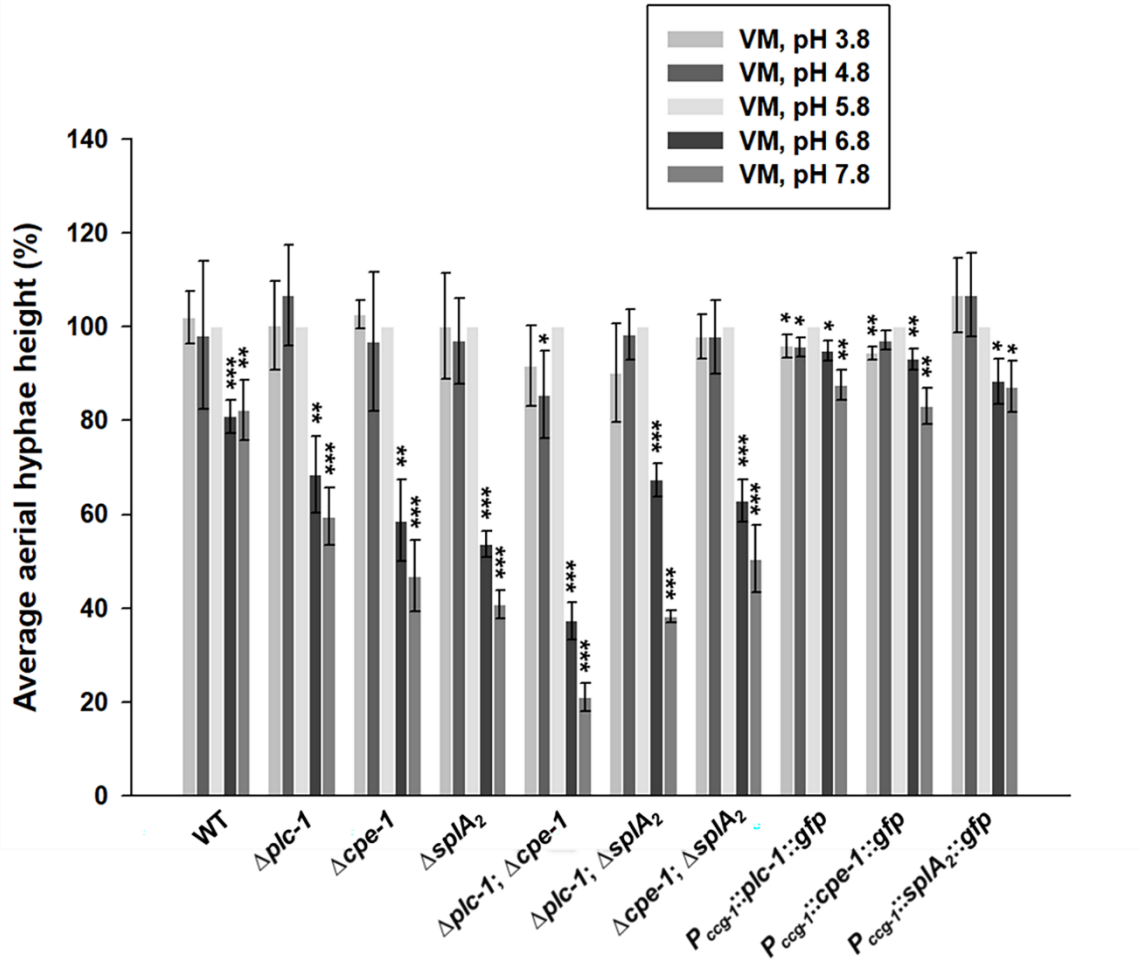

(B)

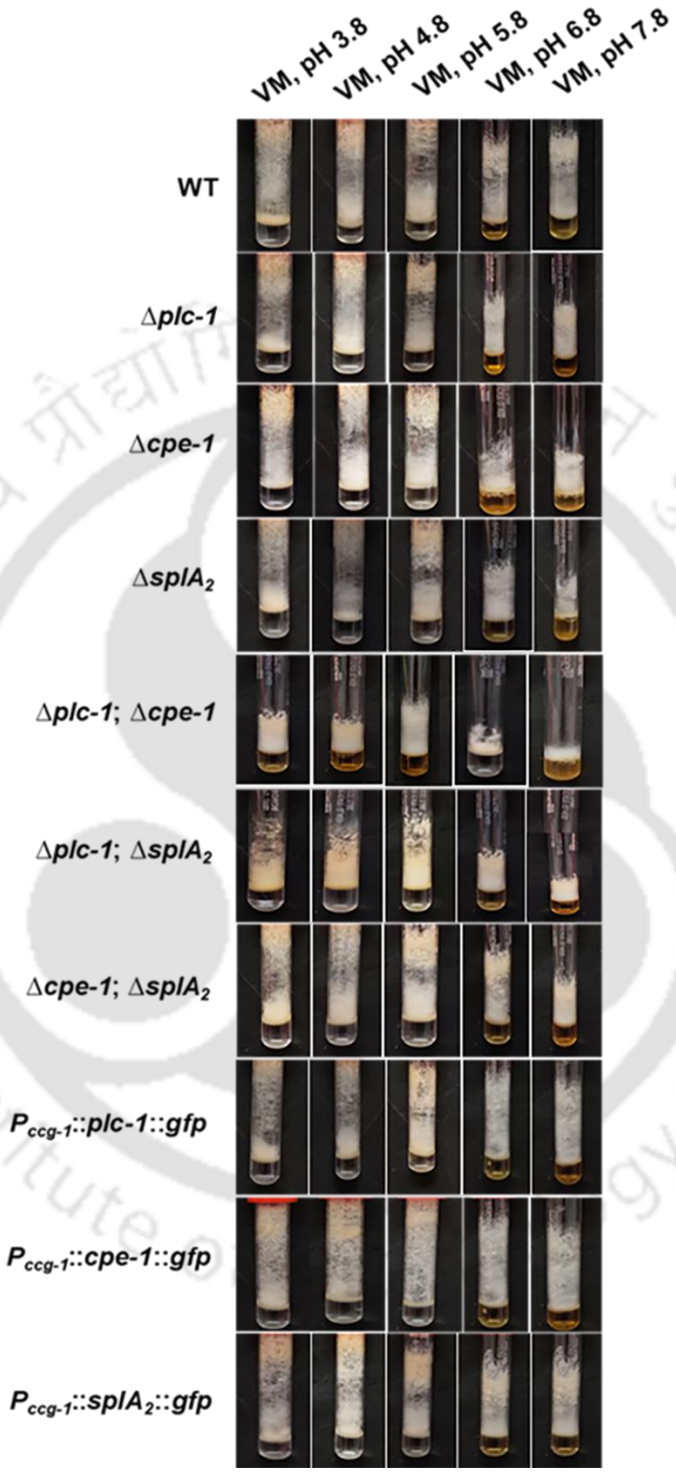

Figure 3.3: The pH tolerance assay of the WT, Δ*plc-1*, Δ*cpe-1*, Δ*splA*$_2$ mutants, and the homokaryotic transformant strains under acidic and alkaline pH conditions. (A) Plot showing the aerial hyphae height (%) in the WT, Δ*plc-1*, Δ*cpe-1*, and Δ*splA*$_2$ single and double mutants, and the homokaryotic transformant strains under acidic and alkaline pH conditions. **(B)** Aerial hyphae of the

WT, Δ*plc-1*, Δ*cpe-1*, Δ*splA*$_2$ single and their double mutant, and the homokaryotic transformant strains in Vogel's Minimal medium (VM) with pH 3.8, 4.8, 5.8, 6.8, and 7.8 (arranged in the columns from left to right). The cultures were incubated at 30 °C for three days, then at room temperature for four days under light, before being photographed. Asterisks indicate statistically significant values, *$P<0.05$, **$P<0.01$, ***$P<0.001$.

3.2.4 Cell Wall Stress Assay

3.2.4.1 The Δ*plc-1*, Δ*cpe-1*, and Δ*splA*$_2$ single and double mutants are insensitive to cell wall stress drugs

The cell wall is an indispensable component of filamentous fungi that safeguards the cell against environmental stresses and enables the cell to assess environmental changes (Maddi et al. 2012). As Δ*plc-1*, Δ*cpe-1*, and Δ*splA*$_2$ mutants were more sensitive to heat stress and alkaline pH, *plc-1*, *cpe-1*, and *splA*$_2$ may play a role in cell wall integrity in *N. crassa*. To test this hypothesis, I examined the growth of the Δ*plc-1*, Δ*cpe-1*, and Δ*splA*$_2$ mutants on VM agar media containing the cell wall stress drugs Congo Red (1 mg/ml) and SDS (0.01%), both of which bind chitin and inhibit chitin-glucan cross-linking (Maddi et al. 2012). However, the Δ*plc-1*, Δ*cpe-1*, and Δ*splA*$_2$ single and double mutants were resistant to these agents (Table 3.5; Fig. 3.4).

Table 3.5: Average colony growth rate (%) of the WT, Δ*plc-1*, Δ*cpe-1*, Δ*splA*$_2$ single and double mutant strains in the presence of cell wall stress drugs

Strains	[+]Percent growth in the presence of cell wall stress drugs		
	VM	**Congo Red**	**SDS**
WT	100 ± 0.00	59.58 ± 01.26 (***)	64.94 ± 08.21 (**)
Δ*plc-1*	100 ± 0.00	59.52 ± 10.29 (**)	66.40 ± 11.47 (**)
Δ*cpe-1*	100 ± 0.00	60.97 ± 07.15 (***)	66.77 ± 01.64 (***)
Δ*splA*$_2$	100 ± 0.00	68.57 ± 06.35 (***)	60.18 ± 11.46 (**)
Δ*plc-1*; Δ*cpe-1*	100 ± 0.00	69.89 ± 07.08 (**)	61.72 ± 02.92 (***)
Δ*plc-1*; Δ*splA*$_2$	100 ± 0.00	65.00 ± 06.92 (***)	59.84 ± 02.76 (***)
Δ*cpe-1*; Δ*splA*$_2$	100 ± 0.00	68.39 ± 12.97 (*)	61.93 ± 05.62 (***)

[+]Results are shown as mean ± standard deviation for three independent experiments (n = 3) with *P-values* < 0.05 (*), < 0.01 (**), and < 0.001 (***) compared with the control condition (VM without drug) as measured by a one-way ANOVA test.

(A)

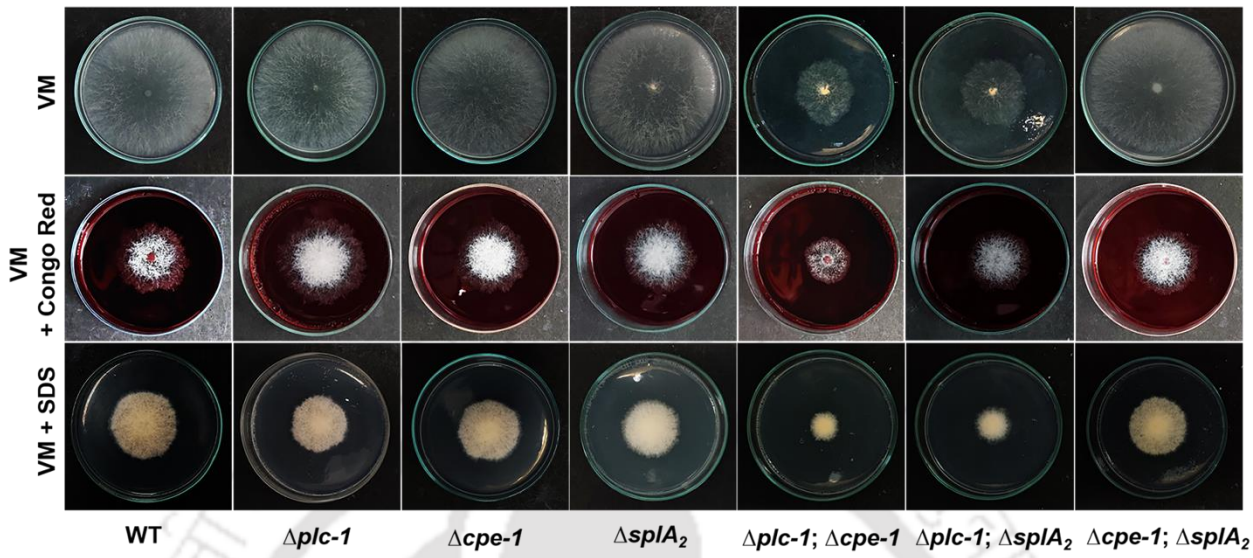

(B)

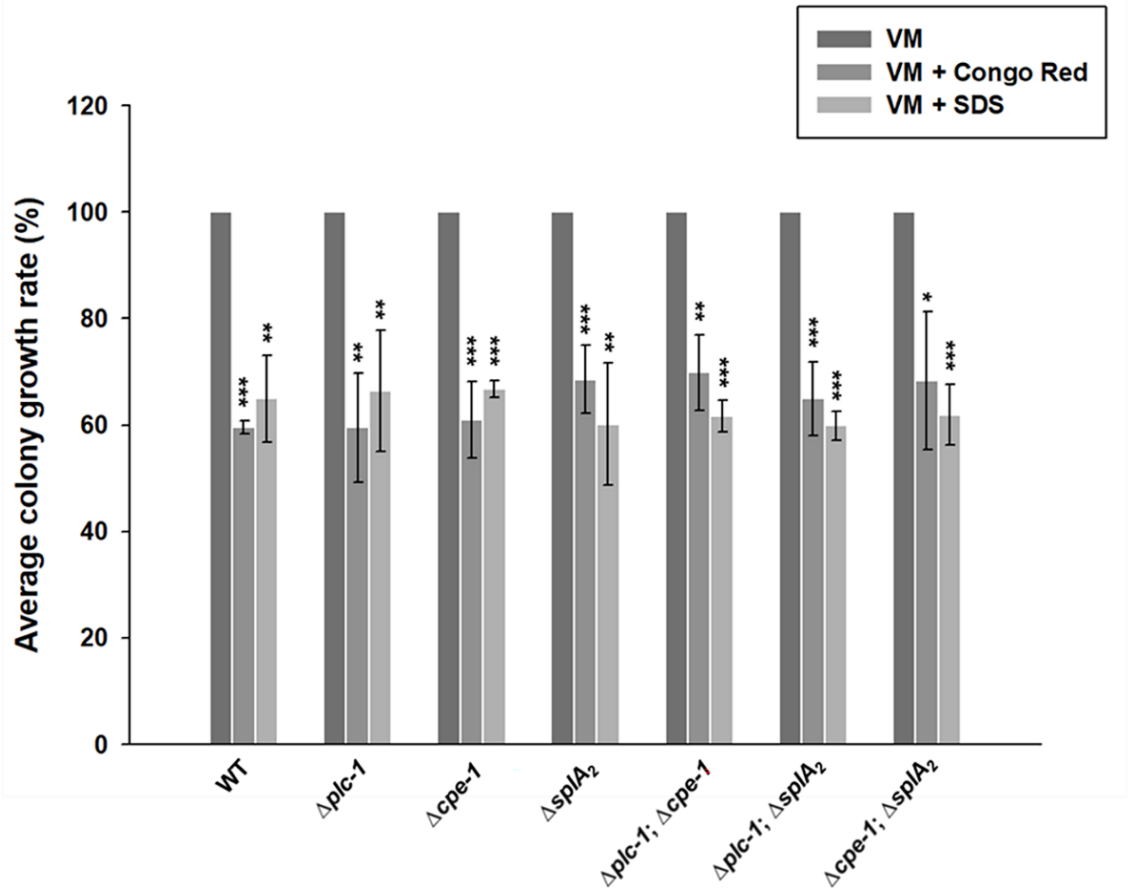

Figure 3.4: Cell wall stress assay of the WT, Δ*plc-1*, Δ*cpe-1*, Δ*splA*$_2$ single and double mutant strains. (A) Colony growth of the WT, Δ*plc-1*, Δ*cpe-1*, Δ*splA*$_2$ single and double mutant strains when grown in the presence of cell wall stress drugs, Congo Red and SDS. **(B)** Graph showing the average colony growth rate (%) of the WT, Δ*plc-1*, Δ*cpe-1*, Δ*splA*$_2$ single and double mutant strains when grown in the presence of cell wall stress drugs, Congo Red and SDS. Asterisks indicate statistically significant values, *$P<0.05$, **$P<0.01$, ***$P<0.001$.

3.2.5 Endoplasmic Reticulum (ER) Stress Assay

3.2.5.1 The Δ*splA*$_2$ mutant showed a growth defect in response to ER stress

The ER plays a central role in the correct folding and maturation of the membrane and secretory proteins. The protein folding capacity of ER is transiently saturated when it encounters excessive protein flux or intractable heterologous proteins, resulting in a secretory route traffic jam that causes ER stress (Ron and Walter 2007; Hetz 2012). The ER activates the signal transduction pathway in response to the accumulation of unfolded proteins in its lumen, a mechanism known as the unfolded protein response (UPR; Bravo et al. 2012). To examine the role of *plc-1*, *cpe-1*, and *splA*$_2$ genes in the ER stress response, the WT, Δ*plc-1*, Δ*cpe-1*, and Δ*splA*$_2$ single and their double mutants were treated with various concentrations (0 mM, 0.5 mM, 1 mM, and 2 mM) of ER stress inducing agent dithiothreitol (DTT), which prevents disulphide bond formation, and development of aerial hyphae in the strains were observed. The Δ*splA*$_2$ single mutant displayed reduced aerial hyphae growth at 2 mM DTT (Table 3.6; Fig. 3.5). In addition, the Δ*plc-1*; Δ*cpe-1* and Δ*plc-1*; Δ*splA*$_2$ double mutants had shorter aerial hyphae at 0.5 mM DTT (Table 3.6; Fig. 3.5). However, the WT, Δ*plc-1*, and Δ*cpe-1* single mutants showed no growth abnormalities at 2 mM DTT (Table 3.6; Fig. 3.5). In addition, the $P_{ccg\text{-}1}$::*plc-1*::*gfp*, $P_{ccg\text{-}1}$::*cpe-1*::*gfp*, and $P_{ccg\text{-}1}$::*splA*$_2$::*gfp* homokaryotic strains behaved like the WT at 2 mM DTT (Table 3.6; Fig. 3.5). Thus, this data revealed that *splA*$_2$ plays a role in the ER response pathway and that *plc-1* is epistatic to *cpe-1* and *splA*$_2$ for survival under the ER stress condition.

Table 3.6: Average aerial hyphae height (%) of the WT, Δ*plc-1*, Δ*cpe-1*, Δ*splA*$_2$ mutants and homokaryotic transformants in response to ER stress

Strains	[+]Average aerial hyphae height (%) in the presence of DTT			
	0 mM	**0.5 mM**	**1 mM**	**2 mM**
WT	100 ± 0.00	85.32 ± 4.33 (**)	84.71 ± 5.33 (**)	74.12 ± 3.59 (***)
Δ*plc-1*	100 ± 0.00	89.94 ± 9.68	87.42 ± 3.93 (**)	83.65 ± 6.06 (**)
Δ*cpe-1*	100 ± 0.00	90.82 ± 6.54	93.62 ± 6.04	73.24 ± 3.26 (***)
Δ*splA*$_2$	100 ± 0.00	91.72 ± 4.34 (*)	90.40 ± 7.30	43.38 ± 2.19 (***)
Δ*plc-1*; Δ*cpe-1*	100 ± 0.00	72.80 ± 4.60 (***)	61.20 ± 5.64 (***)	48.60 ± 5.18 (***)
Δ*plc-1*; Δ*splA*$_2$	100 ± 0.00	58.60 ± 9.87 (**)	55.94 ± 8.69 (***)	49.56 ± 4.52 (***)
Δ*cpe-1*; Δ*splA*$_2$	100 ± 0.00	96.79 ± 4.84	89.11 ± 6.94 (*)	87.31 ± 8.20
P$_{ccg-1}$::*plc-1*::*gfp*	100 ± 0.00	100.23 ± 2.99	95.84 ± 3.91	80.39 ± 3.63 (***)
P$_{ccg-1}$::*cpe-1*::*gfp*	100 ± 0.00	94.30 ± 4.18 (*)	93.23 ± 4.22 (*)	77.28 ± 2.55 (***)
P$_{ccg-1}$::*splA*$_2$::*gfp*	100 ± 0.00	96.13 ± 1.48 (**)	92.46 ± 5.23 (*)	78.71 ± 4.63 (***)

[+]Results are shown as mean ± standard deviation for three independent experiments (n = 3) with *P-values* < 0.05 (*), < 0.01 (**), and < 0.001 (***) compared with the control condition (0 mM) as measured by a one-way ANOVA test.

(A)

(B)

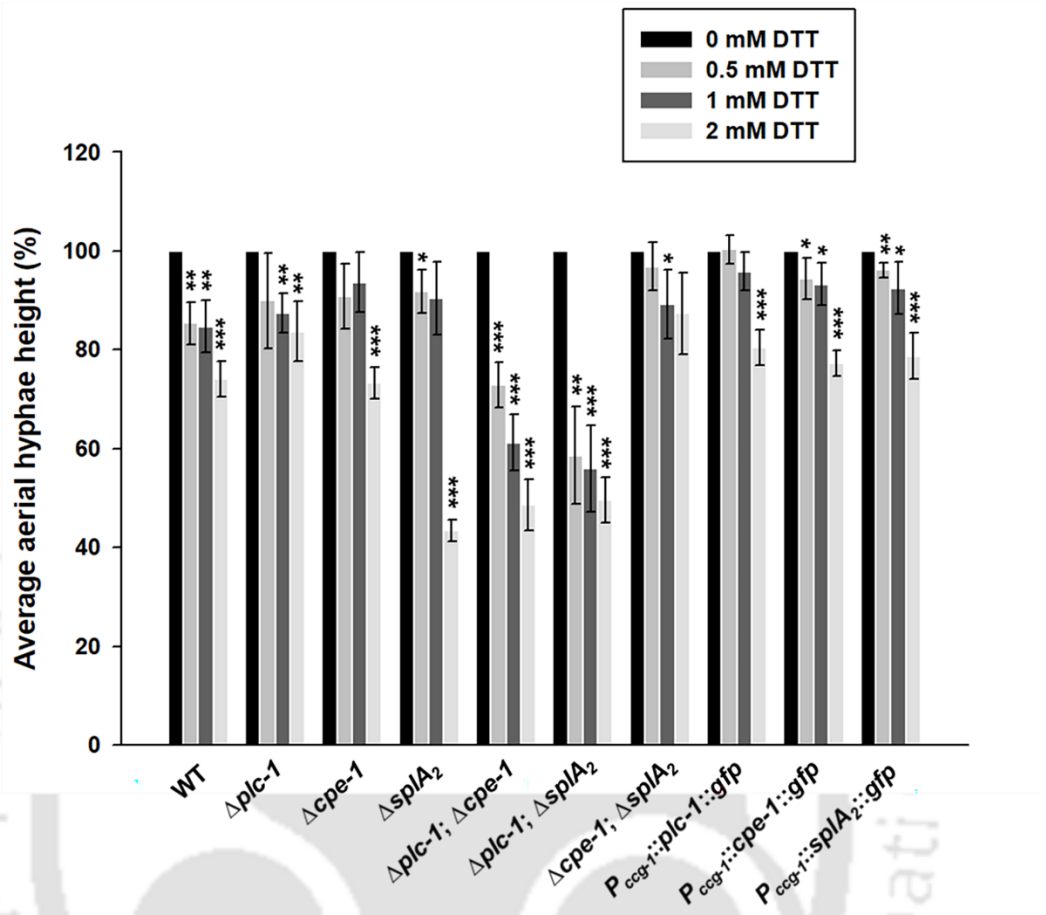

Figure 3.5: ER stress assay of the WT, Δ*plc-1*, Δ*cpe-1*, Δ*splA*$_2$ mutants, and the homokaryotic transformant strains. **(A)** Aerial hyphae of the WT, Δ*plc-1*, Δ*cpe-1*, Δ*splA*$_2$ mutants, and the homokaryotic transformant strains on Vogel's Minimal medium (VM) supplemented with 0 mM, 0.5 mM, 1 mM, and 2 mM DTT. Strains were incubated at 30 °C for three days in the dark, and further incubated at room temperature for four days under light and photographed. **(B)** Plot of average aerial hyphae height (%) in the presence of DTT in the WT, Δ*plc-1*, Δ*cpe-1*, Δ*splA*$_2$ single and double mutants, and the homokaryotic transformant strains. Asterisks indicate statistically significant values, **P<0.05*, ***P<0.01*, ****P<0.001*.

3.2.6 Cellulose Degradation Assay

3.2.6.1 The *splA*$_2$ gene is involved in cellulose degradation in *N. crassa*

Many microorganisms, particularly filamentous fungi, produce hydrolytic enzymes that aid in the degradation of plant cell wall components such as cellulose, hemicellulose, and lignin (Carroll and Somerville 2009). Plant cell wall degrading enzymes from filamentous fungi have been studied for the

development of sustainable and affordable lignocellulosic biofuels. The PLC-1 mediated Ca^{2+} signaling pathway is necessary for the regulation of cellulase overexpression under cellulase-inducing conditions in the filamentous fungus *T. reesei* (Chen et al. 2021). Due to the availability of a nearly complete genome deletion set, *N. crassa* has recently gained importance as a model organism for studying the physiology of lignocellulose degradation in fungi. Therefore, I investigated the ability of the WT, Δ*plc-1*, Δ*cpe-1*, Δ*splA*$_2$ single and their double mutants to utilize cellulose, a natural substrate. Surprisingly, the Δ*splA*$_2$ mutant displayed better cellulose degradation ability than the WT when grown on Vogel's Minimal media with 2% microcrystalline cellulose supplemented as the sole carbon source. The Δ*splA*$_2$ mutant devoured the supplemented amount of microcrystalline cellulose in two days, while the WT required five days (Fig. 3.6A). However, the Δ*plc-1* and Δ*cpe-1* mutants were unable to fully utilize the cellulose till five days. Furthermore, the Δ*plc-1*; Δ*cpe-1* and Δ*plc-1*; Δ*splA*$_2$ double mutants were also unable to utilize microcrystalline cellulose, but the Δ*cpe-1*; Δ*splA*$_2$ double mutant could degrade cellulose like the Δ*splA*$_2$ single mutant (Fig. 3.6A). I also determined the total amount of protein secreted and glucose accumulated in the culture supernatant on days 2 and 5. Both Δ*splA*$_2$ and Δ*cpe-1*; Δ*splA*$_2$ showed higher protein secretion and glucose accumulation in the culture supernatant compared to the WT (Fig. 3.6B, C). In addition, the homokaryotic strains utilize microcrystalline cellulose in a similar manner like the WT; thus, the *plc-1*, *cpe-1*, and *splA*$_2$ alleles complement the mutant phenotype (Fig. 3.6A). The protein secretion and amount of extracellular glucose produced in the homokaryotic strains were also similar to the WT (Fig. 3.6B, C).

(A)

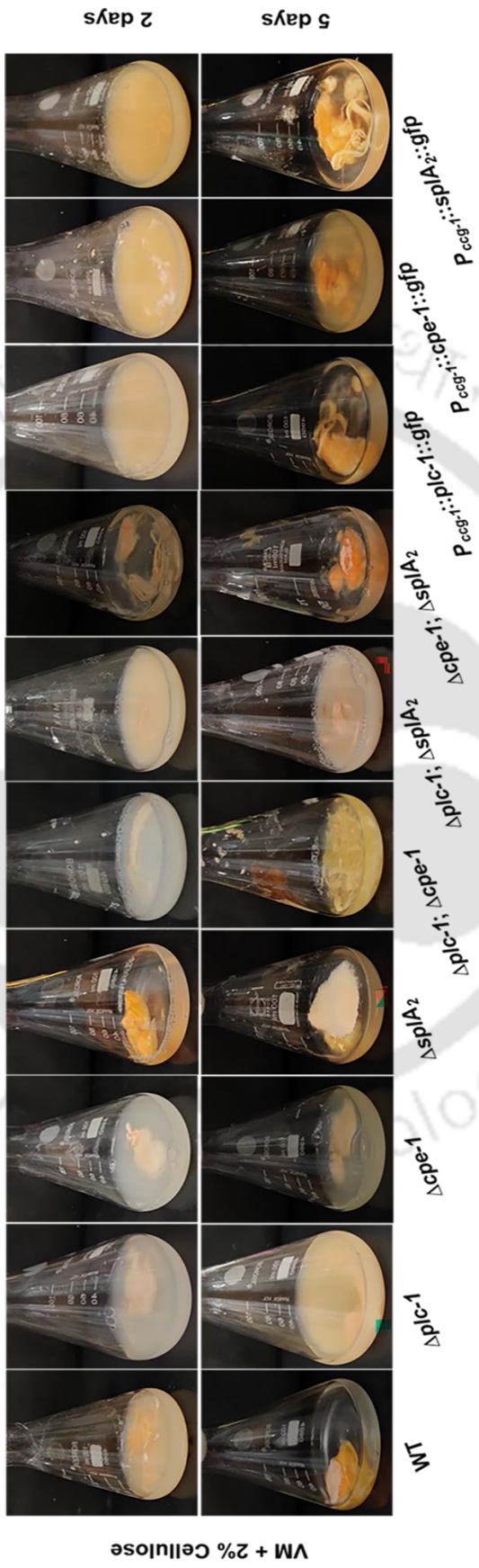

(B)

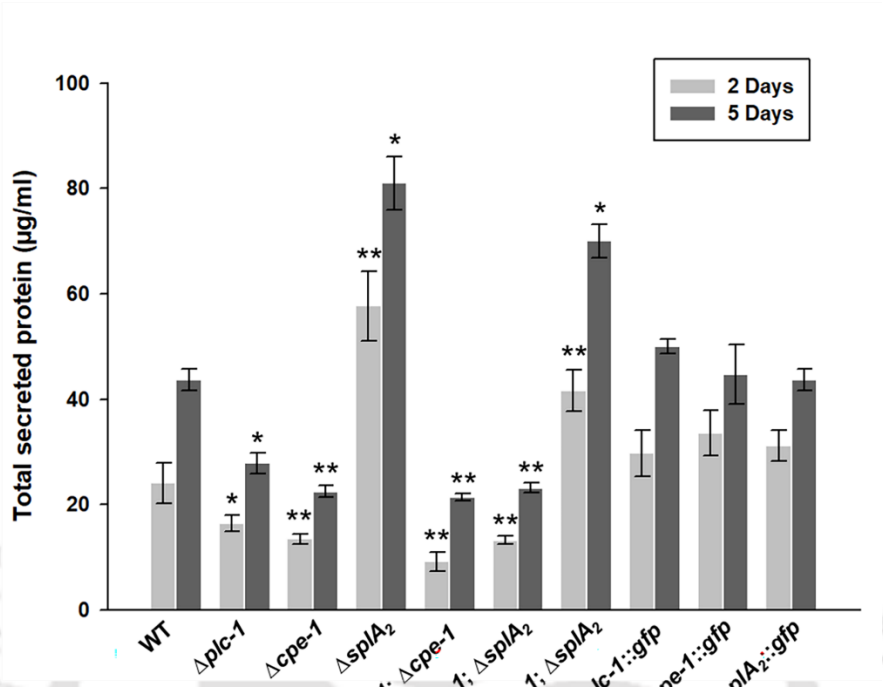

(C)

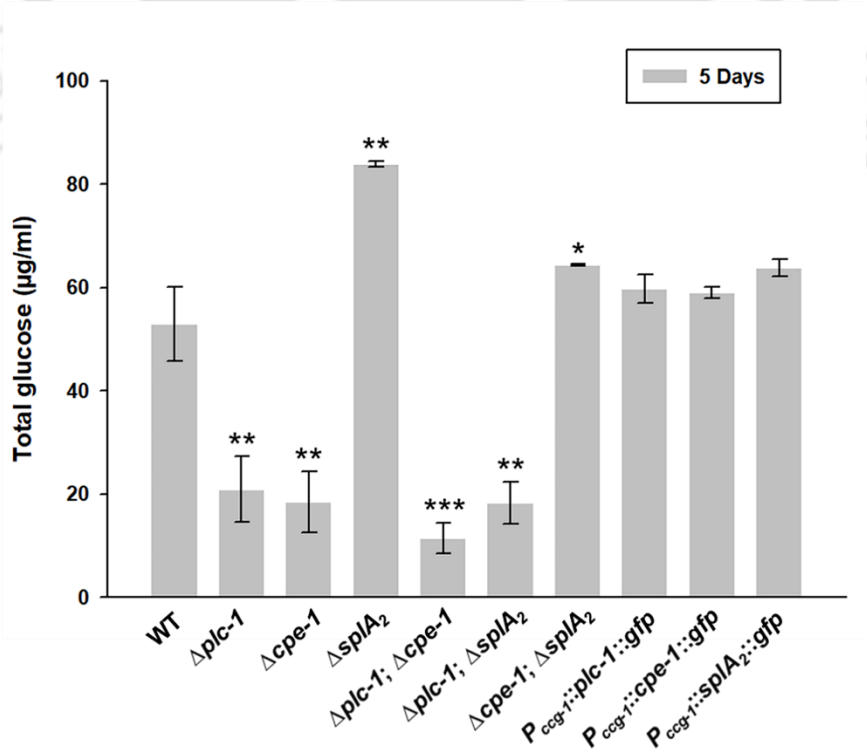

Figure 3.6: Cellulose degradation assay of the WT, Δ*plc-1*, Δ*cpe-1*, Δ*splA*$_2$ mutants, and the homokaryotic transformant strains. **(A)** The WT, Δ*plc-1*, Δ*cpe-1*, Δ*splA*$_2$ mutants, and the homokaryotic transformant strains grown on Vogel's media with 2% microcrystalline cellulose as the sole carbon source for 2 days (Top panel) and 5 days (Bottom panel). **(B)** Total secreted protein in the 2 days and 5 days culture supernatants of WT, Δ*plc-1*, Δ*cpe-1*, Δ*splA*$_2$ mutants, and the homokaryotic transformant strains grown on Vogel's media with 2% microcrystalline cellulose as the sole carbon source. **(C)** Total glucose in the culture supernatants of WT, Δ*plc-1*, Δ*cpe-1*, Δ*splA*$_2$ mutants, and the homokaryotic transformant strains grown on Vogel's media with 2% microcrystalline cellulose as the sole carbon source for 5 days. Error bars indicate standard deviations calculated from the data for three independent experiments (n = 3). Asterisks indicate statistically significant values, **P<0.05*, ***P<0.01*, ****P<0.001*.

3.2.6.2 The Δ*plc-1*, Δ*cpe-1*, Δ*splA*$_2$ single and double mutants showed normal growth phenotypes on alternate carbon sources

I studied the ability of the WT, Δ*plc-1*, Δ*cpe-1*, Δ*splA*$_2$ single and their double mutants to utilize different carbon sources. However, the WT and all the mutant strains tested showed no significant differences in growth rate and morphology when grown on sucrose, glucose, xylose, glycerol, and sodium acetate (Table 3.7; Fig. 3.7).

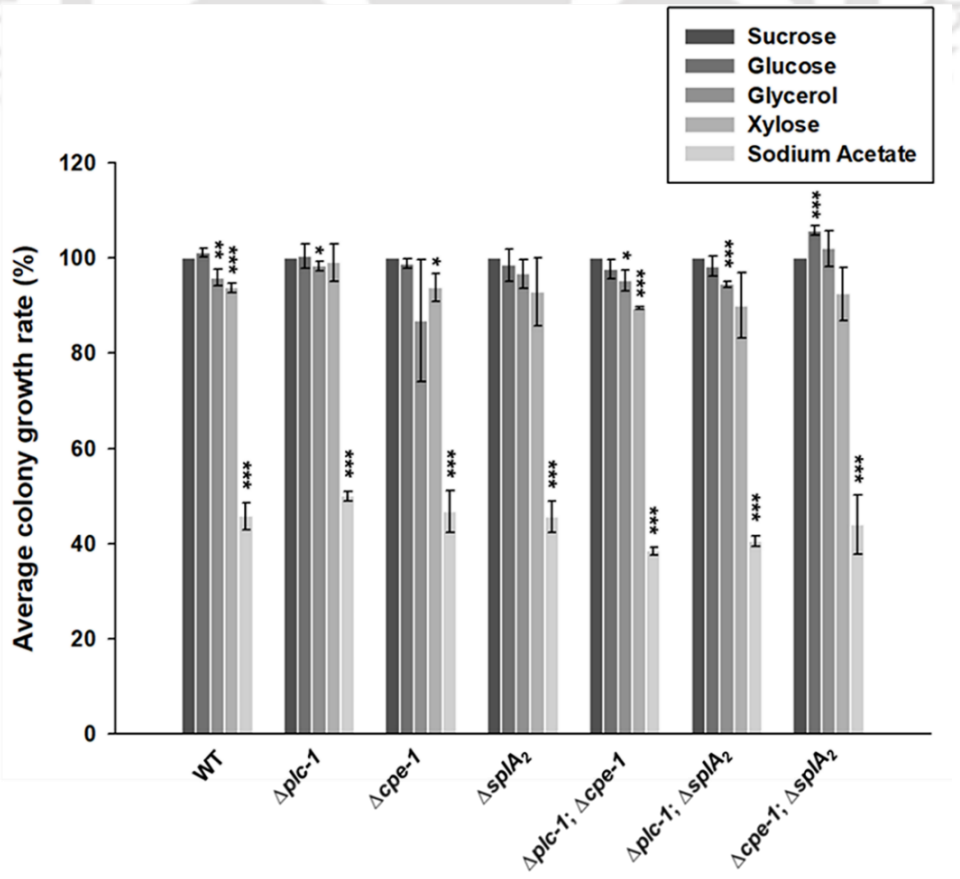

Figure 3.7: Average colony growth rate (%) of the WT, Δ*plc-1*, Δ*cpe-1*, Δ*splA*$_2$ single and double mutant strains on different carbon sources. Graph showing the average colony growth rate (%) of the WT, Δ*plc-1*, Δ*cpe-1*, Δ*splA*$_2$ single and double mutant strains when grown on sucrose, glucose, xylose, glycerol, and sodium acetate as carbon sources. Asterisks indicate statistically significant values, **P<0.05, **P<0.01, ***P<0.001*.

Table 3.7: Average colony growth rate (%) of the WT, Δ*plc-1*, Δ*cpe-1*, Δ*splA*$_2$ single and double mutant strains on different carbon sources

Strains	[+]Percent growth in VM with different carbon sources				
	Sucrose	**Glucose**	**Glycerol**	**Xylose**	**Sodium Acetate**
WT	100 ± 0.00	101.20 ± 0.85	95.96 ± 1.66 (**)	93.79 ± 0.95 (***)	45.79 ± 2.85 (***)
Δ*plc-1*	100 ± 0.00	100.44 ± 2.59	98.35 ± 1.04 (*)	99.12 ± 3.95	49.94 ± 1.01 (***)
Δ*cpe-1*	100 ± 0.00	98.86 ± 1.05	86.91 ± 12.87	93.90 ± 2.95 (*)	46.69 ± 4.48 (***)
Δ*splA*$_2$	100 ± 0.00	98.56 ± 3.39	96.77 ± 3.02	92.96 ± 7.22	45.62 ± 3.27 (***)
Δ*plc-1*; Δ*cpe-1*	100 ± 0.00	97.70 ± 1.99	95.32 ± 2.13 (*)	89.53 ± 0.21 (***)	38.38 ± 0.78 (***)
Δ*plc-1*; Δ*splA*$_2$	100 ± 0.00	98.31 ± 2.16	94.50 ± 0.66 (***)	90.09 ± 6.97	40.53 ± 1.11 (***)
Δ*cpe-1*; Δ*splA*$_2$	100 ± 0.00	105.80 ± 0.99 (***)	102.06 ± 3.80	92.51 ± 5.60	44.00 ± 6.20 (***)

[+]Results are shown as mean ± standard deviation for three independent experiments (n = 3) with *P-values* < 0.05 (*), < 0.01 (**), and < 0.001 (***) compared with the control condition (Sucrose) as measured by a one-way ANOVA test.

3.2.7 Cellulose Degradation Assay during ER stress

3.2.7.1 The Δ*splA*$_2$ mutant is unable to utilize cellulose during ER stress

In *N. crassa*, the lignocellulase secretion pathway and ER stress response pathways crosstalk (Fan et al. 2015); therefore, I assessed the ability of the Δ*splA*$_2$ mutant to degrade microcrystalline cellulose in the ER stress inducing condition to test if the increased protein secretion of the Δ*splA*$_2$ mutant during

cellulose degradation and growth defect during ER stress are correlated. The Δ*splA*$_2$ mutant was unable to utilize microcrystalline cellulose in the presence of 2 mM DTT, whereas the WT could slowly utilize cellulose (Fig. 3.8).

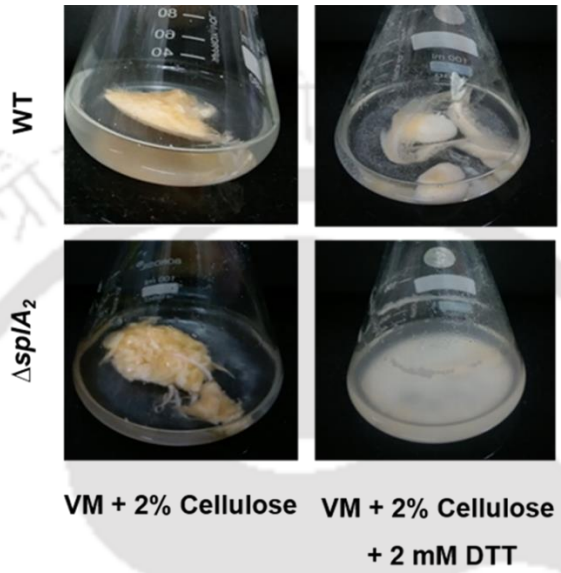

Figure 3.8: Cellulose degradation assay during ER stress in the WT and Δ*splA*$_2$ mutant. The WT and Δ*splA*$_2$ mutant strains were cultured for 5 days in Vogel's media with 2% microcrystalline cellulose as the sole carbon source in the presence of 2 mM DTT, and photographed.

3.3 Discussion

Ca^{2+} is a universal second messenger molecule involved in intracellular signaling in eukaryotes. The $[Ca^{2+}]_c$ regulates several developmental processes in fungi, including *N. crassa*. To maintain cellular Ca^{2+} homeostasis, Ca^{2+} is either pumped out of the cell through the plasma membrane or stored in vacuoles or other cytosolic organelles. PLC/IP_3-mediated signaling is one of the most important pathways for maintaining cytosolic Ca^{2+} homeostasis (Berridge 1987, 1993). In response to the production of IP_3 in the cells, Ca^{2+} is released from vacuoles and other intracellular stores to the cytoplasm (Berridge 1987, 1993). However, IP_3 receptors have not been identified in *N. crassa* and Ca^{2+} signaling mechanisms are still not clearly understood in fungi (Galagan et al. 2003; Borkovich et al. 2004; Zelter et al. 2004). In this chapter, I investigated the functions of three Ca^{2+} signaling genes, *plc-1*, *cpe-1*, and *splA*$_2$, and identified their involvement in diverse cellular functions in *N. crassa*. I

also described the genetic interaction of the *plc-1*, *cpe-1*, and *splA*$_2$ genes using their double mutants in regulating cell functions in *N. crassa*.

Many reports suggest that Ca^{2+} signaling can influence circadian oscillators through multiple pathways. The extracellular signals mediated by Ca^{2+} have been shown to regulate amplitude, phase, and period in mammals (O'Neill and Reddy 2012). A transmembrane Ca^{2+} flow in the hypothalamic suprachiasmatic nucleus (SCN) maintains molecular rhythmicity in mice by regulating clock gene expression (Lundkvist et al. 2005). Inhibition of the inositol 1, 4, 5-trisphosphate receptor (IP_3R) or the endoplasmic reticulum Ca^{2+}-ATPase (SERCA) lengthens the period, suggesting that Ca^{2+} plays a role in modifying the molecular circadian clock in the liver of rats (Báez-Ruiz and Diaz-Munoz 2011). In both prokaryotes and eukaryotes, the Na^{2+}/Ca^{2+} mediated Ca^{2+} signaling is important for temperature compensated circadian rhythms (Kon et al. 2021). In *N. crassa*, increased $[Ca^{2+}]_c$ levels caused by the loss of NCA-2 resulted in shortened circadian period length (Wang et al. 2021). As PLC, CPE-1, and $sPLA_2$ are involved in the sensing and response process to an increase in $[Ca^{2+}]_c$ (Galagan et al. 2003; Borkovich et al. 2004; Barman and Tamuli 2015), I hypothesised that *plc-1*, *cpe-1*, and *splA*$_2$ might have a role in circadian regulated conidiation in *N. crassa*. The Δ*plc-1* knockout mutant exhibited longer periods at 20 °C and 25 °C but normal period length at 30 °C, whereas Δ*cpe-1* and Δ*splA*$_2$ knockout mutants displayed normal periods in all temperatures (Table 3.1; Fig. 3.1). Circadian regulated conidiation studies using the double mutants of *plc-1*, *cpe-1*, and *splA*$_2$ revealed that *plc-1* is epistatic to *cpe-1* and *splA*$_2$ in maintaining the circadian clock period in *N. crassa*. Both Δ*plc-1*; Δ*cpe-1* and Δ*plc-1*; Δ*splA*$_2$ double mutants showed increased period length at 20 °C and 25 °C (Table 3.1; Fig. 3.1).

PLC-1 homologs are required for thermotolerance and growth at non-permissive temperatures in *C. albicans*, *C. parasitica*, and *S. cerevisiae* (Flick and Thorner 1993; Chung et al. 2006; Kunze et al. 2005). In *A. oryzae*, heat shock weakly upregulates *splaB* (Nakahama et al. 2010). In *N. crassa*, the *plc-1*, *cpe-1*, and *splA*$_2$ genes are required for survival in stress conditions (Barman and Tamuli 2015, 2017), I also observed a reduction in induced thermotolerance in the Δ*plc-1*, Δ*cpe-1*, and Δ*splA*$_2$ knockout mutants following exposure to heat shock temperatures (Table 3.3; Fig. 3.2). These data are supported by results in other filamentous fungi that *plc-1* homologs showed increased sensitivity to heat shock. In addition, *plc-1* interacted with *cpe-1* and *splA*$_2$ for the acquisition of induced thermotolerance (Table 3.3; Fig. 3.2). However, neither the WT nor the Δ*plc-1*, Δ*cpe-1*, Δ*splA*$_2$ single and double mutants could survive in the uninduced heat shock condition (Table 3.3; Fig. 3.2). These findings showed that *plc-1*, *cpe-1*, and *splA*$_2$ play a role in survival at lethal temperatures. Furthermore, in *N. crassa*, the alkaline pH and Ca^{2+} signaling pathways are interconnected, and high pH has been shown to modulate the expression of *calcineurin responsive zinc finger-1* (*crz-1*; Virgilio et al. 2017). Studies

on pH tolerance showed that the Δ*plc-1*, Δ*cpe-1*, and Δ*splA*$_2$ single mutants develop abnormal aerial hyphae in alkaline pH (Table 3.4; Fig. 3.3). Moreover, growth defects of the double mutants in alkaline conditions revealed that *plc-1*, *cpe-1*, and *splA*$_2$ interact positively for survival in the alkaline pH condition. However, the normal growth phenotype in an acidic pH condition suggested that the *plc-1*, *cpe-1*, and *splA*$_2$ genes are dispensable for growth in acidic pH (Table 3.4; Fig. 3.3). Further, the well-defined cell wall integrity signal transduction pathway modifies the cell wall under stress conditions. The structure of fungal cell walls is dynamic and their composition changes in response to environmental changes. Fungal cell growth, morphology, and viability are all affected by mutations that affect cell wall synthesis (Maddi et al. 2012). Although *plc-1*, *cpe-1*, and *splA*$_2$ are required for survival during heat and alkaline stress, the mutants of *plc-1*, *cpe-1*, and *splA*$_2$ were insensitive to cell wall stress, indicating that they are not involved in cell wall biosynthesis in *N. crassa* (Table 3.5; Fig. 3.4).

In the filamentous fungus *T. reesei*, the PLC-1 mediated Ca^{2+} signaling pathway plays a crucial role in the regulation of cellulase overexpression under cellulase-inducing conditions (Chen et al. 2021). Therefore, I explored the abilities of Δ*plc-1*, Δ*cpe-1*, and Δ*splA*$_2$ mutants in cellulose consumption for a better understanding of these calcium signaling genes in cellulose utilization in *N. crassa*. The Δ*plc-1* and Δ*cpe-1* mutants were unable to utilize microcrystalline cellulose, but the Δ*splA*$_2$ mutant devoured cellulose better than the WT (Fig. 3.6A). Furthermore, Δ*plc-1*; Δ*cpe-1* and Δ*plc-1*; Δ*splA*$_2$ double mutants could not utilize microcrystalline cellulose, but the Δ*cpe-1*; Δ*splA*$_2$ double mutant behaved like the Δ*splA*$_2$ single mutant (Fig. 3.6A). Both Δ*splA*$_2$ and Δ*cpe-1*; Δ*splA*$_2$ mutants produced significantly more protein and accumulated significantly more glucose in the culture supernatant, indicating a rapid cellulose breakdown capacity (Fig. 3.6B, C). However, Δ*plc-1*, Δ*cpe-1*, Δ*splA*$_2$ single and double mutants showed no significant differences in growth rate or morphology when grown on the media supplemented with sucrose, glucose, xylose, glycerol, and sodium acetate as a carbon source (Table 3.7; Fig. 3.7). Additionally, in *N. crassa*, lignocellulase secretion and ER stress response pathways crosstalk, and the Δ*cre-1* mutant (*carbon catabolite repressor*) with faster cellulose consumption abilities showed ER sensitive phenotype (Fan et al. 2015). Therefore, to induce the ER stress, the Δ*plc-1*, Δ*cpe-1*, Δ*splA*$_2$ single and double mutant strains were treated with the ER stress causing agent dithiothreitol (DTT), which prevents disulphide bond formation. Depending on the severity of ER stress, cells initiate different physiological processes, such as adaptation or death. Strains lacking $sPLA_2$ showed reduced growth in the presence of DTT, suggesting $sPLA_2$ might play a role in the ER response pathway (Table 3.6; Fig. 3.5). Studies on the double mutants showed that *plc-1* genetically interacted with *cpe-1* and *splA*$_2$ in cell survival during ER stress (Table 3.6; Fig. 3.5). Furthermore, during ER stress, Δ*splA*$_2$ mutant was unable to use cellulose (Fig. 3.8). Because the Δ*splA*$_2$ mutant showed

enhanced protein secretion and DTT interferes with normal protein folding, it is possible that the Δ*splA*$_2$ mutant might encounter ER load during cellulose degradation in the presence of DTT.

The homokaryotic transformants expressing the *plc-1*, *cpe-1*, and *splA*$_2$ transgenes complemented the phenotype of the Δ*plc-1*, Δ*cpe-1*, and Δ*splA*$_2$ mutants during the acquisition of thermotolerance (Table 3.3; Fig. 3.2), pH stress (Table 3.4; Fig. 3.3), ER stress (Table 3.6; Fig. 3.5), and cellulose degradation (Fig. 3.6). Therefore, taken together, it may be concluded that the *plc-1*, *cpe-1*, and *splA*$_2$ genes regulate multiple cellular pathways, probably by maintaining the Ca^{2+} homeostasis in *N. crassa*.

I presented the results described in this chapter in parts as posters in (i) National Conference on Fungal Biology: Recent Trends and Future Prospects and 44th Annual Meeting of the Mycological Society of India (MSI), University of Jammu, Jammu, 2017; (ii) Research Conclave, IIT Guwahati, 2017, 2018; (iii) XI International Conference on Biology of Yeasts and Filamentous Fungi, University of Hyderabad, 2019; and (iv) Neurospora 2021, Camp Allen, Texas, 2021.

In the next chapter, I describe the expression of the key molecular regulators in the *N. crassa*, Δ*plc-1*, Δ*cpe-1*, and Δ*splA*$_2$ single and double mutants under the cellular conditions described in this chapter.

Chapter 4: Expression analysis of genes involved in the circadian clock, stress responses, and cellulose degradation in the *N. crassa* Δ*plc-1*, Δ*cpe-1*, and Δ*splA*$_2$ mutants

4.1 Introduction

Several signaling pathways and molecular crosstalk govern key cell functions in fungi, including *N. crassa* (Berridge et al. 2003). GPCR-mediated signaling, MAPK-mediated signaling, and PLC/IP$_3$-mediated Ca^{2+} signaling are the major intracellular signaling pathways that operate in *N. crassa* (Galagan et al. 2003). PLC/IP$_3$-mediated signaling is crucial for maintaining the Ca^{2+} homeostasis in cells (Berridge 1987, 1993). Ca^{2+} accumulated in vacuoles is released back to the cytoplasm in response to IP$_3$ activation in cells, triggering downstream signaling events (Berridge 1987, 1993). The previous chapter described the cell functions of three Ca^{2+} signaling genes, *plc-1*, *cpe-1*, and *splA*$_2$, and their genetic interactions in regulating the circadian clock, acquisition of thermotolerance, tolerance to alkaline pH and ER stress, cellulose degradation, and utilization of alternate carbon sources in *N. crassa*. Therefore, further studies on the molecular players associated with PLC-1, CPE-1, and sPLA$_2$ in regulating these cell processes were critical for understanding the detailed mechanism.

In *N. crassa*, the core circadian clock consists of the *frequency* (*frq*) and *white collars* genes (*wc-1* and *wc*-2; Aronson et al. 1994; Crosthwaite et al. 1997). Exposure of *N. crassa* conidia to sub-lethal heat shock temperatures causes synthesis of heat shock proteins (Kapoor et al. 1995; Yang and Borkovich 1999). Similarly, the Pac-3 transcription factor is one of the central regulators of the *N. crassa* pH signaling pathway (Cupertino et al. 2012; Virgilio et al. 2016). In response to ER stress, cells engage a number of mechanisms, including the unfolded protein response pathway (UPR; Ron and Walter 2007; Bravo et al. 2012). In *N. crassa*, the expression of two UPR marker genes, *grp-78* and *pdi-1*, is used to assess the impact of ER stress (Bravo et al. 2012; Fan et al. 2015). In *N. crassa*, the utilization of microcrystalline cellulose as a carbon source is mediated by the expression of different cellulases encoding genes such as *cbh-1*, *cbh-2*, and *endo-2* (Sun and Glass 2011).

In this chapter, I studied the genetic interactions of *plc-1*, *cpe-1*, and *splA*$_2$ with genes involved in circadian clock regulation, stress responses, and utilization of cellulose to understand the interactions of these genes and crosstalk between various signaling pathways in *N. crassa*.

4.2 Results

4.2.1 Gene expression in the Δ*plc-1*, Δ*cpe-1*, and Δ*splA*$_2$ single and double mutants

4.2.1.1 The period length change is correlated with *frq* and *wc-1* transcript levels

In *N. crassa*, the core components of the circadian clock are *frq*, *wc-1*, and *wc-2* (Aronson et al. 1994; Crosthwaite et al. 1997). WC-1 and WC-2 are two nuclear transcription factors of the GATA zinc finger family that bind to the consensus element in the promoter of light-regulated genes (Ballario et al. 1996; Linden and Macino 1997). The WC proteins play an indispensable role in regulating the *N. crassa* circadian feedback loop (Aronson et al. 1994; Crosthwaite et al. 1997; Garceau et al. 1997).

They interact via their conserved Per-Arnt-Sim (PAS) domains to form a white collar complex (WCC), which regulates rhythmic expression from the *frq* locus and maintains a circadian rhythmicity in constant darkness (Aronson et al. 1994; Crosthwaite et al. 1997; Garceau et al. 1997). FRQ inhibits its own transcription by phosphorylating the WCC complex in a FRQ-dependent manner, forming a negative feedback loop (Aronson et al. 1994; He et al. 2006; Wang et al. 2019). Moreover, FRQ acts positively on WC-1 protein levels post-transcriptionally and on *wc-2* at mRNA levels transcriptionally, thereby forming an interlocked positive feedback loop (Lee et al. 2000; Cheng et al. 2001).

Based on the period length phenotypes observed in the previous chapter (Table 3.1; Fig. 3.1), I performed qRT-PCR to check the transcript levels of *frq* (NCU02265) and *wc-1* (NCU02356) in the *ras-1*^{bd} and the Δ*plc-1*, Δ*cpe-1*, Δ*sp1A*$_2$ single and double mutants at 20 °C and 25 °C. The strains were grown in circadian medium (without agar) under shaking (200 rpm) in light at 20 °C or 25 °C for 2 h and then transferred to darkness for 14 h (Aronson et al. 1994). Mycelia were harvested, and RNA was isolated. The altered period lengths observed in the Δ*plc-1*, Δ*plc-1*; Δ*cpe-1*, and Δ*plc-1*; Δ*splA*$_2$ mutants were related to the transcript levels of *frq* and *wc-1* (Fig. 4.1). The Δ*plc-1*, Δ*plc-1*; Δ*cpe-1*, and Δ*plc-1*; Δ*splA*$_2$ mutants showed significantly higher expression of *frq* and *wc-1* compared to the *ras-1*^{bd} at 20 °C (Fig. 4.1). However, the transcript levels of *frq* and *wc-1* were only marginally higher in the Δ*plc-1*, Δ*plc-1*; Δ*cpe-1*, and Δ*plc-1*; Δ*splA*$_2$ mutants compared to *ras-1*^{bd} at 25 °C (Fig. 4.1). In addition, no change in the *frq* and *wc-1* transcript levels was observed in the Δ*cpe-1*, Δ*splA*$_2$, and Δ*cpe-1*; Δ*splA*$_2$ mutants (Fig. 4.1). Therefore, it could be concluded that *plc-1* regulates the period length by maintaining a proper level of FRQ and WC-1. Studies on the double mutants revealed that *plc-1* is epistatic to *cpe-1* and *splA*$_2$ in regulating the circadian clock in *N. crassa*.

(A)

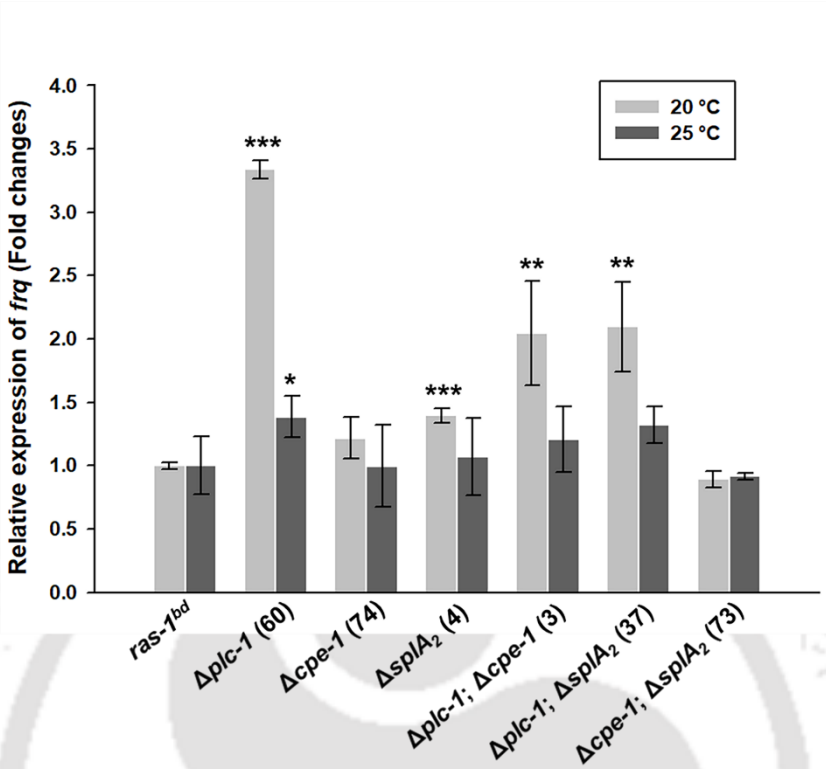

(B)

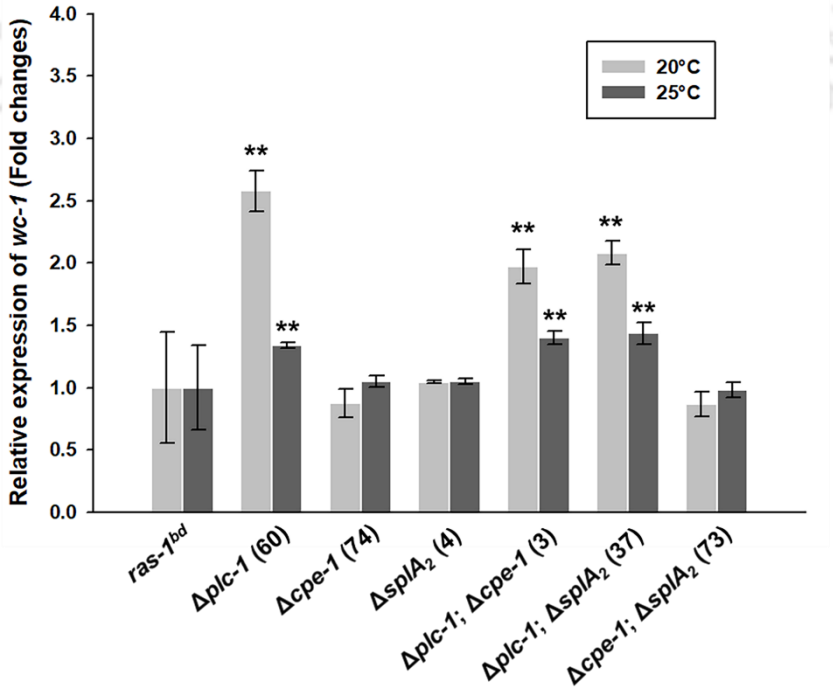

Figure 4.1: Expression of *frq* and *wc-1* during circadian regulated conidiation at 20 °C and 25 °C. RNA was isolated from the *ras-1*^{bd} and the Δ*plc-1*, Δ*cpe-1*, Δ*sp1A*$_2$ single and double mutants cultured under the circadian regulated conidiation conditions at 20 °C or 25 °C, and expression of the *frq* and *wc-1* genes was determined using qRT-PCR with three biological replicates for each strain. The expression of each gene was normalized with that of the *β-tubulin* and expression values were compared with those in the *ras-1*^{bd} control strain. Error bars indicate standard deviations calculated from the data for three independent experiments (n = 3) with *P-values* < 0.05 (*), < 0.01 (**), and < 0.001 (***) relative to the *ras-1*^{bd} strain as measured by a one-way ANOVA test.

4.2.1.2 The *plc-1*, *cpe-1*, and *splA*$_2$ genes regulate the expression of heat shock proteins in *N. crassa*

The heat stress response (HSR) is specified by rapid reprogramming of gene expression, resulting in a transient increase in heat shock proteins (HSPs), which is linked to enhanced thermotolerance (Verghese et al. 2012). HSP60 and HSP90 are two major HSP families involved in a variety of stress responses, including antifungal drug resistance in *C. albicans* and *S. cerevisiae* (Cowen and Lindquist 2005; Cowen et al. 2009), and sexual and asexual developments in *F. graminearum* (Bui et al. 2016). In *A. fumigatus*, *hsp90* is an essential gene and is required for spore viability, conidiation, germination, and cell wall integrity (Lamoth et al. 2012). When *N. crassa* cells are subjected to sub-lethal heat shock temperatures, it leads to the synthesis of heat shock proteins, which provide improved viability in the subsequent exposure to lethal temperatures (Kapoor et al. 1995; Yang and Borkovich 1999). In *N. crassa*, the HSR is demonstrated by the abundant production of HSP60, HSP80, and HSP90; and HSP80 is a member of the HSP90 family of HSPs (Borkovich et al. 2004).

As the Δ*plc-1*, Δ*cpe-1*, and Δ*splA*$_2$ mutants showed increased sensitivity to heat shock (Table 3.3; Fig. 3.2), I performed heat stress induced transcription studies to understand the effect of *plc-1*, *cpe-1*, and *splA*$_2$ deletion on the transcript levels of *hsp60* (NCU01589) and *hsp80* (NCU04142) in the Δ*plc-1*, Δ*cpe-1*, Δ*splA*$_2$ single and double mutants. For heat stress induced expression studies, the strains were grown in VM medium at normal growth temperature of 28 °C, 200 rpm for 15 h, and then heat shocked at 48 °C for 1 h (Kapoor and Lewis 1987). Upon heat shock, Δ*plc-1*, Δ*cpe-1*, Δ*splA*$_2$ single mutants, and the Δ*plc-1*; Δ*cpe-1* and Δ*plc-1*; Δ*splA*$_2$ double mutants showed reduced expression of *hsp60* and *hsp80* compared to the WT (Fig. 4.2A), which correlates with the increased sensitivity of the mutants to heat stress (Fig. 3.2). On the other hand, the transcript levels of *hsp60* and *hsp80* in the Δ*cpe-1*; Δ*splA*$_2$ mutant were comparable to the WT (Fig. 4.2A).

I also tested the expression levels of *plc-1*, *cpe-1*, and *splA*$_2$ under the heat stress condition in the WT. RNA was isolated from non heat shocked, heat shocked, and heat shock-recovered cultures of the WT, and expression analysis was performed. Following heat shock, the expression of *plc-1* was

elevated nearly 2.5-fold compared to the non heat shocked condition (Fig. 4.2B), which also corresponds to the increased susceptibility of the Δ*plc-1* mutant to lethal temperatures (Fig. 3.2). In addition, after heat shock, only a modest upregulation of *cpe-1* and *splA*$_2$ was observed (Fig. 4.2B) in contrast to a 50% reduction in the survival of Δ*cpe-1* and Δ*splA*$_2$ (Fig. 3.2). However, compared to the heat shocked condition, the transcript levels of *plc-1*, *cpe-1*, and *splA*$_2$ decreased when the cells were allowed to recover at 28 °C following heat shock for 30 min (Fig. 4.2B). These results suggested that *plc-1*, *cpe-1*, and *splA*$_2$ are induced upon heat stress, and probably protect the cell by mediating the expression of heat shock proteins. Therefore, it can be concluded that the genetic interactions of *plc-1*, *cpe-1*, and *splA*$_2$ are important for regulating the expression of heat shock proteins in *N. crassa.*

(A)

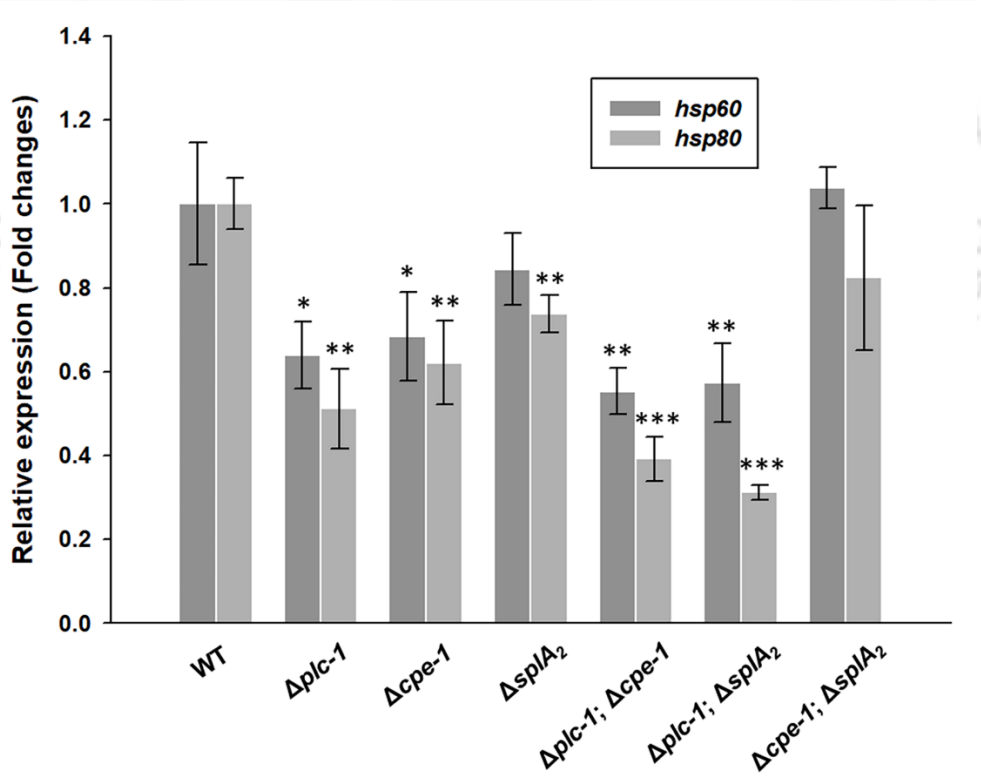

(B)

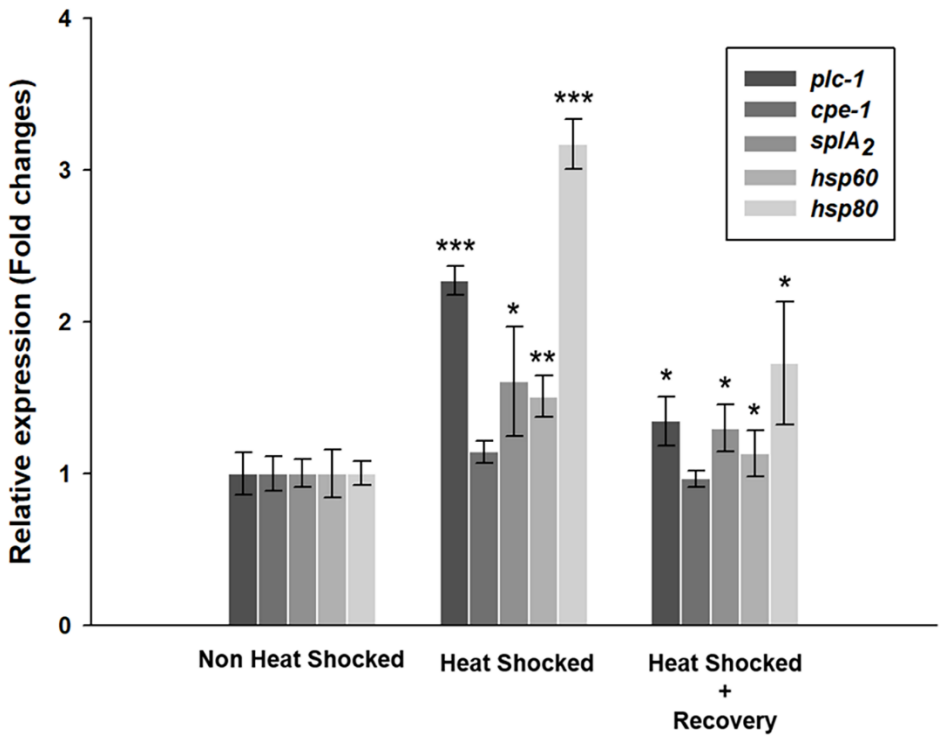

Figure 4.2: Heat stress induced expression studies. (A) RNA was extracted from the WT, Δ*plc-1*, Δ*cpe-1*, Δ*splA*$_2$ single and double mutants cultured in VM medium at 28 °C for 15 h, and heat shocked at 48 °C for 1 h. Then, the expression of *hsp60* and *hsp80* was determined by qRT-PCR on three biological replicates of each strain. **(B)** The expression of *plc-1*, *cpe-1*, and *splA*$_2$ was measured by qRT-PCR using RNA extracted from the non heat shocked, heat shocked, and heat shock-recovered cultures of the WT strain. The expression levels of each gene were normalized with the *β-tubulin* and compared to the **(A)** WT and **(B)** non heat shocked condition. Error bars indicate standard deviations calculated from the data for three independent experiments (n = 3) with *P-values* < 0.05 (*), < 0.01 (**), and < 0.001 (***) compared to the **(A)** WT and **(B)** non heat shocked conditions as measured by a one-way ANOVA test.

4.2.1.3 *plc-1*, *cpe-1*, and *splA*$_2$ positively interact to regulate *pac-3* expression under alkaline conditions in *N. crassa*

The physiological responses to ambient pH have been extensively studied in the model filamentous fungus *A. nidulans* and yeast species, including *S. cerevisiae*. In *A. nidulans* and *S. cerevisiae*, the transcription factor PacC/Rim101 serves as the central regulator of the pH signaling pathway (Tilburn et al. 1995; Peñalva and Arst 2004). The PacC/Rim101 activates the alkaline-responsive genes, which mediate the adaptation of the cell from neutral to alkaline transition (Arst and Peñalva 2003; Peñalva et al. 2008; Maeda 2012). In *S. cerevisiae*, the response to high pH also involves a transient increase in

$[Ca^{2+}]_c$, which in turn activates the calcineurin-Crz1p mediated signaling pathway (Serrano et al. 2002; Viladevall et al. 2004). In *S. cerevisiae*, pH-responsive genes were identified as the targets of Crz1p (Serrano et al. 2002; Viladevall et al. 2004). *N. crassa* shares all components of the pH signaling pathway with *A. nidulans* and *S. cerevisiae* (Virgilio et al. 2016). In *N. crassa*, the *pacC* ortholog, *pac-3* is highly expressed in alkaline condition compared to that at ambient pH 5.8 (Cupertino et al. 2012). In addition, the alkaline pH regulates the expression of *crz-1*, a crucial downstream target of the Ca^{2+} signaling pathway in *N. crassa* (Virgilio et al. 2017).

To investigate if the increased sensitivity of the Δ*plc-1*, Δ*cpe-1*, and Δ*splA*$_2$ mutants to alkaline stress (Table 3.4; Fig. 3.3) was caused by the alteration in *pac-3* (NCU00090) expression, I analysed the mRNA level of *pac-3* in the Δ*plc-1*, Δ*cpe-1*, Δ*splA*$_2$ single and double mutants during pH stress. For pH induced expression studies, the conidia were cultured in VM medium (pH 5.8) at 30 °C with shaking at 200 rpm for 16 h. After this, the cultures were filtered, and mycelia were transferred into fresh VM medium containing 0.5% sucrose at pH 3.8 (for acidic stress) and 7.8 (for alkaline stress), and RNA was isolated after 30 min of incubation essentially as described previously (Cupertino et al. 2012). In alkaline stress, the Δ*plc-1*, Δ*cpe-1*, Δ*splA*$_2$ single, and Δ*plc-1*; Δ*cpe-1*, Δ*plc-1*; Δ*splA*$_2$, and Δ*cpe-1*; Δ*splA*$_2$ double mutants showed reduced expression of *pac-3* (Fig. 4.3A), which was correlated with the increased sensitivity of the mutants to alkaline stress (Fig. 3.3). However, at ambient and acidic pH, *pac-3* transcript levels remain basal in all the mutants, indicating that Pac-3 has no significant role in this condition, consistent with the mutants' phenotypes (Fig. 3.3).

I also analysed the expression of *plc-1*, *cpe-1*, and *splA*$_2$ in the WT strain cultured at ambient pH 5.8, and then subjected to acidic (pH 3.8) or alkaline (pH 7.8) stress conditions. The *plc-1*, *cpe-1*, and *splA*$_2$ genes showed ~ 4, 3, and 2.5-fold upregulation in the alkaline condition (Fig. 4.3B). However, no significant changes in the expression of *plc-1*, *cpe-1*, and *splA*$_2$ were observed in the acidic condition (Fig. 4.3B). Therefore, these data suggested that the *plc-1*, *cpe-1*, and *splA*$_2$ positively interact for survival of *N. crassa* in alkaline condition.

(A)

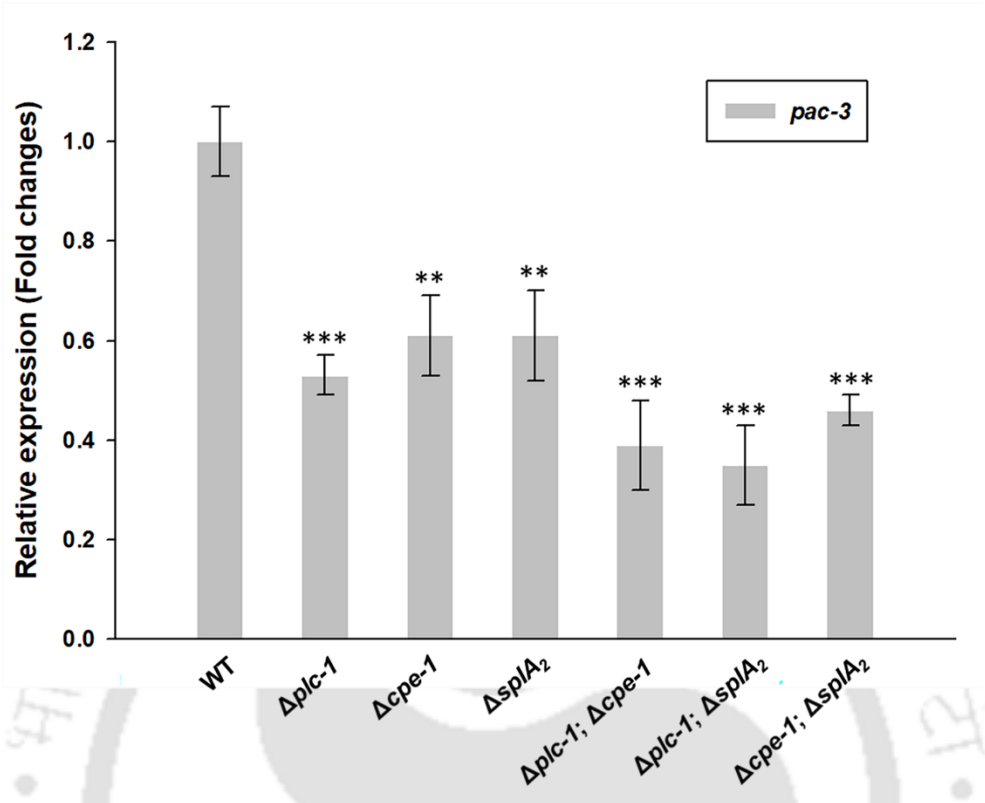

(B)

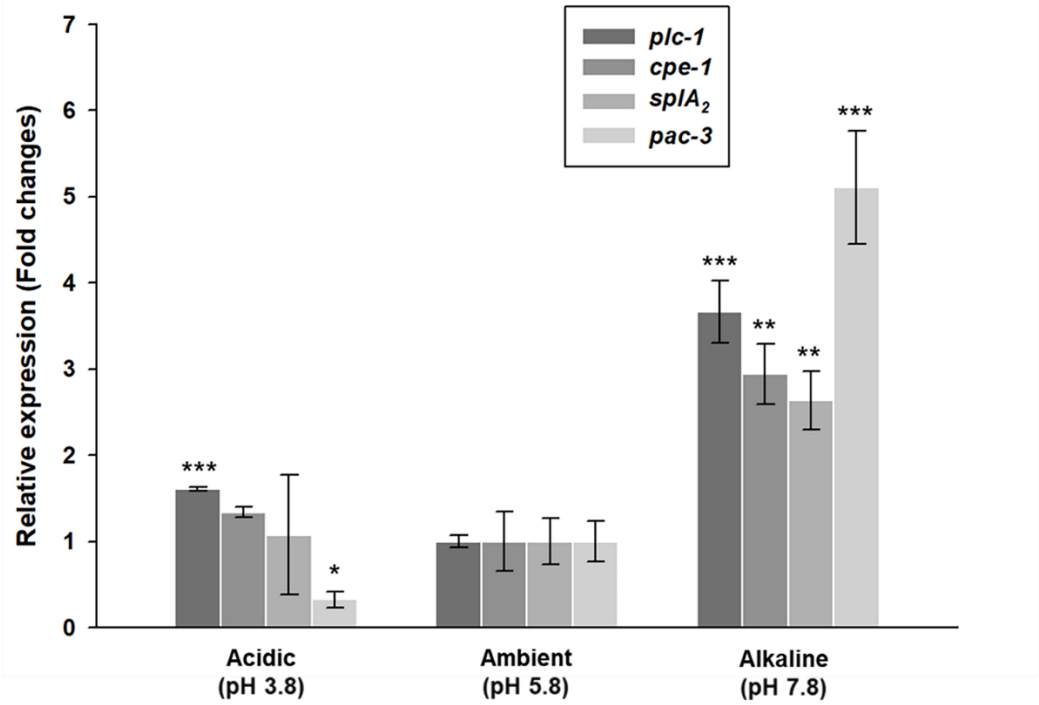

Figure 4.3: Gene expression analysis under pH stress conditions. (A) Cells from the WT and the Δ*plc-1*, Δ*cpe-1*, Δ*splA*$_2$ single and double mutants were cultured at pH 5.8 for 16 h and shifted to alkaline (pH 7.8) condition for 30 min. Mycelial samples were collected and used to extract total RNA, and the expression of *pac-3* was determined by qRT-PCR for three biological replicates of each strain. **(B)** RNA was isolated from the WT strain grown in acidic and alkaline conditions, and the expression of *plc-1*, *cpe-1*, and *splA*$_2$ was determined for three biological replicates for each condition. The expression of each gene was normalized with the *β-tubulin* and expression values were compared with those of the **(A)** WT and **(B)** ambient condition (pH 5.8). Error bars indicate standard deviations calculated from the data for three independent experiments (n = 3) with *P-values* < 0.05 (*), < 0.01 (**), and < 0.001 (***) compared with the **(A)** WT and **(B)** ambient condition (pH 5.8) as measured by a one-way ANOVA test.

4.2.1.4 ER stress induced growth defects in the Δ*splA*$_2$, Δ*plc-1*; Δ*cpe-1*, and Δ*plc-1*; Δ*splA*$_2$ mutants are due to altered transcript levels of UPR markers

In filamentous fungi, high protein secretion capability necessitates an incredibly effective system for protein synthesis, folding, and transport. When normal ER function is compromised or the folding capacity of the ER is exceeded, misfolded proteins build up, which triggers an adaptive ER response referred to as the Unfolded Protein Response (UPR; Bravo et al. 2012; Hetz 2012). The UPR promotes misfolded protein breakdown, increases overall ER volume, and increases chaperone abundance in order to restore organelle homeostasis (Schröder 2008; Hetz 2012). During ER stress, the expression of two well-known UPR marker genes *grp-78* and *pdi-1* is upregulated in *N. crassa* (Bravo et al. 2012; Fan et al. 2015).

In the previous chapter, I described that Δ*splA*$_2$, Δ*plc-1*; Δ*cpe-1*, and Δ*plc-1*; Δ*splA*$_2$ mutants showed growth defects during ER stress (Table 3.6; Fig. 3.5). Therefore, I measured the transcript levels of *grp-78* (NCU03928) and *pdi-1* (NCU09223) to assess the impact of ER stress in the Δ*plc-1*, Δ*cpe-1*, Δ*splA*$_2$ single and double mutants. For ER stress induced expression studies, cells were initially grown in VM medium at 30 °C and 200 rpm. After 16 h, 2 mM DTT was added to the cultures and incubated for another 1 h in the dark to induce ER stress (Fan et al. 2015). The mycelia were harvested, and RNA was isolated. The transcript levels of *grp-78* and *pdi-1* in the Δ*plc-1*, Δ*cpe-1*, and Δ*cpe-1*; Δ*splA*$_2$ mutants were comparable to those in the WT (Fig. 4.4A), in agreement with their phenotypes described in the previous chapter (Fig. 3.5). However, the Δ*splA*$_2$, Δ*plc-1*; Δ*cpe-1*, and Δ*plc-1*; Δ*splA*$_2$ mutants showed reduced expression of *grp-78* and *pdi-1*, which corresponds to the growth defects in these mutants (Fig. 4.4A).

To investigate the effect of ER stress, I also analysed the transcript levels of *plc-1*, *cpe-1*, and

splA$_2$ using the RNA of WT mycelia. The expression of *splA*$_2$ is upregulated nearly 3-fold in DTT-treated cells, whereas the transcript levels of *plc-1* and *cpe-1* were similar in both DTT-treated and non-treated conditions (Fig. 4.4B). These results indicated that *splA*$_2$ and the genetic interactions of *plc-1* with *cpe-1* and *splA*$_2$ are crucial for the ER response pathway in *N. crassa*.

(A)

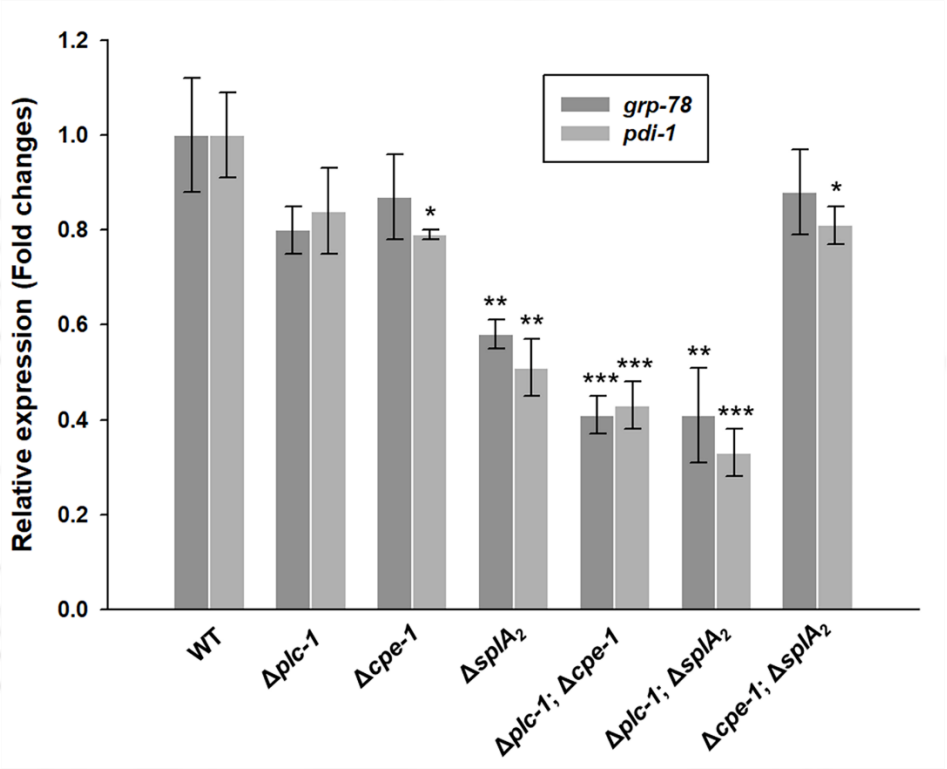

(B)

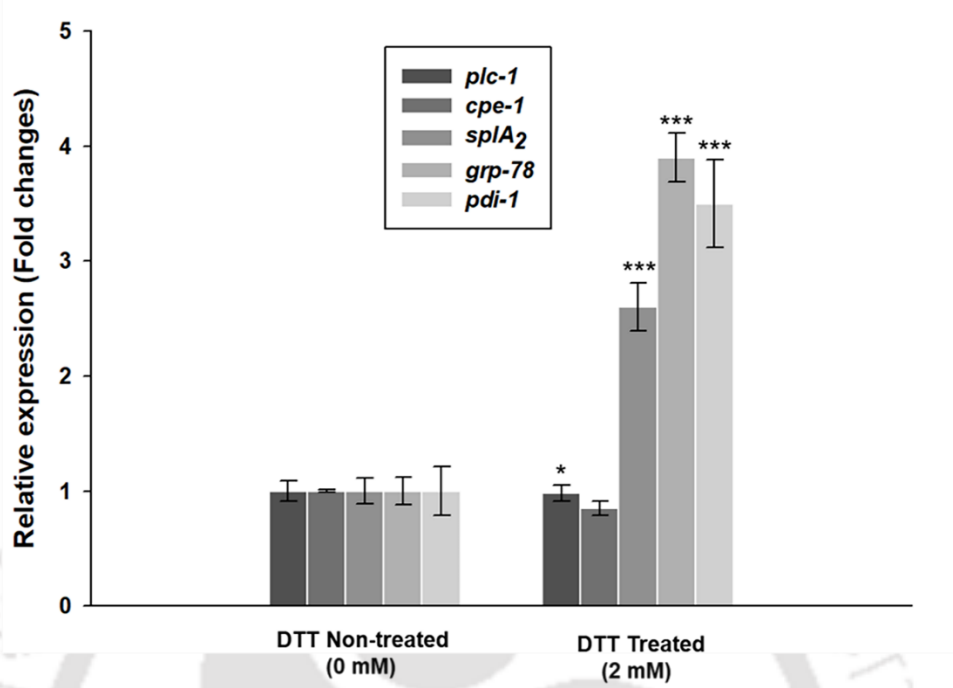

Figure 4.4: Gene expression analysis in response to the ER stress conditions. **(A)** RNA was extracted from the WT, Δ*plc-1*, Δ*cpe-1*, Δ*splA*$_2$ single and double mutants cultured in VM medium for 16 h, followed by 1 h growth in 2 mM DTT in the dark, and the expression of *grp-78* and *pdi-1* was determined by qRT-PCR in three biological replicates of each strain. **(B)** RNA was isolated from ER stress induced (DTT treated) and non-induced (DTT non-treated) cultures of WT and the expression of *plc-1*, *cpe-1*, and *splA*$_2$ was measured by qRT-PCR in three biological replicates for each condition. The expression of each gene was normalized with the *β-tubulin* and expression values were compared with those of the **(A)** WT and **(B)** non-treated condition. Error bars indicate standard deviations calculated from the data for three independent experiments (n = 3) with *P-values* < 0.05 (*), < 0.01 (**), and < 0.001 (***) compared with the **(A)** WT and **(B)** non-treated condition as measured by a one-way ANOVA test.

4.2.1.5 The Δ*splA*$_2$ and Δ*cpe-1*; Δ*splA*$_2$ mutants showed increased expression of cellulolytic genes, which was correlated with the rapid cellulose degradation ability of the mutants

To determine whether increased cellulase/endoglucanase activity and protein secretion in the Δ*splA*$_2$ and Δ*cpe-1*; Δ*splA*$_2$ mutants (Fig. 3.6) was due to an increased expression level of cellulolytic genes, I determined the expression levels of three major cellulase genes, *cbh-1* (NCU07340), *cbh-2* (NCU09680), and *endo-2* (NCU00762), in the WT and Δ*plc-1*, Δ*cpe-1*, Δ*splA*$_2$ single and double mutant

strains. Conidia of these strains were cultured in VM medium at 30 °C and 200 rpm for 16 h, then transferred to 2% Avicel as the sole carbon source and incubated for 4 h, and RNA was isolated (Sun and Glass 2011). As predicted, expression of the *cbh-1*, *cbh-2*, and *endo-2* genes was significantly increased in the Δ*splA*$_2$ and Δ*cpe-1*; Δ*splA*$_2$ mutants compared to the WT (Fig. 4.5A). However, *cbh-1*, *cbh-2*, and *endo-2* genes were downregulated in the Δ*plc-1*, Δ*cpe-1*, Δ*plc-1*; Δ*cpe-1*, and Δ*plc-1*; Δ*splA*$_2$ mutants (Fig. 4.5A), in agreement with the phenotypes described in the previous chapter (Fig. 3.6).

I also cultured the WT strain in VM liquid for 16 h and then transferred to 2% sucrose or 2% Avicel for an additional 4 h, and then analysed the expression of *plc-1*, *cpe-1*, and *splA*$_2$. The expression of *splA*$_2$ was reduced > 50% when the culture was transferred to 2% Avicel (Fig. 4.5B); however, no significant changes in the *plc-1* and *cpe-1* transcript levels were observed (Fig. 4.5B). These results suggested that *plc-1* and *cpe-1* act as positive regulators, whereas *splA*$_2$ plays a repressive role during growth on microcrystalline cellulose in *N. crassa*.

(A)

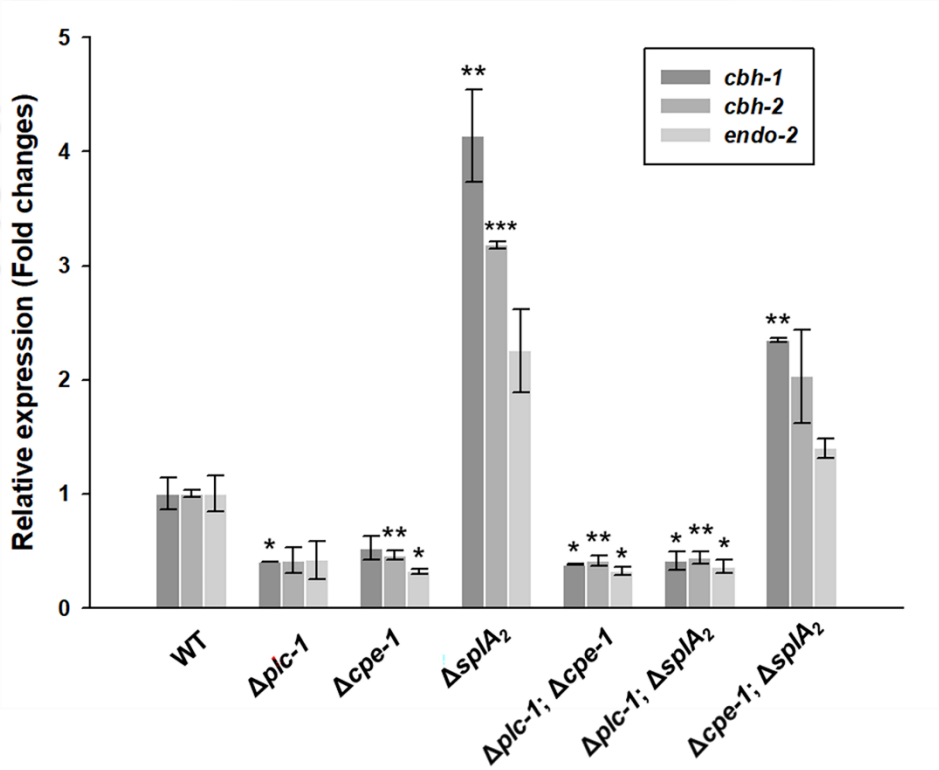

(B)

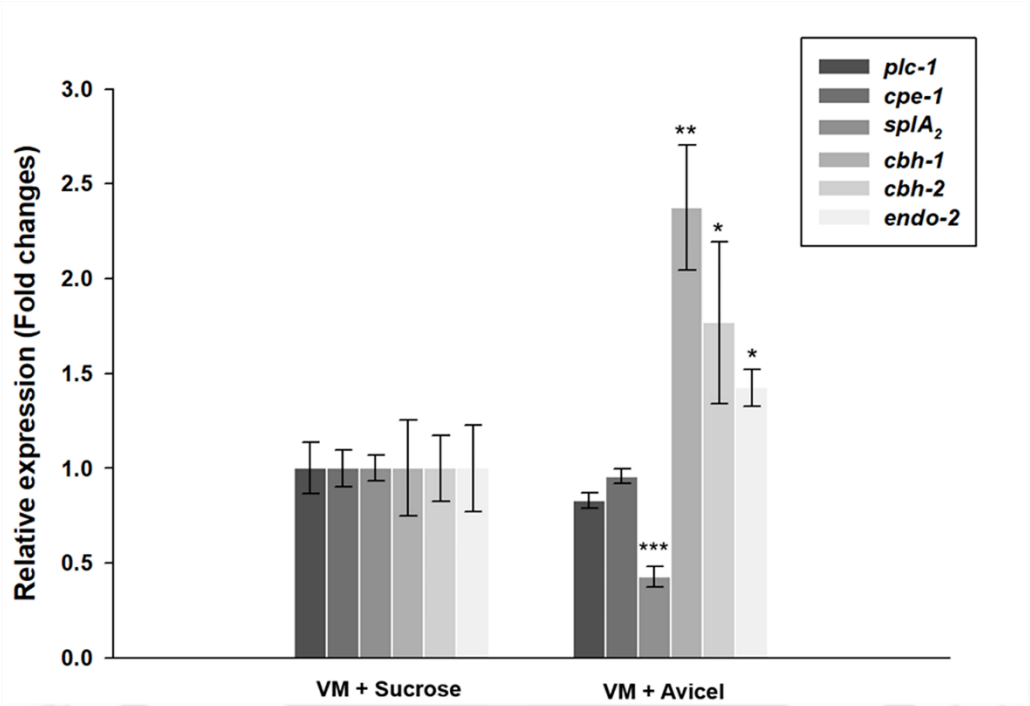

Figure 4.5: Gene expression analysis during growth on microcrystalline cellulose. (A) RNA was extracted from WT, and Δ*plc-1*, Δ*cpe-1*, Δ*splA*$_2$ single and double mutants grown in VM medium for 16 h followed by 4 h on 2% Avicel, and the expression of *cbh-1*, *cbh-2*, and *endo-2* was determined by qRT-PCR using three biological replicates of each strain. **(B)** The expression of *plc-1*, *cpe-1*, and *splA*$_2$ in three biological replicates of WT strain grown on VM medium and then transferred to 2% sucrose or 2% Avicel for 4 h. The expression of each gene was normalized with the *β-tubulin* and expression values were compared to the **(A)** WT and **(B)** WT cultures grown in 2% sucrose. Error bars indicate standard deviations calculated from the data for three independent experiments (n = 3) with *P-values* < 0.05 (*), < 0.01 (**), and < 0.001 (***) compared with the **(A)** WT and **(B)** WT cultures grown in 2% sucrose as measured by a one-way ANOVA test.

4.2.2 Promoter analysis

4.2.2.1 Analysis of the promoter regions of the *plc-1*, *cpe-1*, and *splA*$_2$ genes in *N. crassa*

As transcription factor binding elements regulate the expression of a gene, I used the MatInspector Program (Quandt et al. 1995; Cartharius et al. 2005) to analyse the putative promoter regions of *plc-1*, *cpe-1*, and *splA*$_2$ genes. This analysis revealed putative binding sequences for different transcription factors in the promoter regions of *plc-1*, *cpe-1*, and *splA*$_2$ genes (Table 4.1). The presence of these sequences further supports the findings that PLC-1, CPE-1, and sPLA$_2$ are critical for circadian clock regulation, stress survival, and cellulose utilization in *N. crassa*.

Table 4.1: Functions of the transcriptional regulatory elements in the promoter region of the *plc-1*, *cpe-1*, and *splA*$_2$ genes in *N. crassa*

Transcriptional Regulatory Elements	Functions
cAMP-element responsive binding proteins	Regulation of cellular DNA-dependent transcription
Carbon source responsive elements	Zinc cluster transcriptional activator binding to carbon source responsive elements (CSRE)
Circadian control factors	Circadian clock associated 1
ER stress-response elements (ERSE I)	(ER stress-response element I)-like motif
Fungal basic leucine zipper family	Transcriptional regulation of growth and development, nutrient utilization, pathogenicity, and stress responses
pH responsive regulators (PACC)	pH responsive regulator from *Aspergillus*
Yeast GC-Box Proteins (MIG1)	Zinc finger protein mediates glucose repression
Yeast GC-Box Proteins (MIG3)	Zinc finger transcriptional repressor
Yeast heat shock factors (HSF1)	Trimeric heat shock transcription factor
Yeast stress response elements (MSN2)	Transcriptional activator for genes in multistress response

4.2.3 Possible mechanism of the PLC-1, CPE-1, and sPLA$_2$ mediated pathways in circadian clock, stress survival, and cellulose degradation in *N. crassa*

When *N. crassa* is exposed to external stimuli such as alkaline pH, high temperature, ER stress, or the presence of cellulose in the media, GPCR gets activated, which in turn activates PLC-1. PLC-1 hydrolyzes PIP_2 into IP_3, leading to the release of Ca^{2+} from intracellular storage, and DAG activates PKC. The elevated Ca^{2+} and/or activated PKC likely interact with sPLA$_2$ and CPE-1. sPLA$_2$ belongs to the Ca^{2+} and/or CaM binding protein family (Soragni et al. 2001; Barman and Tamuli 2015; Takayanagi et al. 2015), and CPE-1 encodes a vacuolar Ca^{2+}/H^+ exchanger involved in Ca^{2+} maintenance (Zelter et al. 2004; Barman and Tamuli 2015). In *N. crassa*, the PLC-1, CPE-1, and sPLA$_2$ work together to maintain the intracellular Ca^{2+} homeostasis (Barman and Tamuli 2017). Increased $[Ca^{2+}]_c$ level activates Ca^{2+} sensors, including CaM, which in turn activates CRZ-1 via the calcineurin-CRZ-1 signaling pathway and heat shock factors (Tamuli et al. 2016; Kumar et al. 2020; Roy et al. 2022). Further, PAC-3, the central regulator involved in pH signaling cross regulates the Ca^{2+} signaling and the alkaline pH signaling pathways in *N. crassa* (Cupertino et al. 2012; Virgilio et al. 2016, 2017). In addition, the ER stress upregulates the Ca^{2+}-dependent UPR markers, like GRP-78 and PDI-1 (Rizutto et al. 2004; Bravo et al. 2012; Fan et al. 2015). Furthermore, sPLA$_2$ is under the CRE-1 regulon in *N. crassa*, and their interaction is studied in the next chapter; therefore depicted as dotted lines. These events activate specific promoters of target genes that provide tolerance to different stress conditions

and cellulose degradation in *N. crassa*. Thus, loss of PLC-1, CPE-1, and sPLA$_2$ result in aberrant Ca^{2+} homeostasis and triggers different morphological defects in *N. crassa*.

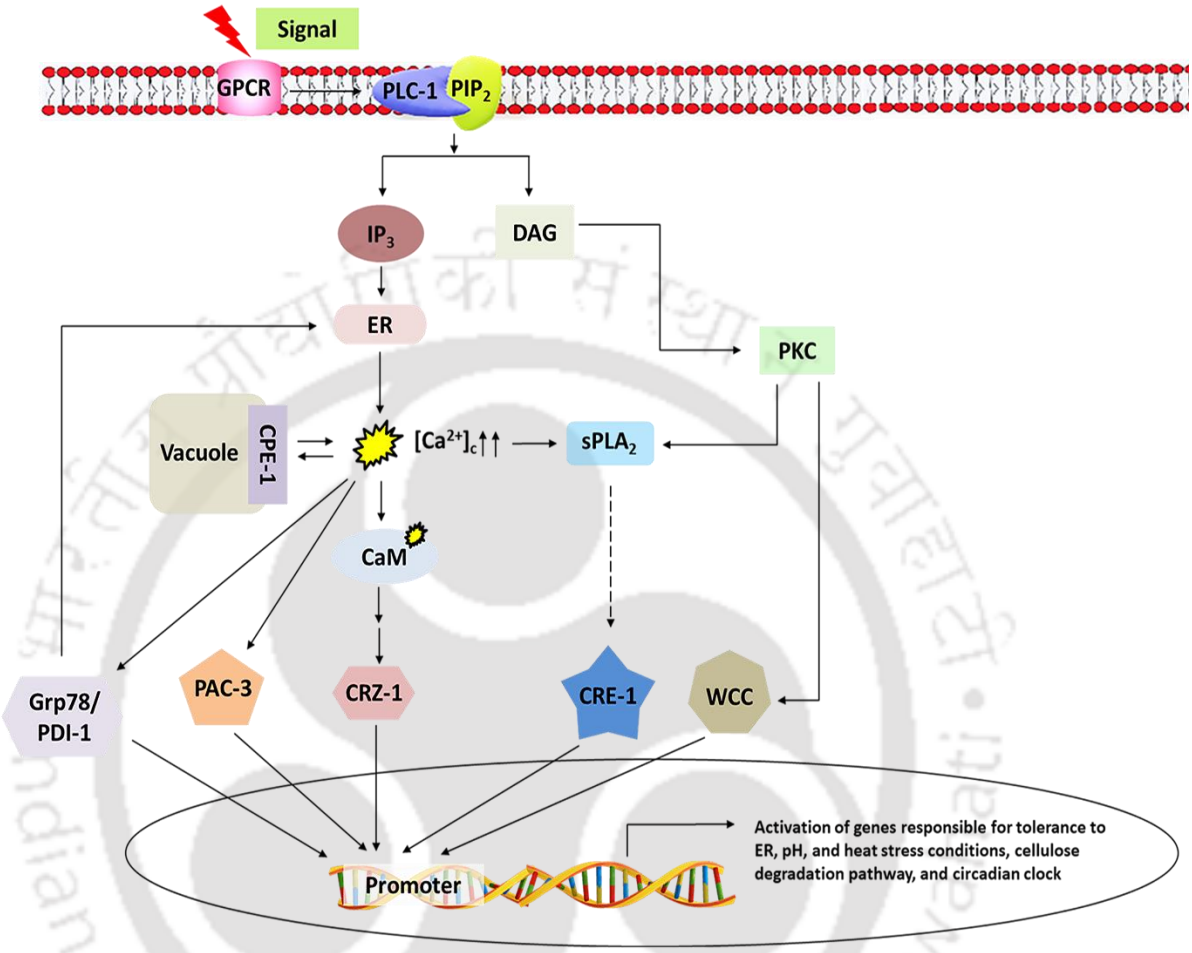

Figure 4.6: Possible mechanism of the PLC-1, CPE-1, and sPLA$_2$ mediated pathways in circadian clock, stress survival, and cellulose degradation in *N. crassa*. The *plc-1*, *cpe-1*, and *splA*$_2$ genes act in coordination to maintain the intracellular Ca^{2+} homeostasis. Aberration of Ca^{2+} homeostasis triggers a number of morphological and physiological changes in *N. crassa*. GPCR: G-Protein coupled receptor; PLC-1: phospholipase C-1; PIP$_2$: phosphatidylinositol 4, 5-bisphosphate; IP$_3$: inositol-1, 4, 5-trisphosphate; DAG: diacylglycerol; PKC: protein kinase C; CPE-1: Ca^{2+}/H^{+} exchanger; sPLA$_2$: secretory phospholipase A$_2$; CaM: calmodulin; PDI-1: protein disulphide-isomerase; PAC-3: pH response transcription factor; CRZ-1: calcineurin responsive zinc finger-1; CRE-1: carbon catabolite repressor; WCC: white collar complex.

4.3 Discussion

All living cells can respond and adapt to environmental changes by integrating environmental sensing and signal transduction pathways, resulting in the induction or repression of specific genes. I found that PLC-1, CPE-1, and sPLA$_2$ are involved in circadian regulated conidiation, thermotolerance acquisition, survival during alkaline pH and ER stress, cellulose utilization, and growth on alternate carbon sources in *N. crassa* (described in Chapter 3). In this chapter, I described the findings of the expression analysis of some important cellular genes involved in the circadian clock, stress responses, and utilization of cellulose in *N. crassa*.

I determined the expression of two major circadian regulators, *frq* and *wc-1* at two different temperatures (20 °C and 25 °C). At 20 °C, the transcript levels of the *frq* and *wc-1* genes were increased more than 2-fold in the Δ*plc-1* single, and Δ*plc-1*; Δ*cpe-1* and Δ*plc-1*; Δ*splA*$_2$ double mutants (Fig. 4.1). However, at 25 °C, the transcript levels of *frq* and *wc-1* were only marginally higher than *ras-1*^{bd} (Fig. 4.1). The membrane-bound phosphoinositide-specific phospholipase C (PLC) hydrolyzes phosphatidylinositol-4, 5-bisphosphate (PIP$_2$) to generate inositol 1,4,5-trisphosphate (IP$_3$) and diacylglycerol (DAG), two important second messengers. IP$_3$ causes the release of intracellular Ca^{2+}, and DAG activates PKC (Rhee and Bae 1997). In *N. crassa*, PKC negatively regulates the light-responsive genes and *frq* expression through the blue light receptor, WC-1 (Arpaia et al. 1999; Franchi et al. 2005). When activated, PKC interacts with the WCC complex and phosphorylates it. Because the hyperphosphorylated WCC complex cannot bind to the *frq* promoter and drive its expression, *frq* transcript levels are maintained (Franchi et al. 2005). Downregulation of PKC abolishes its effect on WC-1, resulting in increased *wc-1* mRNA expression and enhanced WC-1 protein stability (Franchi et al. 2005). Thus, in the Δ*plc-1*, Δ*plc-1*; Δ*cpe-1*, and Δ*plc-1*; Δ*splA*$_2$ mutants, the absence of PLC-1 might have an effect on the DAG level, causing PKC to remain inactive. Inactive PKC is unable to phosphorylate the WCC complex, leading to increase expression of *frq* and *wc-1* in the Δ*plc-1* single and double mutants (Fig. 4.1).

Heat stress is an important environmental factor affecting the growth and development of organisms. Heat stress results in the activation of specific proteins, referred to as heat shock proteins (HSPs; Verghese et al. 2012). HSP60, HSP80, HSP90, and a few small molecular HSPs (sHSPs) are among the most abundantly expressed HSPs (Borkovich et al. 2004). Previous evidence showed that the accumulation of HSPs is regulated by cytosolic Ca^{2+} under heat stress in fungi (Zhang et al. 2016). In *C. albicans*, *C. parasitica*, and *S. cerevisiae*, the *plc-1* homologs are required for thermotolerance and growth at non-permissive temperatures (Flick and Thorner 1993; Chung et al. 2006; Kunze et al. 2005). In *Ganoderma lucidam*, heat stress increases the expression of numerous genes that regulate $[Ca^{2+}]_c$, including *Ca^{2+}-permeable channel* (*cch*) and *plc* (Zhang et al. 2016). In *G. lucidam*, *plc* also

participates in regulating heat shock protein expression upon heat stress (Zhang et al. 2016). Heat shock weakly upregulates *splaB* in *A. oryzae* (Nakahama et al. 2010). In *N. crassa*, *plc-1*, *cpe-1*, and *splA*$_2$ regulate Ca^{2+} homeostasis (Barman and Tamuli 2015, 2017). I found reduced expression of *hsp60* and *hsp80* in the Δ*plc-1*, Δ*cpe-1*, Δ*splA*$_2$ single mutants, and the Δ*plc-1*; Δ*cpe-1* and Δ*plc-1*; Δ*splA*$_2$ double mutants (Fig. 4.2A), which further supported the increased sensitivity reported in these mutants (Fig. 3.2). The increased expression of *plc-1*, *cpe-1*, and *splA*$_2$ after heat shock and gradual decrease when the *N. crassa* strains were kept for recovery after heat shock (Fig. 4.2B), suggested that these genes are induced upon heat stress possibly to protect the cell by mediating expression of heat shock proteins.

Further, microbes, including fungi, frequently encounter pH stress, another critical environmental condition for survival. Therefore, regulation of gene expression by pH has also been widely investigated. In *A. nidulans* and *S. cerevisiae*, a cascade of proteins regulates pH by activating the transcription factor PacC, the central regulator in the pH signaling pathway (Arst and Peñalva 2003; Peñalva et al. 2008; Maeda 2012). In *S. cerevisiae*, alkaline-regulated genes are calcineurin-dependent, indicating that the Ca^{2+}-induced signaling pathway may be implicated in the pH-responsiveness (Serrano et al. 2002; Viladevall et al. 2004). In *N. crassa*, the response to external pH is also influenced by the transcription factor, Pac-3 (Cupertino et al. 2012). I observed reduced expression of *pac-3* in the Δ*plc-1*, Δ*cpe-1*, Δ*splA*$_2$ single mutants, and Δ*plc-1*; Δ*cpe-1*, Δ*plc-1*; Δ*splA*$_2$, and Δ*cpe-1*; Δ*splA*$_2$ double mutants (Fig. 4.3A), confirming that the genetic interactions of *plc-1*, *cpe-1*, and *splA*$_2$ are critical for the expression of *pac-3* during alkaline stress. However, under acidic stress, *pac-3* transcript levels were basal in all mutants, demonstrating Pac-3 has no effect in acidic conditions (Data not shown). I also observed increased expression of *plc-1*, *cpe-1*, and *splA*$_2$ in the alkaline condition (Fig. 4.3B). These results further supported that the effects of an alkaline pH on the growth sensitivity of these mutants (Fig. 3.3) were indeed due to the reduced level of PAC-3 transcription factor.

The ER performs multiple cellular roles. The lumen of the ER acts as the reservoir of Ca^{2+} in the cell, and its oxidative environment is essential for disulphide bond formation and the correct folding of secreted or membrane proteins. Due to its function in protein folding and transport, the ER is abundant in Ca^{2+}-dependent molecular chaperones such as Grp78 and calreticulin that stabilise protein folding (Rizutto et al. 2004). Aberration of Ca^{2+} homeostasis in the ER causes protein unfolding because of the Ca^{2+}-dependent nature of the molecular chaperones (Ma and Hendershot 2004). If the capacity of ER to cope adequately with protein folding is exceeded due to an increase in protein load and/or a disruption in the conditions required for appropriate folding, the URP is activated (Bravo et al. 2012; Hetz 2012). In *N. crassa*, *plc-1*, *cpe-1*, and *splA*$_2$ and their genetic interactions are important for maintaining the Ca^{2+} homeostasis (Barman and Tamuli 2017). In this study, I observed significant downregulation of two UPR markers, *grp-78* and *pdi-1* in the Δ*splA*$_2$, Δ*plc-1*; Δ*cpe-1*, and Δ*plc-1*;

Δ*splA*$_2$ mutants (Fig. 4.4A), suggesting their sensitivity to DTT during ER stress (Fig. 3.5). In addition, the expression level of *splA*$_2$ was found to be upregulated during ER stress, whereas there was no change in the expression of *plc-1* and *cpe-1* (Fig. 4.4B). It is possible that impaired Ca^{2+} homeostasis could lead to the ER response pathway in these mutants.

Filamentous fungi are the primary producers of hydrolytic enzymes for the degradation of lignocellulosic biomass. In the filamentous fungus *T. reesei*, an increase in the levels of cAMP activates the PLC-1 mediated Ca^{2+} signaling pathway to regulate cellulase overexpression under cellulase-inducing conditions (Chen et al. 2021). In response to growth on plant cell walls and crystalline cellulose (Avicel), *N. crassa* exhibits a robust cellulolytic response that includes the production and release of several cellulases and hemicellulases (Tian et al. 2009). The *plc-1*, *cpe-1*, and *splA*$_2$ genes were not previously found to be involved in cellulose degradation; however, I observed a severe reduction in the expression of the cellulolytic genes, *cbh-1*, *cbh-2*, and *endo-2* in the Δ*plc-1*, Δ*cpe-1*, Δ*plc-1*; Δ*cpe-1*, and Δ*plc-1*; Δ*splA*$_2$ mutants compared to WT when grown on Avicel (Fig. 4.5A). However, Δ*splA*$_2$ and Δ*cpe-1*; Δ*splA*$_2$ mutants showed significantly increased expression of the cellulolytic genes, especially *cbh-1* and *cbh-2* (Fig. 4.5A). Furthermore, the expression levels of *plc-1*, *cpe-1*, and *splA*$_2$ during growth on avicel (Fig. 4.5B) were correlated with the phenotypes (Fig. 3.6) described in the previous chapter. These results suggested that PLC-1 and CPE-1 act as positive regulators, whereas sPLA$_2$ plays a repressive role during growth on cellulose. Moreover, *plc-1* shows epistatic interaction with *cpe-1* and *splA*$_2$ in regulating cellulose degradation pathway in *N. crassa*.

Thus, the *plc-1*, *cpe-1*, and *splA*$_2$ genes regulate multiple cellular pathways in *N. crassa*. Moreover, the presence of putative binding sites for different transcription factors (Table 4.1) further supported that *plc-1*, *cpe-1*, and *splA*$_2$ are critical for circadian clock regulation, stress survival, and utilization of cellulose in *N. crassa*.

I presented the results described in this chapter in part as posters at (i) National Conference on Fungal Biology: Recent Trends and Future Prospects and 44th Annual Meeting of the Mycological Society of India (MSI), University of Jammu, Jammu, 2017; (ii) Research Conclave, IIT Guwahati, 2017, 2018; (iii) XI International Conference on Biology of Yeasts and Filamentous Fungi, University of Hyderabad, 2019; and (iv) Neurospora 2021, Camp Allen, Texas, 2021.

In the next chapter, I describe the molecular basis of sPLA$_2$ mediated cellulose degradation in *N. crassa*.

Chapter 5: The *splA*$_2$ gene interacts with the transcription factor CRE-1 to regulate growth and cellulose degradation in *N. crassa*

5.1 Introduction

In the previous chapter, I described the role of *splA*$_2$ gene in cellulose degradation and ER response pathways in *N. crassa*. The Δ*splA*$_2$ knockout mutant exhibited significantly higher expression of the major cellulolytic genes, suggesting that *splA*$_2$ plays a repressive role during the growth on microcrystalline cellulose (Avicel). Moreover, mutants with enhanced lignocellulose degradation capabilities showed an ER sensitive phenotype, suggesting that the lignocellulase secretion and the ER stress response pathways crosstalk in *N. crassa* (Fan et al. 2015). I found that the Δ*splA*$_2$ mutant showed ER stress sensitivity and was unable to use microcrystalline cellulose during ER stress. Homokaryotic strain expressing the *splA*$_2$ transgene complements the phenotype of the Δ*splA*$_2$ knockout mutant grown on microcrystalline cellulose and also results in the repression of extracellular protein secretion, endoglucanase activity, and ER stress sensitivity in *N. crassa*.

The zinc finger transcription factor CreA/CRE-1, the *S. cerevisiae* Mig1 homolog, which encodes a carbon catabolite repressor protein, *regulates* the utilization of alternate carbon sources in the filamentous ascomycete fungi (Sun and Glass 2011). In *N. crassa*, the deletion of *cre-1* results in an enhanced cellulolytic activity and increased expression of cellulolytic genes during growth on microcrystalline cellulose (Sun and Glass 2011). In addition, the Δ*cre-1* mutant showed an increased sensitivity to ER stress in *N. crassa* (Fan et al. 2015). In addition, the Δ*cre-1* knockout mutant consumed Avicel faster than the WT, secreted more extracellular protein, and showed enhanced endoglucanase activity, when grown on 2% Avicel as a sole carbon source. Furthermore, the *splA*$_2$ gene is under the CRE-1 regulon in *N. crassa* (Sun and Glass 2011).

Therefore, in this chapter, I generated the double mutant of *splA*$_2$ and *cre-1* to understand the cell functions regulated by their genetic interactions in *N. crassa*. I also predicted the three-dimensional protein structures of sPLA$_2$ and CRE-1 using the homology modelling approach.

5.2 Results

5.2.1 Generation and confirmation of the Δ*cre-1*; Δ*splA*$_2$ double mutant

The Δ*splA*$_2$ and Δ*cre-1* single mutants were initially generated and confirmed by the *Neurospora* functional genomics project (https://www.broadinstitute.org/fungal-genomeinitiative/neurospora-crassa-genome-project; http://geiselmed.dartmouth.edu/dunlaploros/genome/; Colot et al. 2006). I described the genetic loci and knockout mutant of the *splA*$_2$ gene in Chapter 1. In *N. crassa*, the *cre-1* gene, encoded by NCU08807, is genetically mapped from position 5176440-5178927 (-) at the right arm of linkage group four in the super contig four, and its genomic sequence has only one exon (LG IVR). To generate the Δ*cre-1*; Δ*splA*$_2$ double mutant, the single mutant strains of opposite mating types were crossed (Fig. 5.1A). After 21 days, ascospores from these crosses were harvested and germinated

on Vogel's sorbose agar medium following a heat shock at 60 °C for 45 min. The germinated ascospores were then transferred to VM agar medium and incubated for three days at 30 °C and one day in the light. The f_1 progenies were then screened for the resistance to hygromycin B (Hyg^R) phenotype, and the knockout alleles were confirmed using gene specific forward primers HI-NCU06650-F and HI-NCU08807-F (Entries 3–4, Table 2.3) for the Δ*splA*$_2$ and Δ*cre-1* mutants, respectively, and the common reverse primer 5HPHR (Entry 5, Table 2.3) specific for the *hph* cassette used in the generation of the knockout mutants. PCR amplified products of size ~ 2.044 and 2.5 kb indicated the presence of the Δ*splA*$_2$ and Δ*cre-1* knockout alleles, respectively, in the corresponding mutant strain (Fig. 5.1B).

(A)

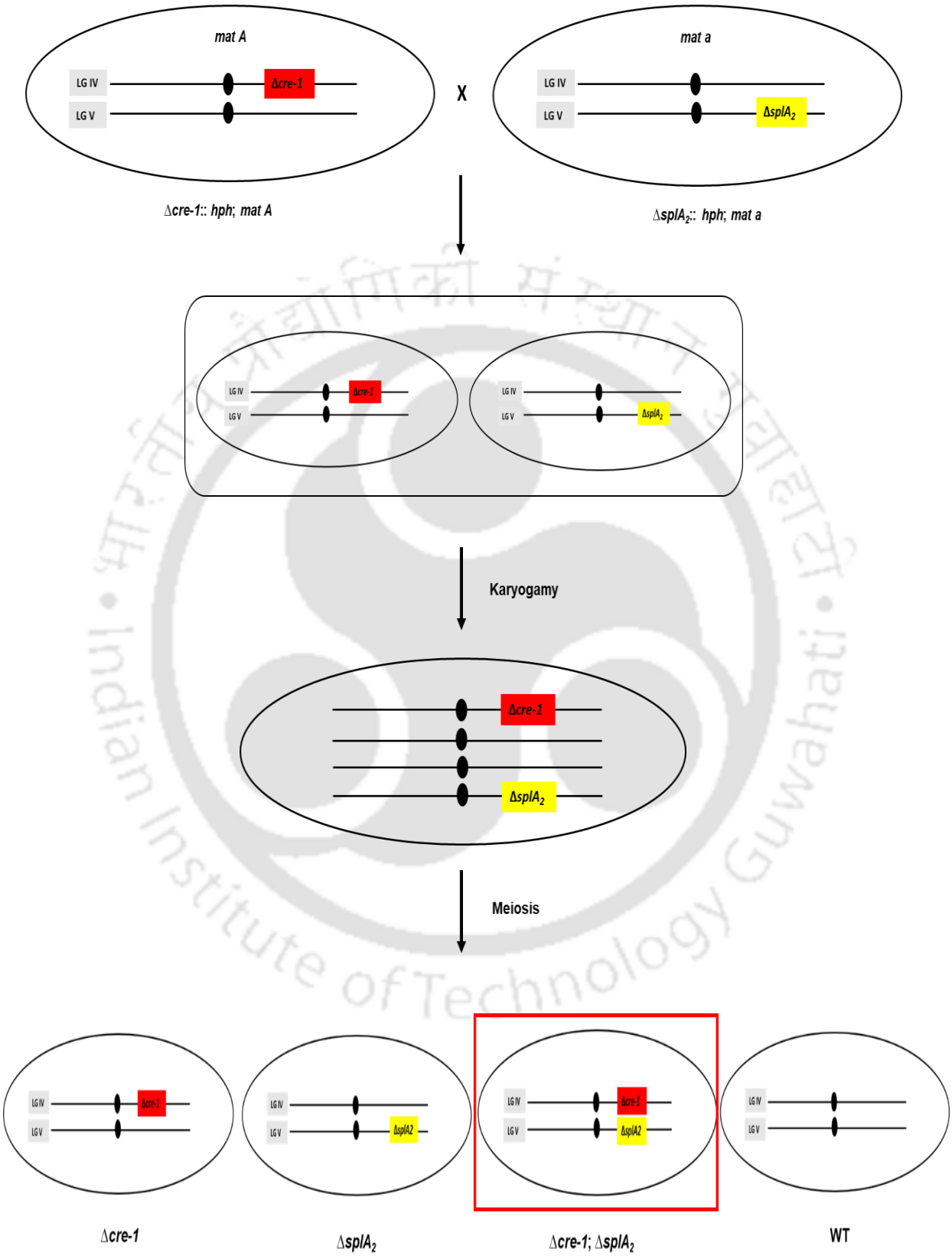

(B)

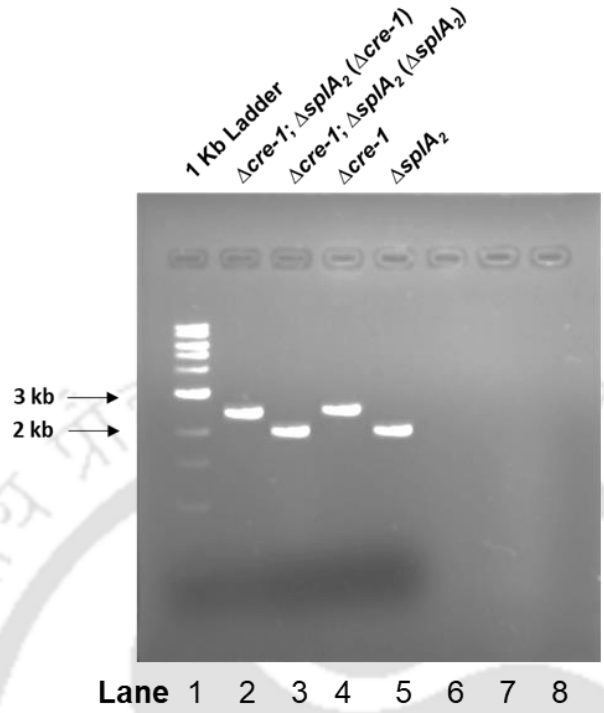

Figure 5.1: Generation and confirmation of the Δ*cre-1*; Δ*splA*$_2$ double mutant. (A) A schematic representation of the crosses of Δ*splA*$_2$ and Δ*cre-1* single mutant strains of opposite mating type for generating the double mutant. **(B)** Confirmation of the Δ*cre-1*; Δ*splA*$_2$ double mutant by PCR analysis. The Δ*cre-1*; Δ*splA*$_2$ double mutant was verified by using the forward primers HI-NCU06650-F and HI-NCU08807-F (Entries 3–4, Table 2.3), specific for upstream of the open reading frame of the *splA*$_2$ and *cre-1* genes, respectively, along with the common reverse primer HPHR (Entry 5, Table 2.3) specific for the *hph* cassette used to generate the knockout mutants (Colot et al. 2006; Deka et al. 2011). Amplification of PCR products of size ~ 2.044 kb and 2.5 kb respectively, indicate the presence of the Δ*splA*$_2$ and Δ*cre-1* knockout alleles in the double mutant. PCR products of the Δ*cre-1* (lane 2) and Δ*splA*$_2$ (lane 3) knockout alleles from the Δ*cre-1*; Δ*splA*$_2$ double mutant, Δ*cre-1* allele from the Δ*cre-1* single mutant (lane 4), and Δ*splA*$_2$ allele from the Δ*splA*$_2$ single mutant (lane 5) were used as positive control, and WT (lanes 6, 7) was used as negative control for both the single mutant alleles, were visualized in a 1.2% agarose gel. The Δ*splA*$_2$ and Δ*cre-1* single mutants were generated by the *N. crassa* genome project (Colot et al. 2006).

5.2.2 The Δ*cre-1*; Δ*splA*$_2$ double mutant showed distinct colony and hyphal morphology

To study the morphology of the WT, Δ*splA*$_2$, Δ*cre-1*, Δ*cre-1*; Δ*splA*$_2$, $P_{ccg\text{-}1}$::*splA*$_2$::*gfp*, and *Pn-cre-1*, mycelial plugs of the strains were inoculated in VM agar medium and incubated at 30 °C for three days

in the dark followed by four days under light. The Δ*cre-1*; Δ*splA*$_2$ double mutant exhibited a colonial morphology distinct from that of the WT and the parental single mutants, with severely reduced mycelial growth and pigmentation (Fig. 5.2A, B). The morphological phenotype exhibited by the Δ*cre-1*; Δ*splA*$_2$ double mutant was different from the WT and both parental single mutants.

To study hyphal morphology, the strains were incubated at 30 °C in VM agar medium for 12 h and observed under the microscope. The Δ*cre-1*; Δ*splA*$_2$ double mutant displayed reduced hyphal branching, whereas the single mutants and the homokaryotic strains exhibited normal hyphal morphology and branching patterns like the WT (Fig. 5.2C).

(A)

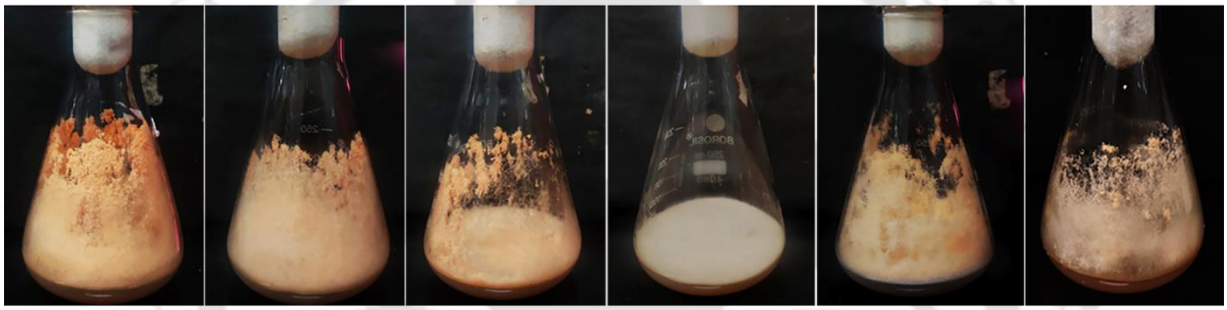

(B)

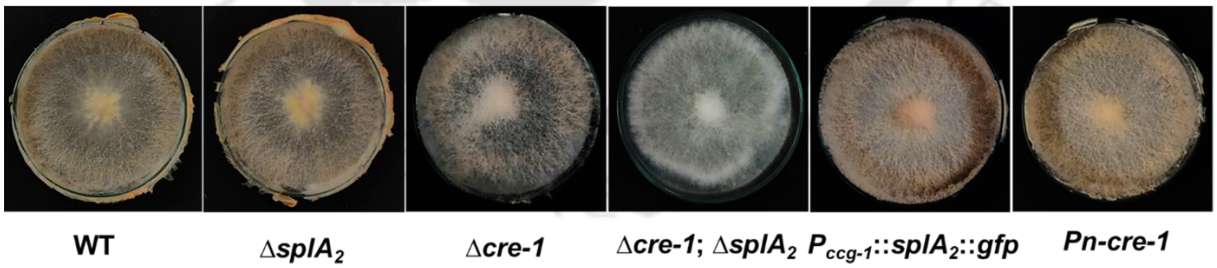

(C)

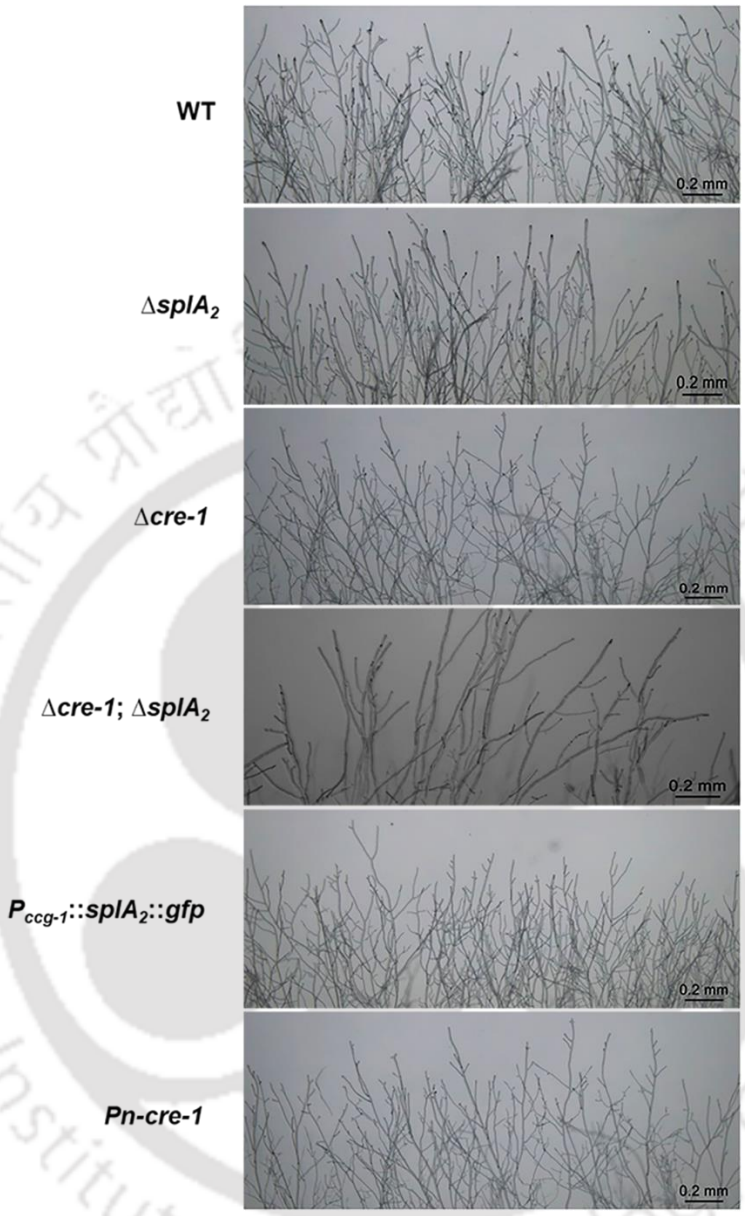

Figure 5.2: Morphology of the WT, Δ*splA*$_2$, Δ*cre-1*, Δ*cre-1*; Δ*splA*$_2$, *P*$_{ccg-1}$::*splA*$_2$::*gfp*, and *Pn-cre-1* strains. **(A)** Colony morphology of the strains grown on VM agar medium in flasks. **(B)** Colony morphology of the strains grown on VM agar medium in 90-mm Petri dishes. For colony morphology, the strains were incubated for three days in the dark at 30 °C followed by four days under light at room temperature, and then photographed. **(C)** Hyphal morphology of the strains grown on VM agar medium for 12 h at 30 °C under a Trinocular inverted microscope (Leica). Scale bar 20 µm.

5.2.3 The Δ*cre-1*; Δ*splA*$_2$ double mutant showed severely reduced growth

For radial and apical growth, the WT, Δ*splA*$_2$, Δ*cre-1*, Δ*cre-1*; Δ*splA*$_2$, *P*$_{ccg-1}$::*splA*$_2$::*gfp*, and *Pn-cre-1* strains were inoculated in sterile 90-mm Petri dishes and race tubes, respectively, containing VM agar medium and incubated at 30 °C to measure the mycelial growth. Hyphal growth fronts were measured as described in Materials and Methods. The Δ*cre-1*; Δ*splA*$_2$ double mutant showed severely reduced growth compared to the WT and the parental single mutants (Table 5.1, 5.2; Fig. 5.3A, B). The Δ*splA*$_2$ single mutant and both homokaryotic strains displayed growth similar to the WT; however, Δ*cre-1* mutant showed a slightly reduced growth compared to the WT (Table 5.1, 5.2; Fig. 5.3A, B).

(A)

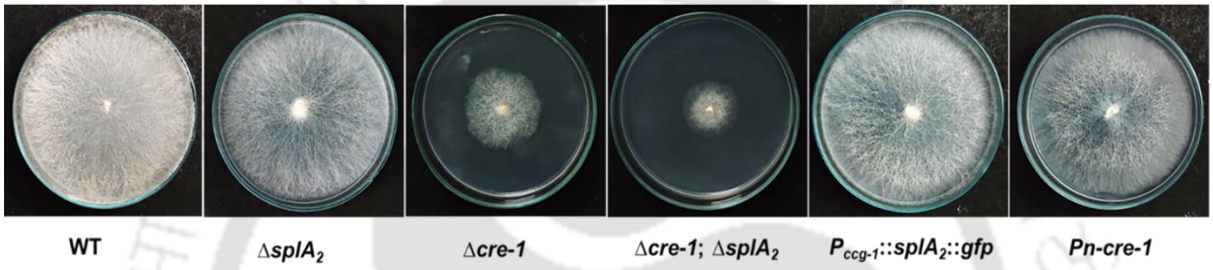

(B)

Figure 5.3: Growth phenotype of the WT, Δ*splA*$_2$, Δ*cre-1*, Δ*cre-1*; Δ*splA*$_2$, *P*$_{ccg-1}$::*splA*$_2$::*gfp*, and *Pn-cre-1* strains. **(A)** Colony growth. The colony growth rate of the strains was measured and photographed after 24 h of incubation at 30 ºC in Petri dishes containing VM agar medium. **(B)** Apical growth. The apical growth of the strains was measured at 30 ºC using race tubes over a 72 h period on VM agar medium. Error bars indicate standard deviations calculated from the data for three independent experiments (n = 3) with *P-values* < 0.05 (*), < 0.01 (**), and < 0.001 (***) compared with the WT as measured by a one-way ANOVA test.

Table 5.1: Average growth rate of the WT, Δ*splA*$_2$, Δ*cre-1*, Δ*cre-1*; Δ*splA*$_2$, *P*$_{ccg-1}$::*splA*$_2$::*gfp*, and *Pn-cre-1* strains

Strains	[+]Growth rate (cm/h)
WT	0.43 ± 0.02
Δ*splA*$_2$	0.41 ± 0.01
Δ*cre-1*	0.28 ± 0.00 (***)
Δ*cre-1*; Δ*splA*$_2$	0.12 ± 0.01 (***)
P$_{ccg-1}$::*splA*$_2$::*gfp*	0.41 ± 0.02
Pn-cre-1	0.36 ± 0.02 (**)

Table 5.2: Average apical growth of the WT, Δ*splA*$_2$, Δ*cre-1*, Δ*cre-1*; Δ*splA*$_2$, *P*$_{ccg-1}$::*splA*$_2$::*gfp*, and *Pn-cre-1* strains

Strains	[+]Average apical growth at different time point (cm)		
	24 h	48 h	72 h
WT	7.05 ± 0.30	19.28 ± 1.02	31.35 ± 0.97
Δ*splA*$_2$	6.87 ± 0.22	19.27 ± 0.32	31.30 ± 0.17
Δ*cre-1*	2.98 ± 0.49	8.54 ± 0.75	14.14 ± 0.75
Δ*cre-1*; Δ*splA*$_2$	1.72 ± 0.16	4.02 ± 0.50	6.80 ± 1.31
P$_{ccg-1}$::*splA*$_2$::*gfp*	5.82 ± 0.30	18.68 ± 2.12	30.22 ± 1.93
Pn-cre-1	7.08 ± 0.24	18.52 ± 0.25	29.78 ± 0.52

5.2.4 The Δ*cre-1*; Δ*splA*$_2$ double mutant showed reduced aerial hyphae and conidiation

I also investigated whether the double deletions affect the aerial hyphal development and conidiation in the Δ*cre-1*; Δ*splA*$_2$ double mutant. To study aerial hyphae, ~1 × 10^6 conidia of the WT, Δ*splA*$_2$, Δ*cre-1*, Δ*cre-1*; Δ*splA*$_2$, $P_{ccg\text{-}1}$::*splA*$_2$::*gfp*, and *Pn-cre-1* strains were inoculated in the VM liquid medium and incubated for three days in the dark at 30 °C, and then four days in the light for conidiation. The Δ*cre-1*; Δ*splA*$_2$ double mutant produced significantly shorter aerial hyphae as compared to the WT and the parental single mutants (Table 5.3; Fig. 5.4).

To determine conidiation, mycelial plugs of the WT, Δ*splA*$_2$, Δ*cre-1*, Δ*cre-1*; Δ*splA*$_2$, $P_{ccg\text{-}1}$::*splA*$_2$::*gfp*, and *Pn-cre-1* strains were inoculated in VM agar medium and incubated at 30 °C for three days in the dark, and four days under light at 22 °C. After thorough resuspension of conidia in sterile distilled water, conidia were counted using a haemocytometer. The Δ*cre-1*; Δ*splA*$_2$ double mutant produced significantly fewer conidia and showed > 50% reduction in conidiation compared to the WT and parental single mutants (Table 5.4). Therefore, these data indicated that the interactions of *cre-1* with *splA*$_2$ play an important role for normal aerial hyphae development and conidiation in *N. crassa*.

(A)

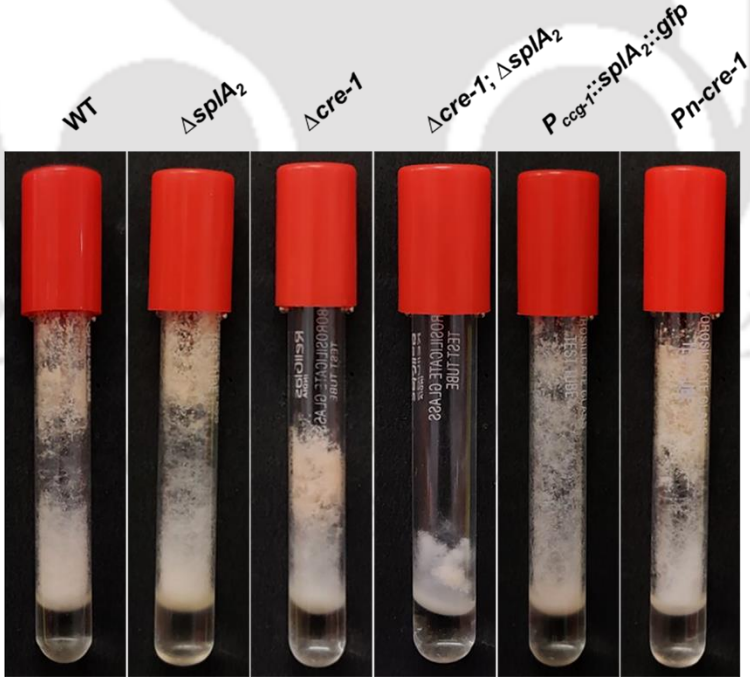

Figure 5.4: Aerial hyphae growth of the WT, Δ*splA*$_2$, Δ*cre-1*, Δ*cre-1*; Δ*splA*$_2$, $P_{ccg\text{-}1}$::*splA*$_2$::*gfp*, and *Pn-cre-1* strains. Strains were grown in VM liquid medium and incubated at 30 °C for three days in the dark, then kept in the light at room temperature for four days and photographed.

Table 5.3: Average aerial hyphae growth of the WT, Δ*splA*$_2$, Δ*cre-1*, Δ*cre-1*; Δ*splA*$_2$, *P*$_{ccg-1}$::*splA*$_2$::*gfp*, and *Pn-cre-1* strains

Strains	[+]Average aerial hyphae growth (cm)
WT	6.5 ± 0.20
Δ*splA*$_2$	6.8 ± 0.20
Δ*cre-1*	4.2 ± 0.06 (***)
Δ*cre-1*; Δ*splA*$_2$	2.4 ± 0.15 (***)
P$_{ccg-1}$::*splA*$_2$::*gfp*	6.2 ± 0.26
Pn-cre-1	6.03 ± 0.15 (*)

Table 5.4: Average conidial count of the WT, Δ*splA*$_2$, Δ*cre-1*, Δ*cre-1*; Δ*splA*$_2$, *P*$_{ccg-1}$::*splA*$_2$::*gfp*, and *Pn-cre-1* strains

Strains	[+]Average count of conidia (conidia /ml)
WT	32.5 x 10^7
Δ*splA*$_2$	28.7 x 10^7
Δ*cre-1*	26.2 x 10^7
Δ*cre-1*; Δ*splA*$_2$	60.6 x 10^5
P$_{ccg-1}$::*splA*$_2$::*gfp*	33.7 x 10^7
Pn-cre-1	38.0 x 10^7

5.2.5 The Δ*cre-1*; Δ*splA*$_2$ double mutant showed irregular septation

I investigated whether the reduced vegetative growth and slower apical extension rate of the Δ*cre-1*; Δ*splA*$_2$ double mutant were caused by improper septation in the growing vegetative hyphae using the fluorescent probe calcofluor white (CFW; Fig. 5.5A), which binds specifically to cell walls composed of cellulose and chitin. The germlings and vegetative hyphae of the Δ*cre-1*; Δ*splA*$_2$ double mutant, after staining with CFW and visualization by fluorescence microscopy, showed irregular septation in contrast to an even septation pattern in the WT and individual single mutants (Fig. 5.5B). However, the Δ*cre-1*; Δ*splA*$_2$ double mutant stained as deeply with CFW as those of WT, and the individual single mutants, which indicated deposition of cellulose and chitin, were not affected in the double mutant (Fig. 5.5B).

(A)

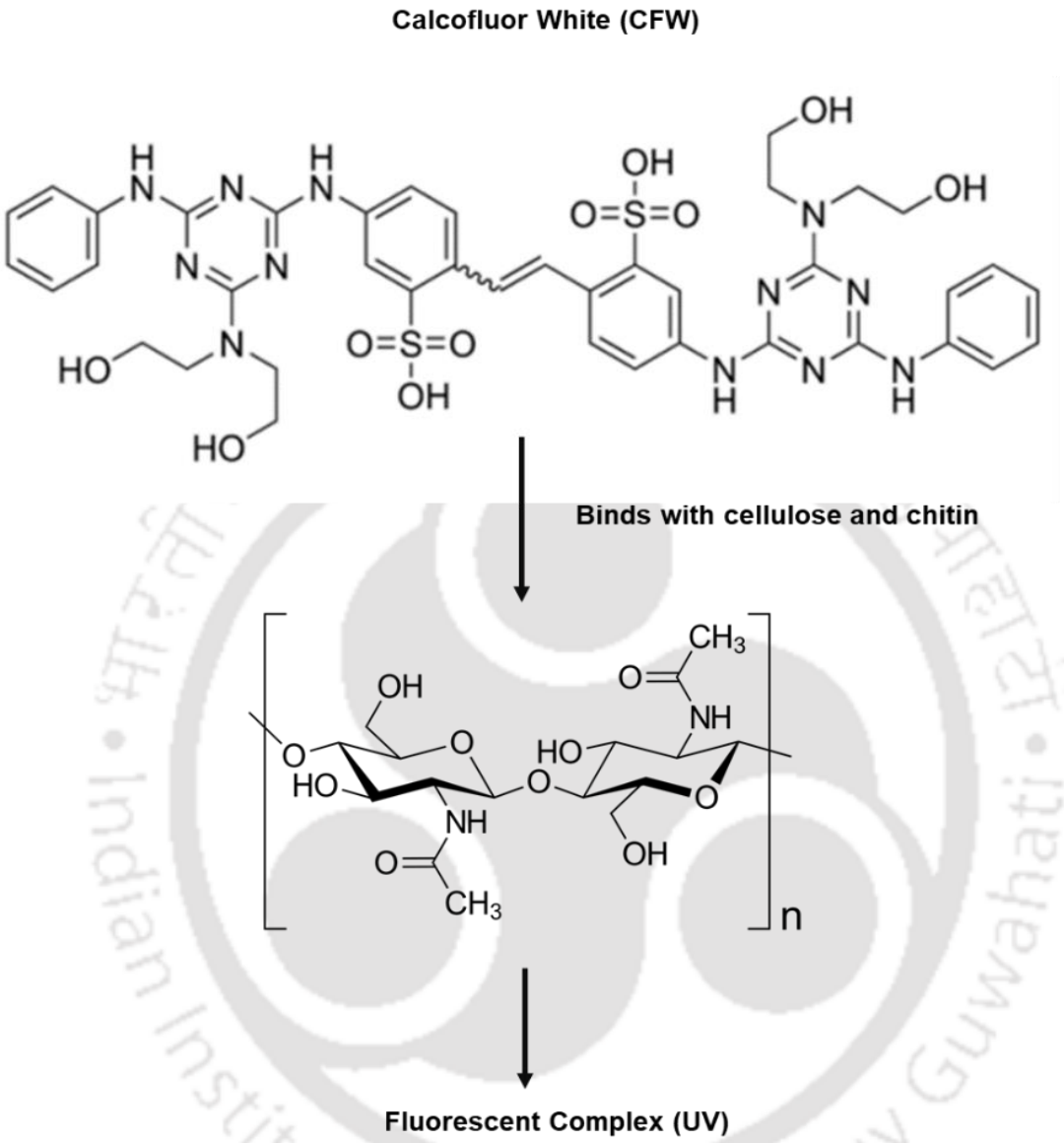

(B)

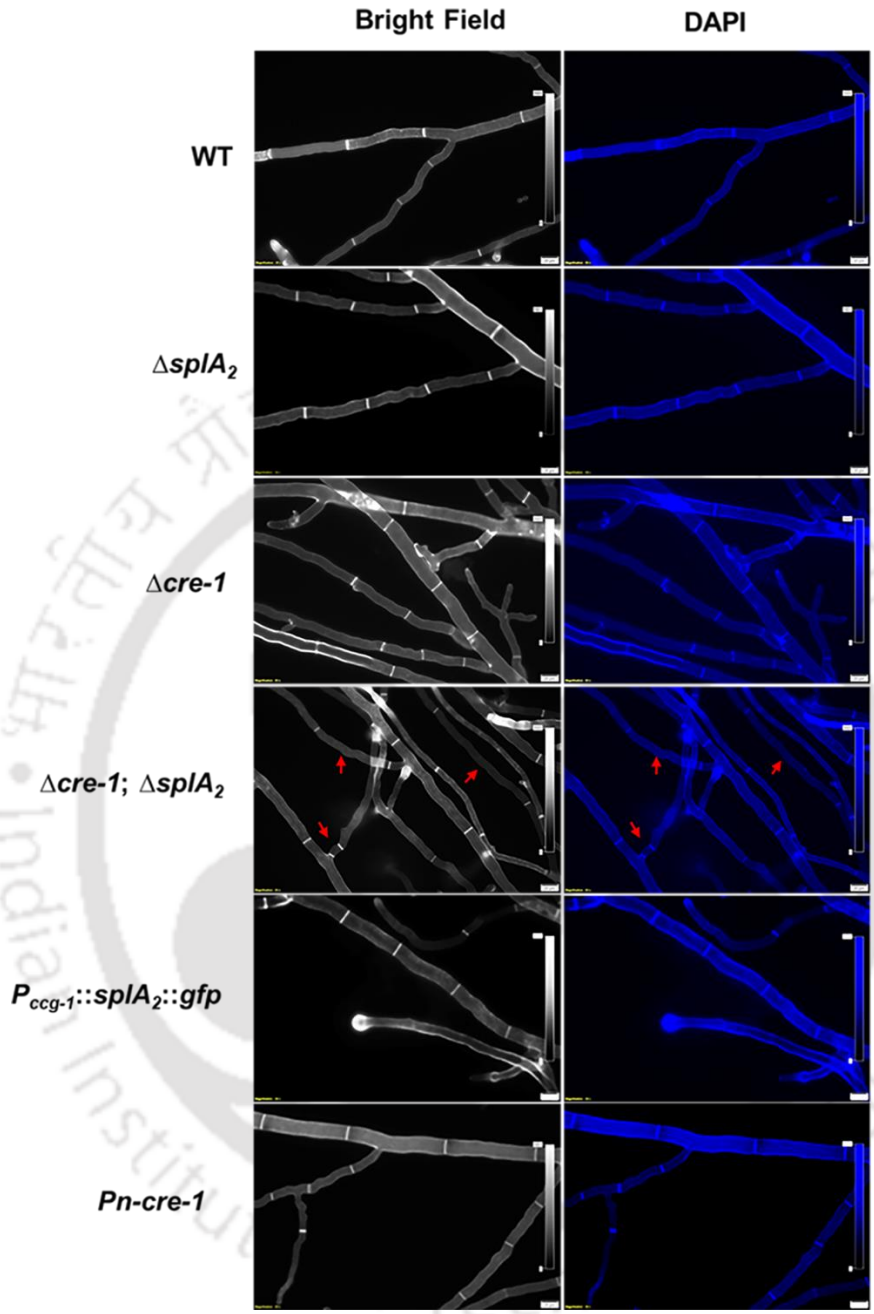

Figure 5.5: Assay for visualization of internal septation of germlings and vegetative hyphae of the WT, Δ*splA*$_2$, Δ*cre-1*, Δ*cre-1*; Δ*splA*$_2$, *P*$_{ccg-1}$::*splA*$_2$::*gfp*, and *Pn-cre-1* strains. (A) Chemical structure of calcofluor white (CFW; λ_{ex}= 355 nm; λ_{em}= 420 nm). CFW, a non-specific fluorochrome binds to cellulose and chitin present in the cell walls of fungi and other organisms. **(B)** Germlings and hyphae of the strains stained with CFW (0.1% in 0.05 M PBS). The sample slides were incubated in the dark for 20 min and observed under a Trinocular inverted fluorescence microscope (AxioVert A1 FL, Carl Zeiss) with DAPI filters and an exposure time of 300-400 ms. Scale bar 20 µm.

5.2.6 The Δ*cre-1*; Δ*splA*$_2$ double mutant was highly sensitive to cell wall stress drugs

I also investigated if the double deletions affected the cell wall integrity of the Δ*cre-1*; Δ*splA*$_2$ double mutant. To test this hypothesis, I assessed the growth of the WT, Δ*splA*$_2$, Δ*cre-1*, Δ*cre-1*; Δ*splA*$_2$, *P*$_{ccg-1}$::*splA*$_2$::*gfp*, and *Pn-cre-1* strains on VM agar medium containing the cell wall stress drugs, Congo Red and SDS that bind chitin and block chitin-glucan cross-linking (Maddi et al. 2012). The Δ*cre-1*; Δ*splA*$_2$ double mutant was unable to grow in the presence of cell wall stressors, indicating that *splA*$_2$ and *cre-1* interactions were required for maintaining cell wall integrity in *N. crassa*. The single mutants and both homokaryotic strains displayed growth patterns similar to the WT (Fig. 5.6).

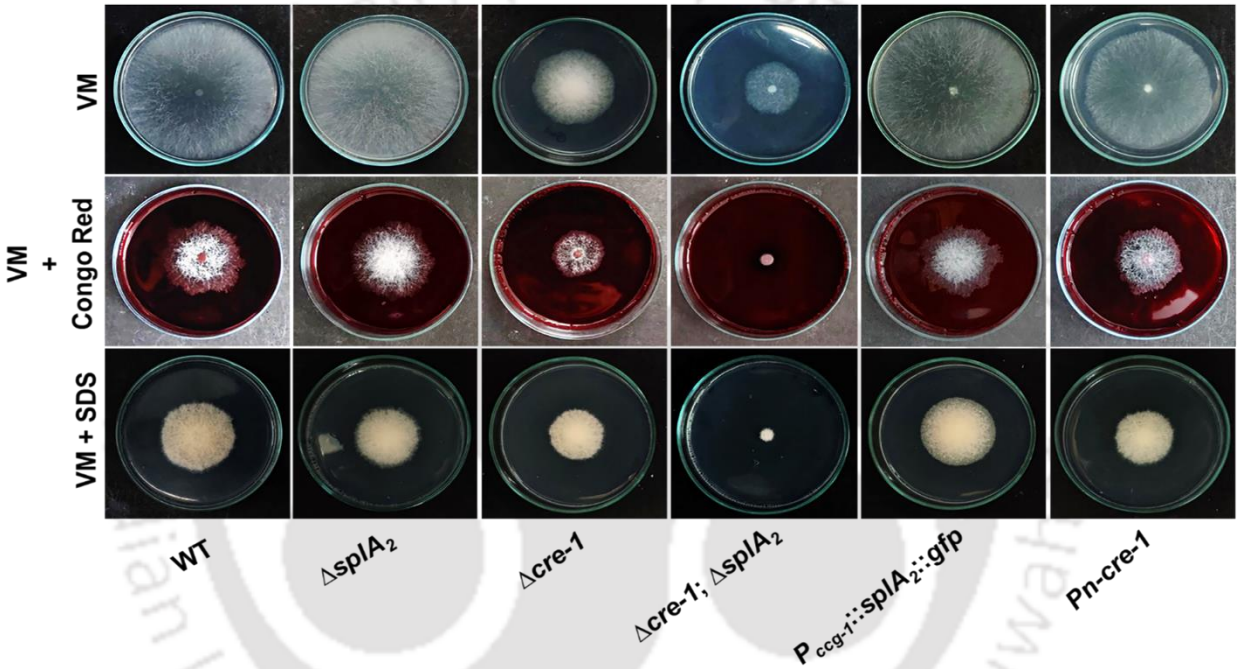

Figure 5.6: Cell wall stress assay of the WT, Δ*splA*$_2$, Δ*cre-1*, Δ*cre-1*; Δ*splA*$_2$, *P*$_{ccg-1}$::*splA*$_2$::*gfp*, and *Pn-cre-1* strains. Colony growth of the strains grown on VM agar medium in the presence of cell wall stress drugs, Congo Red and SDS. Strains were incubated at 30 °C for 24 h in the dark, and then photographed.

5.2.7 The Δ*cre-1*; Δ*splA*$_2$ double mutant was unable to grow in response to ER stress

In a previous study, the *splA*$_2$ and *cre-1* deletions were previously shown to increase the sensitivity to DTT induced ER stress in *N. crassa* (Table 3.4 and Fig. 3.5, Chapter 3; Fan et al. 2015); therefore, I studied the ability of the Δ*cre-1*; Δ*splA*$_2$ double mutant to grow in DTT induced ER stress conditions. In contrast to the reduced growth in both the parental single mutants, the Δ*cre-1*; Δ*splA*$_2$ double mutant undergoes a severe growth retardation in the presence of 2 mM DTT (Fig. 5.7). The homokaryotic

strains displayed a growth pattern similar to the WT (Fig. 5.7). This finding suggested the interaction of *splA*$_2$ with *cre-1* may be critical in response to ER stress in *N. crassa*.

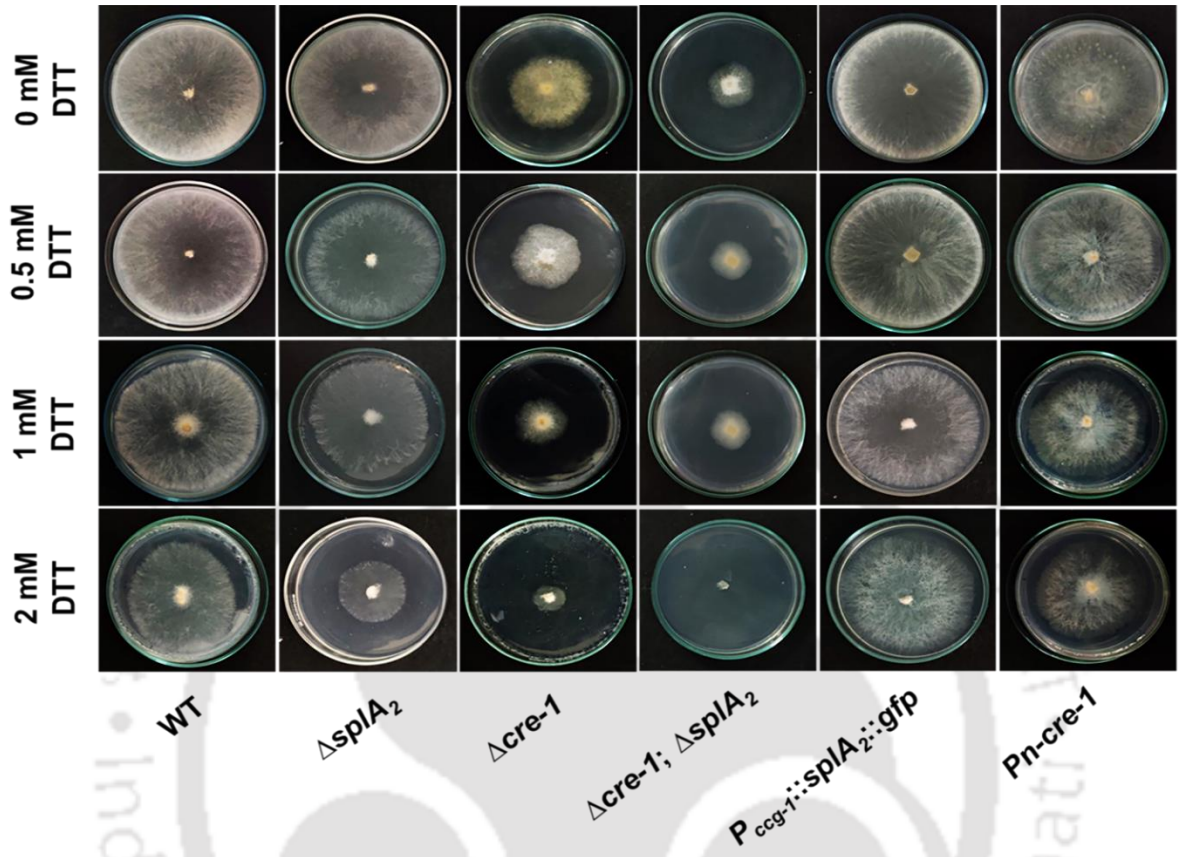

Figure 5.7: ER stress assay of the WT, Δ*splA*$_2$, Δ*cre-1*, Δ*cre-1*; Δ*splA*$_2$, *P*$_{ccg-1}$*::splA*$_2$*::gfp*, and *Pn-cre-1* strains. Colony growth of the strains on VM agar supplemented with 0 mM, 0.5 mM, 1 mM, and 2 mM DTT. Strains were incubated at 30 °C for 24 h in the dark, and then photographed.

5.2.8 The Δ*cre-1*; Δ*splA*$_2$ double mutant exhibited enhanced cellulose degradation ability

Deletion of *splA*$_2$ and *cre-1* results in increased cellulolytic activity, increased protein secretion, and higher endoglucanase activity during growth on microcrystalline cellulose in *N. crassa*. Therefore, to investigate the effect of double deletions, I assessed the cellulose degradation ability of the Δ*cre-1*; Δ*splA*$_2$ double mutant on VM media supplemented with 2% microcrystalline cellulose as the sole carbon source. The Δ*splA*$_2$ and Δ*cre-1* single mutants devoured the supplemented amount of microcrystalline cellulose in two days, while the WT required five days (Fig. 3.6A, Chapter 3; Sun and Glass 2011). Both Δ*splA*$_2$ and Δ*cre-1* showed higher protein secretion and glucose accumulation in the culture supernatant compared to the WT (Fig. 3.6B, C, Chapter 3; Sun and Glass 2011). The Δ*cre-1*; Δ*splA*$_2$ double mutant exhibited enhanced cellulose degradation ability, secreted significantly higher extracellular protein, and accumulated higher glucose compared to the WT and the parental single

mutants (Fig. 5.8A, B, C). But, unlike the Δ*splA*$_2$ and Δ*cre-1* single mutants, the Δ*cre-1*; Δ*splA*$_2$ double mutant did not form mycelial aggregates and remained as isolated colonies. I also assessed the ability of the Δ*cre-1*; Δ*splA*$_2$ double mutant to utilize different carbon sources. However, the Δ*cre-1*; Δ*splA*$_2$ mutants did not show significant differences in growth rate and morphology when grown on sucrose, glucose, xylose, glycerol and sodium acetate (Fig. 5.8D). These findings revealed that interaction of *splA*$_2$ and *cre-1* is involved in the regulation of cellulose degradation pathway in *N. crassa*.

(A)

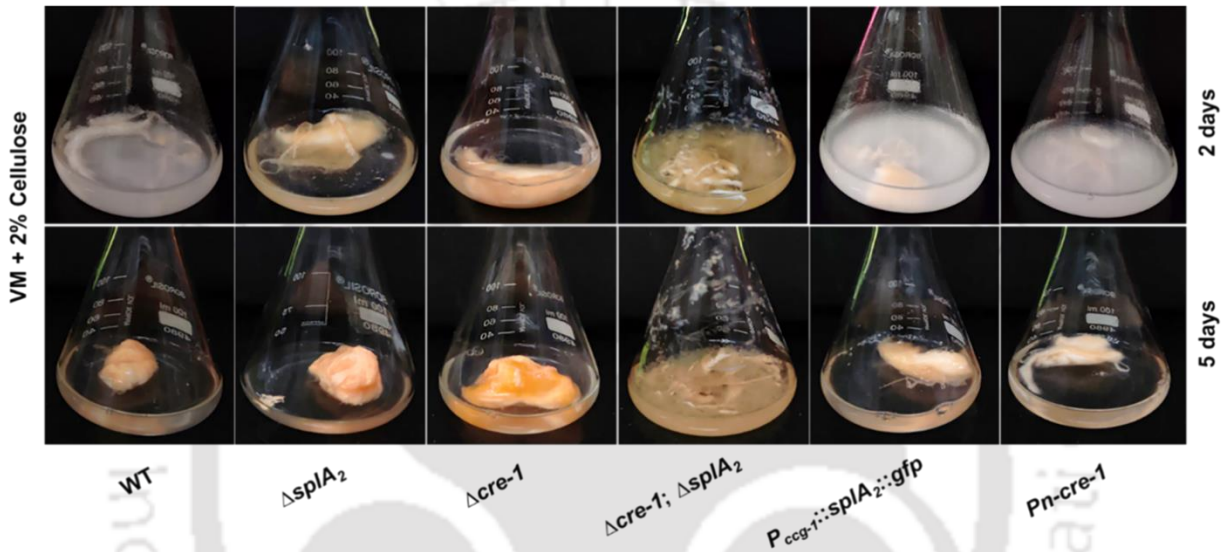

(B)

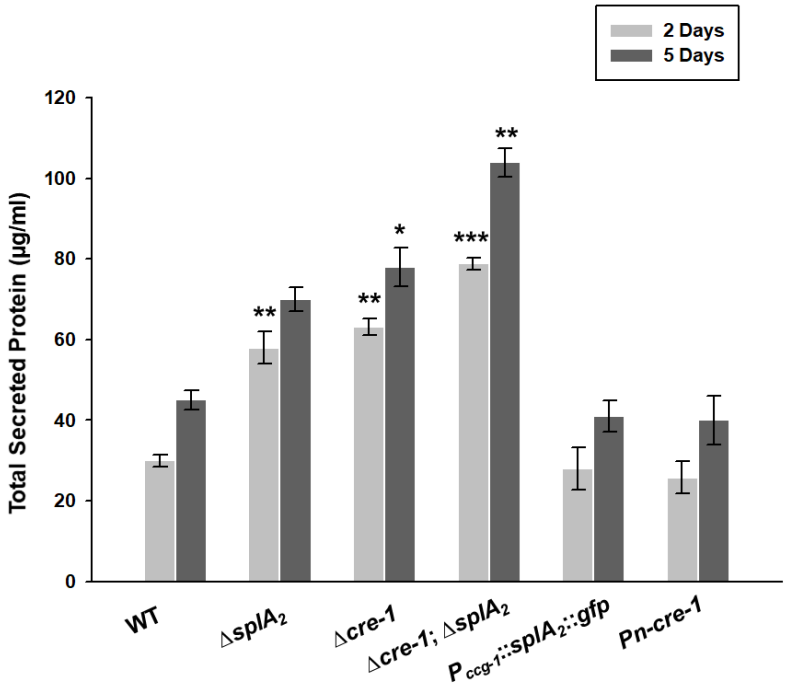

(C)

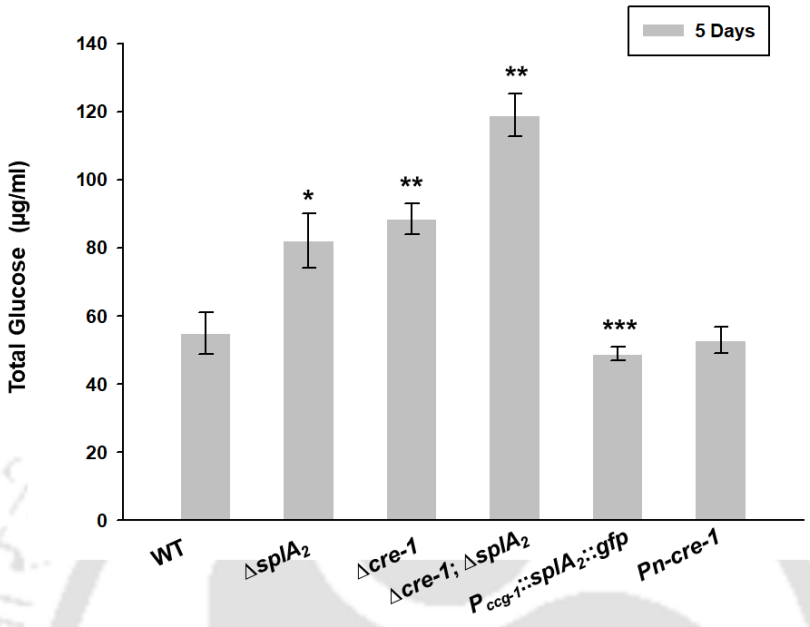

(D)

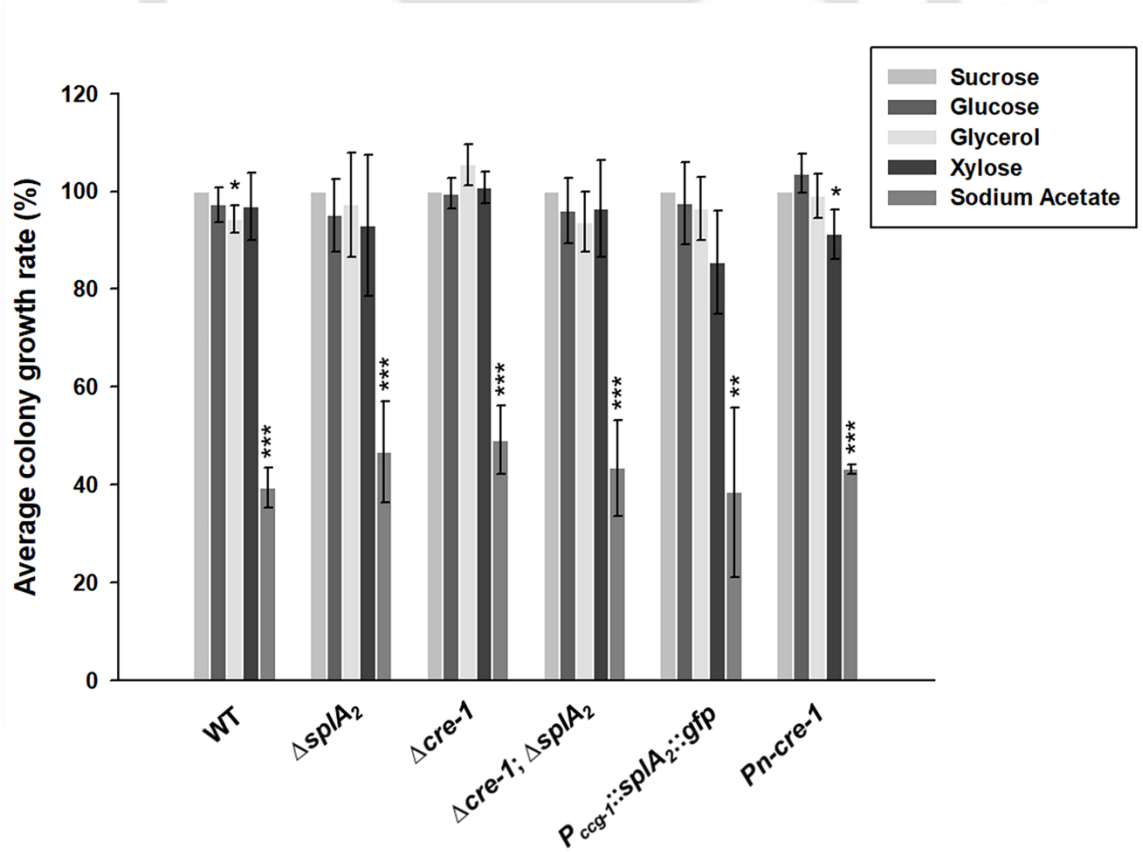

Figure 5.8: Growth of the WT, Δ*splA₂*, Δ*cre-1*, Δ*cre-1*; Δ*splA₂*, *P*$_{ccg-1}$::*splA₂*::*gfp*, and *Pn-cre-1* strains on alternate carbon sources. (**A)** Strains grown in Vogel's media with 2% microcrystalline cellulose as the sole carbon source for 2 days (Top panel) and 5 days (Bottom panel). **(B)** Total secreted protein in the 2 days and 5 days culture supernatants of strains grown in Vogel's media with 2% microcrystalline cellulose as the sole carbon source. **(C)** Total glucose in the culture supernatants of the strains grown in Vogel's media with 2% microcrystalline cellulose as the sole carbon source for 5 days. **(D)** Graph showing the average colony growth rate (%) of the strains when grown on sucrose, glucose, xylose, glycerol, and sodium acetate as carbon source. Error bars indicate standard deviations calculated from the data for three independent experiments (n = 3). Asterisks indicate statistically significant values, **P<0.05, **P<0.01, ***P<0.001*.

Table 5.5: Average colony growth rate (%) of WT, Δ*splA₂*, Δ*cre-1*, Δ*cre-1*; Δ*splA₂*, *P*$_{ccg-1}$::*splA₂*::*gfp*, and *Pn-cre-1* strains on different carbon sources

Strains	[+]Percent growth in VM with different carbon sources				
	Sucrose	**Glucose**	**Glycerol**	**Xylose**	**Sodium Acetate**
WT	100 ± 0.00	97.29 ± 3.56	94.25 ± 2.81 (*)	96.98 ± 6.87	39.43 ± 4.14 (***)
Δ*splA₂*	100 ± 0.00	95.12 ± 7.36	97.24 ± 10.67	93.01 ± 14.41	46.70 ± 10.35 (***)
Δ*cre-1*	100 ± 0.00	99.60 ± 3.10	105.50 ± 4.15	100.83 ± 3.23	49.14 ± 6.96 (***)
Δ*cre-1*; Δ*splA₂*	100 ± 0.00	96.06 ± 6.58	93.79 ± 6.06	96.46 ± 9.97	43.44 ± 9.78 (***)
P$_{ccg-1}$::*splA₂*::*gfp*	100 ± 0.00	97.58 ± 8.37	96.46 ± 6.52	85.45 ± 10.54	38.46 ± 17.39 (**)
Pn-cre-1	100 ± 0.00	103.70 ± 3.92	99.03 ± 4.48	91.27 ± 5.1 (*)	43.18 ± 0.93 (***)

[+]Results are shown as mean ± standard deviation for three independent experiments (n = 3) with *P-values* < 0.05 (*), < 0.01 (**), and < 0.001 (***) compared with the control condition (sucrose) as measured by a one-way ANOVA test.

5.2.9 The *splA₂* and *cre-1* interacts to regulate the expression of UPR markers and the cellulolytic genes in *N. crassa*

I also measured the transcript levels of the UPR markers, *grp-78* and *pdi-1* (as described in Chapter 4) to assess the impact of ER stress in the Δ*cre-1*; Δ*splA₂* double mutant. The Δ*splA₂* and Δ*cre-1* single mutants also showed reduced expression of *grp-78* and *pdi-1*; however, the transcript levels of *grp-78* and *pdi-1* in the Δ*cre-1*; Δ*splA₂* double mutant were drastically downregulated compared to the WT and

the parental single mutants (Fig. 5.9A), in agreement with the phenotype described for ER stress conditions (Fig. 5.7).

Further to investigate if the increased cellulase/endoglucanase activity and protein secretion in the Δ*cre-1*; Δ*splA*$_2$ mutant (Fig. 5.8A, B, C) was due to increased expression of cellulases, I determined the expression levels of three major cellulolytic genes, *cbh-1*, *cbh-2*, and *endo-2* (as described in Chapter 4). During growth on microcrystalline cellulose, the Δ*cre-1*; Δ*splA*$_2$ mutant showed increased expression of *cbh-1* and *cbh-2* compared to the WT and parental single mutants; however, the expression of *endo-2* was comparable to the parental single mutants (Fig. 5.9B). I also analysed the transcript levels of *splA*$_2$ in the Δ*cre-1* mutant. The expression of *splA*$_2$ was upregulated nearly 3-fold in the Δ*cre-1* single mutant, whereas the transcript levels of *splA*$_2$ were similar in both WT and the *Pn-cre-1* homokaryotic strain (Fig. 5.9C).

(A)

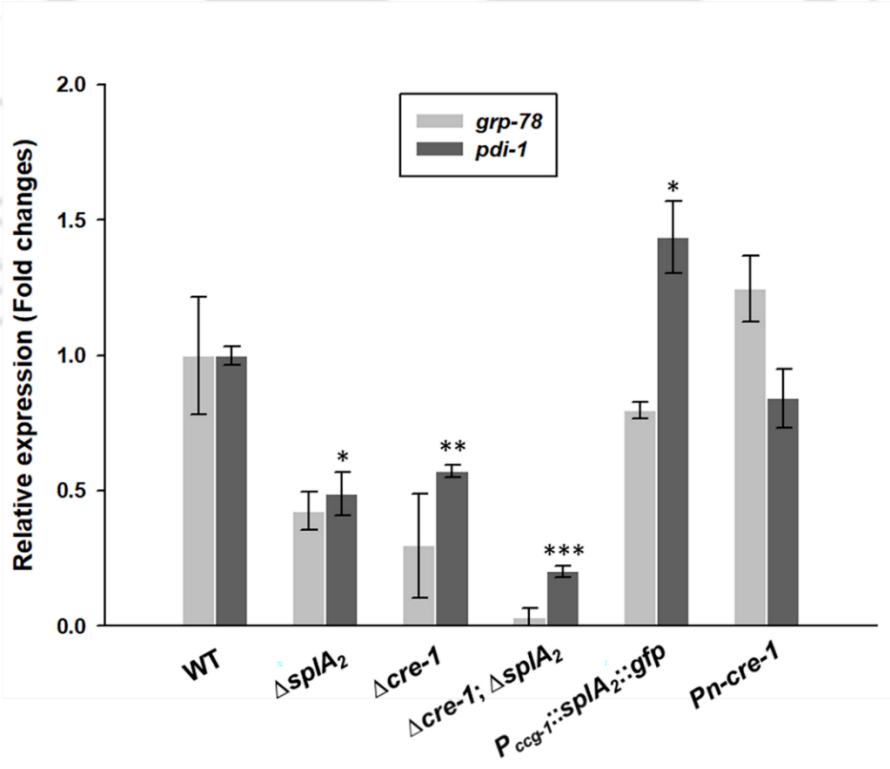

(B)

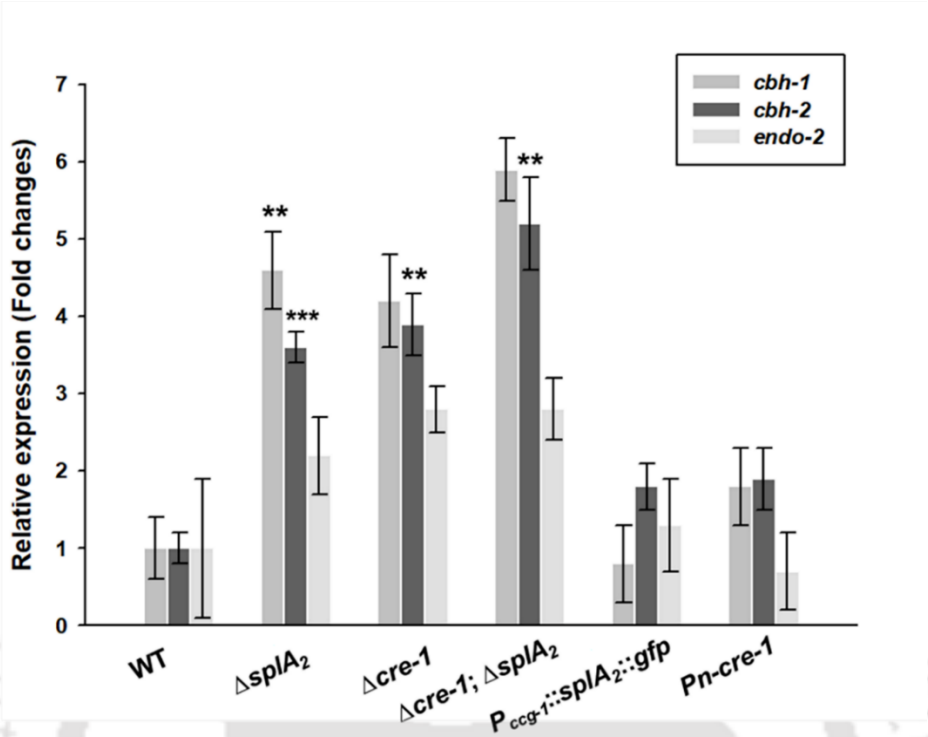

(C)

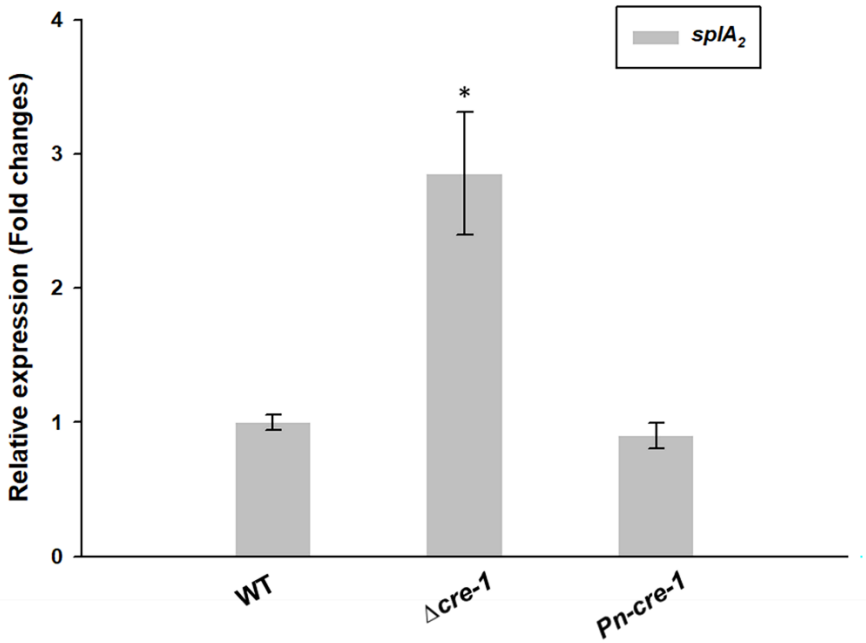

Figure 5.9: Gene expression analysis in response to ER stress and growth on microcrystalline cellulose. RNA was extracted from the *N. crassa* strains cultured in **(A)** VM medium supplemented with 2 mM DTT and the expression of *grp-78* and *pdi-1* was determined, **(B)** VM medium supplemented with 2% microcrystalline cellulose and the expression of *cbh-1*, *cbh-2*, and *endo-2* was determined and **(C)** VM medium supplemented with 2% microcrystalline cellulose and the expression of *splA*$_2$ was determined. The expression of these genes were determined by qRT-PCR using three biological replicates of each strain. The expression of each gene was normalized with the *β-tubulin* and expression values were compared with those of the WT. Error bars indicate standard deviations calculated from the data for three independent experiments (n = 3) with *P-values* < 0.05 (*), < 0.01 (**), and < 0.001 (***) compared to the WT as measured by a one-way ANOVA test.

5.2.10 The modelled structures of sPLA$_2$ and CRE-1 are found to be stereochemically reliable and structurally stable

5.2.10.1 3D Protein Structure Prediction, Refinement, and Molecular Dynamics Simulation Analysis of sPLA$_2$ and CRE-1

In *N. crassa*, secretory phospholipase A$_2$ (sPLA$_2$) and the zinc finger transcription factor CRE-1 comprises of 185 and 430 amino acids, respectively. The unique protein identities of sPLA$_2$ and CRE-1 with respect to the FungiDB and UniProtKB databases, from which the FASTA format of the respective amino acid sequences was obtained (Table 5.6). The FASTA format of the amino acid sequences obtained was used to model the sPLA$_2$ and CRE-1 proteins. As a result of threading and ab-initio based modelling performed by I-TASSER, five different structural models were obtained for both sPLA$_2$ and CRE-1. The best structure for each protein was selected based on the stereochemical quality analysis of the Ramachandran plot. As described in Materials and Methods, the best possible I-TASSER modelled structures of sPLA$_2$ and CRE-1 were subjected to Molecular Dynamics Simulation analysis in order to improve the quality of the modelled structures and understand the stability of the modelled proteins in the simulated environment. MD Simulation of the proteins was performed for a time period of 100 ns at an equilibrated pressure and temperature of 1 atm and 300 K, using GROMACS and the high-end supercomputing facility.

Table 5.6: Unique protein identities of sPLA$_2$ and CRE-1 protein

Protein Name	FungiDB Id	UniProtKB Id	No. of Amino acids
sPLA$_2$	NCU06650	Q1K6W0	185
CRE-1	NCU08807	O59958	430

5.2.10.2 Validation of the modelled structures of sPLA$_2$ and CRE-1

The models obtained after Molecular Dynamics Simulation were also subjected to a stereochemical quality analysis. More interestingly, the simulated models of sPLA$_2$ and CRE-1 showed a significant increase in the stereochemical quality. In the case of sPLA$_2$, the residues in the most favoured regions of the Ramachandran plot were found to have significantly increased from 67.9% to 86.7% (112 to 143 residues), and there was also a notable decrease of 9.0% to 1.2% (15 to 2 residues) in the residues found in the outlier or disallowed regions of the Ramachandran plot after the refinement of the modelled structure (Fig. 5.10A, B). Similarly, for CRE-1, after Molecular Dynamics Simulation refinement of the modelled structure, the residues in the most favoured regions of the Ramachandran plot were found to be significantly increased from 54.8% to 86.1% (189 to 297 residues), and there was a remarkable decrease of 6.9% to 0.6% (24 to 2 residues) in the residues found in the outlier or disallowed regions of the Ramachandran plot (Fig. 5.11A, B).

Table 5.7: Summary of the Ramachandran plots before and after refinement of sPLA$_2$ and CRE-1

	sPLA$_2$		CRE-1	
	Before refinement	**After refinement**	**Before refinement**	**After refinement**
Residues in most favoured regions	112 (67.9%)	143 (86.7%)	189 (54.8%)	297 (86.1%)
Residues in additionally allowed regions	38 (23.0%)	20 (12.1%)	132 (38.3%)	46 (13.3%)
Residues in disallowed regions	15 (9.0%)	2 (1.2%)	24 (6.9%)	2 (0.6%)

(A) sPLA$_2$ before refinement

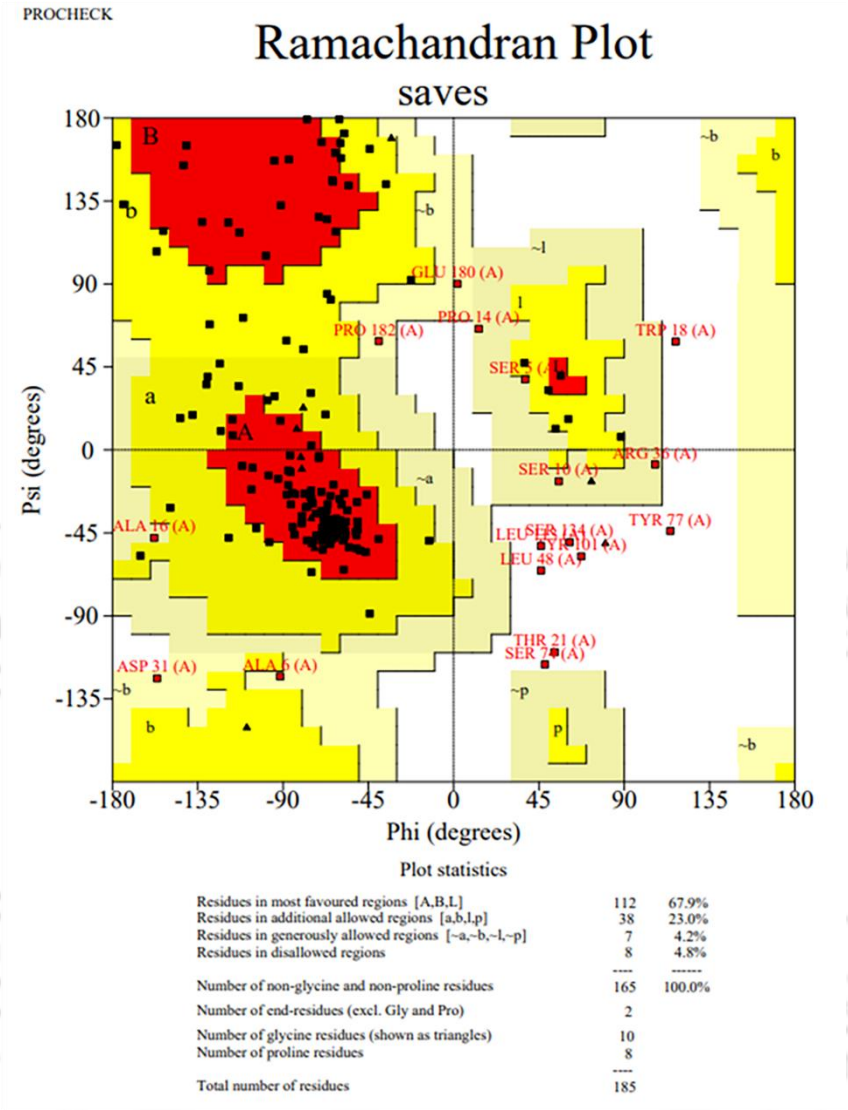

(B) sPLA$_2$ after refinement

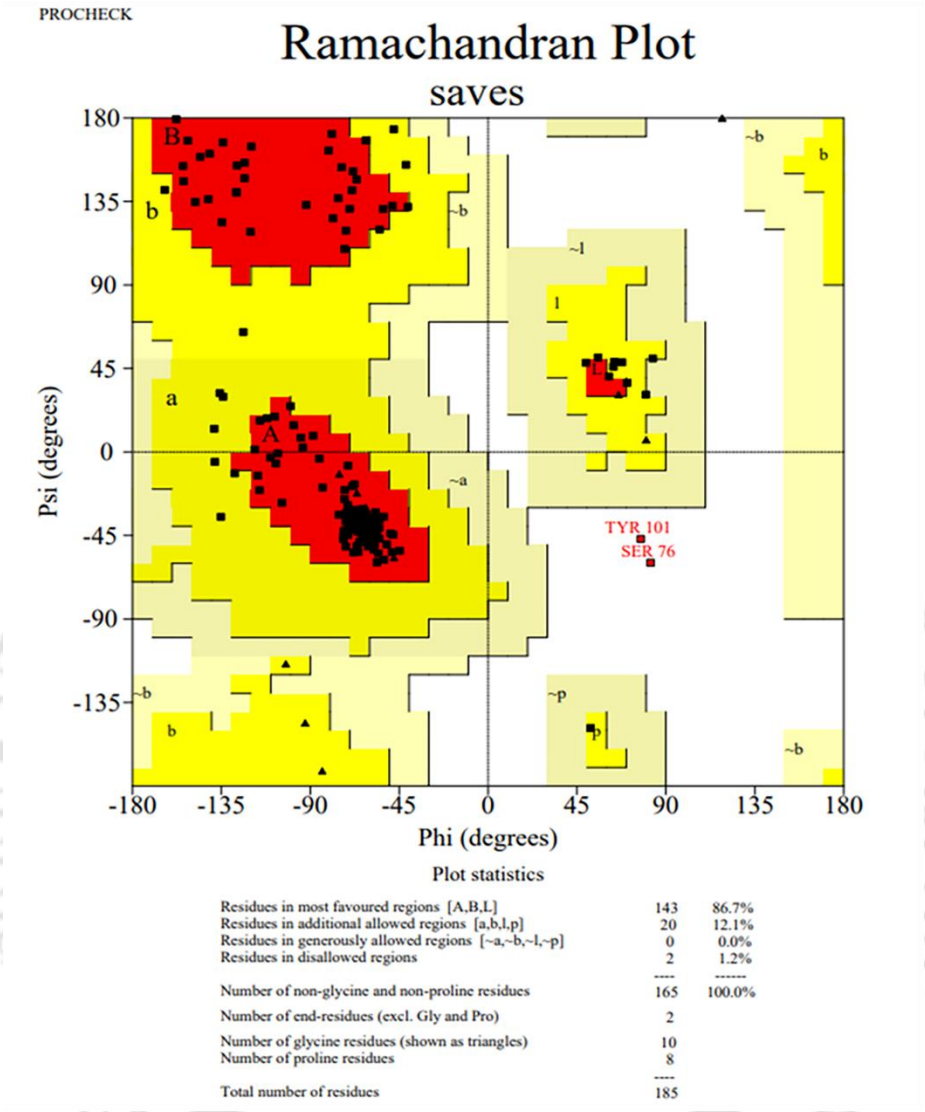

Figure 5.10: Ramachandran plot of sPLA$_2$ protein before and after Molecular Dynamics Simulation refinement. **(A)** Before refinement. **(B)** After refinement. The residues within the disallowed regions of the Ramachandran plot are highlighted in red.

(A) CRE-1 before refinement

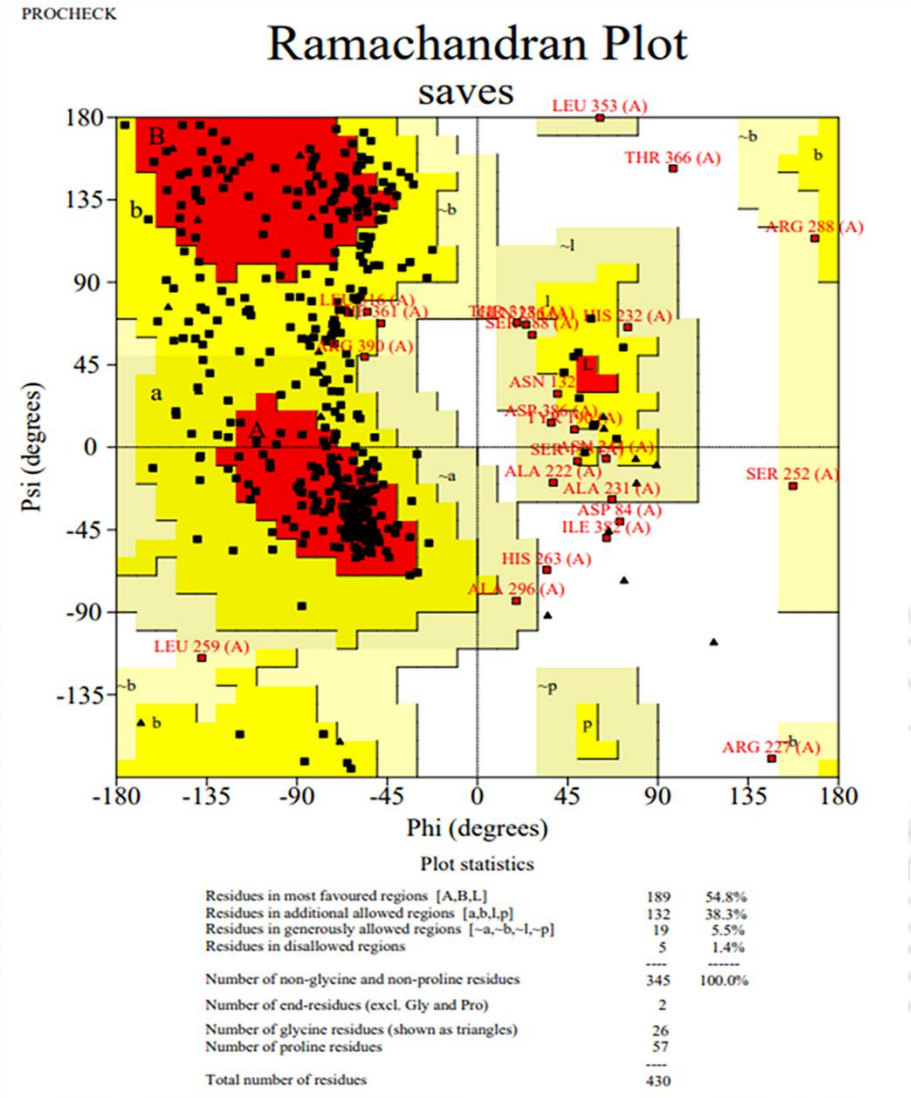

(B) CRE-1 after refinement

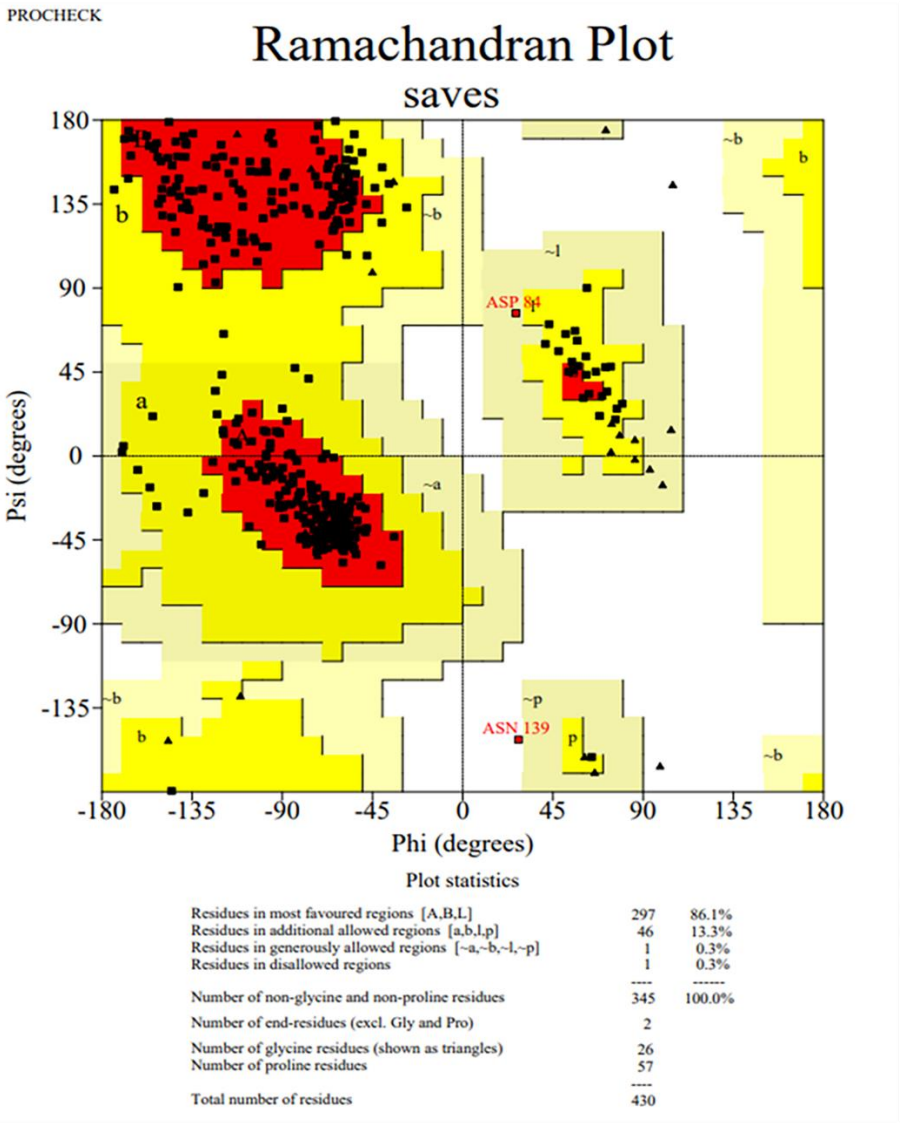

Figure 5.11 Ramachandran plot of CRE-1 protein before and after Molecular Dynamics Simulation refinement. (A) Before refinement. **(B)** After refinement. The residues within the disallowed regions of the Ramachandran plot are highlighted in red.

To further validate the quality of the stereochemically reliable MD simulated protein structures of sPLA$_2$ and CRE-1, ProSA analysis was performed. The ProSA tool computes an overall quality score (Z-score) for the modelled structures derived from knowledge based C_α potentials of mean force, and this Z-score is plotted in a graph with the Z-scores of all experimental structures in the PDB. It is expected that the Z-score of the model will lie within the range of Z-scores that are typical for experimentally determined protein structures of similar size. From the Z-score plot obtained, it can be found that the Z-scores of the simulated structures of sPLA$_2$ and CRE-1 were found to be –5.83 and –

5.18, respectively, which clearly lies within the accepted region in the Z-score plot (Fig. 5.12A, B), thus validating the simulated structures of sPLA$_2$ and CRE-1 reliable for further structural analysis.

(A)

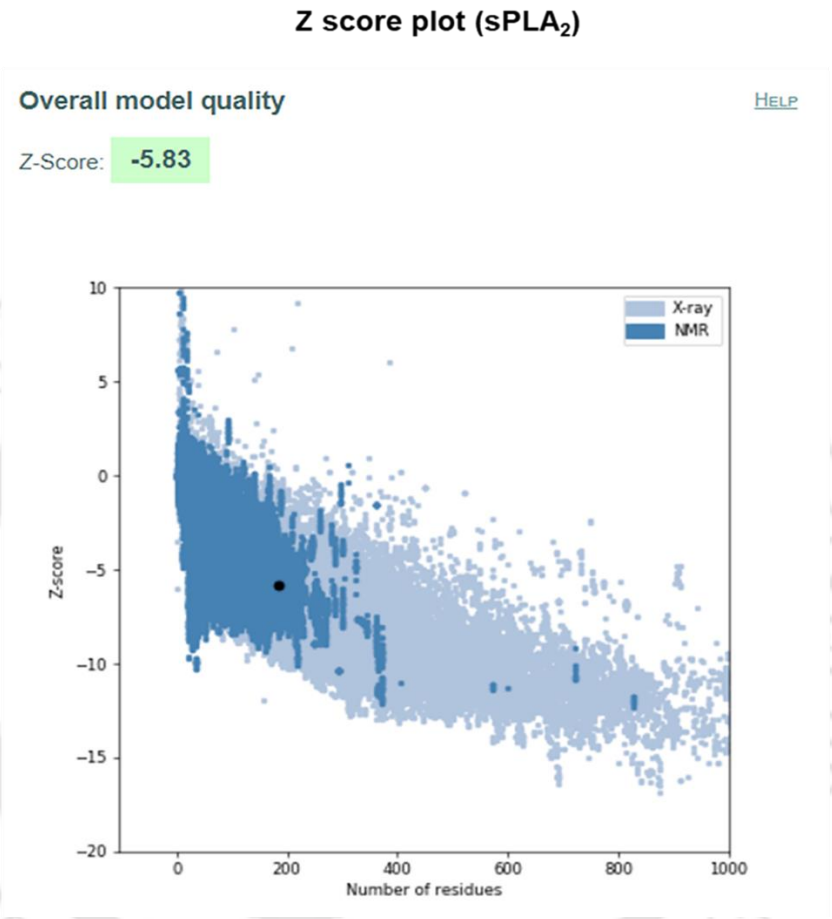

(B)

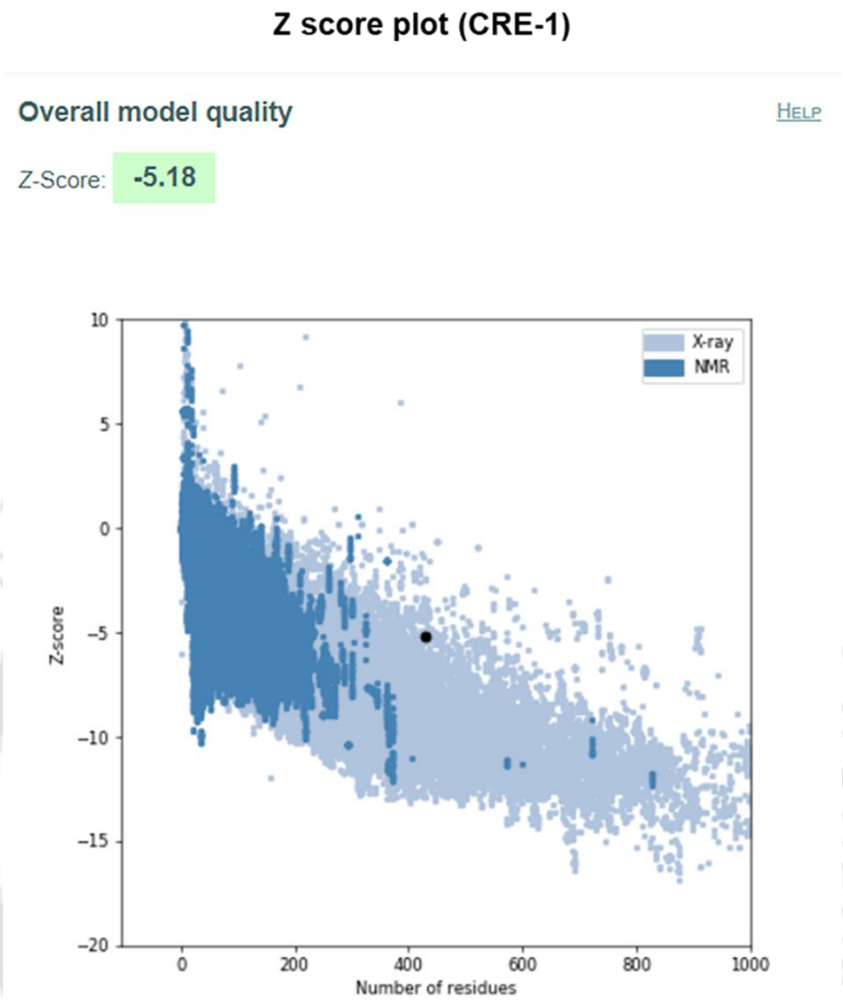

Figure 5.12: Z-score plot of experimental structures of sPLA$_2$ and CRE-1. Z-score plot of experimental structures with the black dot representing the Z-score of the modelled and refined **(A)** sPLA$_2$ and **(B)** CRE-1 structure.

Root Mean Square Deviation (RMSD) is a parameter used to calculate the deviations in the conformational stability of the protein from the backbone structure to the initial starting structure over a period of 100 ns. The backbone of sPLA$_2$ was stabilised between 0.5 and 1 nm after 25 ns of simulation time. And in the case of CRE-1, the backbone was stabilized between 1.5 and 2 nm after 10 ns of the simulation time. The significant increase in RMSD values from the initial structure indicates that the structure underwent a drastic conformational change from the initially modelled structure during the first 25 ns and 10 ns of simulation, respectively, for sPLA$_2$ and CRE-1 (Fig. 5.13A, B). After that time period, the RMSD also seems to have stabilized without any major fluctuations, indicating the stability of the structures. Furthermore, it was clear from the previously discussed Ramachandran plot

analysis that these conformational changes occurred during the MD simulation and only served to improve or refine the stereochemical quality of the I-TASSER modelled structures.

(A)

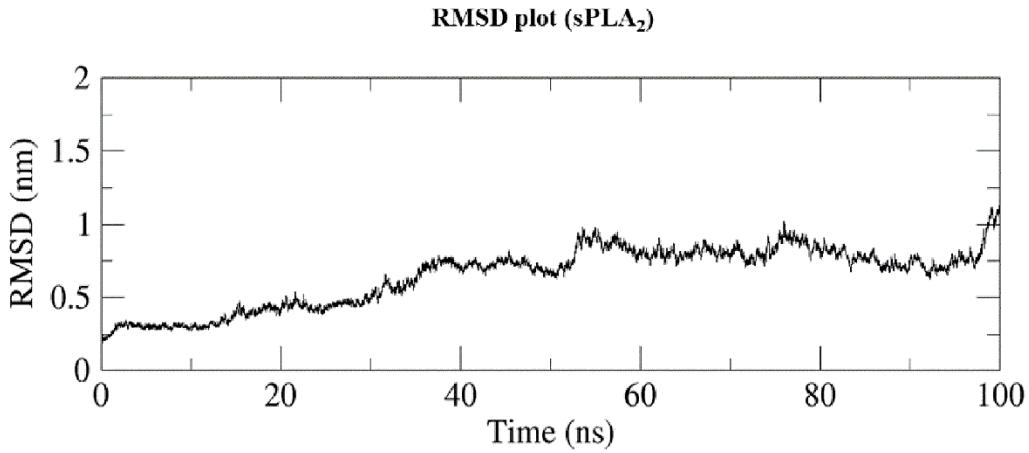

(B)

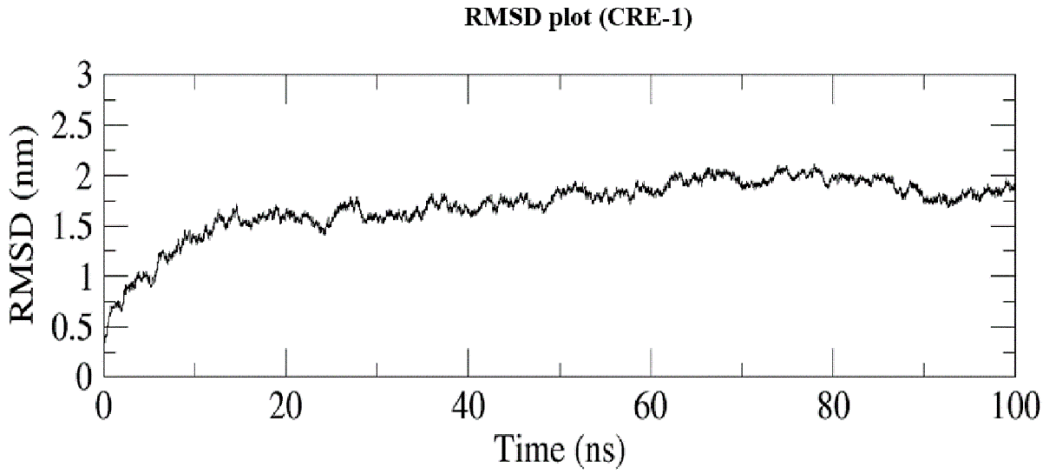

Figure 5.13: Root Mean Square Deviation plot of sPLA$_2$ and CRE-1. **(A)** RMSD plot of sPLA$_2$ over a 100 ns timescale. **(B)** RMSD plot of CRE-1 over a 100 ns timescale.

5.2.10.3 Secondary Structure Prediction in the simulated models of sPLA$_2$ and CRE-1

I also analysed the percentage of amino acids in the different secondary structures of the simulated models of sPLA$_2$ and CRE-1. In the case of sPLA$_2$, which comprises only helices and coiled structures, the percentage of residues involved in the helices (53.2%) was higher than that of the random coiled

structures (46.8%). Furthermore, the random coiled structure of CRE-1 was found to comprise a large percentage of the protein, which was around 70.4%. The secondary structures, helices and sheets, contribute only around 22.6% and 7.0% respectively, of the CRE-1 protein (Table 5.8).

Table 5.8: The percentage of amino acids in the different secondary structures of sPLA$_2$ and CRE-1

	Helices	Sheets	Coil
sPLA$_2$	53.2%	0.0%	46.8%
CRE-1	22.6%	7.0%	70.4%

5.2.10.4 Molecular Visualization of the MD simulated sPLA$_2$ and CRE-1 structure

The three-dimensional structure of the MD simulated sPLA$_2$ and CRE-1 structures was visualised using PyMOL (Fig. 5.14A, B). The sPLA$_2$ was found to comprise 7 helical structures highlighted in red, and the remaining is randomly coiled regions (Fig. 5.14A). The CRE-1 protein contains 13 helical structures, 6 beta-sheet structures, and the random coiled regions (Fig. 5.14B).

(A)

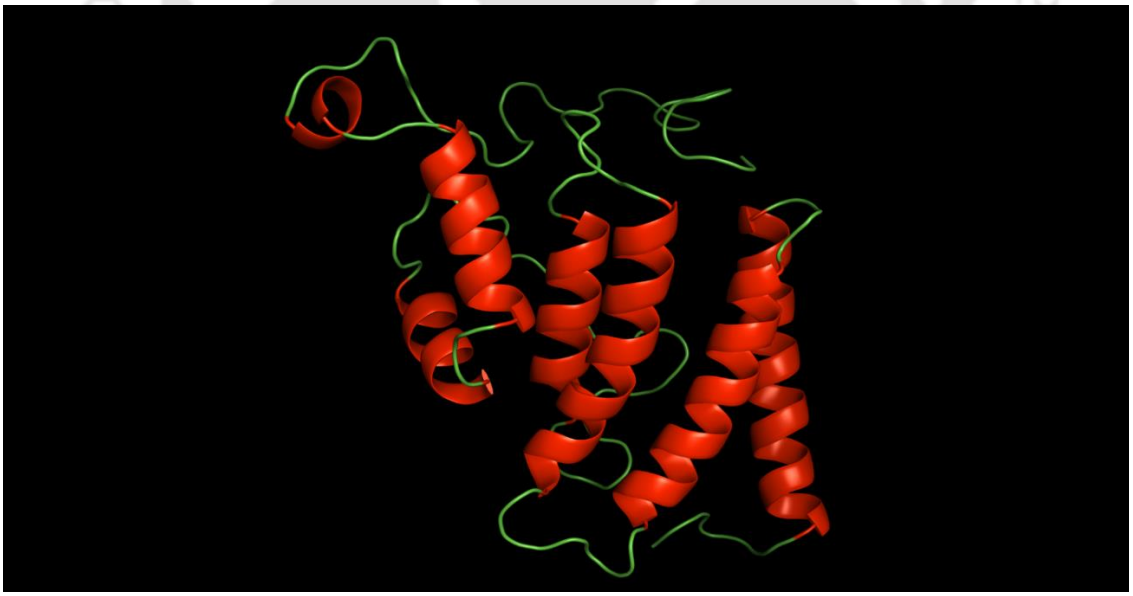

(B)

Figure 5.14: Molecular Visualization of the MD simulated sPLA$_2$ and CRE-1 structure. **(A)** Three-dimensional structure of the modelled and MD refined **(A)** sPLA$_2$ and **(B)** CRE-1 proteins obtained using PyMOL. Helices are highlighted in red, beta-sheets are highlighted in yellow, and coils are highlighted in green.

5.3 Discussion

Mutations in two different genes could lead to a phenotype that is significantly distinct from the individual mutations. Genetic interactions are characterized by two models, a 'between pathway model,' in which one pathway compensates for defects in the other, and a 'within pathway model,' in which both genes function in the same pathway, the function of which is diminished by each mutation (Boone et al. 2007).

In this chapter, I generated and analysed the double mutant of *splA*$_2$ and *cre-1*. The Δ*cre-1*; Δ*splA*$_2$ double mutant was generated by crossing the single mutant strains of opposite mating type (Fig. 5.1) and phenotypes of the double mutant were studied to determine the genetic interactions of the *splA*$_2$ and *cre-1* genes in *N. crassa*. The Δ*cre-1*; Δ*splA*$_2$ double mutant synthetically showed numerous phenotypes such as colonial growth (Fig. 5.2), slower growth rate (Table 5.1, 5.2; Fig. 5.3), reduced aerial hyphae with decreased conidiation (Table 5.3, 5.4; Fig. 5.4). One of the GTP-binding protein (GTPase) mutants in *B. cinerea*, *Rho3*, a member of the Rho superfamily, exhibited reduced vegetative growth and conidiation, as well as increased distance between the septa of individual hyphae (Bang et al. 2015). Similar to the *Rho3* RIP mutant, the Δ*cre-1*; Δ*splA*$_2$ double mutant has pleiotropic phenotypes

including colonial morphology with a slower apical extension rate and decreased conidiation (Bang et al. 2015). The vegetative hyphae of the Δ*cre-1*; Δ*splA*$_2$ double mutant after staining with CFW also showed irregular pattern of septation, unlike the WT and the individual single mutants (Fig. 5.5B). In addition, the Δ*cre-1*; Δ*splA*$_2$ double mutant was unable to grow in the presence of cell wall stress drugs, suggesting their interaction is essential for maintaining cell wall integrity in *N. crassa* (Fig. 5.6). Together, these findings suggest that loss of *splA*$_2$ along with *cre-1* resulted in a variety of morphological defects, including colonial growth morphology; which might be due to impaired cell wall integrity.

In *N. crassa*, the CRE-1 acts as a global transcription factor and influences gene activation and repression both directly and indirectly. In the presence of glucose, CRE-1 represses the genes involved in utilizing alternative carbon source. Under cellulolytic conditions, CRE-1 directly binds to adjacent motifs in promoter regions and also competes with positive regulatory factors to regulate the expression of genes involved in plant cell wall utilization. As Δ*splA*$_2$ and Δ*cre-1* single mutants showed increased sensitivity to ER stress and increased cellulolytic activity, our main purpose in generating the Δ*cre-1*; Δ*splA*$_2$ double mutant was to assess its sensitivity to ER stress and its ability to degrade microcrystalline cellulose. During ER stress, the Δ*cre-1*; Δ*splA*$_2$ double mutant was unable to grow at 2 mM DTT (Fig. 5.7). I also observed significant downregulation of *grp-78* and *pdi-1* (Fig. 5.9A) in the Δ*cre-1*; Δ*splA*$_2$ double mutant, in agreement with the DTT sensitive phenotype (Fig. 5.7). Further, the Δ*cre-1*; Δ*splA*$_2$ double mutant exhibited enhanced cellulose degradation with increased protein secretion and endoglucanase activity compared to the WT and the parental single mutants (Fig. 5.8). The expression levels of the cellulolytic genes, *cbh-1* and *cbh-2* in the Δ*cre-1*; Δ*splA*$_2$ double mutant during growth on avicel (Fig. 5.9B) were correlated with the phenotype observed (Fig. 5.8). These results indicated that the genetic interactions of *splA*$_2$ and *cre-1* are crucial for the ER response and cellulose degradation pathways in *N. crassa*.

In *N. crassa*, the *splA*$_2$ gene is under the CRE-1 regulon under cellulolytic conditions (Sun and Glass 2011). Promoter analysis revealed the CRE-1 binding site 5' SYGGRG 3' is absent in the promoter region of the *splA*$_2$ gene. I also observed increased expression of *splA*$_2$ in the Δ*cre-1* mutant (Fig. 5.9C), which was unexpected. These suggest that sPLA$_2$ and CRE-1 proteins interact possibly to regulate the cellulose degradation pathway in *N. crassa*. However, it is clear that compensatory mechanisms such as increased protein secretion and cellulase activity, occur in strains with deletions of genes essential for plant cell wall degradation (Tian et al. 2009). No previous studies linked sPLA$_2$ expression in response to cellulose, although, the sPLA$_2$ homolog, *splaA* was shown to induced under carbon starvation in *A. oryzae* (Nakahama et al. 2010). The sPLA$_2$ was first discovered in the mycorrhizal ascomycete species, *T. borchii*, and is associated with membrane remodelling during plant colonization (Soragni et al. 2001). In mammalian cells, secreted phospholipases are involved in fatty

acids mobilization and are associated with allergic and systemic inflammatory/autoimmune diseases (Granata et al. 2003). Further characterization of the Δ*splA*$_2$ mutant will reveal its detailed mode of action and how it affects secretion and cellulase activity in *N. crassa*.

I also predicted the three-dimensional protein structures of sPLA$_2$ and CRE-1. The experimental structures (XRD, NMR, or Cryo-EM structures) of sPLA$_2$ and CRE-1 are not available in the protein databank (PDB). Homology modelling of sPLA$_2$ and CRE-1 was also hindered by the absence of suitable structural homologs. Therefore, protein structure modelling was performed using the I-TASSER (Iterative Threading ASSEmbly Refinement) tool by Zhang Lab (https://zhanggroup.org/I-TASSER), which uses threading and ab-initio methods. The modelled structures were then subjected to Molecular Dynamics Simulation, which improved the stereochemical quality of the structures significantly. In addition, based on the RMSD plot obtained from MD simulation studies, the modelled structures were found stable in the simulated environment, making them reliable for further structural studies. In this study, it was discovered that the I-TASSER modelled MD refined structures of sPLA$_2$ and CRE-1 were significantly superior to the existing AlphaFold predicted structures.

Therefore, taken together, it may be concluded that *splA*$_2$ genetically interacts with *cre-1* to regulate vegetative growth and cellulose degradation in *N. crassa*. Further the modelled structures of sPLA$_2$ and CRE-1 are found to be stereochemically reliable and structurally stable. In future, a detailed structure-function study will help in use of engineered sPLA$_2$ and CRE-1 in cellulose degradation process.

Chapter 6: Conclusions and Future Perspectives

6.1 Major conclusions of the study

In the current study, I investigated the cell functions of three Ca^{2+} signaling genes *plc-1* (NCU06245), *cpe-1* (NCU06366), and *splA*$_2$ (NCU06650), encoding for a phospholipase C-1 (PLC-1), a Ca^{2+}/H^{+} exchanger (CPE-1), and a secretory phospholipase A_2 (sPLA$_2$) homolog, respectively, in *N. crassa*. In this study, I found that the Δ*plc-1* knockout mutant exhibited an increase in period lengths and showed loss of temperature compensation. The Δ*plc-1*, Δ*cpe-1*, and Δ*splA*$_2$ mutants had decreased survival during induced thermotolerance and showed increased sensitivity to alkaline pH in *N. crassa*. In addition, the Δ*splA*$_2$ mutant displayed hypersensitivity in the presence of DTT that induces ER stress, consumed microcrystalline cellulose more quickly than the WT, showed enhanced protein secretion, and accumulated higher glucose in the culture supernatants. However, the WT, and the Δ*plc-1*, Δ*cpe-1*, and Δ*splA*$_2$ mutants did not exhibit any variations in growth rate or morphology when cultured on sucrose, glucose, xylose, glycerol, and sodium acetate. Moreover, the Δ*splA*$_2$ mutant was unable to grow on microcrystalline cellulose during ER stress.

Studies on the double mutants of *plc-1*, *cpe-1*, and *splA*$_2$ revealed that they synthetically regulate the circadian clock, acquisition of thermotolerance induced by heat shock, responses to alkaline pH and ER stress, and utilization of cellulose and other alternate carbon sources in *N. crassa*. Complementation studies using the homokaryotic transformants expressing *plc-1*, *cpe-1*, and *splA*$_2$ transgenes under the constitutive promoter *ccg-1* further supported that *plc-1*, *cpe-1*, and *splA*$_2$ are involved in circadian clock, stress responses, and growth on alternate carbon sources in *N. crassa*.

Further, to understand the molecular pathways associated with PLC-1, CPE-1, and sPLA$_2$ in *N. crassa*, I performed qRT-PCR of some important genes involved in regulating the cell processes mentioned. The Δ*plc-1*, Δ*cpe-1*, and Δ*splA*$_2$ single mutants, and their double mutants displayed differential expression of the clock oscillators *frq* and *wc-1*, *hsp60* and *hsp80* during heat stress, and the alkaline pH regulator *pac-3*. The expression of the UPR markers, *grp-78* and *pdi-1* also showed a decrease in the mutants having growth defects during ER stress. I also showed that the increased cellulolytic activities of the Δ*splA*$_2$ and Δ*cpe-1*; Δ*splA*$_2$ mutants are associated with the increased expression of the cellulolytic genes, *cbh-1*, *cbh-2*, and *endo-2* in *N. crassa*. Further, I proposed a possible mechanistic model for PLC-1, CPE-1, and sPLA$_2$ mediated pathways in circadian clock, stress responses, and cellulose degradation in *N. crassa*. Therefore, I conclude that *plc-1*, *cpe-1*, and *splA*$_2$ genes are involved in a complex genetic interaction to regulate numerous cell functions in *N. crassa*.

In addition, I showed a novel genetic interaction between *splA*$_2$ and *cre-1* that regulates vegetative development and cellulose degradation in *N. crassa*. The Δ*cre-1*; Δ*splA*$_2$ double mutant exhibited numerous growth defects, including colonial morphology, slower growth with reduced hyphal branching, reduced aerial hyphae and conidiation, irregular septation, and increased sensitivity to cell

wall and ER stress inducing agents. However, the Δ*cre-1*; Δ*splA*$_2$ double mutant, in contrast to the WT and the parental single mutants, degraded microcrystalline cellulose more rapidly with increased cellulolytic gene expression, secreted noticeably more protein, and accumulated significantly higher glucose in the culture supernatants. Further, I predicted the three dimensional protein structures of sPLA$_2$ and CRE-1. The I-TASSER modelled MD simulated structures of sPLA$_2$ and CRE-1 were found to be stereochemically reliable and structurally stable. The sPLA$_2$ protein has 7 helical structures with random coiled regions, whereas the CRE-1 protein possesses 13 helical structures, 6 beta-sheet structures, and random coiled regions.

6.2 Future perspectives of the work

Future direction of this research will focus on the following areas: (i) further detailed studies on the pathways involving PLC-1, CPE-1, and sPLA$_2$ to understand the mechanism of stress tolerance in *N. crassa*; (ii) to identify additional molecular targets of *N. crassa* PLC-1, CPE-1, and sPLA$_2$ for understanding the mechanism of cellulose degradation; and (iii) to gain insights into the structure-function relationship of the *N. crassa* PLC-1, CPE-1, and sPLA$_2$, specifically the low molecular weight sPLA$_2$. Therefore, it is anticipated that more detailed information about the mechanisms of PLC-1, CPE-1, and sPLA$_2$ will be available in the near future.

Appendix-I

A-I.1 Plasmid Map

pMF272: The 8.4 kb plasmid vector pMF272 has a GFP variant gene (*sgfp*), a *lacZ′* sequence containing the SP6 and T7 promoters, ampicillin as a bacterial selection marker, and a multiple cloning site (MCS) for translational fusion of *Neurospora* genes to *sgfp* (Fig. A-I.1; Freitag et al. 2004). The *sgfp* gene encodes a GFP variant with a serine to threonine substitution at position 65 (S65T), which increases the brightness and shifts the codon bias toward that of humans. This vector contains the *N. crassa ccg-1* promoter (P_{ccg-1}) that is strongly induced by stress or glucose deprivation (McNally and Free 1988). The pBM60 backbone was used to create the P_{ccg-1}::*sgfp* cassette, which allows for *his-3* targeting of the transgene by gene replacement (Margolin et al. 1997).

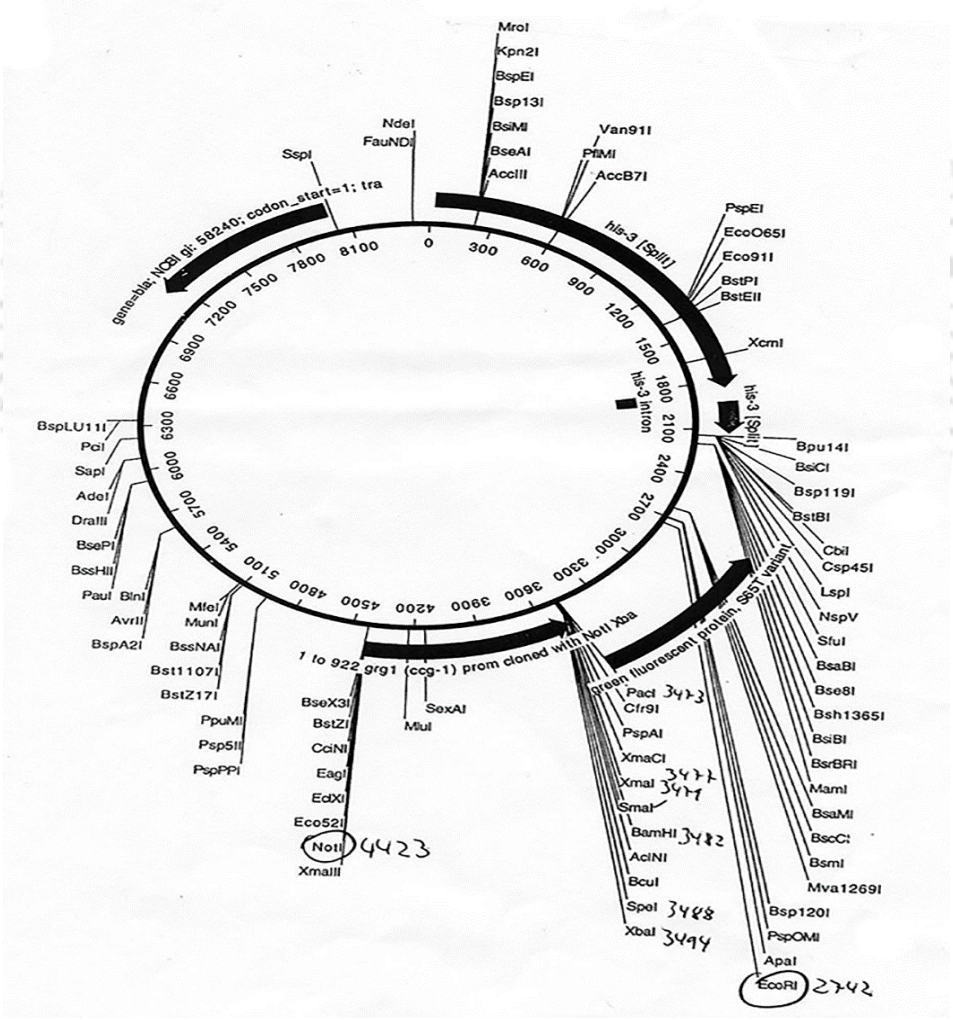

Fig. A-I.1: Schematic of the pMF272 vector. The pMF272 vector is of 8.4 kb size and contains an MCS region with unique restriction sites. The plasmid map is available at http://www.fgsc.net/plasmid/image/609.jpg.

Appendix-II

A-II.1 Generation and confirmation of strains for circadian regulated conidiation assay

In *N. crassa,* conidia accumulate as a discrete band every 22 h, displaying a free-running circadian rhythm in the vegetative developmental program (Nakashima 1981; Bell-Pederson et al. 1992; Aronson et al. 1994). However, in the WT strain, rhythmic conidiation is suppressed due to the accumulation of CO_2, a respiratory by-product. Therefore, all strains used in the circadian regulated conidiation study carry the *ras-1*^{bd} allele, which allows clear visualization of the conidial bands despite the CO_2 accumulation without affecting the clock mechanism (Fig. A-II.1; Sargent and Kaltenborn 1972; Belden et al. 2007). The *ras-1*^{bd}, also known as the *band* (*bd*) mutant, has a T79I point mutation in the *ras-1* gene (Belden et al. 2007). To generate the Δ*plc-1*, Δ*cpe-1*, and Δ*splA*$_2$ mutations in the *ras-1*^{bd} background (Δ*plc-1*; *ras-1*^{bd}, Δ*cpe-1*; *ras-1*^{bd}, and Δ*splA*$_2$; *ras-1*^{bd} strains), each of the three single mutant strains was crossed with the *ras-1*^{bd} strain of opposite mating type. The f_1 progenies were screened for hygromycin B resistance phenotype (Hyg^R) and the presence of the knockout alleles were confirmed using gene specific forward primers HI-NCU06245-F, HI-NCU06366-F, and HI-NCU06650-F (Table 2.3; Entries 1-3) for the Δ*plc-1*, Δ*cpe-1*, and Δ*splA*$_2$ mutants, respectively, and the common reverse primer 5HPHR (Table 2.3; Entry 5) specific for the *hph* cassette used in the generation of the knockout mutants. PCR products of size 2 kb, ~ 1.981 kb, and ~ 2.044 kb, indicate the presence of the Δ*plc-1*, Δ*cpe-1* and Δ*splA*$_2$ knockout alleles, respectively (Fig. A-II.1B). The Hyg^R progenies were then screened for the *ras-1*^{bd} allele on race tubes for circadian regulated conidiation as observed in the *ras-1*^{bd} strain (Sargent and Kaltenborn 1972; Belden et al. 2007). For the generation of the Δ*plc-1*; Δ*cpe-1*; *ras-1*^{bd}, Δ*plc-1*; Δ*splA*$_2$; *ras-1*^{bd}, and Δ*cpe-1*; Δ*splA*$_2$; *ras-1*^{bd} mutants, each of the confirmed single mutants carrying the *ras-1*^{bd} allele was crossed among themselves, followed by PCR confirmation (Fig. A-II.1C).

Appendix-II

(A)

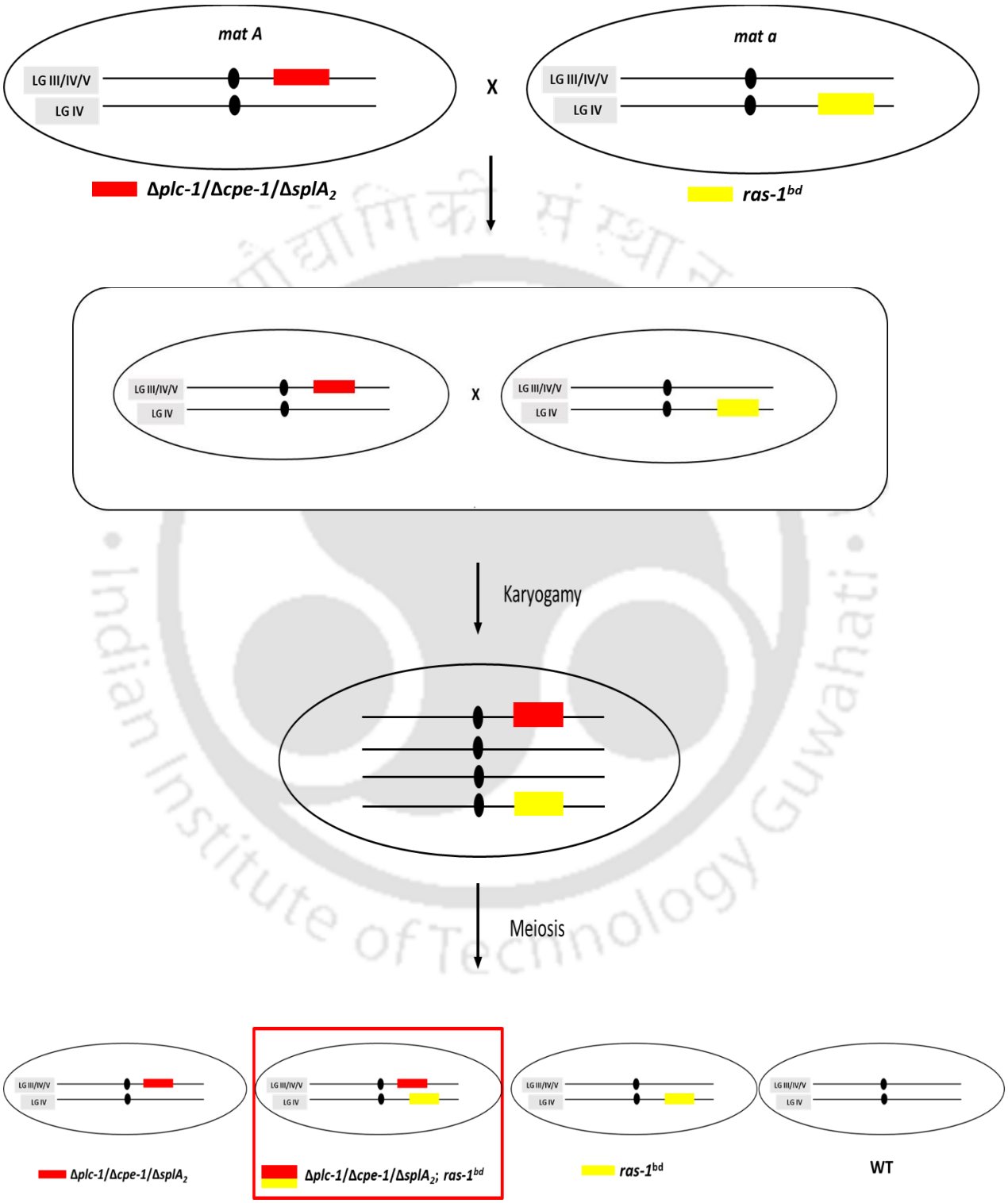

Appendix-II

(B)

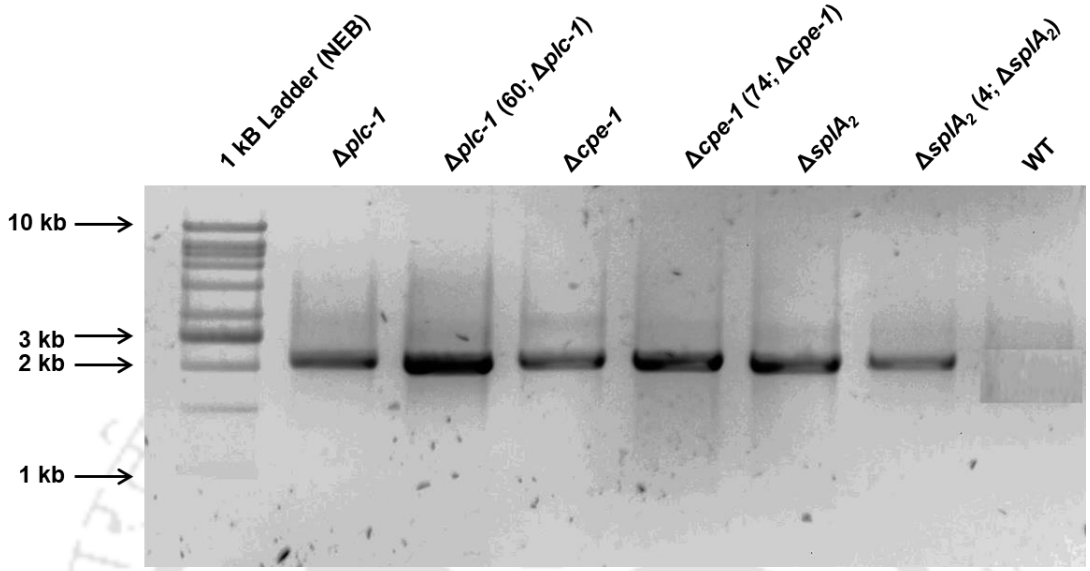

(C)

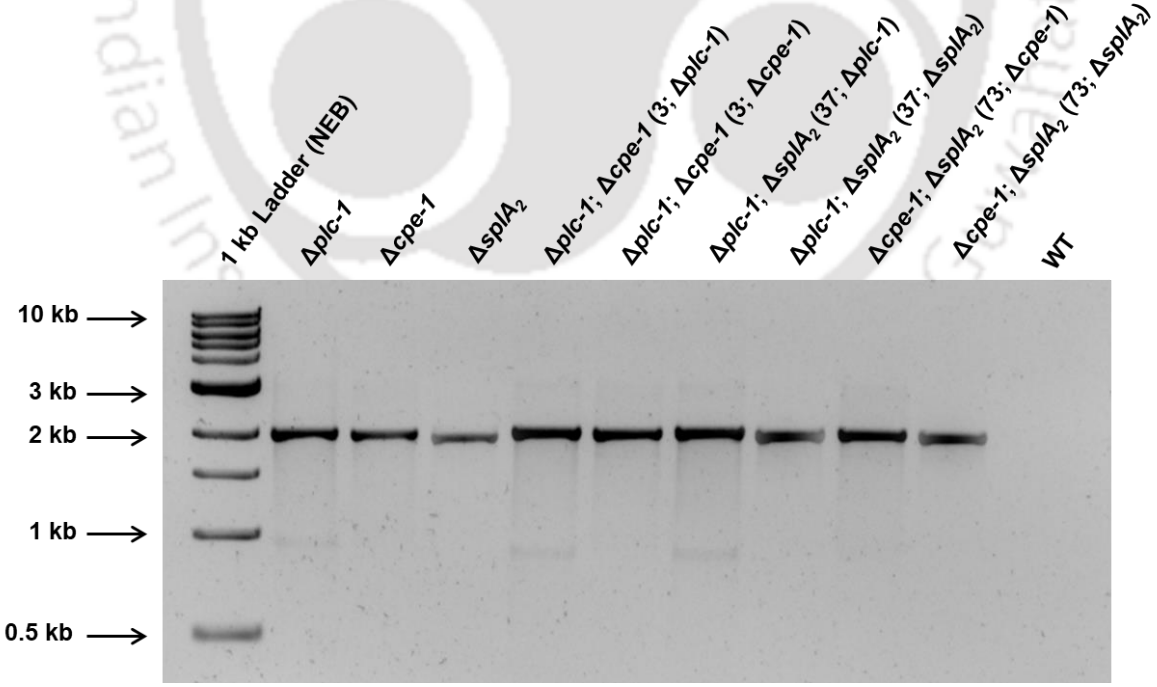

Figure A-II.1: Generation and confirmation of strains for circadian regulated conidiation. (A) A schematic representation showing the crosses of Δ*plc-1*, Δ*cpe-1*, and Δ*splA*$_2$ single mutants with the *ras-1*^{bd} strain. The strains with respective knockout mutant alleles and the *ras-1*^{bd} mutation were

Appendix-II

selected for the circadian regulated conidiation assay. For the generation of the Δ*plc-1*; Δ*cpe-1*, Δ*plc-1*; Δ*splA*$_2$, and Δ*cpe-1*; Δ*splA*$_2$ double mutants in the *ras-1*^{bd} background, each of the confirmed single mutants carrying the *ras-1*^{bd} allele was crossed among themselves. **(B)** and **(C)** Amplification of PCR amplicons of sizes ~ 2 kb, ~ 1.981 kb, and ~ 2.044 kb, respectively, indicate the presence of the Δ*plc-1*, Δ*cpe-1* and Δ*splA*$_2$ alleles in the single and double mutants, respectively. The number in parentheses represent the progeny which carries the knockout alleles in the *ras-1*^{bd} background for each of the single and double mutants.

Appendix-III

Table A-III.1: List of primers used in the qRT-PCR analysis

Primers	Sequence (5'-3')	Source
RT-PLC-1-FW	GCACGGGTACACGCTAACTA	Laboratory stock (Barman and Tamuli 2017)
RT-PLC-1-RV	TCGAGACTGACGATCAGAGG	Laboratory stock (Barman and Tamuli 2017)
RT-CPE-1-FW	CCGCTGTCTTGCTCATCATC	Laboratory stock (Barman and Tamuli 2017)
RT-CPE-1-RV	GATCAGAGTGAGGCGATGAC	Laboratory stock (Barman and Tamuli 2017)
RT-sPLA$_2$-FW	AAACCATCCAGCAGACGACG	Laboratory stock (Barman and Tamuli 2017)
RT-sPLA$_2$-RV	CATGACGATTGCAAGCAGGC	Laboratory stock (Barman and Tamuli 2017)
RT-Q-Tub-FW	CCCAAGAACATGATGGCTGC	Laboratory stock (Barman and Tamuli 2017)
RT-Q-Tub-RV	TTGTTCTGAACGTTGCGCATC	Laboratory stock (Barman and Tamuli 2017)
RT-HSP60-FW	GTCCTCATCGAGTCCAGCTT	Laboratory stock (Roy and Tamuli 2022)
RT-HSP60-RV	CCGAGGTTCTCGAACTTGTC	Laboratory stock (Roy and Tamuli 2022)
RT-HSP80-FW	CGAACAAGACCCTCACCATC	Laboratory stock (Roy and Tamuli 2022)
RT-HSP80-RV	GAGCGGGCAATAGTACCAAG	Laboratory stock (Roy and Tamuli 2022)
RT-FRQ-FW	GAATCGACATCGCAGAGGAG	This study
RT-FRQ-RV	GCCCGTCGACATAGAGTTGT	This study
RT-WC-1-FW	GCGGGAATCGAGATCTATGC	This study
RT-WC-1-RV	TGAGTTCTTGGTAGCGGTGG	This study
RT-PAC-3-FW	CCAAAACGGTGGCATGAATG	This study
RT-PAC-3-RV	GTACTGTGCGTGGTAGTAAC	This study
RT-Grp-78-FW	CGCTGAGTATATTGCACTGTT	This study
RT-Grp-78-RV	GAAATCCATCATTGAGGTTCC	This study
RT-PDI-1-FW	ATCAAGCAGTCTCTTCCCTC	This study
RT-PDI-1-RV	CGAGAGCAGCATCACTGCT	This study
RT-CBH-1-FW	CAAGTACGGTACCGGTTACT	This study
RT-CBH-1-RV	TCGCACATGTGCTGTTCGAT	This study
RT-CBH-2-FW	CATTCCTTCCATGACTGGCA	This study
RT-CBH-2-RV	TCGTAGACGACAAAGTGAGC	This study
RT-ENDO-2-FW	TCAAGTGGTTCGGTGTCAAC	This study
RT-ENDO-2-RV	GCCAACACGGAAGATGTTGT	This study

Appendix-III

Table A-III.2: Relative expression of *frq* during circadian regulated conidiation in the Δ*plc-1*, Δ*cpe-1*, and Δ*splA*$_2$ single and double mutants at 20 °C and 25 °C

Strains	[+]Relative expression of *frq* (Fold changes)	
	20 ºC	25 ºC
ras-1^{bd}	1.00 ± 0.03	1.00 ± 0.23
Δ*plc-1* (60)	3.34 ± 0.07 (***)	1.38 ± 0.16 (*)
Δ*cpe-1* (74)	1.22 ± 0.16	0.99 ± 0.32
Δ*splA*$_2$ (4)	1.40 ± 0.06 (***)	1.07 ± 0.30
Δ*plc-1*; Δ*cpe-1* (3)	2.04 ± 0.41 (**)	1.21 ± 0.26
Δ*plc-1*; Δ*splA*$_2$ (37)	2.09 ± 0.35 (**)	1.32 ± 0.14
Δ*cpe-1*; Δ*splA*$_2$ (73)	0.89 ± 0.06	0.91 ± 0.03

Table A-III.3: Relative expression of *wc-1* during circadian regulated conidiation in the Δ*plc-1*, Δ*cpe-1*, and Δ*splA*$_2$ single and double mutants at 20 °C and 25 °C

Strains	[+]Relative expression of *wc-1* (Fold changes)	
	20 ºC	25 ºC
ras-1^{bd}	1.00 ± 0.44	1.00 ± 0.34
Δ*plc-1* (60)	2.58 ± 0.16 (**)	1.34 ± 0.02 (**)
Δ*cpe-1* (74)	0.87 ± 0.11	1.05 ± 0.04
Δ*splA*$_2$ (4)	1.04 ± 0.01	1.05 ± 0.02
Δ*plc-1*; Δ*cpe-1* (3)	1.97 ± 0.14 (**)	1.40 ± 0.05 (**)
Δ*plc-1*; Δ*splA*$_2$ (37)	2.08 ± 0.10 (**)	1.43 ± 0.09 (**)
Δ*cpe-1*; Δ*splA*$_2$ (73)	0.87 ± 0.10	0.98 ± 0.06

Appendix-III

Table A-III.4: Relative expression of *hsp60* and *hsp80* in the Δ*plc-1*, Δ*cpe-1*, and Δ*splA*$_2$ single and double mutants during heat stress

Strains	[+]Relative expression (Fold changes)	
	hsp60	***hsp80***
WT	1.00 ± 0.14	1.00 ± 0.06
Δ*plc-1*	0.64 ± 0.08 (*)	0.51 ± 0.09 (**)
Δ*cpe-1*	0.68 ± 0.10 (*)	0.62 ± 0.10 (**)
Δ*splA*$_2$	0.84 ± 0.08	0.74 ± 0.04 (**)
Δ*plc-1*; Δ*cpe-1*	0.55 ± 0.06 (**)	0.39 ± 0.05 (***)
Δ*plc-1*; Δ*splA*$_2$	0.57 ± 0.09 (**)	0.31 ± 0.02 (***)
Δ*cpe-1*; Δ*splA*$_2$	1.04 ± 0.05	0.82 ± 0.17

Table A-III.5: Relative expression of *plc-1*, *cpe-1*, and *splA*$_2$ in the WT strain during heat stress

	[+]Relative expression (Fold changes)		
Genes	**Non Heat shocked**	**Heat shocked**	**Heat shocked + Recovery**
plc-1	1.00 ± 0.14	2.30 ± 0.09 (***)	1.30 ± 0.16 (*)
cpe-1	1.00 ± 0.11	1.14 ± 0.07	0.96 ± 0.05
splA$_2$	1.00 ± 0.09	1.60 ± 0.36 (*)	1.30 ± 0.12 (*)
hsp60	1.00 ± 0.16	1.50 ± 0.13 (**)	1.13 ± 0.15 (*)
hsp80	1.00 ± 0.08	3.17 ± 0.17 (***)	1.70 ± 0.41 (*)

Table A-III.6: Relative expression of *pac-3* in the Δ*plc-1*, Δ*cpe-1*, and Δ*splA*$_2$ single and double mutants during alkaline pH condition

Strains	[+]Relative expression (Fold changes)
	pac-3
WT	1.00 ± 0.07
Δ*plc-1*	0.53 ± 0.04 (***)

Appendix-III

Δ*cpe-1*	0.61 ± 0.08 (**)
Δ*splA*$_2$	0.62 ± 0.09 (**)
Δ*plc-1*; Δ*cpe-1*	0.39 ± 0.09 (***)
Δ*plc-1*; Δ*splA*$_2$	0.35 ± 0.08 (***)
Δ*cpe-1*; Δ*splA*$_2$	0.46 ± 0.03 (***)

Table A-III.7: Relative expression of *plc-1*, *cpe-1*, and *splA*$_2$ in the WT strain during different pH conditions

	[+]Relative expression (Fold changes)		
Genes	**pH 3.8 (Acidic)**	**pH 5.8 (Ambient)**	**pH 7.8 (Alkaline)**
plc-1	1.60 ± 0.02 (***)	1.00 ± 0.07	3.66 ± 0.36 (***)
cpe-1	1.34 ± 0.06	1.00 ± 0.35	2.94 ± 0.35 (**)
splA$_2$	1.07 ± 0.70	1.00 ± 0.27	2.64 ± 0.34 (**)
pac-3	0.32 ± 0.10 (*)	1.00 ± 0.24	5.11 ± 0.66 (***)

Table A-III.8: Relative expression of *grp-78* and *pdi-1* in the Δ*plc-1*, Δ*cpe-1*, and Δ*splA*$_2$ single and double mutants in response to ER stress

	[+]Relative expression (Fold changes)	
Strains	***grp-78***	***pdi-1***
WT	1.00 ± 0.12	1.00 ± 0.09
Δ*plc-1*	0.80 ± 0.05	0.84 ± 0.09
Δ*cpe-1*	0.87 ± 0.09	0.79 ± 0.01 (*)
Δ*splA*$_2$	0.58 ± 0.03 (**)	0.51 ± 0.06 (**)
Δ*plc-1*; Δ*cpe-1*	0.41 ± 0.04 (***)	0.43 ± 0.05 (***)
Δ*plc-1*; Δ*splA*$_2$	0.41 ± 0.10 (**)	0.33 ± 0.05 (***)
Δ*cpe-1*; Δ*splA*$_2$	0.88 ± 0.09	0.81 ± 0.04 (*)

Appendix-III

Table A-III.9: Relative expression of *plc-1*, *cpe-1*, and *splA₂* in the WT strain in response to ER stress

Genes	[+]Relative expression (Fold changes)	
	DTT Non-treated	DTT Treated
plc-1	1.00 ± 0.09	0.98 ± 0.07 (*)
cpe-1	1.00 ± 0.01	0.85 ± 0.06
splA₂	1.00 ± 0.11	2.60 ± 0.21 (***)
grp-78	1.00 ± 0.12	3.90 ± 0.21 (***)
pdi-1	1.00 ± 0.21	3.50 ± 0.38 (***)

Table A-III.10: Relative expression of *cbh-1*, *cbh-2*, and *endo-2* in the Δ*plc-1*, Δ*cpe-1*, and Δ*splA₂* single and double mutants during growth on microcrystalline cellulose (Avicel)

Strains	[+]Relative expression (Fold changes)		
	cbh-1	*cbh-2*	*endo-2*
WT	1.00 ± 0.14	1.00 ± 0.03	1.00 ± 0.16
Δ*plc-1*	0.41 ± 0.02 (*)	0.42 ± 0.11	0.42 ± 0.17
Δ*cpe-1*	0.52 ± 0.10	0.46 ± 0.04 (**)	0.32 ± 0.02 (*)
Δ*splA₂*	4.14 ± 0.40 (**)	3.18 ± 0.03 (***)	2.25 ± 0.36
Δ*plc-1*; Δ*cpe-1*	0.38 ± 0.00 (*)	0.41 ± 0.04 (**)	0.32 ± 0.03 (*)
Δ*plc-1*; Δ*splA₂*	0.41 ± 0.08 (*)	0.44 ± 0.05 (**)	0.36 ± 0.06 (*)
Δ*cpe-1*; Δ*splA₂*	2.35 ± 0.02 (**)	2.03 ± 0.41	1.40 ± 0.08

Table A-III.11: Relative expression of *grp-78* and *pdi-1* in the WT, Δ*splA₂*, Δ*cre-1*, Δ*cre-1*; Δ*splA₂*, $P_{ccg\text{-}1}$::*splA₂*::*gfp*, and *Pn-cre-1* in response to ER stress

Strains	[+]Relative expression (Fold changes)	
	grp-78	*pdi-1*
WT	1.00 ± 0.26	1.00 ± 0.03
Δ*splA₂*	0.42 ± 0.07	0.49 ± 0.08 (*)
Δ*cre-1*	0.29 ± 0.19	0.57 ± 0.02 (**)

Δ*cre-1*; Δ*splA*$_2$	0.03 ± 0.04	0.20 ± 0.02 (***)
P$_{ccg-1}$::*splA*$_2$::*gfp*	0.79 ± 0.03	1.44 ± 0.13 (*)
Pn-cre-1	1.24 ± 0.12	0.84 ± 0.11

Table A-III.12: Relative expression of *splA*$_2$ in the Δ*cre-1* and *Pn-cre-1* during growth on microcrystalline cellulose (Avicel)

	[+]Relative expression (Fold changes)
Strains	***splA*$_2$**
WT	1.00 ± 0.06
Δ*cre-1*	2.85 ± 0.46 (*)
Pn-cre-1	0.89 ± 0.09

[+]Results are shown as mean ± standard deviation for three independent experiments (n = 3) with *P-values* < 0.05 (*), < 0.01 (**), and < 0.001 (***) compared with the WT strain or the control condition as measured by a one-way ANOVA test.

Bibliography

Altschul SF, Gish W, Miller W, Myers EW, Lipman DJ. Basic local alignment search tool. **Journal of Molecular Biology. 1990 Oct;215(3):403-10.**

Altschul SF, Madden TL, Schäffer AA, Zhang J, Zhang Z, Miller W, Lipman DJ. Gapped BLAST and PSI-BLAST: a new generation of protein database search programs. **Nucleic Acids Research. 1997 Sep;25(17):3389-402.**

Altschul SF, Wootton JC, Gertz EM, Agarwala R, Morgulis A, Schäffer AA, Yu YK. Protein database searches using compositionally adjusted substitution matrices. **The FEBS Journal. 2005 Oct;272(20):5101-9.**

An B, Li B, Qin G, Tian S. Function of small GTPase Rho3 in regulating growth, conidiation and virulence of *Botrytis cinerea*. **Fungal Genetics and Biology. 2015 Feb 1;75:46-55.**

Andaluz E, Coque JJ, Cueva R, Larriba G. Sequencing of a 4.3 kbp region of chromosome 2 of *Candida albicans* reveals the presence of homologues of *SHE9* from *Saccharomyces cerevisiae* and of bacterial phosphatidylinositol-phospholipase C. **Yeast. 2001 Jun;18(8):711-21.**

Andoh T, Kato Jr T, Matsui Y, Toh-e A. Phosphoinositide-specific phospholipase C forms a complex with 14-3-3 proteins and is involved in expression of UV resistance in fission yeast. **Molecular and General Genetics. 1998 Apr;258(1):139-47.**

Andoh T, Yoko-O T, Matsui Y, Toh-E A. Molecular cloning of the *plc1*$^{+}$ gene of *Schizosaccharomyces pombe*, which encodes a putative phosphoinositide-specific phospholipase C. **Yeast. 1995 Feb;11(2):179-85.**

Arioka M, Cheon SH, Ikeno Y, Nakashima S, Kitamoto K. A novel neurotrophic role of secretory phospholipases A_2 for cerebellar granule neurons. **FEBS Letters. 2005 May;579(12):2693-701.**

Aronson BD, Johnson KA, Dunlap JC. Circadian clock locus frequency: protein encoded by a single open reading frame defines period length and temperature compensation. **Proceedings of the National Academy of Sciences. 1994 Aug;91(16):7683-7.**

Aronson BD, Johnson KA, Loros JJ, Dunlap JC. Negative feedback defining a circadian clock: autoregulation of the clock gene *frequency*. **Science. 1994 Mar;263(5153):1578-84.**

Arpaia G, Cerri F, Baima S, Macino G. Involvement of protein kinase C in the response of *Neurospora crassa* to blue light. **Molecular and General Genetics. 1999 Sept;262(2):314-22.**

Arst Jr HN, Peñalva MA. pH regulation in *Aspergillus* and parallels with higher eukaryotic regulatory systems. **Trends in Genetics. 2003 Apr;19(4):224-31.**

Avello PA, Davis SJ, Ronald J, Pitchford JW. Heat the clock: entrainment and compensation in *Arabidopsis* circadian rhythms. **Journal of Circadian Rhythms. 2019 May;17(5):1-11.**

Báez-Ruiz A, Díaz-Muñoz M. Chronic inhibition of endoplasmic reticulum calcium-release channels and calcium-ATPase lengthens the period of hepatic clock gene *Per1*. **Journal of Circadian Rhythms. 2011 Dec;9(1):1-10.**

Ballario P, Vittorioso P, Magrelli A, Talora C, Cabibbo A, Macino G. White collar-1, a central regulator of blue light responses in *Neurospora*, is a zinc finger protein. **The EMBO Journal. 1996 Apr;15(7):1650-7.**

Bibliography

Balestrieri B, Maekawa A, Xing W, Gelb MH, Katz HR, Arm JP. Group V secretory phospholipase A_2 modulates phagosome maturation and regulates the innate immune response against *Candida albicans*. **Journal of Immunology. 2009 Apr;182(8):4891-8.**

Barman A, Gohain D, Bora U, Tamuli R. Phospholipases play multiple cellular roles including growth, stress tolerance, sexual development, and virulence in fungi. **Microbiological Research. 2018 Apr;209:55-69.**

Barman A, Tamuli R. Multiple cellular roles of *Neurospora crassa plc-1*, *splA*$_2$, and *cpe-1* in regulation of cytosolic free calcium, carotenoid accumulation, stress responses, and acquisition of thermotolerance. **Journal of Microbiology. 2015 Apr;53(4):226-35.**

Barman A, Tamuli R. The pleiotropic vegetative and sexual development phenotypes of *Neurospora crassa* arise from double mutants of the calcium signaling genes *plc-1*, *splA*$_2$, and *cpe-1*. **Current Genetics. 2017 Oct;63(5):861-75.**

Beadle GW, Tatum EL. Genetic control of biochemical reactions in *Neurospora*. **Proceedings of the National Academy of Sciences. 1941 Nov;27(11):499-506.**

Belden WJ, Larrondo LF, Froehlich AC, Shi M, Chen CH, Loros JJ, Dunlap JC. The *band* mutation in *Neurospora crassa* is a dominant allele of *ras-1* implicating RAS signaling in circadian output. **Genes and Development. 2007 Jun;21(12):1494-505.**

Bell-Pedersen D, Dunlap JC, Loros JJ. The *Neurospora* circadian clock-controlled gene, *ccg-2*, is allelic to *eas* and encodes a fungal hydrophobin required for formation of the conidial rodlet layer. **Genes and Development. 1992 Dec;6(12a):2382-94.**

Benito B, Garciadeblás B, Rodríguez-Navarro A. Molecular cloning of the calcium and sodium ATPases in *Neurospora crassa*. **Molecular Microbiology. 2000 Mar;35(5):1079-88.**

Bennett DE, McCreary CE, Coleman DC. Genetic characterization of a phospholipase C gene from *Candida albicans*: presence of homologous sequences in *Candida* species other than *Candida albicans*. **Microbiology. 1998 Jan;144(1):55-72.**

Berridge MJ. Inositol trisphosphate and diacylglycerol: two interacting second messengers. **Annual Review of Biochemistry. 1987 Jul;56(1):159-93.**

Berridge MJ. Inositol trisphosphate and calcium signaling. **Nature. 1993 Jan;361(6410):315-25.**

Berridge MJ, Bootman MD, Lipp P. Calcium-a life and death signal. **Nature. 1998 Oct;395(6703):645-8.**

Berridge MJ, Bootman MD, Roderick HL. Calcium signaling: dynamics, homeostasis, and remodelling. **Nature Reviews Molecular Cell Biology. 2003 Jul;4(7):517-29.**

Berridge MJ, Cobbold PH, Cuthbertson KS. Spatial and temporal aspects of cell signaling. **Philosophical Transactions of the Royal Society of London. B, Biological Sciences. 1988 Jul;320(1199):325-43.**

Berridge MJ, Irvine RF. Inositol trisphosphate, a novel second messenger in cellular signal transduction. **Nature. 1984 Nov;312(5992):315-21.**

Berridge MJ, Lipp P, Bootman MD. The versatility and universality of calcium signaling. **Nature Reviews Molecular Cell Biology. 2000 Oct;1(1):11-21.**

Bibliography

Boilard E, Lai Y, Larabee K, Balestrieri B, Ghomashchi F, Fujioka D, Gobezie R, Coblyn JS, Weinblatt ME, Massarotti EM, Thornhill TS. A novel anti-inflammatory role for secretory phospholipase A_2 in immune complex-mediated arthritis. **EMBO Molecular Medicine. 2010 May;2(5):172-87.**

Boone C, Bussey H, Andrews BJ. Exploring genetic interactions and networks with yeast. **Nature Reviews Genetics. 2007 Jun;8(6):437-49.**

Bootman MD, Collins TJ, Peppiatt CM, Prothero LS, MacKenzie L, De Smet P, Travers M, Tovey SC, Seo JT, Berridge MJ, Ciccolini F. Calcium signaling-an overview. **In Seminars in Cell and Developmental Biology. 2001 Feb;12(1):3-10.**

Borkovich KA, Alex LA, Yarden O, Freitag M, Turner GE, Read ND, Seiler S, Bell-Pedersen D, Paietta J, Plesofsky N, Plamann M. Lessons from the genome sequence of *Neurospora crassa*: tracing the path from genomic blueprint to multicellular organism. **Microbiology and Molecular Biology Reviews. 2004 Mar;68(1):1-108.**

Bowman BJ, Abreu S, Margolles-Clark E, Draskovic M, Bowman EJ. Role of four calcium transport proteins, encoded by *nca-1*, *nca-2*, *nca-3*, and *cax*, in maintaining intracellular calcium levels in *Neurospora crassa*. **Eukaryotic Cell. 2011 May;10(5):654-61.**

Bravo R, Gutierrez T, Paredes F, Gatica D, Rodriguez AE, Pedrozo Z, Chiong M, Parra V, Quest AF, Rothermel BA, Lavandero S. Endoplasmic Reticulum: ER stress regulates mitochondrial bioenergetics. **International Journal of Biochemistry and Cell Biology. 2012 Jan;44(1):16-20.**

Bristol A, Hall SM, Kriz RW, Stahl ML, Fan YS, Byers MG, Eddy RL, Shows TB, Knopf JL. Phospholipase C-148: chromosomal location and deletion mapping of functional domains. **In Cold Spring Harbor Symposia on Quantitative Biology. 1988 Jan;53:915-20.**

Brock TD. Lower pH limit for the existence of blue-green algae: evolutionary and ecological implications. **Science. 1973 Feb;179(4072):480-3.**

Brown EM, Gamba G, Riccardi D, Lombardi M, Butters R, Kifor O, Sun A, Hediger MA, Lytton J, Hebert SC. Cloning and characterization of an extracellular Ca^{2+}-sensing receptor from bovine parathyroid. **Nature. 1993 Dec;366(6455):575-80.**

Bui DC, Lee Y, Lim JY, Fu M, Kim JC, Choi GJ, Son H, Lee YW. Heat shock protein 90 is required for sexual and asexual development, virulence, and heat shock response in *Fusarium graminearum*. **Scientific Reports. 2016 Jun;6(1):1-11.**

Cambareri EB, Jensen BC, Schabtach E, Selker EU. Repeat-induced GC to AT mutations in *Neurospora*. **Science. 1989 Jun;244(4912):1571-5.**

Campbell AK. Intracellular calcium, its universal role as regulator. **Wiley. 1983:483-537.**

Campbell AK. Calcium as an intracellular regulator. **Calcium in Human Biology. 1988:261-316.**

Capelli N, Van Tuinen D, Perez RO, Arrighi JF, Turian G. Molecular cloning of a cDNA encoding calmodulin from *Neurospora crassa*. **FEBS Letters. 1993 Apr;321(1):63-8.**

Carafoli E. Intracellular calcium homeostasis. **Annual Review of Biochemistry. 1987 Jul;56(1):395-433.**

Carneiro P, Duarte M, Videira A. The external alternative NAD(P)H dehydrogenase NDE3 is localized both in the mitochondria and in the cytoplasm of *Neurospora crassa*. **Journal of Molecular Biology. 2007 May;368(4):1114-21.**

Bibliography

Carroll A, Somerville C. Cellulosic biofuels. **Annual Review of Plant Biology. 2009 Jun;60(1):165-82.**

Carugo O, Djinović K, Rizzi M. Comparison of the co-ordinative behaviour of calcium (II) and magnesium (II) from crystallographic data. **Journal of the Chemical Society, Dalton Transactions. 1993(14):2127-35.**

Case RM, Eisner D, Gurney A, Jones O, Muallem S, Verkhratsky A. Evolution of calcium homeostasis: from birth of the first cell to an omnipresent signaling system. **Cell Calcium. 2007 Oct;42(4-5):345-50.**

Cartharius K, Frech K, Grote K, Klocke B, Haltmeier M, Klingenhoff A, Frisch M, Bayerlein M, Werner T. MatInspector and beyond: promoter analysis based on transcription factor binding sites. **Bioinformatics. 2005 Jul;21(13):2933-42.**

Cavazzini D, Meschi F, Corsini R, Bolchi A, Rossi GL, Einsle O, Ottonello S. Autoproteolytic activation of a symbiosis-regulated truffle phospholipase A_2. **Journal of Biological Chemistry. 2013 Jan;288(3):1533-47.**

Cerella C, Diederich M, Ghibelli L. The dual role of calcium as messenger and stressor in cell damage, death, and survival. **International Journal of Cell Biology. 2010 Mar;2010:1-14.**

Chafouleas JG, Bolton WE, Means AR. Potentiation of bleomycin lethality by anticalmodulin drugs: a role for calmodulin in DNA repair. **Science. 1984 Jun;224(4655):1346-8.**

Chard PA. DNA repair in human cells: methods for the determination of calmodulin involvement. **Methods in Enzymology. 1987 Jan;139:715-730.**

Chayakulkeeree M, Sorrell TC, Siafakas AR, Wilson CF, Pantarat N, Gerik KJ, Boadle R, Djordjevic JT. Role and mechanism of phosphatidylinositol-specific phospholipase C in survival and virulence of *Cryptococcus neoformans*. **Molecular Microbiology. 2008 Aug;69(4):809-26.**

Chen Y, Fan X, Zhao X, Shen Y, Xu X, Wei L, Wang W, Wei D. cAMP activates calcium signaling via phospholipase C to regulate cellulase production in the filamentous fungus *Trichoderma reesei*. **Biotechnology for Biofuels. 2021 Dec;14(1):1-13.**

Cheng P, Yang Y, Liu Y. Interlocked feedback loops contribute to the robustness of the *Neurospora* circadian clock. **Proceedings of the National Academy of Sciences. 2001 Jun;98(13):7408-13.**

Chin D, Means AR. Calmodulin: a prototypical calcium sensor. **Trends in Cell Biology. 2000 Aug;10(8):322-8.**

Choi J, Kim KS, Rho HS, Lee YH. Differential roles of the phospholipase C genes in fungal development and pathogenicity of *Magnaporthe oryzae*. **Fungal Genetics and Biology. 2011 Apr;48(4):445-55.**

Chung HJ, Kim MJ, Lim JY, Park SM, Cha BJ, Kim YH, Yang MS, Kim DH. A gene encoding phosphatidyl inositol-specific phospholipase C from *Cryphonectria parasitica* modulates the *lac*1 expression. **Fungal Genetics and Biology. 2006 May;43(5):326-36.**

Clapham DE. Calcium signaling. **Cell. 2007 Dec;131(6):1047-58.**

Colot HV, Park G, Turner GE, Ringelberg C, Crew CM, Litvinkova L, Weiss RL, Borkovich KA, Dunlap JC. A high-throughput gene knockout procedure for *Neurospora* reveals functions for multiple transcription factors. **Proceedings of the National Academy of Sciences. 2006 Jul;103(27):10352-7.**

Bibliography

Cortat M, Turian G. Conidiation of *Neurospora crassa* in submerged culture without mycelial phase. **Archives of Microbiology. 1974 Dec;95(1):305-9.**

Cornelius G, Gebauer G, Techel D. Inositol trisphosphate induces calcium release from *Neurospora crassa* vacuoles. **Biochemical and Biophysical Research Communications. 1989 Jul;162(2):852-6.**

Cowen LE, Lindquist S. Hsp90 potentiates the rapid evolution of new traits: drug resistance in diverse fungi. **Science. 2005 Sep;309(5744):2185-9.**

Cowen LE, Singh SD, Köhler JR, Collins C, Zaas AK, Schell WA, Aziz H, Mylonakis E, Perfect JR, Whitesell L, Lindquist S. Harnessing Hsp90 function as a powerful, broadly effective therapeutic strategy for fungal infectious disease. **Proceedings of the National Academy of Sciences. 2009 Feb;106(8):2818-23.**

Crosthwaite SK, Dunlap JC, Loros JJ. *Neurospora wc-1* and *wc-2*: transcription, photoresponses, and the origins of circadian rhythmicity. **Science. 1997 May;276(5313):763-9.**

Cunningham KW, Fink GR. Calcineurin inhibits *VCX1*-dependent H^+/Ca^{2+} exchange and induces Ca^{2+} ATPases in *Saccharomyces cerevisiae*. **Molecular and Cellular Biology. 1996 May;16(5):2226-37.**

Cupertino FB, Freitas FZ, de Paula RM, Bertolini MC. Ambient pH controls glycogen levels by regulating glycogen synthase gene expression in *Neurospora crassa*. New insights into the pH signaling pathway. **Plos One. 2012 Aug;7(8):e44258.**

Davis RH. *Neurospora*: contributions of a model organism. **Oxford University Press. 2000 Aug.**

Davis RH, de Serres FJ. Genetic and microbiological research techniques for *Neurospora crassa*. **Methods in Enzymology. 1970 Jan;17(A):79-143.**

Davis RH, Perkins DD. *Neurospora*: a model of model microbes. **Nature Reviews Genetics. 2002 May;3(5):397-403.**

Deka R, Kumar R, Tamuli R. *Neurospora crassa* homologue of Neuronal Calcium Sensor-1 has a role in growth, calcium stress tolerance, and ultraviolet survival. **Genetica. 2011 Jul;139(7):885-94.**

Deka R, Tamuli R. *Neurospora crassa ncs-1*, *mid-1*, and *nca-2* double-mutant phenotypes suggest diverse interaction among three Ca^{2+}-regulating gene products. **Journal of Genetics. 2013 Dec;92(3):559-63.**

Dennis EA, Cao J, Hsu YH, Magrioti V, Kokotos G. Phospholipase A_2 enzymes: physical structure, biological function, disease implication, chemical inhibition, and therapeutic intervention. **Chemical Reviews. 2011 Oct;111(10):6130-85.**

Dodge BO. Some problems in the genetics of the fungi. **Science. 1939 Oct;90(2339):379-85.**

Fan F, Ma G, Li J, Liu Q, Benz JP, Tian C, Ma Y. Genome-wide analysis of the endoplasmic reticulum stress response during lignocellulase production in *Neurospora crassa*. **Biotechnology for Biofuels. 2015 Dec;8(1):1-17.**

Fankhauser H, Schweingruber AM, Edenharter E, Schweingruber ME. Growth of a mutant defective in a putative phosphoinositide-specific phospholipase C of *Schizosaccharomyces pombe* is restored by low concentrations of phosphate and inositol. **Current Genetics. 1995 Jul;28(2):199-203.**

Felsenstein J. Confidence limits on phylogenies: an approach using the bootstrap. **Evolution. 1985 Jul;39(4):783-91.**

Bibliography

Flick JS, Thorner J. Genetic and biochemical characterization of a phosphatidylinositol-specific phospholipase C in *Saccharomyces cerevisiae*. **Molecular and Cellular Biology. 1993 Sep;13(9):5861-76.**

Franchi L, Fulci V, Macino G. Protein kinase C modulates light responses in *Neurospora* by regulating the blue light photoreceptor WC-1. **Molecular Microbiology. 2005 Apr;56(2):334-45.**

Freitag M, Hickey PC, Raju NB, Selker EU, Read ND. GFP as a tool to analyze the organization, dynamics and function of nuclei and microtubules in *Neurospora crassa*. **Fungal Genetics and Biology. 2004 Oct;41(10):897-910.**

Galagan JE, Calvo SE, Borkovich KA, Selker EU, Read ND, Jaffe D, FitzHugh W, Ma LJ, Smirnov S, Purcell S, Rehman B. The genome sequence of the filamentous fungus *Neurospora crassa*. **Nature. 2003 Apr;422(6934):859-68.**

Garceau NY, Liu Y, Loros JJ, Dunlap JC. Alternative initiation of translation and time-specific phosphorylation yield multiple forms of the essential clock protein FREQUENCY. **Cell. 1997 May;89(3):469-76.**

Gardner GF, Feldman JF. Temperature compensation of circadian period length in clock mutants of *Neurospora crassa*. **Plant Physiology. 1981 Dec;68(6):1244-8.**

Garnjobst L, Tatum EL. A survey of new morphological mutants in *Neurospora crassa*. **Genetics. 1967 Nov;57(3):579-604.**

Gavric O, dos Santos DB, Griffiths A. Mutation and divergence of the phospholipase C gene in *Neurospora crassa*. **Fungal Genetics and Biology. 2007 Apr;44(4):242-9.**

Ghannoum MA. Potential role of phospholipases in virulence and fungal pathogenesis. **Clinical Microbiology Reviews. 2000 Jan;13(1):122-43.**

Gifford JL, Walsh MP, Vogel HJ. Structures and metal-ion-binding properties of the Ca^{2+}-binding helix-loop-helix EF-hand motifs. **Biochemical Journal. 2007 Jul;405(2):199-221.**

Gilroy S, Blowers DP, Trewavas A. Calcium: a regulation system emerges in plant cells. **Development. 1987 Jun;100(2):181-4.**

Gerloff GC, Fishbeck KA. Quantitative cation requirements of several green and blue-green algae[2]. **Journal of Phycology. 1969 Jun;5(2):109-14.**

Granata F, Balestrieri B, Petraroli A, Giannattasio G, Marone G, Triggiani M. Secretory phospholipases A2 as multivalent mediators of inflammatory and allergic disorders. **International Archives of Allergy and Immunology. 2003 July;131(3):153-63.**

Guignard R, Grange F, Turian GT. Microcycle conidiation induced by partial nitrogen deprivation in *Neurospora crassa*. **Canadian Journal of Microbiology. 1984 Oct;30(10):1210-5.**

Hao L, Rigaud JL, Inesi G. Ca^{2+}/H^{+} countertransport and electrogenicity in proteoliposomes containing erythrocyte plasma membrane Ca^{2+}-ATPase and exogenous lipids. **Journal of Biological Chemistry. 1994 May;269(19):14268-75.**

Halachmi D, Eilam Y. Cytosolic and vacuolar Ca^{2+} concentrations in yeast cells measured with the Ca^{2+}-sensitive fluorescence dye indo-1. **FEBS Letters. 1989 Oct;256(1-2):55-61.**

Bibliography

He Q, Cha J, He Q, Lee HC, Yang Y, Liu Y. CKI and CKII mediate the FREQUENCY-dependent phosphorylation of the WHITE COLLAR complex to close the *Neurospora* circadian negative feedback loop. **Genes and Development. 2006 Sep;20(18):2552-65.**

Hetz C. The unfolded protein response: controlling cell fate decisions under ER stress and beyond. **Nature Reviews Molecular Cell Biology. 2012 Feb;13(2):89-102.**

Hong Y, Zhao J, Guo L, Kim SC, Deng X, Wang G, Zhang G, Li M, Wang X. Plant phospholipases D and C and their diverse functions in stress responses. **Progress in Lipid Research. 2016 Apr;62:55-74.**

Hu Y, Wang J, Ying SH, Feng MG. Five vacuolar Ca^{2+} exchangers play different roles in calcineurin-dependent Ca^{2+}/Mn^{2+} tolerance, multistress responses, and virulence of a filamentous entomopathogen. **Fungal Genetics and Biology. 2014 Dec;73:12-9.**

Huang Y, Li Y, Li D, Bi Y, Prusky DB, Dong Y, Wang T, Zhang M, Zhang X, Liu Y. Phospholipase C from *Alternaria alternata* is induced by physiochemical cues on the pear fruit surface that dictate infection structure differentiation and pathogenicity. **Frontiers in Microbiology. 2020 Jun;11:1279.**

Iida H, Yagawa Y, Anraku Y. Essential role for induced Ca^{2+} influx followed by $[Ca^{2+}]_i$ rise in maintaining viability of yeast cells late in the mating pheromone response pathway: a study of $[Ca^{2+}]_i$ in single *Saccharomyces cerevisiae* cells with imaging of fura-2. **The Journal of Biological Chemistry. 1990 Aug;265(22):13391-9.**

Jaiswal JK. Calcium-how and why? **Journal of Biosciences. 2001 Sep;26(3):357-63.**

Johannes E, Brosnan JM, Sanders D. Calcium channels and signal transduction in plant cells. **BioEssays. 1991 Jul;13(7):331-6.**

Kapoor M, Curle CA, Runham C. The hsp70 gene family of *Neurospora crassa*: cloning, sequence analysis, expression, and genetic mapping of the major stress-inducible member. **Journal of Bacteriology. 1995 Jan;177(1):212-21.**

Kapoor M, Lewis J. Heat shock induces peroxidase activity in *Neurospora crassa* and confers tolerance toward oxidative stress. **Biochemical and Biophysical Research Communications. 1987 Sep;147(3):904-10.**

Kapoor M, Sreenivasan GM, Goel N, Lewis J. Development of thermotolerance in *Neurospora crassa* by heat shock and other stresses eliciting peroxidase induction. **Journal of Bacteriology. 1990 May;172(5):2798-801.**

Kazmierczak J, Kempe S, Kremer B. Calcium in the early evolution of living systems: a biohistorical approach. **Current Organic Chemistry. 2013 Aug;17(16):1738-50.**

Kim H, Wright SJ, Park G, Ouyang S, Krystofova S, Borkovich KA. Roles for receptors, pheromones, G proteins, and mating type genes during sexual reproduction in *Neurospora crassa*. **Genetics. 2012 Apr;190(4):1389-404.**

Klee CB, Crouch TH, Krinks MH. Calcineurin: a calcium-and calmodulin-binding protein of the nervous system. **Proceedings of the National Academy of Sciences. 1979 Dec;76(12):6270-3.**

Kmetzsch L, Staats CC, Cupertino JB, Fonseca FL, Rodrigues ML, Schrank A, Vainstein MH. The calcium transporter Pmc1 provides Ca^{2+} tolerance and influences the progression of murine cryptococcal infection. **The FEBS Journal. 2013 Oct;280(19):4853-64.**

Bibliography

Kmetzsch L, Staats CC, Simon E, Fonseca FL, de Oliveira DL, Sobrino L, Rodrigues J, Leal AL, Nimrichter L, Rodrigues ML, Schrank A. The vacuolar Ca^{2+} exchanger Vcx1 is involved in calcineurin-dependent Ca^{2+} tolerance and virulence in *Cryptococcus neoformans*. **Eukaryotic Cell. 2010 Nov;9(11):1798-805.**

Knechtle P, Goyard S, Brachat S, Ibrahim-Granet O, d'Enfert C. Phosphatidylinositol-dependent phospholipases C Plc2 and Plc3 of *Candida albicans* are dispensable for morphogenesis and host-pathogen interaction. **Research in Microbiology. 2005 Aug;156(7):822-9.**

Kobayashi T, Abe K, Asai K, Gomi K, Juvvadi PR, Kato M, Kitamoto K, Takeuchi M, Machida M. Genomics of *Aspergillus oryzae*. **Bioscience, Biotechnology, and Biochemistry. 2007 Mar;71(3):646-70.**

Köhler GA, Brenot A, Haas-Stapleton E, Agabian N, Deva R, Nigam S. Phospholipase A_2 and phospholipase B activities in fungi. **Biochimica et Biophysica Acta (BBA)-Molecular and Cell Biology of Lipids. 2006 Nov;1761(11):1391-9.**

Kon N, Wang HT, Kato YS, Uemoto K, Kawamoto N, Kawasaki K, Enoki R, Kurosawa G, Nakane T, Sugiyama Y, Tagashira H. Na^+/Ca^{2+} exchanger mediates cold Ca^{2+} signaling conserved for temperature-compensated circadian rhythms. **Science Advances. 2021 Apr;7(18):eabe8132.**

Kothe GO, Free SJ. Calcineurin subunit B is required for normal vegetative growth in *Neurospora crassa*. **Fungal Genetics and Biology. 1998 Apr;23(3):248-58.**

Kretsinger RH, Wasserman RH. Structure and evolution of calcium-modulated protein. **Critical Reviews in Biochemistry. 1980 Jan;8(2):119-74.**

Kumar R, Tamuli R. Calcium/calmodulin-dependent kinases are involved in growth, thermotolerance, oxidative stress survival, and fertility in *Neurospora crassa*. **Archives of Microbiology. 2014 Apr;196(4):295-305.**

Kumar A, Roy A, Deshmukh MV, Tamuli R. Dominant mutants of the calcineurin catalytic subunit (CNA-1) showed developmental defects, increased sensitivity to stress conditions, and CNA-1 interacts with CaM and CRZ-1 in *Neurospora crassa*. **Archives of Microbiology. 2020 May;202:921-34.**

Kunze D, Melzer I, Bennett D, Sanglard D, MacCallum D, Nörskau J, Coleman DC, Odds FC, Schäfer W, Hube B. Functional analysis of the phospholipase C gene *CaPLC1* and two unusual phospholipase C genes, *CaPLC2* and *CaPLC3*, of *Candida albicans*. **Microbiology. 2005 Oct;151(10):3381-94.**

Lakin-Thomas PL. Choline depletion, *frq* mutations, and temperature compensation of the circadian rhythm in *Neurospora crassa*. **Journal of Biological Rhythms. 1998 Aug;13(4):268-77.**

Lamoth F, Juvvadi PR, Fortwendel JR, Steinbach WJ. Heat shock protein 90 is required for conidiation and cell wall integrity in *Aspergillus fumigatus*. **Eukaryotic Cell. 2012 Nov;11(11):1324-32.**

Laxmi V, Tamuli R. The *Neurospora crassa cmd*, *trm-9*, and *nca-2* genes play a role in growth, development, and survival in stress conditions. **Genomics and Applied Biology. 2015 Oct 14;6.**

Laxmi V, Tamuli R. The calmodulin gene in *Neurospora crassa* is required for normal vegetative growth, ultraviolet survival, and sexual development. **Archives of Microbiology. 2017 May;199(4):531-42.**

Lee K, Loros JJ, Dunlap JC. Interconnected feedback loops in the *Neurospora* circadian system. **Science. 2000 Jul;289(5476):107-10.**

Bibliography

Lev S, Desmarini D, Li C, Chayakulkeeree M, Traven A, Sorrell TC, Djordjevic JT. Phospholipase C of *Cryptococcus neoformans* regulates homeostasis and virulence by providing inositol trisphosphate as a substrate for Arg1 kinase. **Infection and Immunity. 2013 Apr;81(4):1245-55.**

Lew RR, Abbas Z, Anderca MI, Free SJ. Phenotype of a mechanosensitive channel mutant, *mid-1*, in a filamentous fungus, *Neurospora crassa*. **Eukaryotic Cell. 2008 Apr;7(4):647-55.**

Lew RR, Giblon RE, Lorenti MS. The phenotype of a phospholipase C (*plc-1*) mutant in a filamentous fungus, *Neurospora crassa*. **Fungal Genetics and Biology. 2015 Sep;82:158-67.**

Li L, Borkovich KA. GPR-4 is a predicted G-protein-coupled receptor required for carbon source-dependent asexual growth and development in *Neurospora crassa*. **Eukaryotic cell. 2006 Aug;5(8):1287-300.**

Lindegren CC. A six-point map of the sex-chromosome of *Neurospora crassa*. **Journal of Genetics. 1936 Apr;32(2):243-56.**

Linden H, Macino G. White collar 2, a partner in blue-light signal transduction, controlling expression of light-regulated genes in *Neurospora crassa*. **The EMBO Journal. 1997 Jan;16(1):98-109.**

Liu Y, Bell-Pedersen D. Circadian rhythms in *Neurospora crassa* and other filamentous fungi. **Eukaryotic Cell. 2006 Aug;5(8):1184-93.**

Livak KJ, Schmittgen TD. Analysis of relative gene expression data using real-time quantitative PCR and the $2^{-\Delta\Delta CT}$ method. **Methods. 2001 Dec;25(4):402-8.**

Lundkvist GB, Kwak Y, Davis EK, Tei H, Block GD. A calcium flux is required for circadian rhythm generation in mammalian pacemaker neurons. **Journal of Neuroscience. 2005 Aug;25(33):7682-6.**

Luque EM, Gutierrez G, Navarro-Sampedro L, Olmedo M, Rodríguez-Romero J, Ruger-Herreros C, Tagua VG, Corrochano LM. A relationship between carotenoid accumulation and the distribution of species of the fungus *Neurospora* in Spain. **PLoS One. 2012 Mar;7(3):e33658.**

Lytton J. Na^+/Ca^{2+} exchangers: three mammalian gene families control Ca^{2+} transport. **Biochemical Journal. 2007 Sep;406(3):365-82.**

Ma Y, Hendershot LM. ER chaperone functions during normal and stress conditions. **Journal of Chemical Neuroanatomy. 2004 Sep;28(1-2):51-65.**

Machida M, Asai K, Sano M, Tanaka T, Kumagai T, Terai G, Kusumoto KI, Arima T, Akita O, Kashiwagi Y, Abe K. Genome sequencing and analysis of *Aspergillus oryzae*. **Nature. 2005 Dec;438(7071):1157-61.**

Maddi A, Fu C, Free SJ. The *Neurospora crassa dfg5* and *dcw1* genes encode α-1, 6-mannanases that function in the incorporation of glycoproteins into the cell wall. **PLoS One. 2012 Jun;7(6):e38872.**

Maeda T. The signaling mechanism of ambient pH sensing and adaptation in yeast and fungi. **The FEBS Journal. 2012 Apr;279(8):1407-13.**

Marchler-Bauer A, Anderson JB, Chitsaz F, Derbyshire MK, DeWeese-Scott C, Fong JH, Geer LY, Geer RC, Gonzales NR, Gwadz M, He S. CDD: specific functional annotation with the Conserved Domain Database. **Nucleic Acids Research. 2009 Jan;37(suppl_1):D205-10.**

Marchler-Bauer A, Bryant SH. CD-Search: protein domain annotations on the fly. **Nucleic Acids Research. 2004 Jul;32(suppl_2):W327-31.**

Bibliography

Margolin BS, Freitag M, Selker EU. Improved plasmids for gene targeting at the *his-3* locus of *Neurospora crassa* by electroporation. **Fungal Genetics Newsletter. 1997:34-6.**

Matoba Y, Katsube Y, Sugiyama M. The crystal structure of prokaryotic phospholipase A_2. **Journal of Biological Chemistry. 2002 May;277(22):20059-69.**

Mattern DL, Forman LR, Brody S. Circadian rhythms in *Neurospora crassa*: a mutation affecting temperature compensation. **Proceedings of the National Academy of Sciences. 1982 Feb;79(3):825-9.**

McCluskey K, Wiest A, Plamann M. The Fungal Genetics Stock Centre: a repository for 50 years of fungal genetics research. **Journal of Biosciences. 2010 Mar;35(1):119-26.**

McNally MT, Free SJ. Isolation and characterization of a *Neurospora* glucose-repressible gene. **Current Genetics. 1988 Dec;14(6):545-51.**

Melo AM, Duarte M, Møller IM, Prokisch H, Dolan PL, Pinto L, Nelson MA, Videira A. The external calcium-dependent NADPH dehydrogenase from *Neurospora crassa* mitochondria. **Journal of Biological Chemistry. 2001 Feb;276(6):3947-51.**

Melo AM, Duarte M, Videira A. Primary structure and characterisation of a 64 kDa NADH dehydrogenase from the inner membrane of *Neurospora crassa* mitochondria. **Biochimica et Biophysica Acta (BBA)-Bioenergetics. 1999 Aug;1412(3):282-7.**

Miller AJ, Vogg G, Sanders D. Cytosolic calcium homeostasis in fungi: roles of plasma membrane transport and intracellular sequestration of calcium. **Proceedings of the National Academy of Sciences. 1990 Dec;87(23):9348-52.**

Miozzi L, Balestrini R, Bolchi A, Novero M, Ottonello S, Bonfante P. Phospholipase A_2 up-regulation during mycorrhiza formation in *Tuber borchii*. **New Phytologist. 2005 Jul;167(1):229-38.**

Mirzayans R, Famulski KS, Enns L, Fraser M, Paterson MC. Characterization of the signal transduction pathway mediating gamma ray-induced inhibition of DNA synthesis in human cells: indirect evidence for involvement of calmodulin but not protein kinase C nor p53. **Oncogene. 1995 Oct;11(8):1597-605.**

Miseta A, Kellermayer R, Aiello DP, Fu L, Bedwell DM. The vacuolar Ca^{2+}/H^{+} exchanger Vcx1p/Hum1p tightly controls cytosolic Ca^{2+} levels in *S. cerevisiae*. **FEBS Letters. 1999 May;451(2):132-6.**

Møller JV, Juul B, le Maire M. Structural organization, ion transport, and energy transduction of P-type ATPases. **Biochimica et Biophysica Acta (BBA)-Reviews on Biomembranes. 1996 May;1286(1):1-51.**

Montagne C. Quatrieme centurie plantes cellulaires exotiques nouvelles. Decades VIII, IX, X. **Annual Science Natural Botany. 1843;20(2):352-9.**

Murakami M, Kudo I. Secretory phospholipase A_2. **Biological and Pharmaceutical Bulletin. 2004;27(8):1158-64.**

Murray NE, Perkins DD. Stanford *Neurospora* methods. ***Neurospora*** **News l4. 1963:21-5.**

Nakahama T, Nakanishi Y, Viscomi AR, Takaya K, Kitamoto K, Ottonello S, Arioka M. Distinct enzymatic and cellular characteristics of two secretory phospholipases A_2 in the filamentous fungus *Aspergillus oryzae*. **Fungal Genetics and Biology. 2010 Apr;47(4):318-31.**

Bibliography

Nakashima H. A liquid culture method for the biochemical analysis of the circadian clock of *Neurospora crassa*. **Plant and Cell Physiology. 1981 Apr;22(2):231-8.**

Nakashima S, Ikeno Y, Yokoyama T, Kuwana M, Bolchi A, Ottonello S, Kitamoto K, Arioka M. Secretory phospholipases A_2 induce neurite outgrowth in PC12 cells. **Biochemical Journal. 2003 Dec;376(3):655-66.**

Nakayama S, Kretsinger RH. Evolution of the EF-hand family of proteins. **Annual Review of Biophysics and Biomolecular Structure. 1994 Jun;23(1):473-507.**

Nevalainen TJ, Cardoso JC, Riikonen PT. Conserved domains and evolution of secreted phospholipases A_2. **The FEBS Journal. 2012 Feb;279(4):636-49.**

Nevalainen TJ, Morgado I, Cardoso JC. Identification of novel phospholipase A_2 group IX members in metazoans. **Biochimie. 2013 Aug;95(8):1534-43.**

Nicholas KB. GeneDoc: analysis and visualization of genetic variation. **Embnew News. 1997;4:14.**

Nishizuka Y. The role of protein kinase C in cell surface signal transduction and tumour promotion. **Nature. 1984 Apr;308(5961):693-8.**

Nguyen QB, Kadotani N, Kasahara S, Tosa Y, Mayama S, Nakayashiki H. Systematic functional analysis of calcium-signaling proteins in the genome of the rice-blast fungus, *Magnaporthe oryzae*, using a high-throughput RNA-silencing system. **Molecular Microbiology. 2008 Jun;68(6):1348-65.**

Ochiai EI. Why calcium? Principles and applications in bioorganic chemistry-IV. **Journal of Chemical Education. 1991 Jan;68(1):10-2.**

Oh YT, Ahn CS, Lee KJ, Kim JG, Ro HS, Kim JW, Lee CW. The activity of phosphoinositide-specific phospholipase C is required for vegetative growth and cell wall regeneration in *Coprinopsis cinerea*. **Journal of Microbiology. 2012 Aug;50(4):689-92.**

O'Neill JS, Reddy AB. The essential role of cAMP/Ca^{2+} signaling in mammalian circadian timekeeping. **Biochemical Society Transactions. 2012 Feb;40(1):44-50.**

Pall ML. The use of Ignite (Basta; glufosinate; phosphinothricin) to select transformants of bar-containing plasmids in *Neurospora crassa*. **Fungal Genetics Reports. 1993;40(1):58.**

Palma-Guerrero J, Hall CR, Kowbel D, Welch J, Taylor JW, Brem RB, Glass NL. Genome wide association identifies novel loci involved in fungal communication. **PLoS Genetics. 2013 Aug;9(8):e1003669.**

Park S, Lee K. Inverted race tube assay for circadian clock studies of the *Neurospora* accessions. **Fungal Genetics Reports. 2004;51(1):12-4.**

Pavelić K. Calmodulin antagonist W 13 prevents DNA repair after bleomycin treatment of human urological tumour cells growing on extracellular matrix. **The International Journal of Biochemistry. 1987 Jan;19(11):1091-5.**

Payen AD. Extrait d'un rapport adresse a M. Le Marechal Duc de Dalmatie, Ministre de la Guerre, President du Conseil, sur une alteration extraordinaire du pain de munition. **Annual Chim. Phys. 3rd Ser. 1843;9:5-21.**

Bibliography

Payne WE, Fitzgerald-Hayes M. A mutation in *PLC1*, a candidate phosphoinositide-specific phospholipase C gene from *Saccharomyces cerevisiae*, causes aberrant mitotic chromosome segregation. **Molecular and Cellular Biology. 1993 Jul;13(7):4351-64.**

Peñalva MA, Arst Jr HN. Recent advances in the characterization of ambient pH regulation of gene expression in filamentous fungi and yeasts. **Annual Review of Microbiology. 2004 Oct;58:425-51.**

Peñalva MA, Tilburn J, Bignell E, Arst Jr HN. Ambient pH gene regulation in fungi: making connections. **Trends in Microbiology. 2008 Jun;16(6):291-300.**

Perkins DD. *Neurospora*: the organism behind the molecular revolution. **Genetics. 1992 Apr;130(4):687-701.**

Perkins DD, Davis RH. *Neurospora* at the millennium. **Fungal Genetics and Biology. 2000 Dec;31(3):153-67.**

Pickard RT, Chiou XG, Strifler BA, DeFelippis MR, Hyslop PA, Tebbe AL, Yee YK, Reynolds LJ, Dennis EA, Kramer RM, Sharp JD. Identification of essential residues for the catalytic function of 85-kDa cytosolic phospholipase A_2: probing the role of histidine, aspartic acid, cysteine, and arginine. **Journal of Biological Chemistry. 1996 Aug;271(32):19225-31.**

Pittendrigh CS. Circadian rhythms and the circadian organization of living systems. **In Cold Spring Harbor Symposia on Quantitative Biology. 1960 Jan;25:159-84.**

Pittman JK, Cheng NH, Shigaki T, Kunta M, Hirschi KD. Functional dependence on calcineurin by variants of the *Saccharomyces cerevisiae* vacuolar Ca^{2+}/H^{+} exchanger Vcx1p. **Molecular Microbiology. 2004 Nov;54(4):1104-16.**

Plesofsky-Vig N, Light D, Brambl R. Paedogenetic conidiation in *Neurospora crassa*. **Experimental Mycology. 1983 Sep;7(3):283-6.**

Prokisch H, Yarden O, Dieminger M, Tropschug M, Barthelmess IB. Impairment of calcineurin function in *Neurospora crassa* reveals its essential role in hyphal growth, morphology, and maintenance of the apical Ca^{2+} gradient. **Molecular and General Genetics. 1997 Sep;256(2):104-14.**

Quandt K, Frech K, Karas H, Wingender E, Werner T. Matlnd and Matlnspector: new fast and versatile tools for detection of consensus matches in nucleotide sequence data. **Nucleic Acids Research. 1995 Dec;23(23):4878-84.**

Raju NB. Meiosis and ascospore genesis in *Neurospora*. **European Journal of Cell Biology. 1980 Dec;23(1):208-23.**

Raju NB. Genetic control of the sexual cycle in *Neurospora*. **Mycological Research. 1992 Apr;96(4):241-62.**

Rhee SG, Bae YS. Regulation of phosphoinositide-specific phospholipase C isozymes. **Journal of Biological Chemistry. 1997 Jun;272(24):15045-8.**

Rho HS, Jeon J, Lee YH. Phospholipase C-mediated calcium signaling is required for fungal development and pathogenicity in *Magnaporthe oryzae*. **Molecular Plant Pathology. 2009 May;10(3):337-46.**

Rizzuto R, Duchen MR, Pozzan T. Flirting in little space: the ER/mitochondria Ca^{2+} liaison. **Science's STKE. 2004 Jan;2004(215):re1**

Bibliography

Romano N, Macino G. Quelling: transient inactivation of gene expression in *Neurospora crassa* by transformation with homologous sequences. **Molecular Microbiology. 1992 Nov;6(22):3343-53.**

Ron D, Walter P. Signal integration in the endoplasmic reticulum unfolded protein response. **Nature Reviews Molecular Cell Biology. 2007 Jul;8(7):519-29.**

Roy A, Tamuli R. Heat shock proteins and the calcineurin-crz1 signaling regulate stress responses in fungi. **Archives of Microbiology. 2022 May;204(5):1-3.**

Roy A, Tamuli R. Regulation of Hsp80 involved in the acquisition of induced thermotolerance, and NCA-2 involved in calcium stress tolerance by the calcineurin-CRZ-1 signaling pathway in *Neurospora crassa.* **Mycological Progress. 2022 Oct;21(10):84.**

Ryan FJ, Beadle GW, Tatum EL. The tube method of measuring the growth rate of *Neurospora*. **American Journal of Botany. 1943 Dec;30(10):784-99.**

Rzhetsky A, Nei M. Statistical properties of the ordinary least-squares, generalized least-squares, and minimum-evolution methods of phylogenetic inference. **Journal of Molecular Evolution. 1992 Oct;35(4):367-75.**

Sadakane Y, Nakashima H. Light-induced phase shifting of the circadian conidiation rhythm is inhibited by calmodulin antagonists in *Neurospora crassa*. **Journal of Biological Rhythms. 1996 Sep;11(3):234-40.**

Sambrook J, Russell DW. Molecular cloning: a laboratory manual. **Cold Spring Harbor Laboratory Press, Cold Spring Harbor, New York. 2001.**

Sanders D, Pelloux J, Brownlee C, Harper JF. Calcium at the crossroads of signaling. **The Plant Cell. 2002 May;14(suppl_1):S401-17.**

Sargent ML, Kaltenborn SH. Effects of medium composition and carbon dioxide on circadian conidiation in *Neurospora*. **Plant Physiology. 1972 Jul;50(1):171-5.**

Saunders DS. An introduction to biological rhythms. **John Wiley & Sons Incorporated. 1977.**

Schaloske RH, Dennis EA. The phospholipase A_2 superfamily and its group numbering system. **Biochimica et Biophysica Acta (BBA)-Molecular and Cell Biology of Lipids. 2006 Nov;1761(11):1246-59.**

Schmitz HP, Heinisch JJ. Evolution, biochemistry, and genetics of protein kinase C in fungi. **Current Genetics. 2003 Jul;43(4):245-54.**

Schröder M. Endoplasmic reticulum stress responses. **Cellular and Molecular Life Sciences. 2008 Mar;65(6):862-94.**

Schumacher J, Viaud M, Simon A, Tudzynski B. The Gα subunit BCG1, the phospholipase C (BcPLC1) and the calcineurin phosphatase co-ordinately regulate gene expression in the grey mould fungus *Botrytis cinerea*. **Molecular Microbiology. 2008 Mar;67(5):1027-50.**

Scott DL, White SP, Otwinowski Z, Yuan W, Gelb MH, Sigler PB. Interfacial catalysis: the mechanism of phospholipase A_2. **Science. 1990 Dec;250(4987):1541-6.**

Selker EU, Garrett PW. DNA sequence duplications trigger gene inactivation in *Neurospora crassa*. **Proceedings of the National Academy of Sciences. 1988 Sep;85(18):6870-4.**

Bibliography

Serrano R, Ruiz A, Bernal D, Chambers JR, Ariño J. The transcriptional response to alkaline pH in *Saccharomyces cerevisiae*: evidence for calcium-mediated signaling. **Molecular Microbiology. 2002 Dec;46(5):1319-33.**

Shear CL, Dodge BO. Life histories and heterothallism of the red bread-mold fungi of the *Monilia sitophila* group. **Journal of Agricultural Research. 1927 Jun;34(11):1019-42.**

Shiu PK, Raju NB, Zickler D, Metzenberg RL. Meiotic silencing by unpaired DNA. **Cell. 2001 Dec;107(7):905-16.**

Soragni E, Bolchi A, Balestrini R, Gambaretto C, Percudani R, Bonfante P, Ottonello S. A nutrient-regulated, dual localization phospholipase A_2 in the symbiotic fungus *Tuber borchii*. **The EMBO Journal. 2001 Sep;20(18):5079-90.**

Sorek M, Levy O. The effect of temperature compensation on the circadian rhythmicity of photosynthesis in *Symbiodinium*, coral-symbiotic alga. **Scientific Reports. 2012 Jul;2(1):1-8.**

Springer ML. Genetic control of fungal differentiation: the three sporulation pathways of *Neurospora crassa*. **Bioessays. 1993 Jun;15(6):365-74.**

Sun J, Glass NL. Identification of the CRE-1 cellulolytic regulon in *Neurospora crassa*. **PloS One. 2011 Sep;6(9):e25654.**

Suresh K, Subramanyam C. A putative role for calmodulin in the activation of *Neurospora crassa* chitin synthase. **FEMS Microbiology Letters. 1997 May;150(1):95-100.**

Sutton RB, Davletov BA, Berghuis AM, Sudhof TC, Sprang SR. Structure of the first C2 domain of synaptotagmin I: a novel Ca^{2+}/phospholipid-binding fold. **Cell. 1995 Mar;80(6):929-38.**

Swain AL, Amma EL. The co-ordination polyhedron of Ca^{2+}, Cd^{2+} in parvalbumin. **Inorganica Chimica Acta. 1989 Sep;163(1):5-7.**

Takayanagi A, Miyakawa T, Asano A, Ohtsuka J, Tanokura M, Arioka M. Expression, purification, refolding, and enzymatic characterization of two secretory phospholipases A_2 from *Neurospora crassa*. **Protein Expression and Purification. 2015 Nov;115:69-75.**

Tamuli R, Kumar R, Srivastava DA, Deka R. Calcium signaling. **In: D.P. Kasbekar, and McCluskey, K. (eds.),** ***Neurospora*** **Genomics and Molecular Biology 2013;35-57. Norfolk: Caister Academic Press.**

Tamuli R, Deka R, Borkovich KA. Calcineurin subunits A and B interact to regulate growth and asexual and sexual development in *Neurospora crassa*. **PloS One. 2016 Mar;11(3):e0151867.**

Tamura K, Stecher G, Peterson D, Filipski A, Kumar S. MEGA6: molecular evolutionary genetics analysis version 6.0. **Molecular Biology and Evolution. 2013 Dec;30(12):2725-9.**

That TC, Turian G. Ultrastructural study of microcyclic macroconidiation in *Neurospora crassa*. **Archives of Microbiology. 1978 Mar;116(3):279-88.**

Thompson JD, Gibson TJ, Plewniak F, Jeanmougin F, Higgins DG. The CLUSTAL_X windows interface: flexible strategies for multiple sequence alignment aided by quality analysis tools. **Nucleic Acids Research. 1997 Dec;25(24):4876-82.**

Tian C, Beeson WT, Iavarone AT, Sun J, Marletta MA, Cate JH, Glass NL. Systems analysis of plant cell wall degradation by the model filamentous fungus *Neurospora crassa*. **Proceedings of the National Academy of Sciences. 2009 Dec;106(52):22157-62.**

Bibliography

Tilburn J, Sarkar S, Widdick DA, Espeso EA, Orejas M, Mungroo J, Penalva MA, Arst Jr HN. The *Aspergillus* PacC zinc finger transcription factor mediates regulation of both acid- and alkaline-expressed genes by ambient pH. **The EMBO Journal. 1995 Feb;14(4):779-90.**

Tsai HC, Chung KR. Calcineurin phosphatase and phospholipase C are required for developmental and pathological functions in the citrus fungal pathogen *Alternaria alternata*. **Microbiology. 2014 Jul;160(7):1453-65.**

Verghese J, Abrams J, Wang Y, Morano KA. Biology of the heat shock response and protein chaperones: budding yeast (*Saccharomyces cerevisiae*) as a model system. **Microbiology and Molecular Biology Reviews. 2012 Jun;76(2):115-58.**

Verheij HM, Volwerk JJ, Jansen EH, Puyk WC, Dijkstra BW, Drenth J, De Haas GH. Methylation of histidine-48 in pancreatic phospholipase A_2. Role of histidine and calcium ion in the catalytic mechanism. **Biochemistry. 1980 Feb;19(4):743-50.**

Verkhratsky A, Parpura V. Calcium signaling and calcium channels: evolution and general principles. **European Journal of Pharmacology. 2014 Sep;739:1-3.**

Viladevall L, Serrano R, Ruiz A, Domenech G, Giraldo J, Barceló A, Ariño J. Characterization of the calcium-mediated response to alkaline stress in *Saccharomyces cerevisiae*. **Journal of Biological Chemistry. 2004 Oct;279(42):43614-24.**

Virgilio S, Cupertino FB, Ambrosio DL, Bertolini MC. Regulation of the reserve carbohydrate metabolism by alkaline pH and calcium in *Neurospora crassa* reveals a possible cross-regulation of both signaling pathways. **BMC Genomics. 2017 Dec;18(1):1-5.**

Virgilio S, Cupertino FB, Bernardes NE, Freitas FZ, Takeda AA, Fontes MR, Bertolini MC. Molecular components of the *Neurospora crassa* pH signaling pathway and their regulation by pH and the PAC-3 transcription factor. **PloS One. 2016 Aug;11(8):e0161659.**

Vogel HJ. A convenient growth medium for *Neurospora* (Medium N). **Microbial Genetics Bulletin. 1956;13:42-3.**

Vogel HJ. Distribution of lysine pathways among fungi: evolutionary implications. **The American Naturalist. 1964 Nov;98(903):435-46.**

Wakatsuki S, Arioka M, Dohmae N, Takio K, Yamasaki M, Kitamoto K. Characterization of a novel fungal protein, p15, which induces neuronal differentiation of PC12 cells. **The Journal of Biochemistry. 1999 Dec;126(6):1151-60.**

Wakatsuki S, Yokoyama T, Nakashima S, Nishimura A, Arioka M, Kitamoto K. Molecular cloning, functional expression, and characterization of p15, a novel fungal protein with potent neurite-inducing activity in PC12 cells. **Biochimica et Biophysica Acta (BBA)-Gene Structure and Expression. 2001 Dec;1522(2):74-81.**

Wang B, Kettenbach AN, Zhou X, Loros JJ, Dunlap JC. The phospho-code determining circadian feedback loop closure and output in *Neurospora*. **Molecular Cell. 2019 May;74(4):771-84.**

Wang B, Zhou X, Gerber SA, Loros JJ, Dunlap JC. Cellular calcium levels influenced by NCA-2 impact circadian period determination in *Neurospora*. **mBio. 2021 Jun;12(3):e01493-21.**

Watson S, Arkinstall S. G-protein linked effector and second messenger systems. **In the G Protein Linked Receptor Factsbook 1994. Academic Press London.**

Bibliography

Westergaard M, Mitchell HK. *Neurospora* V.A synthetic medium favouring sexual reproduction. **American Journal of Botany. 1947 Dec;34(10):573-7.**

Williams RJ. The evolution of the biochemistry of calcium. **New Comprehensive Biochemistry. 2007 Jan;41:23-48.**

Winkler MA, Merat DL, Tallant EA, Hawkins S, Cheung WY. Catalytic site of calmodulin-dependent protein phosphatase from bovine brain resides in subunit A. **Proceedings of the National Academy of Sciences. 1984 May;81(10):3054-8.**

Yamamoto TA, Takeuchi H, Kanematsu T, Allen V, Yagisawa H, Kikkawa U, Watanabe Y, Nakasima A, Katan M, Hirata M. Involvement of EF-hand motifs in the Ca^{2+}-dependent binding of the pleckstrin homology domain to phosphoinositides. **European Journal of Biochemistry. 1999 Oct;265(1):481-90.**

Yang Q, Borkovich KA. Mutational activation of a $G\alpha_i$ causes uncontrolled proliferation of aerial hyphae and increased sensitivity to heat and oxidative stress in *Neurospora crassa*. **Genetics. 1999 Jan;151(1):107-17.**

Yang Y, Cheng P, Zhi G, Liu Y. Identification of a calcium/calmodulin-dependent protein kinase that phosphorylates the *Neurospora* circadian clock protein FREQUENCY. **Journal of Biological Chemistry. 2001 Nov;276(44):41064-72.**

Yoko-o T, Matsui Y, Yagisawa H, Nojima H, Uno I, Toh-e A. The putative phosphoinositide-specific phospholipase C gene, *PLC1*, of the yeast *Saccharomyces cerevisiae* is important for cell growth. **Proceedings of the National Academy of Sciences. 1993 Mar;90(5):1804-8.**

Zelter A, Bencina M, Bowman BJ, Yarden O, Read ND. A comparative genomic analysis of the calcium signaling machinery in *Neurospora crassa*, *Magnaporthe grisea*, and *Saccharomyces cerevisiae*. **Fungal Genetics and Biology. 2004 Sep;41(9):827-41.**

Zhang X, Ren A, Li MJ, Cao PF, Chen TX, Zhang G, Shi L, Jiang AL, Zhao MW. Heat stress modulates mycelium growth, heat shock protein expression, ganoderic acid biosynthesis, and hyphal branching of *Ganoderma lucidum* via cytosolic Ca^{2+}. **Applied and Environmental Microbiology. 2016 Jul;82(14):4112-25.**

Zhu Q, Zhou B, Gao Z, Liang Y. Effects of phospholipase C on *Fusarium graminearum* growth and development. **Current Microbiology. 2015 Dec;71(6):632-7.**

Zhu Q, Sun L, Lian J, Gao X, Zhao L, Ding M, Li J, Liang Y. The phospholipase C (*FgPLC1*) is involved in regulation of development, pathogenicity, and stress responses in *Fusarium graminearum*. **Fungal Genetics and Biology. 2016 Dec;97:1-9.**

List of Publications, Conferences, and Workshops

Journal Publications

1. Avishek Roy, Ajeet Kumar, **Darshana Baruah,** and Ranjan Tamuli, 2020**.** Calcium signaling is involved in diverse cellular processes in fungi. **Mycology: An International Journal on Fungal Biology, 10-24. (Equal Contribution)**

2. **Darshana Baruah,** Christy Noche K Marak, Avishek Roy, Dibakar Gohain, Ajeet Kumar, Pallavi Das, Katherine A. Borkovich, and Ranjan Tamuli. Multiple calcium signaling genes play a role in *Neurospora crassa* circadian period length. **(FEMS Microbiology Letters; In Press).**

3. **Darshana Baruah** and Ranjan Tamuli. The *Neurospora crassa Phospholipase C-1*, Ca^{2+}/H^{+} *exchanger-1*, and *Secretory phospholipase* A_2 are involved in stress responses and cellulose degradation. **(Manuscript Communicated).**

4. **Darshana Baruah** and Ranjan Tamuli. Molecular basis of Secretory Phospholipase A_2 mediated cellulose degradation in *N. crassa.* **(Manuscript Under Preparation).**

Conference Presentations

1. **Darshana Baruah** and Ranjan Tamuli **(2021).** Understanding the molecular functions of *Phospholipase C-1* and *Secretory phospholipase* A_2 in *Neurospora crassa*. Neurospora 2021, 17-20th Oct, Camp Allen Navasota, Texas (Poster Presented).

2. **Darshana Baruah** and Ranjan Tamuli **(2019).** Understanding the role of *phospholipase C-1* and *secretory phospholipase* A_2 in circadian clock and biomass degradation in *Neurospora crassa.* XI International Conference on Biology of Yeasts and Filamentous Fungi, University of Hyderabad, 27-29th Nov 2019 (Poster Presented).

3. **Darshana Baruah** and Ranjan Tamuli **(2019).** Understanding the interactions of *phospholipase C-1*, *secretory phospholipase* A_2, and Ca^{2+}/H^{+} *exchanger* in circadian regulated conditions, development, and cell survival in *Neurospora crassa.* Research Conclave 2019, IIT Guwahati **(Received Best Poster Presentation Award).**

4. Christy Noche K Marak, **Darshana Baruah,** and Ranjan Tamuli **(2019).** A look into evolution and life through calcium. Research Conclave 2018, IIT Guwahati (Model Presentation).

5. **Darshana Baruah** and Ranjan Tamuli **(2018).** Understanding the role of PLC-δ, $sPLA_2$ and CPE-1 in regulating various cellular processes in *Neurospora crassa.* Research Conclave 2018, IIT Guwahati **(Received 2nd Best Poster Presentation Award).**

6. **Darshana Baruah** and Ranjan Tamuli **(2017).** Understanding the role of *plc-1*, *splA*$_2$ and *cpe-1* genes in regulation of *Neurospora crassa* circadian clock. National Conference on Fungal Biology, University of Jammu, 16-18th Nov 2017 (Poster Presented).

List of Publications, Conferences, and Workshops

Workshops Attended

1. DBT and BCIL sponsored workshop on "Capacity building in grant writing skills and effective management of Intellectual Property Rights (IPR) in Biotechnology by universities and research institutions in the North East Region" held at College of Veterinary Sciences, Assam Agricultural University, Khanapara, Guwahati, India from 28th to 30th December, 2016 (Attended).
2. 1st Departmental Retreat (Biotech Express), Department of Biosciences and Bioengineering, IIT Guwahati, 21st Dec, 2019 (Attended).
3. Skill Development in Molecular Strategies for Understanding Biodiversity and Human Diseases" at NEHU during Feb 27th-Mar 1st, 2019 (Attended).